Assessment of Transformer Energisation Transients and Their Impacts on Power Systems

A thesis submitted to The University of Manchester for the degree of

DOCTOR OF PHILOSOPHY

in the Faculty of Engineering and Physical Sciences

2013

JINSHENG PENG

School of Electrical and Electronic Engineering

Contents

Final word count: 55 909

List of Figures

List of Tables

List of Abbreviations

ATP/EMTP	Alternative Transients Program/Electromagnetic Transients Program
AVR	Automatic Voltage Regulator
CB	Circuit Breaker
CCGT	Combined Cycle Gas Turbine
CT	Current Transformer
DC	Direct Current
FEM	Finite Element Method
FC	Fixed Capacitor
GSU	Generator Step-Up
HV	High Voltage
HVDC	High Voltage Direct Current
LV	Low Voltage
MCTS	Maximum Closing Time Span
MSC	Mechanical Switched Capacitor
NGET	National Grid Electricity Transmission
PCC	Point of Common Coupling
RMS	Root Mean Square
STC	Saturable Transformer Component
SVC	Stativ Var Compensator
TCR	Thyristor Controlled Reactor
UMEC	Unified Magnetic Equivalent Circuit
WCDM	Worst Case Dip Magnitude

Abstract

Transformers are essential components facilitating transmission and distribution of electric power. Energisation of transformers, however, can cause core operating at deep saturation region and thereby induce transient inrush currents of high magnitude and with rich harmonics. This can lead to undesirable effects including potential damage to the transformer itself, relay mal-operation, harmonic resonant overvoltages, and reduced power quality in the system (mainly in the form of voltage dips).

This thesis investigates voltage dips caused by energising generator step-up (GSU) transformers and two types of generation connection are studied: one is a combine cycle gas turbine (CCGT) plant connected to a 400 kV transmission grid and the other is a large offshore wind farm connected to a 132 kV distribution grid. To carry out the investigation, detailed network models were developed in alternative transients program/electromagnetic transients program (ATP/EMTP) and validated with the help of field measurements.

For the connection of generation in the transmission grid, deterministic assessment was conducted to comparatively analyse voltage dips caused by energising large GSU transformers under different energisation conditions and different network conditions; special attention was paid to the energisation cases involving sympathetic inrush between transformers by addressing its prolonging effects on voltage dips, with sensitivity studies further carried out to identify the key influential parameters. In addition, stochastic assessment was conducted by applying Monte Carlo method, which helps identify the dip frequency pattern and the likelihood of reaching the dip magnitude resulted from the commonly agreed worst case energisation condition; their sensitivities to the variation of circuit breaker closing time span, transformer core residual flux, system condition and the number of transformers being energized together were also investigated. Furthermore, possible cost-effective operational approaches to mitigate the voltage dips were explored and compared. For the connection of large offshore wind farm, voltage dips caused by energising wind turbine transformers under different scenarios were assessed; in particular, sympathetic inrush between wind turbine transformers were studied, and the energisation sequence resulting in less sympathetic inrush was deterministically identified and stochastically validated.

The simulation results of deterministic studies indicate that, when carrying out energisation of a large GSU transformer in the transmission grid under the commonly agreed worst case energisation condition, the dip magnitude can reach 9.6% and the duration 2.7 seconds; moreover, when coupled with sympathetic inrush, the duration can be prolonged by 136%, lasting for 6.4 seconds. The sensitivity studies show that transformer core saturation inductance is the key parameter determining dip magnitude and transformer copper losses is the key parameter determining dip duration. Stochastic assessment of voltage dips shows that, out of 1000 stochastic dip events, less than 0.5% of the dips can reach the worst case dip magnitude and about 80% are of magnitudes less than 0.6 pu of the worst case dip magnitude; the dip frequency pattern is found to be insensitive to the circuit breaker closing time variation but can be considerably influenced by the residual flux distribution. In terms of mitigation measures, it was proven that, by adjusting tap changer position, applying static var compensator and even opening coupler circuit breaker in the substation, the degree of voltage dip especially the dip duration can be significantly reduced.

Contrasting to those observed in the transmission grid, voltage dips resulted from energising wind turbine transformers in large offshore wind farms are of less concern; dip magnitudes are no more than 1% in the case of energising a stand-alone wind turbine transformer. However, sympathetic inrush between wind turbine transformers within one feeder was found to be significant and the energisation sequence resulting in less sympathetic inrush is to separately energise the wind turbine transformer from the one closest to the offshore platform to the one farthest away from the platform.

Declaration

I declare that no portion of the work referred to in the thesis has been submitted in support of an application for another degree or qualification of this or any other university or other institute of learning.

Copyright Statement

Acknowledgement

First and foremost I would like to thank my supervisors Dr. Haiyu Li and Prof. Zhongdong Wang.

It is my privilege to be their student and this thesis would not have been possible without their invaluable guidance, generous support and constant inspiration. I much appreciate Dr. Haiyu Li for his generous supervision, forward-looking advices and insightful discussions during my PhD studies. I am deeply grateful to Prof. Zhongdong Wang for providing me the great opportunity to explore and endeavour the PhD journey and the intensive technical guidance; she helped me build up confidence, cultivate academic skills and enlighten my vision of future career.

I am very grateful to Your Manchester Fund at the University of Manchester for providing the Alumni Research Impact Scholarship which partially sponsored my PhD research.

I would like to thank Dr. Foroozan Ghassemi and Prof. Paul Jarman of National Grid, for providing technical support.

Special thanks also to all my colleagues in the transformer research group, in Ferranti Building and our school for their company and support; in particular, I would like to express my gratitude to Dr. Swee Peng Ang for his kind help and interesting discussions during my MSc and PhD studies in the University of Manchester.

With extreme appreciation, I wish to convey my sincere thanks to my family for their continuous care and encouragement. Especially, I am deeply indebted to my beloved wife Xiao Yi whose selfless love and devotion continuously motivate me to overcome difficulties, make progress and achieve my best.

Chapter 1 Introduction

1.1 Background

Modern society critically relies on electric power as the key energy source and constant efforts have been made by power system operators to maintain and operate interconnected electrical systems as reliably as possible.

One of the challenges for the quality of power supply is the disturbances caused by transformer energisation. Due to the nonlinearity of the magnetic characteristic of transformer core, transformer energisation would result in inrush currents of high magnitude and with rich harmonics, causing damage to transformer itself, and influencing the system by harmonic resonant overvoltages, relay mal-operation and reduced power quality mainly in terms of voltage dips [1]. Indeed, a modern high voltage transmission grid normally consists of hundreds of power transformers and a distribution grid may consist of thousands; the topology of some future network configurations, such as in the case of wind farm grids, reflects the tendency that power transformers would be connected more adjacent to one another and it is more likely to simultaneously switch on a group of transformers [2, 3]. Therefore, more intensified inrush transient interactions could occur, which would cause adverse impacts on power system, hence affect industrial and commercial customers. This, without proper management, could lead to significant economic losses; and consequently their associated adverse effects should be carefully assessed to guide system operation and planning so as to ensure the compliance with tightening standards that define secure and high quality supply of electric power [4, 5].

1.1.1 Transformer energisation inrush phenomena

The transformer core is normally made up of steel laminations with non-linear magnetic permeability. This leads to core magnetization exhibiting a hysteresis characteristic, as illustrated in Figure 1-1 (a). By linking the peak points of the hysteresis loops taken under different steady state applied voltages, a simplified magnetization curve can be

obtained, as shown in Figure 1-1 (b). Normally, transformer core operates at the linear region where the core magnetic permeability is high and the core magnetizing current is low. As the voltage is increased, more and more flux is demanded (the flux is proportional with the integral of the applied voltage) and the core would enter the saturation region where a slight increase of flux would result in a significant increase of magnetizing current.

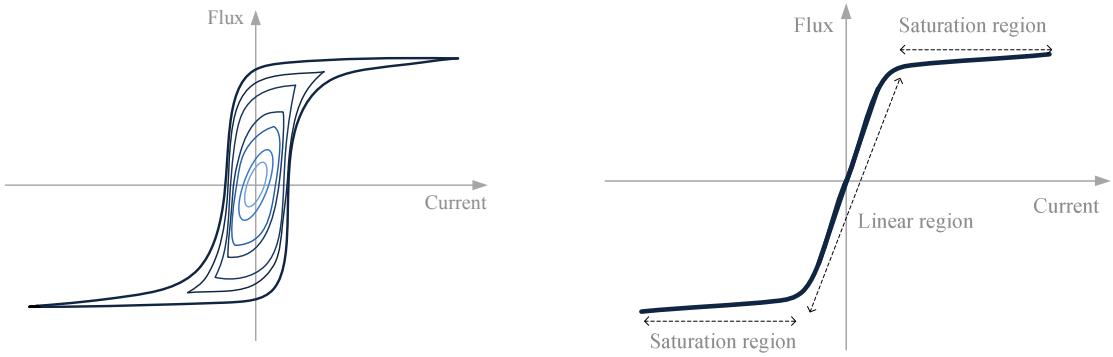

(a) Hysteresis loops (b) Simplified magnetization curve

Figure 1-1 Qualitative illustration of transformer core hysteresis loops and simplified magnetization curve

Figure 1-2 shows the relationship between voltage, magnetic flux, and magnetizing current for a transformer under steady state operation. Due to the transformer core non-linearity, the magnetizing current is non-sinusoidal. It follows the hysteresis loop oscillating between $\pm i_m$ as the flux changes sinusoidally between $\pm \Phi_m$ (the magnitude of i_m is normally between 0.5% and 2% of the transformer rated current).

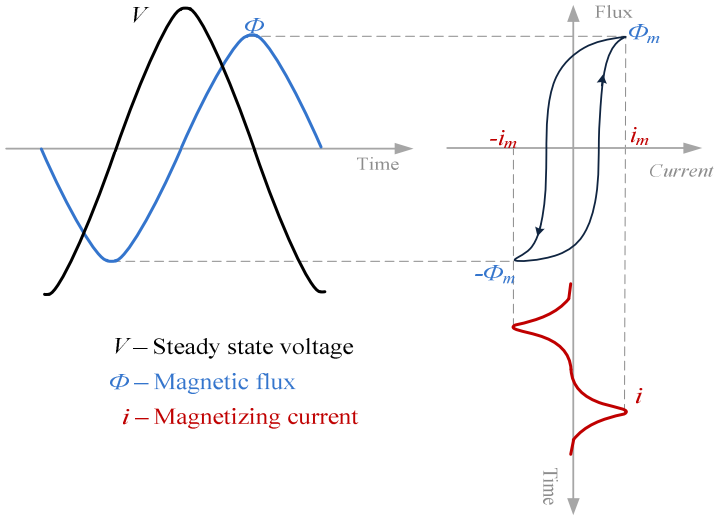

Figure 1-2 Qualitative representation of voltage, flux and magnetizing current for a transformer at steady state operation

Supposing a transformer is energised onto an ideal voltage source at the positive-going zero crossing of the applied voltage, this would require the flux in the core to reach Φ_m

when the voltage peak is reached and continue to increase to $2\Phi_m$ when the voltage returns to zero again (as shown by the dash blue line in Figure 1-3). The excessive demand of flux would saturate the core and result in sharp increase of the magnetizing current. This sharply increased current is termed as inrush current (i_{inrush}) and its magnitude could be many times of the transformer nominal magnetizing current.

Usually, after a transformer is switched off, magnetizing current will follow a hysteresis loop to zero and some residual flux Φ_r could be retained in the core. If this residual flux is taken into account and suppose its polarity is in the direction of flux build-up, the maximum flux resulted from the above-mentioned energisiation would become $2\Phi_m+\Phi_r$ (as indicated by the solid blue line in Figure 1-3), resulting in even larger inrush current.

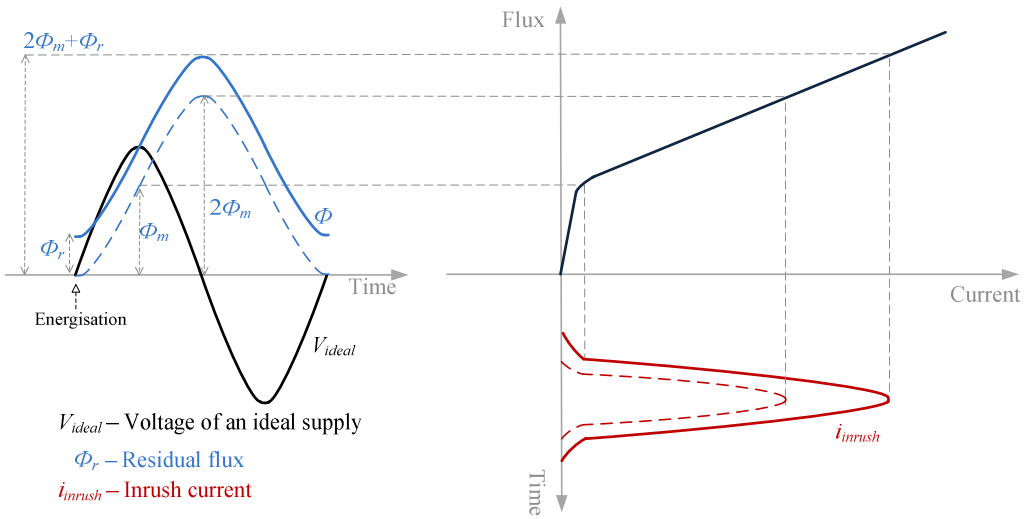

Figure 1-3 Qualitative illustration of inrush phenomena and the effect of residual flux

Figure 1-4 shows a measured inrush current resulting from energising a 155 MVA generator step-up (GSU) transformer [6]. The magnitude of the first peak of inrush current is hundreds of times larger than the magnitude of the nominal magnetizing current. The waveform of the inrush current looks like half cycle sinusoidal wave superimposed by a DC component whose decay is largely influenced by system losses. The inrush current is rich in harmonics especially even harmonics [7].

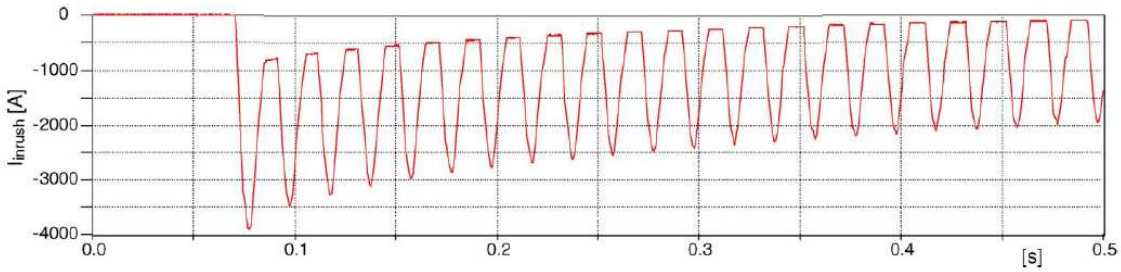

Figure 1-4 Field measured long duration inrush current resulted from energising a 155 MVA GSU transformer [6]

1.1.2 Adverse effects of transformer energisation transients

There are many cases in which transformer energisation caused serious issues in power systems, the key adverse effects include:

Mechanical and electrical stresses

The amplitude of inrush current can be equal to that of the short-circuit current [8], and it lasts longer without enough damping in the system and consequently can seriously damage the windings through excessive mechanical stresses. In fact, the axial forces due to inrush current are always larger than those caused by short circuit current and the radial force applied on transformer high voltage winding can be three times of the corresponding force caused by short circuit condition [9]. These adverse effects on the windings can result in pre-mature failure of a transformer.

Harmonic resonant overvoltages

Transformer inrush currents are rich in harmonics [10]. If one of the harmonic components in the inrush current is close to the resonant frequency of the power system, a sustained overvoltage might be produced [11]. This can be encountered in the following scenarios:

- After system collapse, a black-start process is carried out by energising a remote transformer against minimum generation and loading [12];
- In High-Voltage Direct Current (HVDC) scheme, the ac system can be in resonance with the ac harmonic filters at particular harmonic frequencies, and these resonances can be excited by inrush currents resulted from energising HVDC converter transformers [13];
- In offshore electrical systems, such as offshore wind farms or oil production facilities, the interconnection via a subsea cable introduces a significant shunt capacitance to the source power system, resulting in low resonant frequency, and therefore the resonant overvoltages may be excited by one of the harmonics of the inrush currents caused by energising wind turbine transformers or offshore platform transformers [14].

Harmonic resonant overvoltages may be amplified above the level the system equipment can withstand and if these overvoltages last for a long period of time, they may eventually damage the equipment [15].

Relay mal-operation

Transformer inrush may cause mal-operation of transformer relay protection [7]. During transformer energisation, the inrush current only flows through the energised winding, which has no equivalent currents from the other windings. This unbalance condition may be treated by the transformer differential protection as transformer internal faults, thereby tripping the circuit breaker immediately after transformer energisation. Although the second harmonic of the inrush current can be used to identify the inrush condition and restrain the relay operation, the restraining criteria for setting the relay may affect the relay performance [16]; and in certain cases, ultra-saturation may be induced by transformer energisation, which would inevitably cause tripping of a healthy transformer [17].

Voltage dips

Due to the impedance between the supply source and the energised transformer, the inrush currents may result in temporary voltage dips in the connected system. The dips differ in the magnitudes among three phases and take a long time to recover [18]. If the short circuit level at the transformer busbar is low, the resulted voltage dips can be significant which may affect downstream customers having devices sensitive to power quality variation [19].

Figure 1-5 shows measured three-phase voltage dips on an 11 kV network due to energising a no-load transformer. The voltage dips are in root mean square (RMS) values calculated based on one-cycle window; they are characterized by being non-rectangular and non-symmetrical in three phases (each phase has a dip magnitude different from others due to the different degrees of saturation), with long duration of recovery [18]. The largest RMS dip magnitude is about 0.17 pu and it took about 100 ms to recover by 50%. In addition, for over a two-month period, a total of 109 voltage dip events caused by transformer energisation in the same distribution system were measured. Figure 1-6 shows the frequency of occurrence of the measured RMS voltage dip magnitudes (note that each event constitutes three voltage dip magnitudes and therefore there are in total 327 samples, as derived from Figure 1-6).

Similar voltage dip events were observed in high voltage transmission networks. For example, in [20], voltage dips caused by energising a no-load 750/220/63 kV auto-

transformer were measured on 220 kV side, which are shown in Figure 1-7. Compared to those observed in distribution network shown in Figure 1-5, the dip pattern is similar but the recovery is slower (the dips took about 750 ms to recover by 50%). This slower recovery could be attributed to the larger L/R ratio in the transmission system, as the L/R ratio determines the decaying time constant of the inrush current.

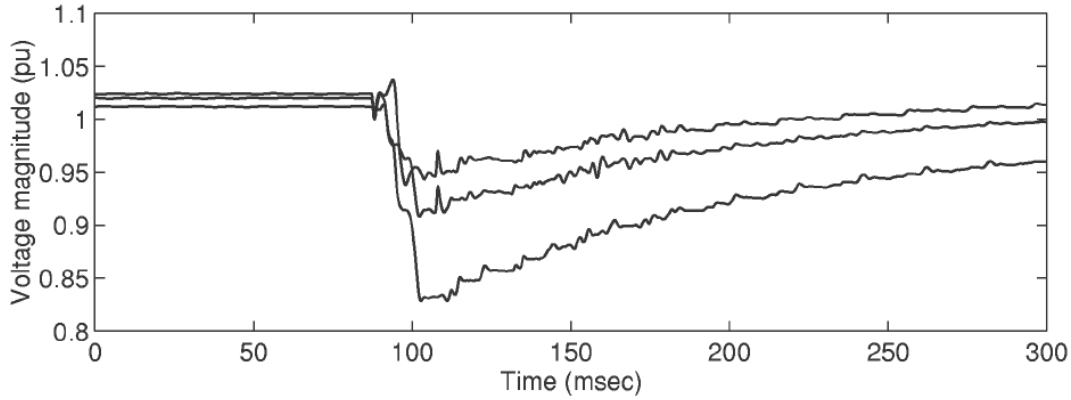

Figure 1-5 Measured RMS voltage dips caused by transformer energising at a 11 kV distribution network [18]

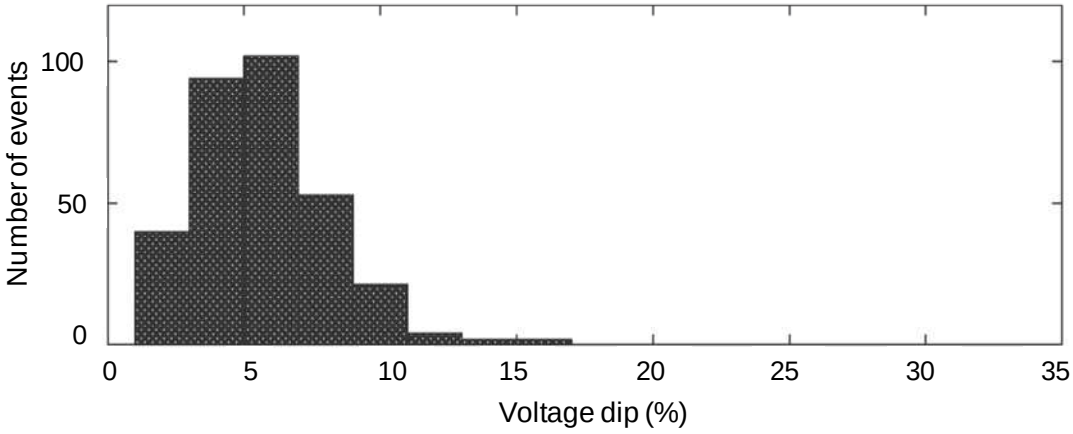

Figure 1-6 Frequency of RMS voltage dip magnitudes out of 109 dip events measured at a 11 kV distribution network [18]

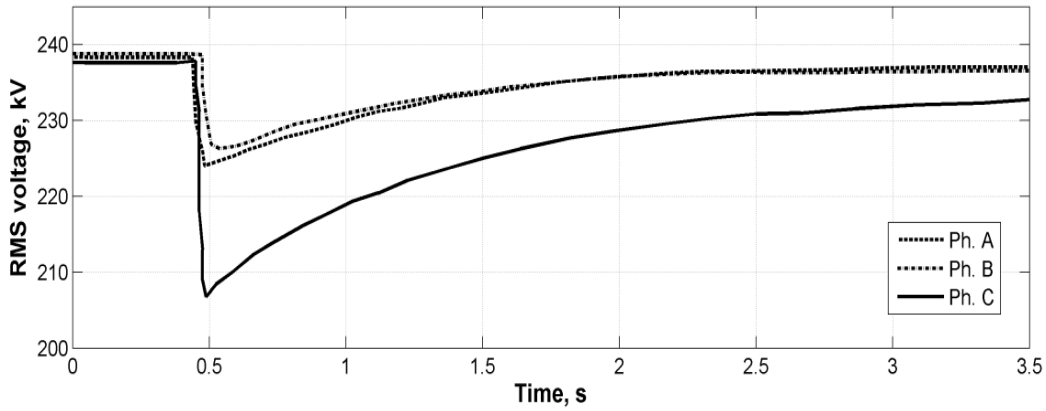

Figure 1-7 RMS voltage dips caused by energising a 750/220/63 kV transformer (voltage dips were measured on 220 kV side) [20]

Recently, connections of wind farms are increasing and they are often located at remote areas where the electrical network can be of relatively low fault level (i.e. the source strength is weak). Voltage dips caused by energising wind turbine transformers have been causing concerns.

Sympathetic inrush

A transformer already connected to the supply system can experience unexpected saturation during the inrush transient of an incoming transformer [21]. This saturation is established by the asymmetrical voltage drop across the system resistance caused by the inrush current in the transformer being energised. It demands offset magnetizing currents of high magnitude in the already connected transformers and hence classified as 'sympathetic'. The sympathetic inrush can significantly prolong the duration of the inrush and therefore exacerbate the above-mentioned adverse effects associated with the inrush phenomena [22].

1.2 Objectives of research

With the help of field measurements and time-domain simulation, this thesis investigates voltage dips and sympathetic inrush caused by energising generator step-up (GSU) transformers, focusing on two types of generation connection: one is a combine cycle gas turbine plant connected to a 400 kV transmission grid and the other is a large offshore wind farm plant connected to a 132 kV distribution grid.

Through the investigation, it is aimed to answer the following questions that have not been addressed before:

- Influence of sympathetic inrush on voltage dips caused by transformer energisation;
- Probability of encountering the worst case voltage dips;
- Energisation sequence resulting in less sympathetic inrush between wind turbine transformers.

To achieve the objectives, the scope of the work covers the following areas:

- Use Alternative Transients Program/Electro-Magnetic Transients Program (ATP/EMTP) to develop network models suitable for studying voltage dips and sympathetic inrush caused by energising transformers;
- Assess and compare voltage dips caused by energising GSU transformers in a

400 kV transmission grid and a 33 kV wind farm collection grid;

- ❖ Investigate the influence of sympathetic inrush on voltage dips caused by transformer energisation;
- ❖ Perform sensitivity assessment to identify the key influential parameters;
- ❖ Stochastically assess the voltage dips caused by transformer energisation, taking into account the influences of various transformer core residual flux and circuit breaker closing time span distributions;
- ❖ Explore possible operational measures to reduce the voltage dips caused by transformer energisation in the 400 kV grid;
- ❖ Assess different energisation sequences to reduce sympathetic inrush between wind turbine transformers in the offshore wind farm grid.

1.3 Outline of the thesis

The thesis consists of seven chapters which are briefly described below:

Chapter 1 Introduction

This chapter presents a general background about transformer inrush and its potential adverse impacts on the power transformer itself and the power system. The objectives and the scope of work of this thesis are presented.

Chapter 2 Literature Review on Transformer Energisation Transients

This chapter summarizes the published work related to transformer energisation transients. First of all, the approaches for calculating transformer inrush currents are presented; network components modelling in ATP/EMTP (mainly include transformer, transmission line and circuit breaker) are further reviewed in detail; this is followed by reviewing simulation studies of transformer energisation transients mainly in terms of sympathetic interaction, harmonic resonant overvoltages and voltage dips. Finally, possible measures for mitigating transformer inrush are presented and compared.

Chapter 3 Field Measurements, Network Model Development and Validation

This chapter reports the field measurements of inrush currents, sympathetic inrush currents and voltage dips caused by energising 400 kV GSU transformers. The network model development is described in detail and also its validation against field measurement results.

Chapter 4 Assessment of Voltage Dips Caused by Transformer Energisation Transients Using Deterministic Approach

This chapter describes the comprehensive assessment on voltage dips in the 400 kV system caused by energising large GSU transformers, including: comparison of voltage dips under different energisation conditions; the network-wide voltage dips under both non-outage and outage scenarios; the influence of sympathetic inrush on voltage dips. It also presents the work that has been done on identification of key influential parameters on voltage dips and exploring operational approaches to cost-effectively reduce voltage dips and sympathetic inrush.

Chapter 5 Assessment of Voltage Dips Caused by Transformer Energisation Transients Using Stochastic Approach

This chapter attempts to extend the deterministic studies carried out in Chapter 4 by taking into account stochastic variables. First, an ATP-EMTP interface to facilitate stochastic assessment using Monte Carlo method is described. Second, the possible stochastic variables are discussed and quantified. Then a preliminary stochastic simulation based on a single phase circuit is presented. Finally, stochastic studies of the three-phase system are presented, which include: calculating the distribution of voltage dip magnitudes and durations; identifying the probability of the worst case voltage dips; and testing the sensitivity of the results to various closing time span and residual flux distributions.

Chapter 6 Assessment of Transformer Energisation Transients Due to Offshore Wind Farm Connection

This chapter applies the modelling and simulation methods proven in Chapter 4 and Chapter 5 to assess transformer inrush transients during offshore wind farm connections. Special attention is focusing on voltage dips and sympathetic inrush between wind turbine transformers. It first describes the development of a wind farm collection grid model and its validation against measurements, and then presents the studies of voltage dips and sympathetic inrush caused by energising wind turbine transformers in a large offshore wind farm collection grid. The studies estimate the possible voltage dips caused by energising wind turbine transformers and assess energisation sequences with the aim to reduce sympathetic inrush between wind turbine transformers.

Chapter 7 Conclusion and Future Work

This chapter summarizes the main finding of this thesis work. Future work is also suggested for several aspects of the research on voltage dips and sympathetic inrush caused by transformer energisation.

Chapter 2 Literature Review on Transformer Energisation Transients

Transients resulted from transformer energisation were first observed by Ferranti when commissioning the Deptford to London 11 kV link in 1890 [23]. Afterwards, abundant publications were devoted to the calculation of transformer inrush current, the assessment of transformer energisation transients and the development of possible mitigation measures.

In this chapter, calculations of inrush current by using analytical and numerical approaches are briefly summarized at the beginning. Thereafter, modelling of system components in EMTP for assessing transformer energisation transients in large-scale networks is systematically reviewed. This is followed by the review on the key issues involved in transformer energisation transients, mainly including: sympathetic interaction, mechanical forces on winding generated by inrush current, energising transformer from a generator of small capacity, harmonic resonant overvoltages, and voltage dips caused by transformer energisation. Finally, possible mitigation approaches reported in the literature are summarized.

2.1 Approaches for calculating transformer inrush current

Calculation of transformer inrush current is the first step for studying the effects of inrush current. At the beginning, transformer inrush currents were analytically calculated. Later, following the advent of computer application, numerical approaches gradually took over analytical approaches and now they have become the preferred way for transformer inrush current calculation.

2.1.1 Simple analytical approaches for calculating inrush current

One early attempt of analytical calculation was made in [1] to predict the first peak of inrush current ($i_{first-peak}$) caused by energising a single-phase transformer at voltage zero crossing. The derived formula is shown below:

$$i_{first-peak} = \frac{B_{air} l}{\mu_0 N} = \frac{l}{\mu_0 N} \cdot \frac{A_c}{A_{air}} (2B_n + B_r - B_s) \quad (2.1)$$

where B_{air} is the magnetic flux density outside the saturated core, B_n is the peak nominal flux density, B_r and B_s are the residual and saturation flux densities, l is the length of the magnetic flux path in air, N is the turn number of the energised winding, A_{air} is the cross-section of the space enclosed by the energised winding, A_c is the cross-section of the iron core and μ_0 is the permeability of the air.

This formula, however, only considers one particular switching time (voltage zero crossing) and assumes infinite short circuit capacity at the transformer terminal; moreover, it neglects the resistance of the energisation circuit R which contributes to the decaying mechanism of inrush current (see Figure 2-1, the circuit resistance would reduce the flux by an amount of $\int_t^{t+2\pi} R \cdot idt$ per cycle, resulting in the attenuation of the inrush current peak).

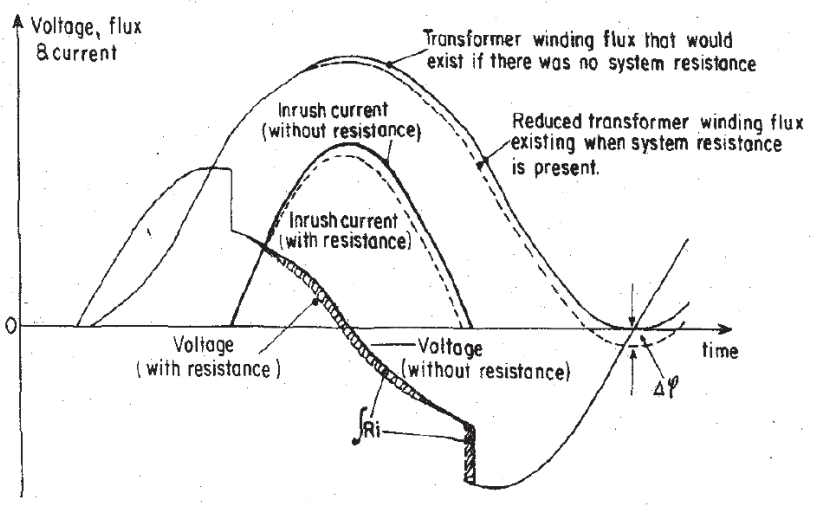

Figure 2-1 Effect of circuit resistance during first cycle when switching in transformer at the positive-going zero crossing of applied voltage [24]

As one step forward, the work presented in [25] suggests an analytical formula which takes into account the effect of switching angle and circuit resistance to predict the first peak of inrush current. The formula was derived as follows:

$$i_{first-peak} = \frac{V_m}{\sqrt{R^2 + (\omega L_{air-core})^2}} \left(\frac{B_r - B_s}{B_n} + cos\theta + 1 \right) \quad (2.2)$$

with additional parameters: V_m the magnitude of the applied voltage, ω the angular frequency, θ the initial phase angle of the voltage source, R the series resistance and $L_{air-core}$ the air-core inductance of the energised winding.

Analytical equations proposed in [26], [27] and [28] extended the estimation of inrush current peak from the first cycle to the following cycles. The work presented in [26] estimates inrush current peaks via the following procedure:

Step 1 - calculate the saturation angle θ_{sat} (i.e., the angle at which saturation occurs):

$$\theta_{sat} = \cos^{-1}\left(\frac{B_s - B_n - B_r}{B_n}\right) \tag{2.3}$$

Step 2 - estimate the inrush peak of the first cycle using:

$$i_{peak} = \frac{\sqrt{2}V_m}{\omega L_{air-core}}(1 - \cos\theta_{sat}) \tag{2.4}$$

Step 3 - update the residual flux B_r:

$$B_r(new) = B_r(old) - B_n \cdot \frac{R}{\omega L_{air-core}} \cdot 2(sin\theta_{sat} - \theta_{sat}cos\theta_{sat}) \tag{2.5}$$

With the updated B_r, steps 1, 2 and 3 are repeated to calculate the inrush peaks of subsequent cycles.

The method given in [26] neglects the integrated $R \cdot i$ term for the first cycle and only gives the peak values of the inrush current rather than the full inrush current waveform. These limitations were overcome by including an exponential transient term in the equations given by [27] and [28], which helps obtain the full current waveform as a function of time, as shown by the following equation:

$$i_{peaks}(t) = \frac{\sqrt{2}V_m}{\sqrt{R^2 + (\omega L_{air-core})^2}} \cdot \left(sin(\omega t - \phi) - e^{-\frac{R}{L_{air-core}}(t - \frac{\theta_{sat}}{\omega})} \cdot sin(\theta_{sat} - \phi)\right) \tag{2.6}$$

where $\phi = \tan^{-1}(\omega L_{air-core}/R)$ = phase angle between voltage and current vectors.

It should be noted that the above analytical approaches can only estimate the inrush current peaks for a single-phase transformer. It might not be suitable to apply them for estimating inrush transient of multi-winding and multi-phase transformers or assessing transformer energisation transient with other network components involved.

2.1.2 Numerical approaches for calculating inrush current

When the nonlinear behavior of the transformer core is considered, it is difficult to get analytical solutions to describe the inrush transients; a preferable alternative way to calculate transformer inrush currents is by utilizing numerical approaches.

Some early attempts, such as those in [10, 29, 30], were focusing on numerical prediction of inrush current in single-phase transformers. Basically, they adopted a time stepping technique which can give successive discrete values of current at successive chosen steps. The main purpose of these attempts was to investigate the effects of varying point-on-wave switching, residual flux and transformer resistance on the harmonic content variation of inrush current. However, they were not extended to study the impacts of inrush transients on system operation in large-scale networks.

Inrush current calculation based on finite element method (FEM) was presented in [31]. In this method, both magnetic field and electrical circuit equations are solved simultaneously. Similar contribution can be found in [32]. The use of FEM calculation allows investigating mechanical stresses on the winding, internal flux distribution and thermal condition. However, it is time consuming, computationally costly and not suitable for studying inrush currents' network impacts.

Up to date, the most frequently used numerical tool for calculating inrush current is the Electromagnetic Transient Program (EMTP). In the EMTP-type simulation packages (including ATP/EMTP and PSCAD/EMTDC), standard available transformer models are provided together with non-linear elements describing transformer core hysteresis and saturation features; models for other system components, including transmission line, cable, circuit breaker, surge arrester, rotating machines and Flexible AC Transmission Systems devices, are also provided. This enables the simulation of complex networks and control systems of arbitrary structure, which make the EMTP a preferable numerical tool for calculating inrush currents as well as simulating their impacts on network operation. In the following section, modelling system components in EMTP for transformer energisation transient studies are reviewed.

2.2 Modelling system components in EMTP for studying transformer energisation transients

According to the report given by CIGRE Working Group 02 of Study Committee 33, the frequency range for the transients of primary interest can be divided into four groups:

- Low frequency transients, from 0.1 Hz to 3 kHz;
- Slow-front transients, from 50/60 Hz to 20 kHz;
- Fast-front transients, from 10 kHz to 3 MHz;
- Very fast-front transients, from 100 kHz to 50 MHz.

In Table 2-1, various origins of transient and their associated frequency ranges are listed.

Table 2-1 Origin of electrical transients and their associated frequency ranges [33]

Origin of transients	Frequency range
Transformer energisation Ferroresonance	(DC) 0.1 Hz – 1 kHz
Load rejection	0.1 Hz – 3 kHz
Fault clearing	50/60 Hz – 3 kHz
Fault initiation	50/60 Hz – 20 kHz
Line energisation	50/60 Hz – 20 kHz
Line reclosing	(DC) 50/60 Hz – 20 kHz
Transient recovery voltage Terminal faults	50/60 Hz – 20 kHz
Short line faults	50/60 Hz – 100 kHz
Multiple re-strikes of circuit breaker	10 kHz – 1 MHz
Lightning surges, faults in substations	10 kHz – 3 MHz
Disconnector switching (single re-strike) Faults in GIS	100 kHz – 50 MHz

Since the transformer energisation transients mainly range between DC to 1 kHz, when modelling system components in EMTP to study transformer energisation transients, the frequency range can be targeted on the range between DC and 1 kHz [34].

2.2.1 Transformer modelling

Modelling transformer to study transformer energisation transients mainly focuses on two parts: representation of windings and representation of the magnetic iron core [35]. In EMTP, the standard available transformer models for assessing transformer energisation transients are Saturable Transformer Component (STC), BCTRAN, Hybrid Transformer (XFMR) and UMEC, which are explained in the following sections.

2.2.1.1 Saturable transformer component (STC model)

As shown in Figure 2-2, the STC model is based on single-phase transformer representation and it can be extended to form a star-circuit representation so as to handle single-phase N-winding transformer. The single-phase N-winding transformer can be described by the following equation:

$$\left[\frac{di}{dt}\right] = [L]^{-1}[v] - [L]^{-1}[R][i] \tag{2.7}$$

Core saturation and hysteresis effects are modelled by a nonlinear inductor connected at the star point which can be located at the primary winding side.

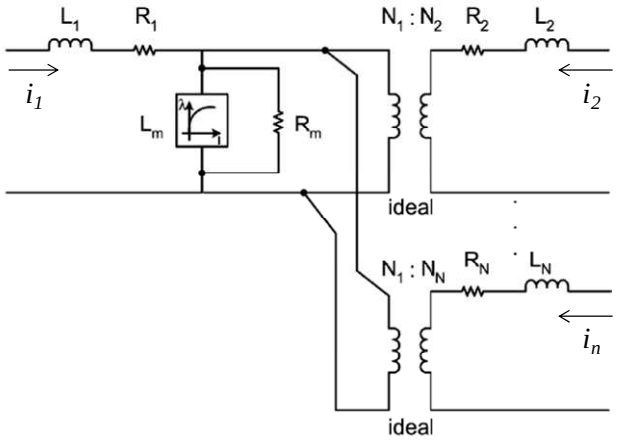

Figure 2-2 Star-circuit representation of single-phase N-winding transformers [35]

The use of three single-phase two-winding STCs to model a three-phase transformer has been applied in many studies [19, 36-39]. As shown in Figure 2-3, three single-phase two-winding STCs were used to model a 315 MVA 138/21 kV, YNd connected GSU transformer, with their primary side connected as grounded-star and secondary side delta [19].

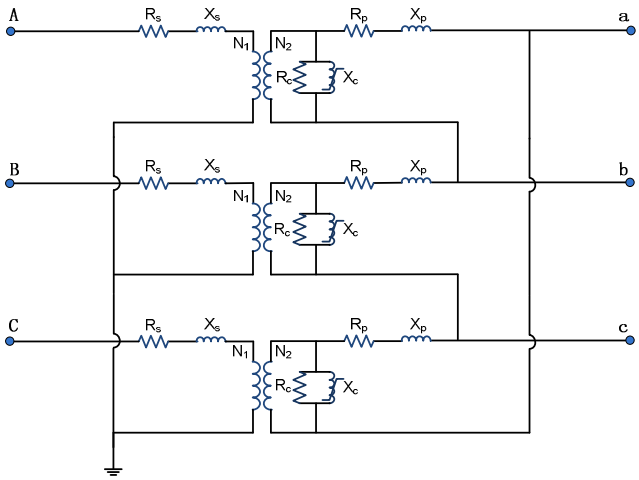

Figure 2-3 Connecting three two-winding STCs to represent a three-phase transformer

2.2.1.2 BCTRAN model

The BCTRAN model uses branch impedances and admittance matrices to represent a three-phase N-winding transformer simply as 3×N coupled branches [40]. The model formulation is based on the steady state equations of a single-phase multi-winding transformer described by a branch impedance equation:

$$[V] = [Z][I] \tag{2.8}$$

To describe multi-winding three-phase transformers, an extension of the above equation is made by replacing any element of $[Z]$ by a (3×3) sub-matrix

$$\begin{bmatrix} Z_s & Z_m & Z_m \\ Z_m & Z_s & Z_m \\ Z_m & Z_m & Z_s \end{bmatrix} \tag{2.9}$$

where Z_s represents the self-impedance of a phase and Z_m represents the mutual impedance among phases.

These impedances can be calculated from positive and zero sequence impedances (Z_1 and Z_0)

$$Z_s = \frac{(Z_0 + 2Z_1)}{3} \tag{2.10}$$

$$Z_m = \frac{(Z_0 - Z_1)}{3} \tag{2.11}$$

For transient calculation, equation 2.8 is rewritten as

$$[v] = [R][i] + [L]\left[\frac{di}{dt}\right] \tag{2.12}$$

being $[R]$ and $[L]$ the real and imaginary part of the branch impedance matrix, respectively.

In the case of a very low excitation current, the transformer should be described by an admittance formulation

$$[I] = [Y][V] \tag{2.13}$$

Accordingly, for transient simulation, the expression 2.12 becomes

$$\left[\frac{di}{dt}\right] = [L]^{-1}[v] - [L]^{-1}[R][i] \tag{2.14}$$

The BCTRAN model takes phase-to-phase coupling into account; it can model core saturation but does not consider core topology. It is linear and is reasonably accurate for frequencies below 1 kHz [41]. The effects of core saturation can be represented by a set of externally connected non-linear inductances which are usually added at the terminals

of the transformer winding nearest to the core, as shown in Figure 2-4. Application of BCTRAN with external core representation has shown satisfactory performance for studying transformer energisation transients in various networks [6, 42-44].

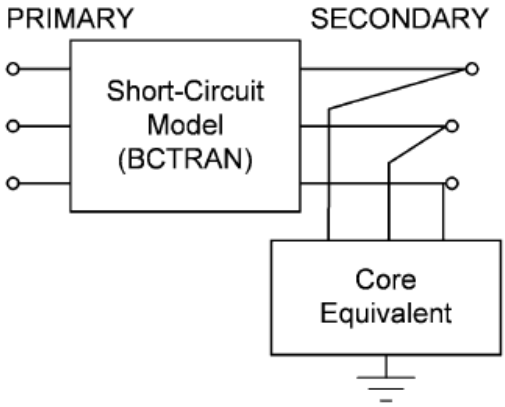

Figure 2-4 Schematic diagram of BCTRAN-based model for two-winding transformer, with an externally connected core representation [35]

2.2.1.3 Hybrid model (XFMR)

The Hybrid transformer model, as shown in Figure 2-5, consists of four parts, including: a equivalent electrical circuit for core representation, an inverse inductance matrix [A] for leakage representation, a [C] matrix for representing capacitive coupling and a set of circuits for modelling frequency dependent winding resistances [45].

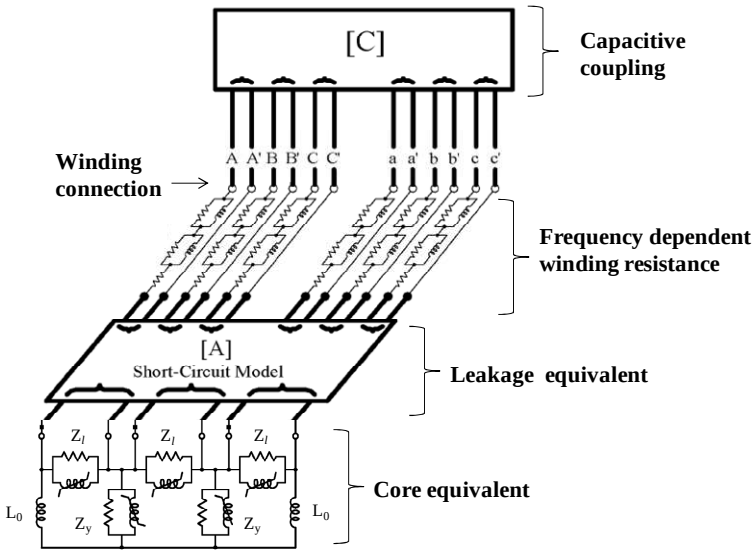

Figure 2-5 Schematic diagram of the Hybrid transformer model [45]

The equivalent circuit for the core modelling is derived from a simplified core magnetic circuit via duality transformation (meshes in the magnetic circuit are transformed to nodes in the electrical dual; reluctances are changed to inductances; sources of

magnetomotive force become current sources) [46, 47]; in the circuit, a constant resistance in parallel with a nonlinear inductance is used to represent each limb (Z_l) and yoke (Z_y); L_0 accounts for the zero-sequence flux paths. The leakage equivalent is an inverse inductance matrix established based on BCTRAN approach.

Hybrid model has been implemented in ATPDraw [48]. Recent development of the Hybrid model suggests the inclusion of type-96 non-linear inductors to produce residual flux after de-energisation and accommodation of user-defined air-core inductance value [49]. However, due to the requirement of core design data and the difficulty of manually initializing residual flux, so far this model has not been widely used.

2.2.1.4 UMEC model

In PSCAD/EMTDC, there is a transformer model called Unified Magnetic Equivalent Circuit (UMEC) model. This model is based on the concept of normalized core. It expects users to scale yoke-to-limb ratio regarding cross-sectional area and length. Thus, this model is difficult to be applied because it requires transformer dimensional data which are usually not available. In most transformer energisation studies carried out in PSCAD/EMTDC, such as [2, 50, 51], three single-phase transformer models without coupling between phases (i.e., three single-phase two-winding STCs) were used instead of the UMEC model.

2.2.1.5 Estimation of core saturation curve

Transformer core saturation curve, especially the section of deep saturation, is of great importance for inrush transient estimation [52]. In many cases, transformer open-circuit test data is the only data source for approximating the saturation curve. The open-circuit test data are usually in the form of RMS voltage versus RMS magnetizing current. For modelling purposes, this form is inconvenient for use and must be converted to 'peak' or 'instantaneous' form. Several approaches have been developed to convert saturation characteristics expressed in RMS values (RMS voltage/current, *V/I*) to peak and instantaneous values (peak flux-linkage/current, λ/i) [53-56], which are summarized in Table 2-2.

They are different from each other in terms of conversion approach, consideration of core losses and handling of delta connection. Taking core losses into account improves the accuracy of the conversion; handling of delta connection counts the fact that, in the

tests carried out with closed delta-coupled windings, the triplen harmonics circulating in the closed delta do not appear in the measured line currents [57]. The analytical approach reported in [54] is the basis of the current main conversion routine (called SATURA) used in ATP/EMTP [58].

Table 2-2 Summary of previous contributions on converting RMS *V/I* to *λ/i* curve

Contributors	Conversion method	Core losses	Delta connection
Talukdar et al. [53]	Numerical	Not considered	Not considered
Prusty and Rao [54]	Analytical	Not considered	Not considered
Neves and Dommel [55]	Analytical	Considered	Not considered
Neves and Dommel [57]	Numerical	Considered	Considered
Chiesa and Høidalen [56]	Analytical	Considered	Considered

In the open-circuit tests carried out by transformer manufacturer, the commonly applied excitation levels are 90%, 100% and 110% of rated operating voltage, because, during operation, system voltage variations are normally controlled to be within ±10% of the nominal operation voltage. Hence, the converted *λ/i* characteristic usually consists of only three points. These points can only form a very crude piecewise nonlinear core saturation curve. Extension of the test report data is needed to form a more complete core saturation curve.

There are two approaches for data extension: one is linear extrapolation and the other is curve fitting. In linear extrapolation, the final segment of the crude piecewise nonlinear curve is linearly extended to form a constant slope for representing *λ/i* characteristic in transformer core deep saturation region. Although this method is simple, it may severely underestimate the current resulted from any excitation level above the 110% excitation level, because at the 110% excitation level the core has not reached the deep saturation. Instead of simple linear extrapolation, curve fitting approach generates new artificial points which form new segments to be added into the crude piecewise nonlinear curve. One commonly used curve fitting function is a two term n^{th} order polynomial function:

$$i = a \cdot \lambda + b \cdot \lambda^n \tag{2.15}$$

This function was first identified in [59] and used to develop an analytical approach to evaluate ferroresnance. It was applied to curve fit non-linear saturation characteristics of potential transformer and substation transformer in [60]. Other more complex functions but rarely used for the curve fitting were documented in [61].

Although curve fitting provides additional points, transformer saturation characteristic beyond the final measured excitation point is unknown and should be better decided by incorporating with the knowledge of transformer air-core inductance. Determination of the value of air-core inductance can be based on transformer winding design data using analytical calculation. The design data include the winding's mean cross-section area A_w, the equivalent height h_{eq} (taking into account fringing effects) and winding turn number N [52, 62]. However, it is frequently encountered that transformer winding design data are not available. As an alternative approach, transformer air-core inductance can be estimated from transformer short-circuit inductance. According to the modelling guideline provided by CIGRE Study Committee 33 [33], the approximation of transformer air-core inductance can be referred to transformer short-circuit inductance L_{sc} as follows:

- Step-down transformer (outer winding): $L_{air\text{-}core}$=2~2.5 L_{sc}
- Step-up transformer (inner winding): $L_{air\text{-}core}$=1~1.5 L_{sc}
- Autotransformer (high voltage side): $L_{air\text{-}core}$=4~5 L_{sc}

The value of air-core inductance is important for the estimation of transformer core saturation inductance which determines the final slope of core saturation curve [52]. In BCTRAN and STC, the saturation inductance L_{sat} is deduced by taking into account short circuit inductance:

$$L_{sat} = L_{air-core} - L_{HL} \tag{2.16}$$

where L_{HL} is transformer short-circuit inductance.

In the case of Hybrid model, the leakage flux between the inner winding and the core are taken into account by L_{LC}; in this case, L_{sat} is calculated by:

$$L_{sat} = L_{air-core} - L_{HL} - L_{LC} \tag{2.17}$$

2.2.2 Overhead line and cable modelling

Being important links for power transportation, overhead lines and cables could also engage transformer energisation transients by interacting with the energised transformers. Hence, modelling of overhead lines and cables should be fully considered. In Figure 2-6, an element dx of a single-phase line is schematically illustrated.

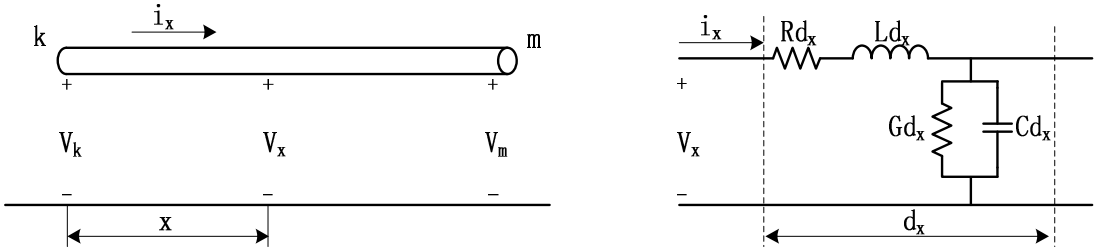

Figure 2-6 Single-phase line with detail of a *dx* section

The frequency-domain description of the single-phase line, either of a cable or an overhead line, can be expressed as:

$$-\frac{\partial V(x,\omega)}{\partial x} = \big(R(\omega) + j\omega L(\omega)\big)I(x,\omega) = Z(\omega)I(x,\omega) \tag{2.18}$$

$$-\frac{\partial I(x,\omega)}{\partial x} = \big(G(\omega) + j\omega C(\omega)\big)V(x,\omega) = Y(\omega)V(x,\omega) \tag{2.19}$$

where $V(x,\omega)$ and $I(x,\omega)$ are the voltage and current of the line, respectively; $R(\omega)$, $L(\omega)$, $G(\omega)$ and $C(\omega)$ are line parameters expressed in per unit length and with frequency dependent; $Z(\omega)$ [=$R(\omega) + L(\omega)$] and $Y(\omega)$ [=$G(\omega) + C(\omega)$] represent line series impedance and shunt admittance in per unit length, respectively.

The characteristic impedance of the line is determined by:

$$Z_c(\omega) = \sqrt{\frac{R(\omega) + j\omega L(\omega)}{G(\omega) + j\omega C(\omega)}} \tag{2.20}$$

Also, the propagation constant of the line is described by:

$$\gamma(\omega) = \sqrt{\big(R(\omega) + j\omega L(\omega)\big) \cdot \big(G(\omega) + j\omega C(\omega)\big)} \tag{2.21}$$

From the line equations above, one can further obtain the well-known relation between the sending and receiving end [63]:

$$\begin{bmatrix} V_k \\ I_k \end{bmatrix} = \begin{bmatrix} \cosh(\gamma l) & Z_c sinh(\gamma l) \\ \dfrac{1}{Z_c} sinh(\gamma l) & cosh(\gamma l) \end{bmatrix} \begin{bmatrix} V_m \\ I_m \end{bmatrix} \tag{2.22}$$

These equations are for describing steady-state conditions and form the basis for deriving transient line models.

For modelling lines in time-domain simulation, two types of model are commonly used:

- Lumped-parameter models, usually known as pi-models, represent line by

lumped parameters whose values are calculated at a single frequency (most commonly used pi-models include: exact pi-model and nominal pi-model);

- Distributed-parameter models, with distributed nature of the line parameters taken into account (they can be categorized into: constant-parameter model (Bergeron model) and frequency-dependent model).

The basic principles of these line models are equally applicable to overhead lines and cables.

2.2.2.1 Exact pi-model

The exact pi-model is derived from equation 2.22 and can be described by the equivalent circuit shown in Figure 2-7. In the circuit,

$$Z_1(\omega) = (Z(\omega) \cdot l)\frac{\sinh(\gamma(\omega)l)}{(\gamma(\omega)l)} \tag{2.23}$$

$$Y_2(\omega) = (Y(\omega) \cdot l)\frac{\tanh(\gamma(\omega)l/2)}{(\gamma(\omega)l/2)} \tag{2.24}$$

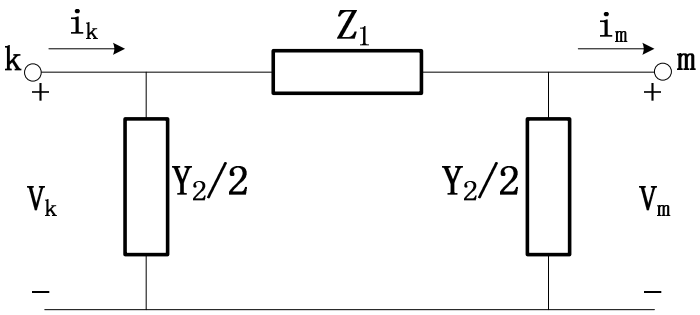

Figure 2-7 Pi-circuit model of a line [64]

The scalar Z and Y can be replaced by corresponding $[Z]$ and $[Y]$ matrixes to describe N-phase transmission line. It is an exact representation of the line at a given frequency and therefore named as exact-pi model. This model is suitable for steady-state or harmonic analysis in which solutions are obtained for one frequency at a time. However, they are difficult to be applied for time-domain transient analysis because the elements in the exact pi-model are two-fold frequency dependent: one due to the line parameters themselves (including Z and Y) and second due to the propagation constant γ. Even by assuming the line parameters as constant, the elements in the exact pi-model are still function of frequency.

2.2.2.2 Nominal pi-model

Nominal pi-model is described by the same equivalent circuit of exact pi-model (as shown in Figure 2-7) but with the branch total series impedance and total shunt admittance equal to $Z(\omega) \cdot l$ and $Y(\omega) \cdot l$, with the hyperbolic correction factors neglected. The nominal pi-model is preferred over the exact pi-model because it can be directly applied to time-domain transient simulations by assuming the line parameters as constant. In addition, it approximates the performance of exact pi-model. In the cases of short lines or low frequencies, the nominal pi-model is effectively identical to the exact pi-model and it may be used for transient simulations in the proximity of the frequency at which line parameter values are calculated. In the cases of long lines and high frequencies, a number of cascaded short nominal pi-model sections, the so called "cascaded nominal pi-model", can be used to approximate the frequency dependent effect of the propagation constant so as to mimic the performance of exact pi-model [12, 36]. However, the treatment of lumped parameters can give rise to spurious oscillations and hence the pi-model is not preferable for representing the frequency dependent line parameters.

2.2.2.3 Bergeron model

Bergeron model is a simple, constant frequency model, based on travelling wave theory. In general, it is a combination of lossless distributed parameter line and lumped series resistances [65].

One important technique utilized to derive the Bergeron model (as well as the frequency dependent model) is the decoupling between the line sending and receiving ends. To understand this, a lossless distributed parameter line can be considered first. The general solution for the wave propagation equations of a lossless line are:

$$i(x,t) = f_1(x - \alpha t) + f_2(x + \alpha t) \tag{2.25}$$

$$v(x,t) = Z_c \cdot f_1(x - \alpha t) - Z_c \cdot f_2(x + \alpha t) \tag{2.26}$$

where Z_c is the characteristic impedance and α is the velocity:

$$Z_c = \sqrt{\frac{L}{C}} \tag{2.27}$$

$$\alpha = \frac{1}{\sqrt{LC}} \tag{2.28}$$

Rearranging (2.25) and (2.26):

$$v(x,t) + Z_c \cdot i(x,t) = 2Z_c \cdot f_1(x - \alpha t) \tag{2.29}$$

$$v(x,t) - Z_c \cdot i(x,t) = -2Z_c \cdot f_2(x + \alpha t) \tag{2.30}$$

Clearly, when $(x-\alpha t)$ is constant, $v(x,t) + Z_c \cdot i(x,t)$ is constant. Given d as the length of the line, the travelling time for a constant wave to travel from the end k to the other end m of the line is:

$$\tau = \frac{d}{\alpha} = d\sqrt{LC} \tag{2.31}$$

Hence

$$v_k(t-\tau) + Z_c \cdot i_{km}(t-\tau) = v_m(t) + Z_c \cdot (-i_{mk}(t)) \tag{2.32}$$

Rearranging the equation (2.32) gives

$$i_{mk}(t) = \frac{1}{Z_c} v_m(t) + I_m(t-\tau) \tag{2.33}$$

where

$$I_m(t-\tau) = -\frac{1}{Z_c} v_k(t-\tau) - i_{mk}(t-\tau) \tag{2.34}$$

Similarly

$$i_{km}(t) = \frac{1}{Z_c} v_k(t) + I_k(t-\tau) \tag{2.35}$$

where

$$I_k(t-\tau) = -\frac{1}{Z_c} v_m(t-\tau) - i_{km}(t-\tau) \tag{2.36}$$

Therefore the lossless line can be represented by an equivalent two-port network as shown in Figure 2-8.

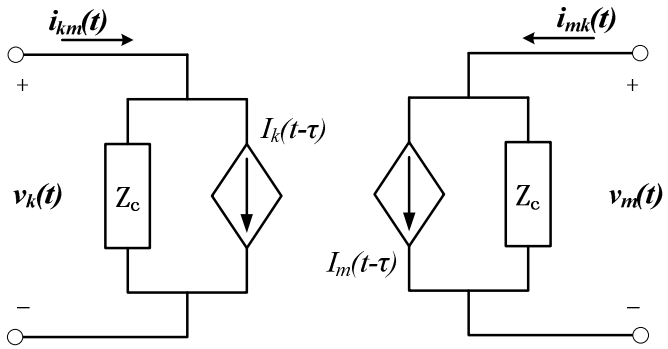

Figure 2-8 Equivalent two-port network for modelling a lossless line

As can be seen, the terminals of the two port network are topologically disconnected, i.e., the sending and receiving ends of the line are effectively decoupled from each other during the solution at time *t*. This is valid in time domain simulation provided that the simulation time step, Δt, is smaller than travelling time of the waves, τ [66].

The Bergeron model is formed by adding lumped series resistances into the lossless line model, with the conductance to ground neglected. This is made by splitting the total line resistance into three lumped parts and locating them at the middle and at the ends of the line, as shown in Figure 2-9. The error incurred in lumping the series resistance as compared to the distributed case is acceptable as long as $R \cdot l \ll Z_c$ [66].

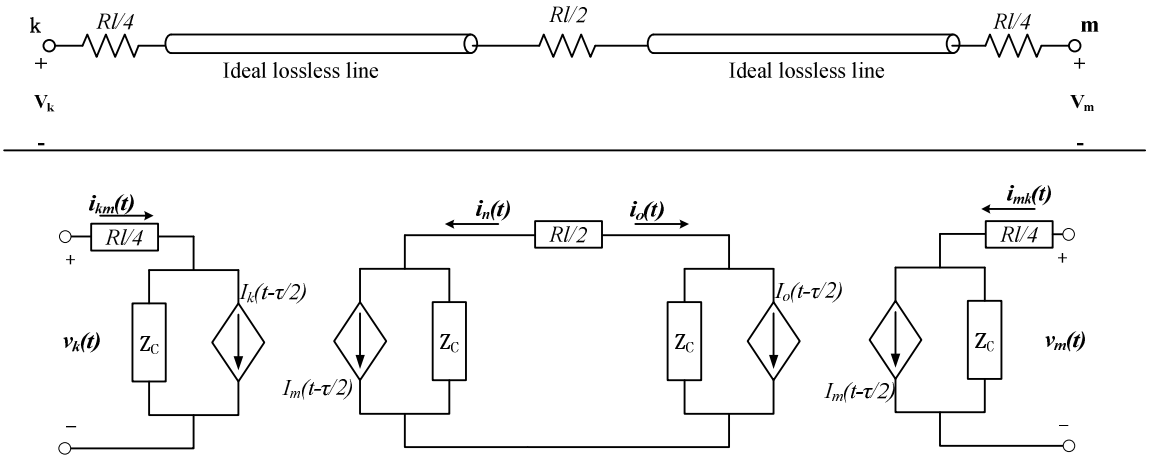

Figure 2-9 Forming of Bergeron model based on two-port network model of lossless line

For studying transformer energisation transients, Bergeron model is accurate enough to represent frequency dependent parameters, because the positive sequence resistance and inductance are fairly constant up to approximately 1 kHz [12, 34, 67]. Nevertheless, the Bergeron model is more efficient and accurate than the nominal pi-model or cascaded nominal pi-model [67].

2.2.2.4 Frequency-dependent model

The frequency-dependent line models commonly available in EMTP include: Semlyen model, Marti model and Noda model. Details of these models are not reviewed here, because they are rarely used in the simulation studies of transformer energisation transients. Since the frequency dependent parameters of transmission lines are fairly constant within the frequency range of transformer energisation transients [12], it is therefore not necessary to use the frequency-dependent models. Even by employing

frequency-dependent line models to study energisation transients, the results obtained are similar to that calculated by the cascaded nominal pi-model [68].

2.2.3 Circuit breaker modelling

Depending on the features of studied transients, circuit breaker can be modelled to different levels of complexity. A guideline was proposed by the CIGRE Study Committee 33 on representing circuit breaker closing and opening operations for studying transients in different frequency ranges, as shown in Table 2-3 [69].

Table 2-3 Guidelines for modelling circuit breaker [69]

<table>
<tr><th colspan="2">Operation</th><th>Low frequency transients
(0.1 Hz – 3 kHz)</th><th>Slow-front transients
(50/60 Hz – 20 kHz)</th><th>Fast-front transients
(10 kHz – 3 MHz)</th><th>Very fast-front transients
(100 kHz – 50 MHz)</th></tr>
<tr><td rowspan="2">Closing</td><td>Mechanical pole spread</td><td>Important</td><td>Very important</td><td>Negligible</td><td>Negligible</td></tr>
<tr><td>Prestrikes</td><td>Negligible</td><td>Important</td><td>Important</td><td>Very important</td></tr>
<tr><td rowspan="4">Opening</td><td>High current interruption</td><td colspan="2">Important only for interruption capability studies</td><td>Negligible</td><td>Negligible</td></tr>
<tr><td>Current chopping</td><td>Negligible</td><td colspan="2">Important only for interruption of small inductive currents</td><td>Negligible</td></tr>
<tr><td>Restrike characteristic</td><td>Negligible</td><td rowspan="2">Important only for interruption of small inductive currents</td><td>Very important</td><td>Very important</td></tr>
<tr><td>High frequency current intteruption</td><td>Negligible</td><td>Very important</td><td>Very important</td></tr>
</table>

It can be seen that for low-frequency transients, such as those of transformer inrush transients, high current and high frequency current interruption, current chopping and re-strike characteristics of circuit breaker can be neglected in modelling opening operation, and the prestrike can be neglected in modelling closing operation; the only important feature that should be considered in detail is the mechanical pole spread, i.e. closing time span (in general breaker poles do not close simultaneously, but with certain time span). Therefore, in many previous studies of transformer inrush transients, such as [6, 39, 70], each pole in a three-phase circuit breaker was modelled as an ideal time-controlled switch: in opening operation, it opens at the first current zero crossing after the ordered tripping instant (a current margin parameter can be included to approximate current chopping); in closing operation, it behaves as an impedance changing instantaneously from an infinite value to a zero value at the closing instant (the closing instant can be at any part of a power cycle). Since three poles are represented by three

separate ideal time-controlled switches, the closing time span between three poles can be represented by closing time differences between the three time-controlled switches.

The circuit breaker closing time and closing time span between circuit breaker poles are of stochastic nature; hence, several approaches have been proposed to construct statistical switches with closing time and closing time span modelled by statistical distributions. In [70], each pole of a circuit breaker was modelled by two contacts (one is named as auxiliary contact and the other is named as main contact), as shown in Figure 2-10.

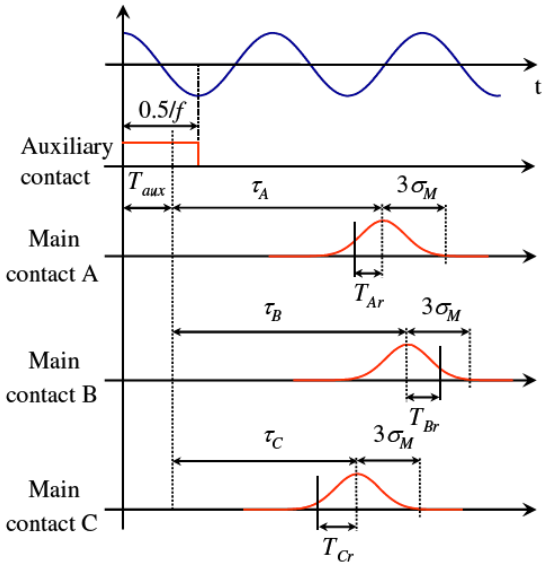

Figure 2-10 Statistical switching model involving closing time span among three phases [70]

The closing time of the auxiliary contact T_{aux} was used to represent the instant at which the closing signal is ordered. It was considered to be the same for three phases and follow a Uniform distribution with a typical range of one power frequency cycle (equal to 20 ms for 50 Hz systems).

The closing times for three main contacts were defined as:

$$\begin{aligned} T_{Aclose} &= T_{aux} + \tau_A \pm T_{Ar} \\ T_{Bclose} &= T_{aux} + \tau_B \pm T_{Br} \\ T_{Cclose} &= T_{aux} + \tau_C \pm T_{Cr} \end{aligned} \tag{2.37}$$

where T_{Ar}, T_{Br} and T_{Cr} represent the closing offset time of three poles (each of them was defined by a Gaussian distribution whose standard deviation was defined by one-sixth of the maximum closing time span (MCTS)); τ_A, τ_B and τ_C represent the time delays between the closing signal ordering and the actual closure of circuit breaker.

Similar to modelling approach used in [70], the circuit breaker closing time span modelled in [43] consists of four parameters:

- Common order time, t_{order}. It was also characterized by a Uniform distribution over a power frequency cycle.
- Random offset time for each pole ($t_{offset,A}$, $t_{offset,B}$ and $t_{offset,C}$). This offset time was assumed to follow a Gaussian distribution, whose mean value is zero (assuming that three poles tend to close simultaneously) and whose standard deviation is MCTS/6.

The exact closing time for each pole was thus determined by:

$$\begin{aligned} T_{Aclose} &= t_{order} \pm t_{offset,A} \\ T_{Bclose} &= t_{order} \pm t_{offset,B} \\ T_{Cclose} &= t_{order} \pm t_{offset,C} \end{aligned} \tag{2.38}$$

It can be seen that in both modelling approaches, the MCTS determines the offset closing time. However, MCTS is an uncertain value. According to [71], it is suggested that the typical MCTS is between 3 and 5 ms. In [72], tests were carried out to study the performance of a 110 kV circuit breakers (minimum oil circuit breaker and air-blast circuit breaker) on energising transmission lines and it was shown that the MCTS is normally smaller than 5 ms but could be as large as 10 ms. In [73], the performance of 400 kV and 220 kV circuit breakers for energising transmission lines in different network topologies were experimentally investigated and it was shown that: for 400 kV circuit breakers (minimum oil, air-blast or SF6 without switching resistance), the MCTS was less than 9 ms; for 220 kV circuit breakers (minimum oil), the MCTS can sometimes reach 16 ms.

2.2.4 Source and network equivalent modelling

According to the guidelines for modelling switching transients [74], the source can be represented by an ideal sinusoidal voltage source; generators can be modelled as an ideal voltage source with a sub-transient impedance. These treatments have also been applied in studies targeted on transformer energisation transients.

In a large network, a proper boundary can be selected to reduce the network to a size only covering the part of the network that is of interest for a specific study. This boundary is normally set at the points where the system is very strong (i.e. large short circuit level). These points can be the supply side of a substation transformer or a main supply bus. The portion of network outside the boundary can be represented by a

network equivalent. In many studies, such as [19, 36, 75, 76], the network equivalent is modelled by an ideal voltage source together with a Thevenin equivalent impedance.

2.2.5 System load modelling

Power system loads are mainly resistive, represented by loads of heating and lighting and the active component of motor loads. The reactive components of motor and fluorescent lighting loads are the other major contributors to power system loads [74].

In the range of low frequency transients, loads are commonly modelled as a constant impedance [77]. Naturally, this treatment also applies in the loads modelling for studying transformer energisation transients; examples can be found in [2, 12, 78]. The constant impedance model can be parallel-connected resistive and inductive elements (loads vary with square of voltage magnitude) or can be of series-connected resistive and inductive elements (loads vary with square of current magnitude). The power factor of the load indicates the relative proportion of the resistive and inductive components in the impedance.

2.3 Investigation case studies on transformer energisation transients

2.3.1 Sympathetic interaction between transformers

Many research addressed the transformer inrush transients caused by energising transformers into a system assuming that there is no other transformers connected to the same system. In practice, however, energisation of transformers is normally conducted either in parallel or in series with other adjacent transformers that are already in operation. These already connected transformers may experience unexpected saturation during the inrush transients of the transformers being energised. This saturation demands offset magnetizing current of high magnitude in the already connected transformers, which in turn affects the inrush transients caused by the energised transformers. This sharing of the transient inrush current is called as sympathetic inrush [21]. Up to date, most of the published papers on this topic mainly studied the sympathetic interaction between transformers connected in parallel and focused on simplified analytical evaluation (e.g., [22, 24, 79, 80]) and parametric study (e.g., [21, 80-82]).

Figure 2-11 shows one commonly used generic circuit for studying sympathetic interaction between two paralleled transformers. In the circuit, transformers TE1 and TE2 are connected to an ideal voltage source through system resistance R_s and inductance L_s ; R_1 and R_2 are transformer winding resistances; $L_{1\sigma}$ and $L_{2\sigma}$ are transformer leakage inductances; L_{1m} and L_{2m} are the magnetization inductances of TE1 and TE2, respectively. V_s is equal to $V_m sin(\omega t + \theta)$, where V_m is the amplitude of source voltage and θ is the energisation phase angle; V_c is the voltage of common busbar; i_s , i_1 and i_2 are the currents flowing through the supply, TE1 and TE2, respectively.

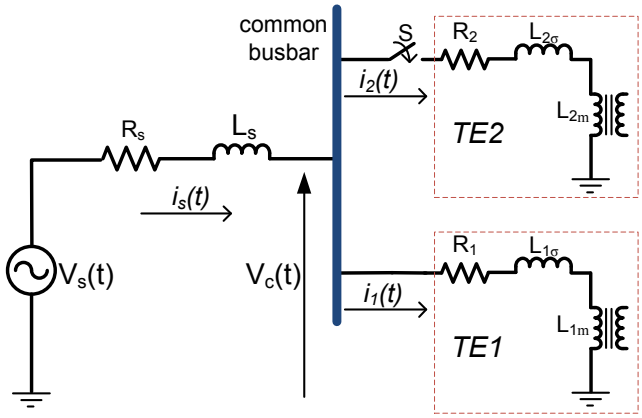

Figure 2-11 Generic circuit for studying sympathetic interaction between transformers connected in parallel

Utilizing the coupled electromagnetic model proposed in [83], simulation was carried out in [24] to study the sympathetic inrush interaction between the two parallel connected transformers, in which case TE1 and TE2 are two identical 230/69 kV, 15 MVA single-phase transformers (referring to Figure 2-11). The simulated currents i_2, i_1 and i_s are illustrated in Figure 2-12 (a), Figure 2-12 (b) and Figure 2-12 (c), respectively. As can be seen, the inrush current i_2 reached maximum peak right after the energisation of TE2 and then decayed gradually, while the sympathetic inrush current i_1 built up in TE1 gradually reached its maximum peak and then gradually decayed; the supply current i_s is the sum of the currents i_1 and i_2, showing the peaks of sympathetic inrush current i_1 and of the inrush current i_2 occur in direction opposite to each other, on alternate half cycles.

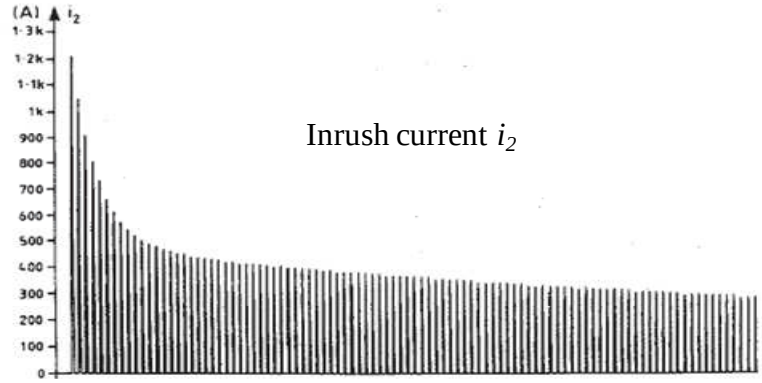

Inrush current i_2

(a) Current observed at TE2

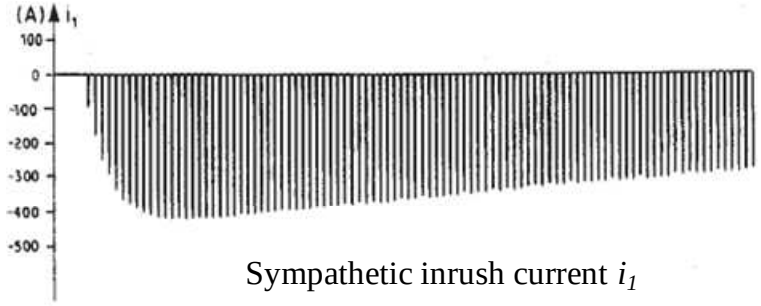

Sympathetic inrush current i_1

(b) Current observed at TE1

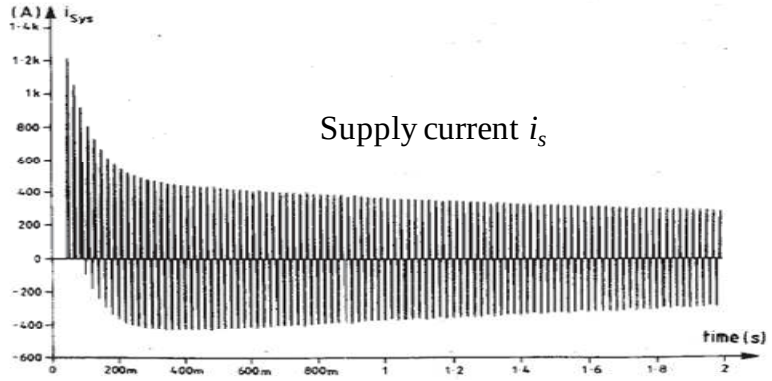

Supply current i_s

(c) Current observed from the source

Figure 2-12 Sympathetic inrush current waveforms simulated in [24]

2.3.1.1 Analytical evaluation

Simplified analytical analysis of sympathetic interaction between two parallel connected transformers was given in [79, 81]. By Applying Kirchhoff's laws, the circuit shown in Figure 2-11 was described by:

$$\begin{cases} R_s i_s + L_s \dfrac{di_s}{dt} + R_1 i_1 + \dfrac{d\lambda_1}{dt} = V_m sin(\omega t + \theta) \\ R_1 i_1 + \dfrac{d\lambda_1}{dt} = R_2 i_2 + \dfrac{d\lambda_2}{dt} \\ i_s = i_1 + i_2 \end{cases} \tag{2.39}$$

where λ_1, λ_2 are the flux-linkages of transformers TE1 and TE2, respectively, and $\lambda_1 = i_1(L_{1\sigma} + L_{1m})$ and $\lambda_2 = i_2(L_{2\sigma} + L_{2m})$.

Due to the nonlinearity of core magnetization inductances, analytical solution for equation 2.39 cannot be readily obtained. To qualitatively show how each electric component contributes to the sympathetic inrush process, an analysis is made by assuming L_{1m} and L_{2m} as constants. Assuming TE1 is identical to TE2, it is possible to get $R_1 = R_2 = R$, $L_{1\sigma} + L_{1m} = L_{2\sigma} + L_{2m} = L$. If TE1 has already been energised, energisation of TE2 would induce changes of λ_1 and λ_2 as a function of time, which can be expressed by:

$$\lambda_1(t) = \frac{L}{Z}V_m \sin(\omega t + \theta - \alpha) - \frac{1}{2}[\lambda_1(0) - \lambda_2(0)]e^{-\left(\frac{R+2R_s}{L+2L_s}\right)t} + \frac{1}{2}[\lambda_1(0) - \lambda_2(0)]e^{-\left(\frac{R}{L}\right)t} \tag{2.40}$$

$$\lambda_2(t) = \frac{L}{Z}V_m \sin(\omega t + \theta - \alpha) - \frac{1}{2}[\lambda_1(0) - \lambda_2(0)]e^{-\left(\frac{R+2R_s}{L+2L_s}\right)t} - \frac{1}{2}[\lambda_1(0) - \lambda_2(0)]e^{-\left(\frac{R}{L}\right)t} \tag{2.41}$$

where $Z = [(R + 2R_s)^2 + (L + 2L_s)^2]^{1/2}$, $\alpha = arctan[\omega(L + 2L_s)/(R + 2R_s)]$; $\lambda_1(0)$ and $\lambda_2(0)$ are the initial flux of TE1 and the residual flux of TE2, respectively.

From equations 2.40 and 2.41, it can be seen that both λ_1 and λ_2 consist of one sinusoidal component and two exponential DC components. The AC component and the first DC component are the same, but the second DC component in λ_1 is opposite to that in λ_2, therefore i_1 and i_2 are opposite to each other and appear alternately. Also, because the DC components in λ_2 are negative, the maximum peak of i_2 would appear right after the energisation of TE2, whilst the DC components in λ_1 are of opposite polarity and the time constant of the first DC component $\tau_1[= (L + 2L_s)/(R + 2R_s)]$ is smaller than that of the second DC component $\tau_2[= L/R]$, so i_1 will gradually reach the maximum peak, and gradually decay afterwards. The simplified analytical analysis shows in a general way the variation of flux-linkages in TE1 and TE2 which depends on the time constants formed by the inductances and resistances of the circuit branches. In real situation, the core inductance is nonlinear and therefore the time constants cannot be so readily determined.

In [22] and [24], the interactions between paralleled transformers were analysed using the voltage drop across circuit resistances, with system and transformer winding inductances neglected, which is summarized as follows (by referring to Figure 2-11).

Before closing S, only the magnetizing current of the unloaded transformer TE1 flows through the system; the source voltage V_s can be described by:

$$V_s = (R_s + R_1) \cdot i_1 + \frac{d\lambda_1}{dt} \tag{2.42}$$

The integration of V_s over one cycle gives:

$$\int_t^{t+\Delta t} V_s \, dt = \int_t^{t+\Delta t} [(R_s + R_1) \cdot i_1] \, dt + \Delta\varphi_1 \tag{2.43}$$

where Δt is of one cycle interval and $\Delta\varphi_1$ represents the flux change per cycle in transformer TE1. Since source voltage V_s is sinusoidal, the following relation is valid:

$$\Delta\varphi_1 = -\int_t^{t+\Delta t} [(R_s + R_1) \cdot i_1] \, dt \tag{2.44}$$

with i_1 being symmetrical, $\Delta\varphi_1$ is zero.

After closing S, saturation of transformer TE2 causes a transient inrush current i_2 which flows through R_s. Due to the unidirectional characteristic of the inrush current, each cycle transformer T_1 experiences an offset flux by an amount of:

$$\Delta\varphi_1 = -\int_t^{t+\Delta t} [(R_s + R_1) \cdot i_1 + R_s \cdot i_2] \, dt \tag{2.45}$$

Meanwhile, an offset flux per cycle $\Delta\varphi_2$ is produced in transformer TE2 by:

$$\Delta\varphi_2 = -\int_t^{t+\Delta t} [(R_s + R_2) \cdot i_2 + R_s \cdot i_1] \, dt \tag{2.46}$$

At the initial stage, both $\Delta\varphi_1$ and $\Delta\varphi_2$ are of the same polarity and mainly depend on the voltage drop caused by the inrush current i_2. The accumulation of $\Delta\varphi_1$ drives transformer TE1 into saturation, while the effect of $\Delta\varphi_2$ is to reduce the initial offset flux in transformer TE2 so as to produce the decay of inrush current i_2.

As the transformer TE1 becomes more and more saturated, a sympathetic inrush current i_1 gradually increases from the steady state magnetizing current to a considerable magnitude. Noted that as the transformer TE1 saturates with the polarity opposite to that of transformer TE2, the peaks of the sympathetic inrush current i_1 are with polarity opposite to that of inrush current i_2, on alternate half cycles. As a result, the voltage asymmetry on transformer terminals caused by the inrush current i_2 during one half cycle is reduced by the voltage drop produced by the sympathetic inrush current i_1 during the subsequent half cycle. This decreases both $\Delta\varphi_1$ and $\Delta\varphi_2$, and therefore

reduces the changing rate of the magnitude of both the increasing sympathetic inrush current i_1 and the decaying inrush current i_2.

After a certain time, the increase of i_1 and decay of i_2 can reach a point that:

$$(R_s + R_1) \cdot i_1 = -R_s \cdot i_2 \tag{2.47}$$

At this point, the flux change per cycle $\Delta\varphi_1$ is zero and hence current i_1 stops increasing. Thereafter, the polarity of $\Delta\varphi_1$ reverses and starts to reduce the offset flux in the transformer TE1, as a result, the sympathetic inrush current i_1 begins to decay (so does the inrush current i_2). Since both decaying currents have the same amplitude but with polarities opposite to each other, no voltage asymmetry is produced on the transformer terminals and the flux change per cycle in each transformer only depends on the winding resistance of each transformer. This is one of the reasons for the inrush current to be significantly prolonged in power systems with large transformers energised, as the winding resistances of these transformers are normally of relatively small value.

2.3.1.2 Parametric study

Sympathetic interaction between two identical single-phase transformers (rated at 333 kVA, 13.8/0.46 kV) was evaluated in the laboratory tests carried out in [81]. The schematic diagram of the circuit used in laboratory tests is the same with that shown in Figure 2-11. In the tests, circuit breaker was set to close at the positive-going zero crossing of the applied voltage and the residual flux of the transformer (both in terms of polarity and magnitude) was fixed by feeding a direct current through the winding before each test for a short period. The effects of line resistance, line inductance, resistance of the transformer loop circuit and transformer loading were investigated and it was found that:

- Line resistance: a key factor in determining the magnitude of the sympathetic inrush current in the transformer already connected; increase of line resistance generates higher maximum peak of sympathetic inrush current and accelerates the build-up to reach the maximum peak;
- Line inductance: increase of line inductance reduces the magnitudes of both inrush currents (the inrush current of the transformer being energised and the sympathetic inrush current of the already connected transformer) but has little effect on the build-up of sympathetic inrush;
- Resistance of the transformer loop circuit: it rapidly reduces the magnitude of

sympathetic inrush current of already connected transformer and speeds up the decay of the sympathetic interaction (this represents the case of two parallel transformers separated by transmission lines of long length instead of a short electrical connection) ;

- Transformer loading: negligibly affects the sympathetic inrush current and the inrush current of the energised transformer.

In [21], using a coupled field-circuit simulation approach, the possible influential factors, including system resistance (i.e., sum of source resistance and line resistance), switching angle, residual flux in the energised transformer and load current were analysed. Again, the configuration of the electrical circuit connection for the analysis is also similar to that shown in Figure 2-11. It was found that: although the increase in system resistance reduces the magnitude of the inrush currents drawn by the energised transformer, it increases the magnitude of the sympathetic inrush current in the already connected transformer (however, it has very little effect on the duration of the sympathetic inrush current); changing circuit breaker closing time and transformer core residual flux would cause significant variation of sympathetic inrush phenomenon; loading the energised transformer under various levels with various power factors only slightly affect the magnitudes of inrush and sympathetic inrush currents.

2.3.1.3 Measurements of sympathetic inrush in real systems

Sympathetic inrush has been encountered in many practical systems and caused significant concerns. In [84], sympathetic interaction between transformers in a 20 kV converter test facility was reported. The configuration of the test facility is shown in Figure 2-13 (a). During converter testing, the active power is circulating between S1-T1-TO-T2-S2-S1 and only the losses are compensated from a 20 kV grid (with 160 MVA short-circuit level). The two transformers T1 and T2 need to be energised on a daily basis for carrying out tests. To reduce inrush current, a 100 Ohm short-circuit current limiting resistor was connected, which is large enough to limit the inrush current magnitude to values below 150 A and to damp out inrush current in less than 50 ms. However, sustaining sympathetic inrush currents were encountered. As shown in Figure 2-13 (b), T1 was energised at 52.2 s and then T2 was energised at 52.26 s; although inrush current caused by energising T1 was damped out in one cycle, long-duration sympathetic inrush currents were induced after energising T2. The damping resistor,

which helped reduce inrush current in the case of energising T1, caused voltage asymmetry which resulted in sympathetic inrush when T2 was energised.

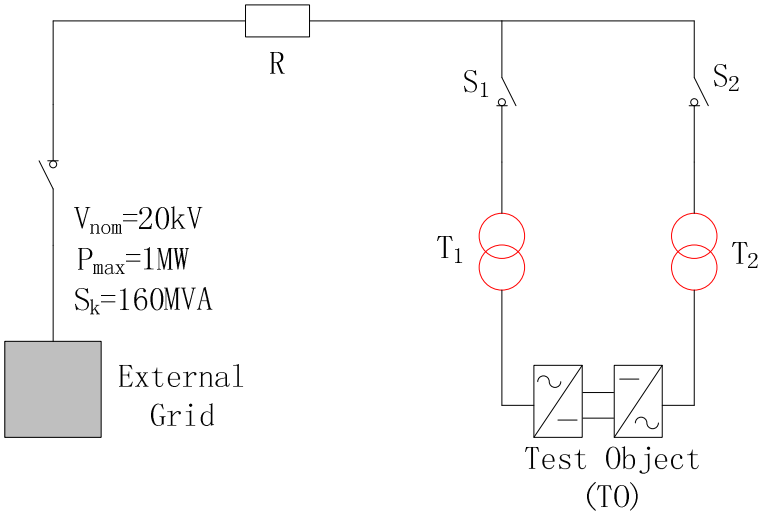

(a) Diagram of the 20 kV converter test facility

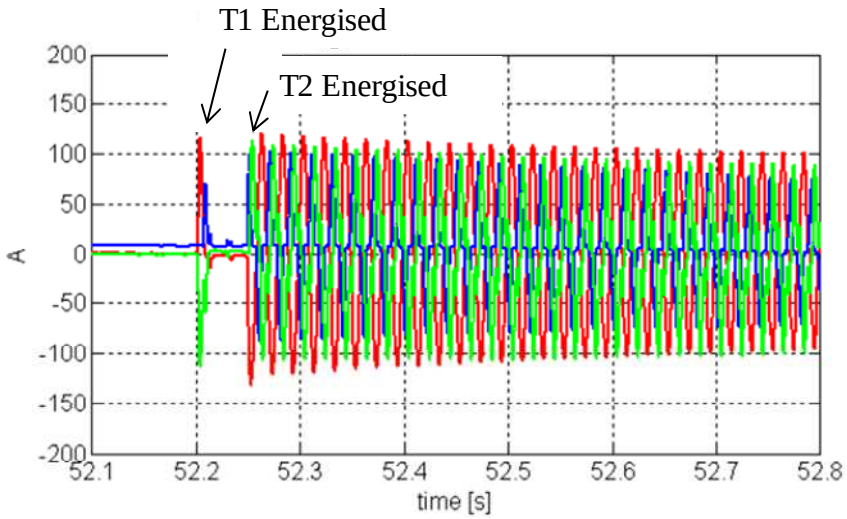

(b) Measured sympathetic inrush current waveforms

Figure 2-13 One-line diagram of 20 kV converter test facility and recorded sympathetic inrush current waveforms [84]

Voltage dips caused by sympathetic inrush between 100 MVA 220/23 kV transformers were reported in [85]. The configuration of the electrical system subjected to sympathetic inrush is shown in Figure 2-14. The substation is fed by two 220 kV overhead lines with length of 178 km; it originally consisted of two 100 MVA, 220/23 kV transformers (T1 and T2) connected in parallel to supply power to mining facilities. A new transformer T3 was added to meet increasing demands. When energising T3, sympathetic inrush was induced in the two already connected transformers T1 and T2. The energisation also resulted in high distortion of voltages and caused tripping of those

equipment connected to 23 kV busbar due to undervoltage. Field measurement of RMS voltage dip waveforms are shown in Figure 2-15. It can be seen that in both cases, the maximum voltage dip magnitudes were no more than 8%, however, the duration to achieve a recovery were over 10 seconds. It shows that, despite of small voltage dip magnitude, voltage dips accompanied by sympathetic inrush lasts much longer and may still trip off sensitive equipment.

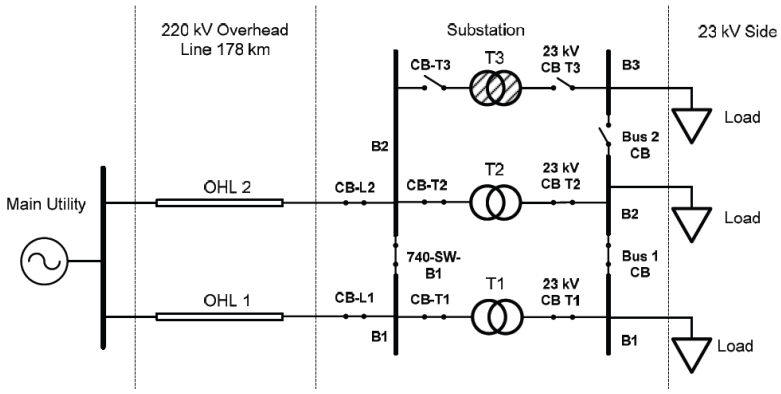

Figure 2-14 Simplified electrical system circuit diagram [85]

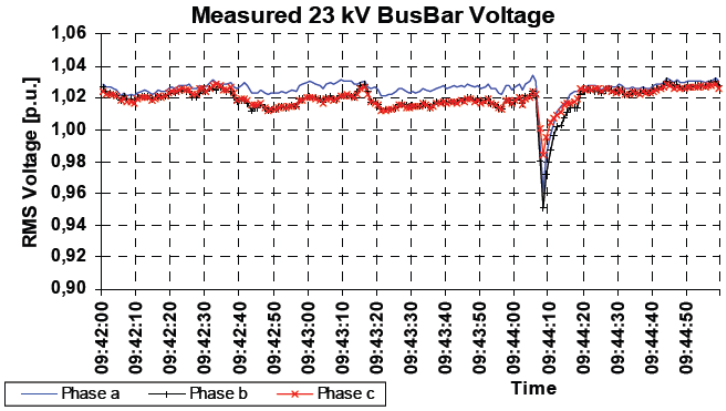

(a) Measurement 1

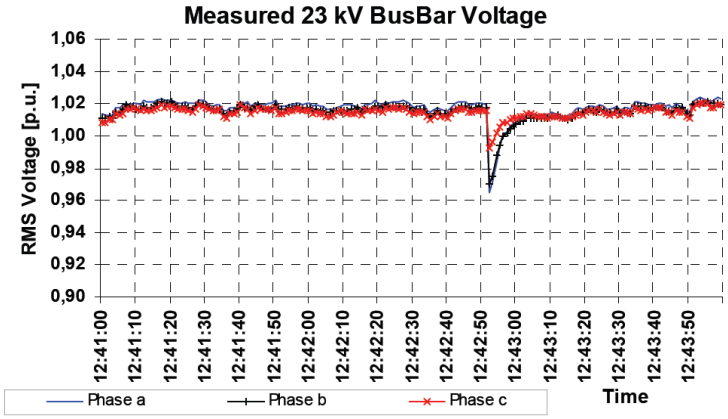

(b) Measurement 2

Figure 2-15 Measured voltage dips at 23 kV busbar [85]

2.3.2 Mechanical forces induced by transformer inrush current

Mechanical force on transformer windings under short-circuit is frequently of main concerns [86]. Since the amplitude of inrush current may be comparable to that of short-circuit current, the mechanical forces built-up on windings under inrush were investigated and compared to those under short-circuit conditions [8, 9].

In [8], how mechanical forces build up under inrush current was investigated, compared to those occurring under short-circuit. The investigation was based on 2D and 3D modelling of a 268 MVA, 525/17.75 kV three-legged step-up transformer. It was found that inrush currents with peaks of more than 70% of the rated short-circuit current magnitude would induce forces higher than those under short-circuit condition; these forces summed up on the high voltage winding (normally the energised winding) can be three times higher.

In [9], the radial and axial electromagnetic forces due to inrush currents were examined for a three-phase, three-legged 66/11 kV, 40 MVA power transformer. The study shows that the axial forces due to inrush current are always larger than those caused by short circuit current and the radial force applied on High-Voltage (HV) winding is about three times the corresponding force under short-circuit condition.

Even though inrush currents are normally smaller than short-circuit current, they are with a much longer duration. In addition, the duration of inrush current can be further prolonged under sympathetic inrush. This may cause winding damage or insulation failures a certain time span after transformer energisation.

2.3.3 Energising transformers from a limited capacity generator

In some industrial and utility installations, an emergency generator is provided to supply essential loads during islanded operation or for system restoration. In such installations, the necessary switching operations may require energising a transformer or a group of transformers from the emergency generator which is of relatively small capacity. The resulted long-duration high magnitude inrush current may generate adverse impacts on the emergency generator [2, 78].

In [78], simulations were performed using EMTP to analyse the inrush transients resulted from energising a 27 MVA transformer from an 8.3 MVA diesel generator

under different operating conditions. The developed network model included generator, generator control, transformer and loads; the governor was not included in the generator control, because the governor time constant is longer than the analysed inrush transients and the level of active power consumption during the transformer energisation is low. The simulation results show that: although the inrush currents are of magnitudes lower than three-phase short-circuit currents, they are much higher than normal operating current and may generate high electromagnetic torch oscillations; these oscillation may subject the shaft to high torsional stresses which could lead to fatigue failure if the transformer energisation from the diesel generator is frequent.

In [2], energisation of wind turbine transformers with an auxiliary diesel generator in a large offshore wind farm during islanded operation was investigated using time-domain PSCAD/EMTDC simulation. The simplified diagram shown in Figure 2-16 illustrates the configuration of the wind farm collection grid during islanded operation.

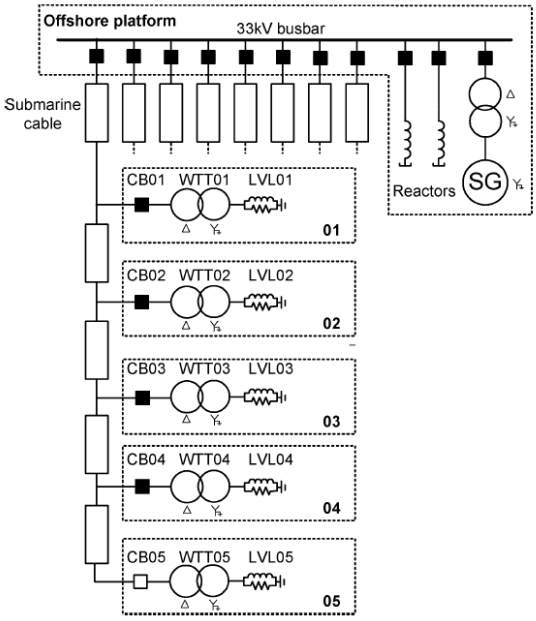

Figure 2-16 Simplified single-line diagram of wind farm collection grid during an emergent islanded condition [2]

As can be seen, it consists of eight cable feeders; each feeder contains five wind turbines and each wind turbine connects a circuit breaker, a wind turbine transformer (4 MVA, 33/0.69 kV, Dyn) and a low-voltage auxiliary load (18 kVA); the emergency diesel generator (1.6 MVA, 33/0.4 kV) is located at the offshore platform together with two shunt reactors (1.5 MVar) which are to balance the reactive power generated by the 33 kV cables.

The collection grid was modelled in PSCAD/EMTDC: the diesel generator was modelled in a way similar to that used in [78]; the 33 kV submarine cable sections were represented by nominal pi-sections (the length of the cable section between two adjacent wind turbines is slightly above 1 km); the loads connected on the low-voltage side of each wind turbine transformer were modelled by constant impedances; the wind turbine transformers were modelled by the PSCAD classical model in which each phase of the transformer is represented by a separate single-phase transformer model with no coupling between phases; additional dc-current sources were connected to the wind turbine transformer low-voltage side to simulate residual flux in the transformer.

In the paper, there were in total five case studies which are summarized in Table 2-4. As can be seen, the case studies mainly considered the effects of residual flux, sympathetic interaction between wind turbine transformers and the response of Automatic Voltage Regulator (AVR). In all the cases, the shunt reactors and 33 kV cables were connected; only the wind turbine transformer located farthest from the platform was energised and the energisation instant was at the positive-going zero crossing of phase-to-ground voltage. It was found that: the sympathetic inrush current induced in the already connected wind turbine transformers imposes further reactive power demand on the diesel generator; increase in the speed of AVR response from medium to high can result in larger sympathetic inrush currents in the already connected wind turbine transformers and hence higher reactive power demand from the diesel generator.

Table 2-4 Summary of case studies carried out in [2]

Case	Energised wind turbine transformers	Adjacent wind turbine transformers	Residual flux	AVR response
1	The wind turbine transformer farthest from the offshore platform	Not connected	Zero	Medium speed
2		Not connected	70%	
3		Connected (With saturation)		
4		Connected (No saturation)		
5		Connected (With saturation)		High speed

2.3.4 Harmonic incursion due to transformer energisation

The inrush current resulted from transformer energisation is rich in harmonics. Evaluating the harmonic content of the transformer inrush current is important for the design of transformer differential protection and the analysis of harmonic resonant overvoltages.

2.3.4.1 Harmonic analysis of inrush current

In most previous contributions, the harmonic analysis of inrush current was performed by looking at the variation of its harmonic content with time. The first contribution showing the harmonic content variation was presented in [10]. In the paper, the magnitude and phase shift of each harmonic component were obtained from a Fourier analysis for each cycle of the inrush separately. This approach was also followed by other contributions in [14, 24, 87, 88]. Typical harmonic analysis results given by [24] are shown in Figure 2-17.

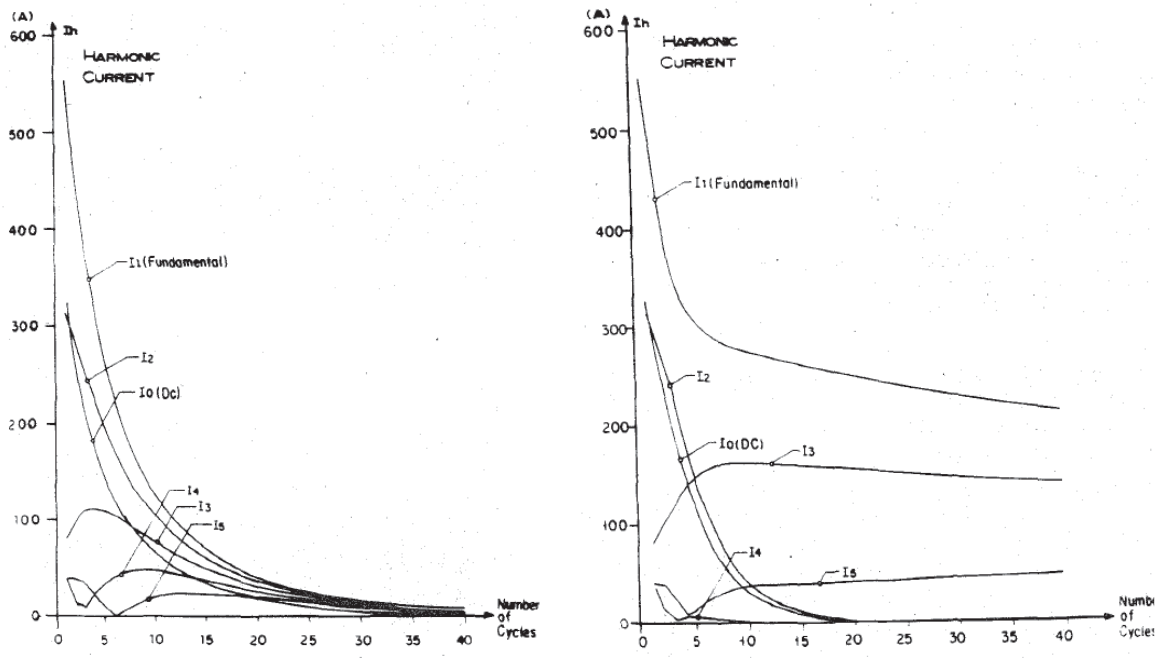

(a) Harmonic contents of the inrush current drawn by the transformer being energised

(b) Harmonic contents of combined inrush current and sympathetic inrush current

Figure 2-17 Variation of harmonic content of inrush current as a function of time [24]

Figure 2-17 (a) illustrates the harmonic components of inrush current alone (without sympathetic inrush current involved). It can be seen that: the amplitude of any harmonic component during one cycle is generally different from its amplitude during another cycle; the second order harmonic is the dominant one; the higher the magnitude of the inrush current at any one cycle, the higher the second order harmonic content of that cycle; the higher the harmonic order, the smaller the magnitude of the corresponding current component in the inrush current; for some harmonics, their highest amplitudes do not appear at the first cycle after transformer energisation, such as the third and fourth order harmonics; some harmonic components change their phase from negative to positive, or vise versa, after their amplitude pass zero, such as the fourth and fifth

order harmonics. Figure 2-17 (b) shows the harmonic components of the current combining inrush current and sympathetic inrush current, in which case, the even order harmonic components decay rather quickly, whereas the odd harmonics increase and continue to stay for a considerable period of time.

2.3.4.2 Use of second harmonic of inrush current in transformer protection

During transformer energisation, the inrush current typically occurs in only one winding of the transformer and thereby produce a differential current that may result in the operation of transformer differential protection [89]. Since transformer inrush is not a fault event, the differential protection must be restrained for this condition.

Harmonic restraint is a classical method to ensure the reliability of transformer differential protection during inrush events. The simplest restraint function uses the ratio between the magnitude of the second harmonic and that of the fundamental frequency component in the differential current; harmonic ratio is typically calculated on a per-phase basis; typical setting of the ratio ranges between 15% and 20%, above which the differential protection is restrained [16].

Experience shows that for most transformer application, the setting can effectively differentiate the inrush events and internal fault events via harmonic restraint. However, it should be aware of the fact that modern transformers may be characterized by lower second harmonic ratios because of higher designed flux density and the use of step-lap type joint [90]; in addition, in the case of transformer ultra-saturation, the percentage of second harmonic can fall below 5%, inevitably leading to mal-operation [17, 91]; furthermore, in the case of current transformer (CT) saturation during internal faults, the fault current transformed to the secondary may contain amounts of second harmonic higher than the setting and thus cause incorrect restraining [16]. In view of the limitations of the second harmonic restraint function, there are other methods proposed, such as a complex second harmonic restraint [92], flux restraint [93], or the use of artificial neutral network [94].

2.3.4.3 Harmonic resonant overvoltages

Rich in harmonics, transformer inrush currents may produce harmonic resonant overvoltages (also called temporary overvoltages) which may subject transmission lines and equipment (e.g., transformers and surge arrestors) to long duration overvoltages

with magnitude over twice the rated voltage for as long as 100 or more cycles, imposing large risk of burning insulators, arresters and damaging transformer insulation. This type of overvoltage has been identified in following cases:

- Energising the convertor transformers in HVDC substations consisting of ac filter circuit [13, 95];
- Restoration of a bulk power supply system [12, 15, 76, 96];
- Energising transformer in systems with long length cables [14, 36];
- Energising transformer in some industrial distribution systems with installation of power factor correction capacitors [97] or pulse-type loads [98].

In these cases, the systems consist of the following common characteristics: pronounced parallel resonance points (such as in the systems with long transmission lines or reactive components like filters and capacitor banks) and low degree of damping (the system is light-loaded or non-loaded). Selected examples corresponding to some of the typical cases are given below.

Normally, the HVDC station is directly fed by generators without local ac loads being connected, i.e., low damping. The ac filter circuit connected at the HVDC stations can form several parallel resonance points in the impedance-frequency characteristic of the system. The inrush currents resulted from energising the converter transformer can repeatedly shock the ac system – ac filter combination once per cycle, and due to the slow decay of the inrush currents, result in overvoltages lasting many cycles, as shown in Figure 2-18.

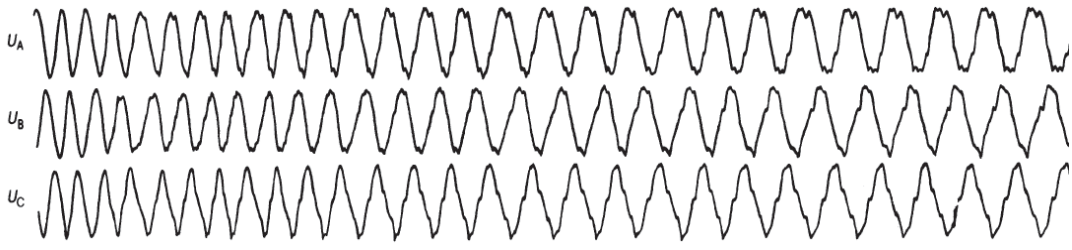

Figure 2-18 Field measured overvoltages caused by transformer energisation in HVDC stations [13, 99]

The value of the overvoltages depends on the value of the harmonic current at which the resonance occurs; the largest value of a certain harmonic might occur a long time after energisation. Measurements show that the peak value of such overvoltages can be 1.7 pu [99], while simulations show that it can be over 2 pu [13, 95].

In [14], harmonic resonance overvoltages excited by transformer inrush current in an inter-connected offshore power system were evaluated. As shown in Figure 2-19 (a), in the studied system, a 4.5 MVA transformer is located at a remote offshore platform which is supplied via an inter-connected circuit consisting of a 11/35 kV, 25 MVA step-up transformer, a 30 km subsea cable and a 35/6 kV, 16 MVA step-down transformer; the onshore plant operates at 11 kV and is equipped with 30 MVA gas turbine generators. A network model was developed in PSCAD/EMTDC to study the resonant overvoltages: the transformer being energised was modelled by the "classical" model in which each phase of the transformer is represented by a separate single-phase transformer model with no coupling between phases; the subsea cable was modelled by cascaded nominal pi-sections; each generator was represented by a dynamic machine model including their AVRs. Simulations were carried out to study the resonant overvoltages caused by energising the 4.5 MVA transformer. The simulated overvoltage and the variation of its harmonic content with time were obtained, as shown in Figure 2-19 (b) and Figure 2-19 (c), respectively.

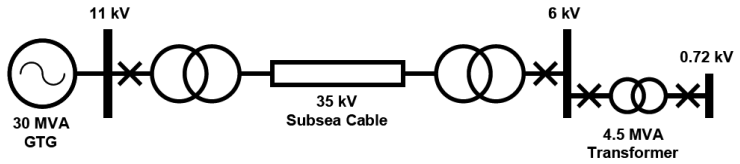

(a) System configuration of an offshore inter-connected circuit

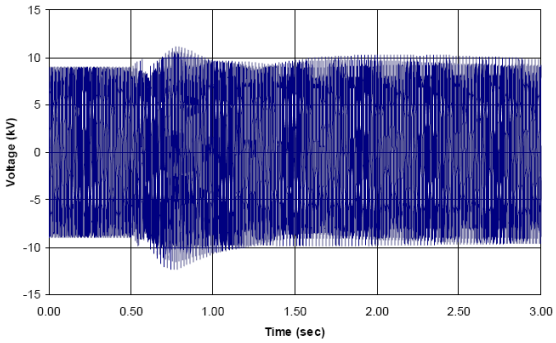

(b) 11 kV line-to-ground voltage

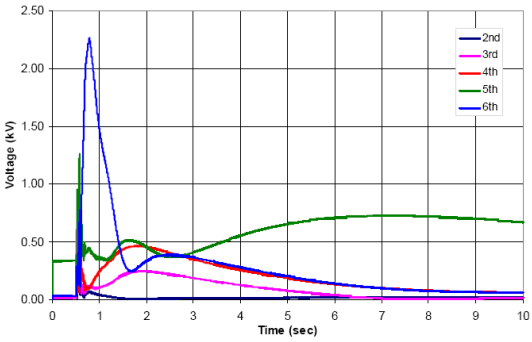

(c) Variation of harmonic content

Figure 2-19 System configuration, simulated harmonic resonant overvoltages and variation of harmonic component [14]

It was also shown that severer overvoltages can be excited by energising the inter-connector link (i.e., energising the step-up transformer, the sub-sea cable and the step-down transformer simultaneously). The authors suggested that the overvoltage problem can become less severe with increased levels of generation and load on the system.

Harmonic resonant overvoltages are also likely to occur during system restoration, because the networks, after a complete or partial collapse, are lightly loaded and with low system resonant frequencies. An example configuration for a system restoration was given in [96] and is shown here in Figure 2-20 (a). The basic procedure to restore such a system would be: start up the generators; connect the local load at busbar B4; energise the transmission line together with the shunt reactor connected to busbar B3; finally, energise the unloaded transformer. The energisation of the unloaded transformer through long transmission line resulted in significant resonant overvoltages at busbar B3, as shown in Figure 2-20 (b). For harmonic resonant overvoltages during system restoration, they can be controlled by several methods [15]: increase resistive loading, bring additional generators on line or decrease the magnitude of generator terminal voltage.

From the harmonic analysis of the system current combining inrush and sympathetic inrush currents (see Figure 2-17 (b)), it can be seen that the sympathetic interaction can probably reduce the severity of harmonic overvoltages for systems resonating at even ordered harmonic frequencies; however, for systems resonating at odd ordered harmonic frequencies, harmonic overvoltages are likely to be prolonged [24].

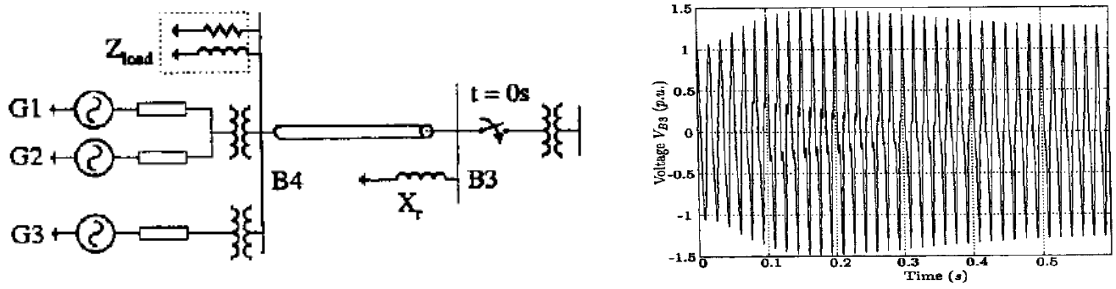

(a) Network configuration at the beginning of system restoration

(b) Simulated harmonic overvoltage

Figure 2-20 System configuration at the beginning of a restoration procedure and overvoltage resulted from energising a transformer [96]

2.3.5 Voltage dips caused by transformer energisation

During recent years, power quality issues associated with voltage dips are gaining more concerns. One reason for this is that customers are becoming more aware of power quality; for instance, flicker caused by voltage dips may lead to customers' complaints. The other important reason is the increasing use of power quality sensitive loads, such as adjustable-speed drives and programmable logic-based process control in paper, mining and electronic chip manufacturing plants [100]; for example, in adjustable-speed

drive, when the voltage drops below a critical level for a long duration, the drive might function abnormally or even shut down.

Transformer energisation is a planned operation and may cause severe voltage dips. It gains increasing attention in recent years due to the need to comply with tightened grid code requirements. In UK, a 3% threshold is normally applied to the voltage dips caused by transformer energisation. This threshold is derived from the Engineering Recommendation P28 (ER-P28) which defines the curve describing tolerable dip magnitude (in other words, the size of voltage change) against the interval between each voltage change, as shown in Figure 2-21 [4].

The curve shows the tolerable size of voltage change increases with the time between each change. For examples, if the time between each change is 1 second, the allowable size of voltage change is 0.4%; if the time between each change is 200 seconds, the limit will be 2%; and when the time between each change is equal to or more than 750 seconds, the maximum allowable size of voltage change is 3%.

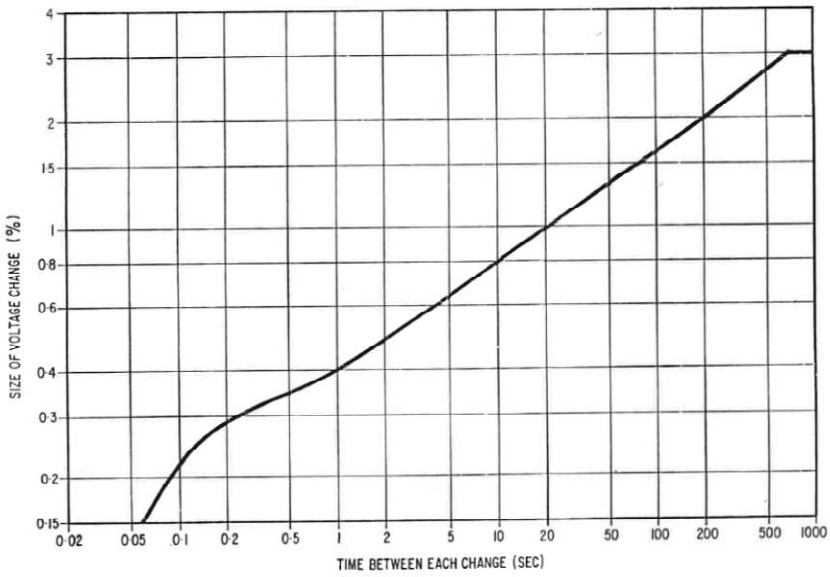

Figure 2-21 Size of voltage change against the time between each change [4]

2.3.5.1 Energising large generator step-up (GSU) transformer

The voltage dips caused by energising large GSU transformers from HV transmission grid were investigated in [19], [51] and [101].

In [19], the system under study comprises generating plants, long transmission lines and power quality sensitive loads, which can be referred to the simplified single-line diagram shown in Figure 2-22.

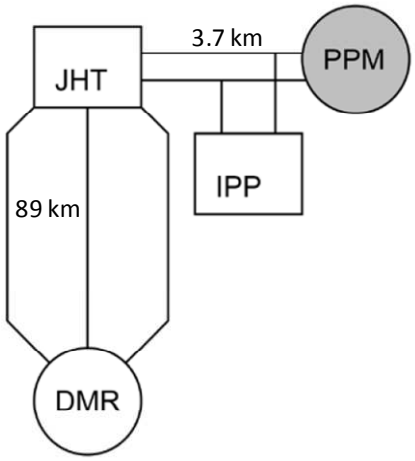

Figure 2-22 Simplified single-line diagram of a 138 kV BC Hydro system [19]

The Dunsmuir Substation (DMR) is a major switching substation connected to BC Hydro grid through two 500 kV ac submarine cables. Three 138 kV transmission lines (with length of 89 km) are connecting between Dunsmuir Substation and the 150 MVA John Hart (JHT) hydroelectric generating plant. A 200 MW pulp and paper mill (PPM), containing power quality sensitive loads, are supplied via two 3.7 km 138 kV lines from the John Hart plant. Between John Hart plant and the mill, there is a new independent power producer (IPP), with a 250 MW gas turbine generator which needs to be connected to the 138 kV network. Since the independent power producer generating plant does not have black start capability, the GSU transformer of the gas turbine generator needs to be energised from BC Hydro grid to power the auxiliary devices for starting the generator. The nameplate data of the GSU transformer are 315 MVA, 138/21 kV, 14.9% impedance and star-delta windings with 138 kV star side being solidly grounded.

An EMTP model of the 138 kV network was developed to carry out assessment of voltage dips caused by energisation of the GSU transformer. In the network model:

- Positive and zero sequence Thevenin impedances were used to represent the remaining network and the 500 kV connection to the main grid;
- Generating plant located at John Hart was represented by an ideal voltage source connected to equivalent sub-transient impedance;
- Transmission lines were modelled by Bergeron model;
- GSU transformer was modelled by three single-phase two-winding STC transformers (the three single-phase transformers are connected in grounded-star on the 138 kV side, and in delta on the 21 kV side); type-96 nonlinear inductors

were used to model core saturation and residual flux.

Simulation assessment was carried out to estimate the voltage dips under the worst energisation condition which was assumed in the study as:

- All three phases simultaneously switched at the zero crossing of phase A voltage;
- Maximum residual flux of negative polarity in phase A and the other two phases with half of the maximum residual flux of positive polarity (the maximum residual flux was assumed to be the flux retained at the instant when the magnetizing current become zero following the core hysteresis curve).

In the simulation of the worst case energisation, it was estimated that the maximum dip magnitude of the RMS voltage dips observed at the mill was about 0.27 pu.

The study carried out in [51] not only assessed voltage dips under the worst energisation condition, but also investigated the influence of network configuration variation on voltage dips. Figure 2-23 shows the network studied in [51].

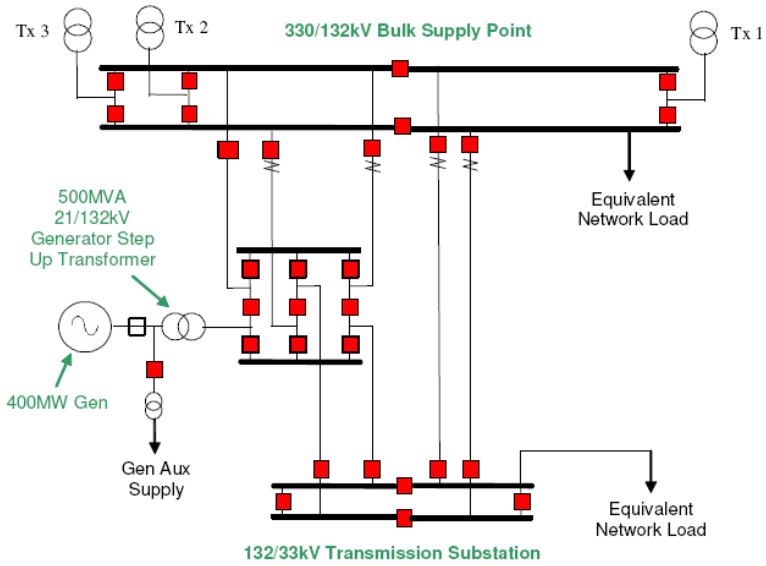

Figure 2-23 Simplified diagram of a HV supply network in Australian system [51]

A power station is located between a bulk supply point and a 132/33 kV transmission substation. The bulk supply point contains three links to higher voltage grid through three 330/132 kV step-down transformers. Network loads are connected to the bulk supply point as well as the transmission substation. There are five feeders going into the power station, two from the transmission substation and three from the bulk supply point. The GSU transformer connected to the 400 MW generator needs to be energised from the 132 kV grid. The nameplate data of the GSU transformer are 500 MVA,

132/21 kV, 18% impedance, YNd11 winding connection with 132 kV star side being solidly grounded and its tapping range is from +15% to -5% (each step is of 1.25%).

The network was modelled in PSCAD/EMTDC, consisting of the supply network and the GSU transformer (the generator was not included in the model). The GSU transformer was represented by three separate single-phase transformers. The effect of residual flux in the GSU transformer was modelled by using adjustable DC current sources in parallel with the transformer HV terminals.

In the assessment, the assumed worst energisation condition was that: energising at zero crossing of one phase voltage and the maximum residual flux was assumed to be 90% of the peak nominal flux. Based on the same energisation condition, voltage dips resulted from energising GSU transformer under three different network configurations were assessed. The three considered network configurations (C1, C2 and C3) are:

- C1, as shown in Figure 2-24 (a), all busbars are made solid; only two supply sources are connected at the bulk supply point; all lines to the substation of the generating plant are switched in;
- C2, as shown in Figure 2-24 (b), all busbars are made solid; all three supply sources are connected at the bulk supply point; the generation plant is only supplied by one single feeder from the bulk supply point;
- C3, as shown in Figure 2-24 (c), the 132 kV busbar at the bulk supply point are split; all lines linking the generator substation and the transmission substation are disconnected.

Under the three network configurations and the same worst case energisation condition, the estimated inrush current (peak, duration) and voltage dip magnitudes observed at the terminal of the GSU transformer and at the transmission substation 132 kV busbar are summarized in Table 2-5. It was found that, by changing configuration from C1 to C3, the RMS dip magnitude observed at the transmission substation 132 kV load bus can be reduced from 16.8% to 6.3%. This is because the point of common coupling connecting all loads and the energised GSU transformer has been effectively moved to 330 kV grid. This increased the electrical distance between the TS and the energised transformer, so the voltages at transmission substation 132 kV busbars become less sensitive to the energisation of GSU transformer.

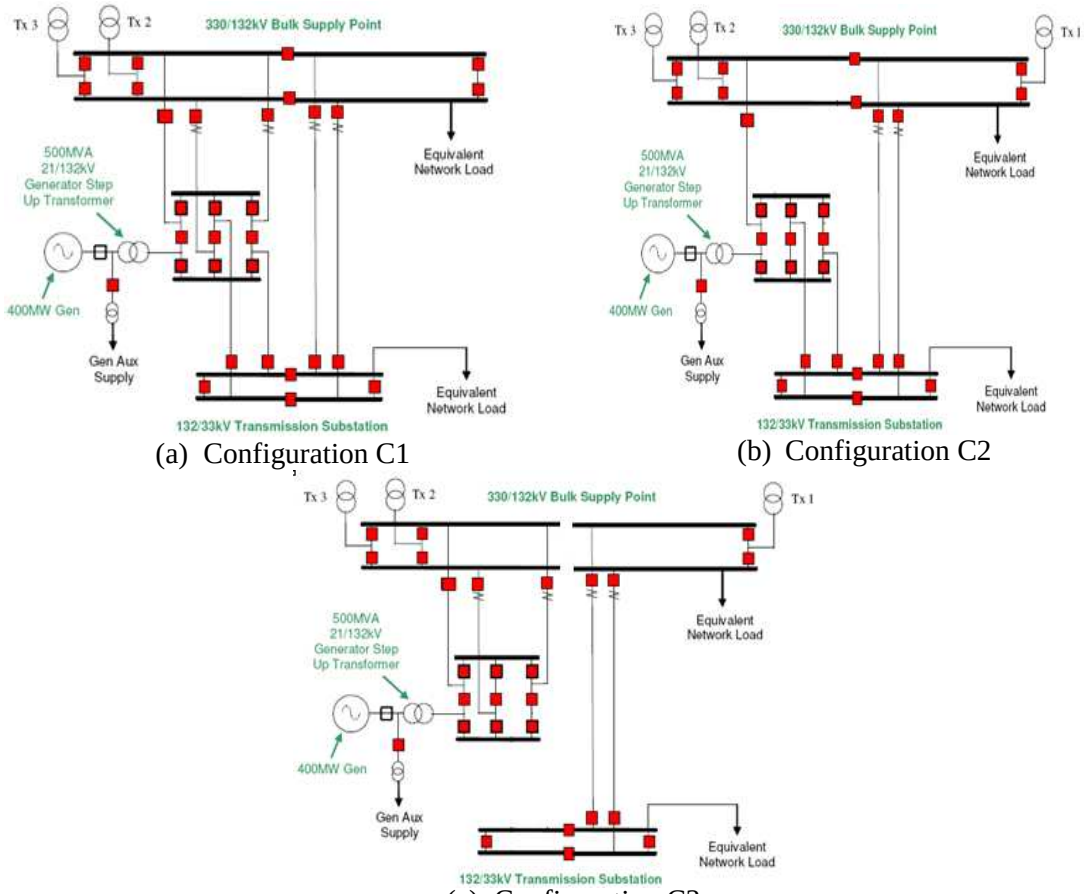

(a) Configuration C1 (b) Configuration C2

(c) Configuration C3

Figure 2-24 Network configurations under comparison

Table 2-5 Estimated inrush current peaks, duration and voltage dip magnitudes resulted from the worst case energisation under different network configurations [51]

Network configuration	Peak inrush current (kA)	Inrush Duration (s)	RMS Voltage dips %	
			Transformer Terminals	TS 132 kV Load Bus
C1	11.3	0.57	22.7	16.8
C2	11.7	0.60	20.6	14.5
C3	8.3	0.68	38.5	6.3

Instead of focusing on the voltage dip observed on a specific busbar, network-wide voltage dips were studied in [101], taking into account the variation of energising angle, residual flux condition and system loading. The configuration of system under study is illustrated in Figure 2-25. It consists of ten busbars in which three busbars are connecting power plants, two busbars are connecting wind turbines and eight busbars are connecting loads. The lengths of the transmission line range from 5.1 to 46 km. The peak loads is 409.09 MW. To connect the power plant to the JN bus, a main GSU transformer needs to be energised first. The nameplate data of the main transformer are 124 MVA, 154/13.8 kV, 11% impedance and star-delta connection.

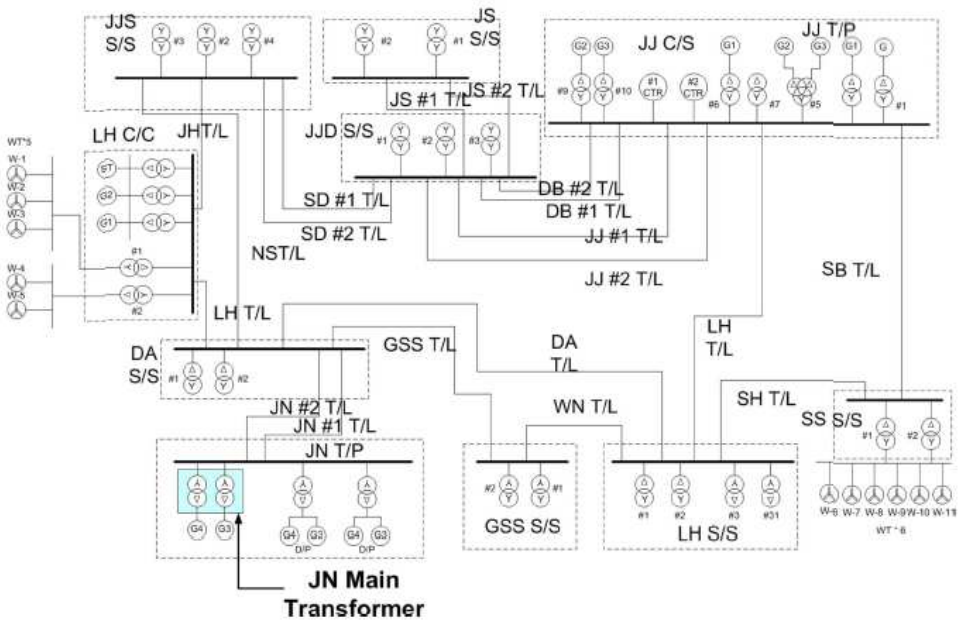

Figure 2-25 Single line diagram of Jeju power system in Korea [101]

The network of Jeju power system in Korea was modelled by following the approaches below:

- Generator was modelled by using the SM model in EMTP;
- Transmission lines were represented by lumped parameter model;
- Main GSU transformers were modelled based on transformer test report data and the core saturation curve was modelled to include hysteresis characteristic;
- Substation transformers were modelled but without considering hysteresis;
- Wind turbine and HVDC system were not considered in the network model.

Energisation of the main GSU transformer was simulated under the conditions shown in Table 2-6. Voltage dip magnitudes at all the substations were observed, as shown in Figure 2-26. It was found that the range of the voltage dip magnitudes is between 0.15 pu and 0.2 pu. The substations with closer distance to the energised transformer are with relatively larger voltage dips. Regarding the effect of the parameter on voltage dip magnitude, the assessment showed that voltage dip magnitude is sensitive to the circuit breaker closing angle, core residual flux and load variation.

Table 2-6 Energisation condition for simulation assessment [101]

Closing angle degree	Residual flux	Load
0	28.3%	Peak
45	15%	Middle
90	0	Off-peak

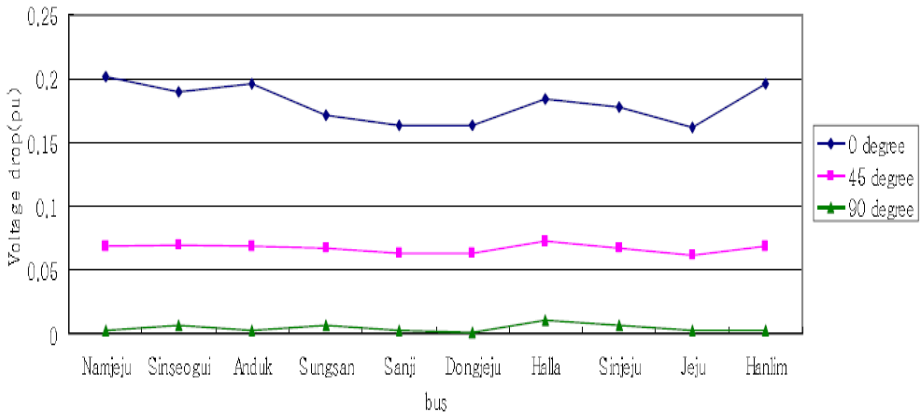

Figure 2-26 Voltage dip magnitudes resulted from different energisation angles when residual flux is 28.3% and system loading is at its peak [101]

2.3.5.2 Energising step-up wind turbine transformer

In recent years, wind farms are becoming more prevalent. A large number of wind farms have been connected to distribution or transmission grids and more are to be designed and commissioned. A common requirement for the connection of wind farm in the UK is that the energisation of transformers should not result in voltage dips exceeding 3%, according to the P28 requirements. A number of contributions have been devoted to transformer inrush studies for wind farm grid connections [50, 75, 102, 103], all of which were performed using PSCAD/EMTDC.

In [102], simulations were conducted to identify the possible voltage dips resulted from energising wind turbine transformers in two wind farm sites: one consists of 20 wind turbines, each rated at 1.5 MVA; the other consists of 17 wind turbines, each rated at 1.0 MVA; both of them are directly connected to 33 kV distribution networks. The simulation studies demonstrated that the voltage dips can be affected by circuit breaker closing time, closing time scatter among three poles, the number of wind turbine transformers to be energised simultaneously and the number of already connected transformers. It was found that, to meet grid code requirements, up to two wind turbine transformers can be energised simultaneously

Similar simulation studies were performed in [75]. Two wind farm sites (named here as A and B) were investigated, as shown in Figure 2-27. Wind farm A contains 15 wind turbine transformers (33/0.69 kV, 1.5 MVA, 6%) which are connected via two 33 kV feeders to the main wind farm switchboard and the point-of-common-coupling (PCC) is at 33 kV busbar; wind farm B contains 52 wind turbine transformers (33/0.69 kV, 2.6 MVA, 8.28%) which are connected via eight radial feeders back to the wind farm 33 kV

main switchboard and the point-of-common-coupling is located at 132 kV busbar. The number of wind turbine transformers consisted in each feeder varies between 1 and 9.

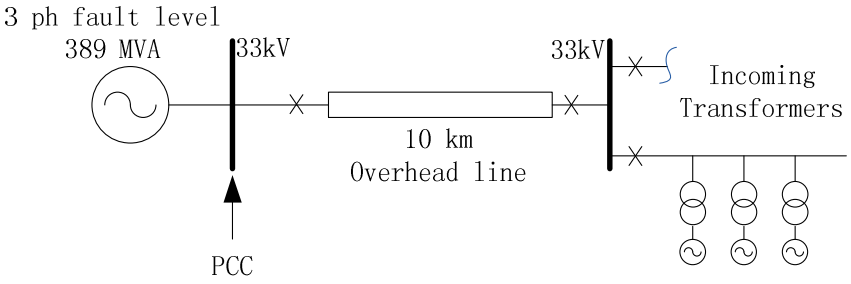

(a) Wind farm A configuration

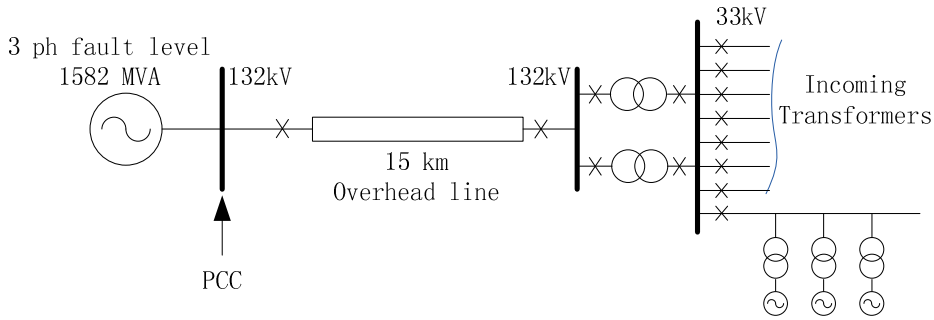

(b) Wind farm B configuration

Figure 2-27 Schematic diagram of two wind farm configurations [75]

Assessment of voltage dips at the point-of-common-coupling was carried out by using the commonly agreed worst case energisation condition, i.e., simultaneously energising transformer at the voltage zero crossing of the phase retaining maximum residual flux with polarity in line with flux build-up. It was found that: to ensure the voltage dip at the point-of-common-coupling does not exceed the 3% limit, the maximum number of wind turbine transformers allowed to be energised simultaneously was 3 in the smaller capacity wind farm connecting to 33 kV grid, whilst for the larger wind farm with a 132 kV grid connection, the maximum number was 9. This can be attributed to the much weaker source strength of 33 kV grid compared to that of 132 kV grid.

Sympathetic inrush in wind farm B was also assessed. The scenario considered was simultaneous energisation of nine 2.6 MVA wind turbine transformers under the worst case energisation condition; the wind turbine transformers on other feeders were assumed already connected, and, for each feeder with N wind turbine transformers, a single equivalent transformer with N×2.6 MVA was used. It was found that the sympathetic inrush current at one adjacent feeder can increase to a peak of 94 A about 12 cycles after the energisation.

In [50], some curves were identified to correlate the system fault level with voltage dips resulted from energising some typical wind turbine transformers. The main contribution of these curves is to allow the P28 assessment to be preliminarily carried out for a proposed wind farm connection before the detailed design information is available.

In [103], voltage dips caused by the sequential energisation of wind turbine transformers in a large offshore wind farm were studied. As shown in Figure 2-28 (a), the wind farm consists of 72 wind turbine transformers (each rated at 2.5 MVA) which were connected to an offshore platform via eight cable feeders (each feeder consists of nine wind turbine transformers). As shown in Figure 2-28 (b), four sequences with different switching time combinations between the energising groups were assessed, focusing on the effects of the switching angle, number of simultaneously energised transformers and energising sequence on voltage dip, current and active and reactive power. It was found that the smallest voltage dips, and the lowest inrush current occur when the wind turbine transformers are switched in one by one (i.e., independent energisation).

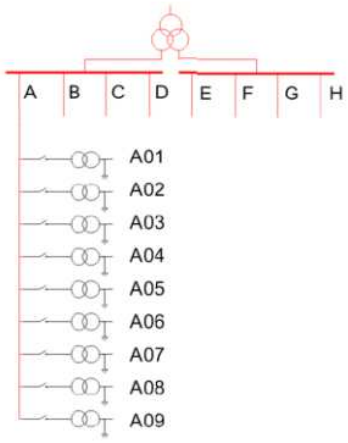

(a) Wind farm topology

	9WTx0s	5WTx5s	2WTx2s	1WTx1s
A01	0,1 s	5,1 s	6,1 s	8,1 s
A02	0,1 s	5,1 s	6,1 s	7,1 s
A03	0,1 s	5,1 s	6,1 s	6,1 s
A04	0,1 s	5,1 s	4,1 s	5,1 s
A05	0,1 s	0,1 s	4,1 s	3,1 s
A06	0,1 s	0,1 s	2,1 s	3,1 s
A07	0,1 s	0,1 s	2,1 s	2,1 s
A08	0,1 s	0,1 s	0,1 s	1,1 s
A09	0,1 s	0,1 s	0,1 s	0,1 s

(b) Energisation sequences

Figure 2-28 Wind farm topology and sequences for energising wind turbine transformers [103]

Based on the four contributions specifically targeted to assess voltage dips caused by energisation of wind turbine transformers for wind farm connections, Table 2-7 summarized the influential parameters that have been considered. In addition, the parameters studied by each paper are illustrated in Table 2-7 as well. As can be seen, none of them could take into account all the possible influential parameters. The most frequently concerned parameters are switching angle, the number of transformer being energised simultaneously (aggregated energisation) and sympathetic inrush.

Table 2-7 Summary of the influential parameters

Parameters	References			
	[102]	[75]	[50]	[103]
Switching angle	+	+	+	+
Closing time span	+	-	-	-
Residual flux	-	-	+	+
System strength	-	-	-	+
Core saturation inductance	+	-	-	+
Aggregated energisation	+	+	+	+
Sympathetic inrush	+	+	+	-
Energisation sequence	-	+	-	-
Voltage dip propagation	+	-	-	-

+: parameter taken into account; -: parameter not considered

2.3.6 Statistical assessment of transformer energisation transients

When carrying out an energisation of a power transformer, the circuit breaker closing time and residual flux are normally stochastic. In three-phase system, the stochastic nature can be more complicated with different closing time span between breaker poles and residual flux distribution in three phases. In addition, system parameters, such as loading and source strength, can stochastically vary within a certain range. In view of the parameter uncertainties, statistical simulation was conducted to evaluate the frequency of occurrence of inrush current or inrush-induced harmonic resonant overvoltages in a number of studies.

In [104], Monte-Carlo method was used to study the frequency of occurrence of inrush current first peak when energising a single-phase transformer at stochastic circuit breaker closing time and with stochastic transformer core residual flux. In the study, it was assumed that: closing time varies in a range of one power frequency cycle; residual flux varies in a range of ±1 pu of peak nominal flux; both ranges were characterized by Uniform distribution. Three cases were simulated, see Table 2-8.

Table 2-8 Cases studies of the influences of stochastic variables on the inrush current of a single-phase transformer

Case	Circuit breaker closing time		Transformer residual flux	
	Range	Distribution	Range	Distribution
1	One cycle (20 ms)	Uniform	Zero	
2	Fixed at positive-going zero crossing of the applied voltage		±1 pu of the peak nominal flux	Uniform
3	One cycle (20 ms)	Uniform		

The result of the Case 3 is shown in Figure 2-29 which suggests, under simultaneous variation of closing time and residual flux, the inrush current first peaks obtained from stochastic simulation runs seem to follow an asymmetrical exponential distribution.

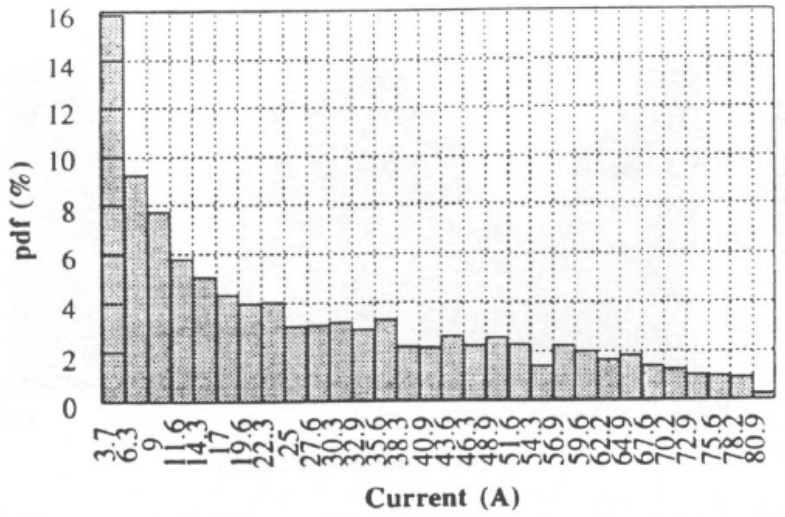

Figure 2-29 Frequency of inrush current first peaks when residual flux and closing time vary stochastically [104]

Statistical studies of energising a three-phase transformer were mainly focused on harmonic resonant overvoltages [38, 43, 95]. In [95], the resonant overvoltages excited by transformer inrush currents in HVDC system were assessed by a series of stochastic simulation tests. In each test, 1000 transformer energisations were carried out with stochastic closings and openings (the maximum time span between circuit breaker poles was assumed to be 3.3 ms); the residual flux was implicitly modelled by the stochastic openings; system source strength and the X/R ratio of equivalent impedance were considered to be deterministic.

Harmonic resonant overvoltages generated by transformer energisation during system restoration process were statistically assessed in [38] and [43] based on a similar network, as shown in Figure 2-30, with an auxiliary transformer energised from a source plant through a 400 kV overhead line.

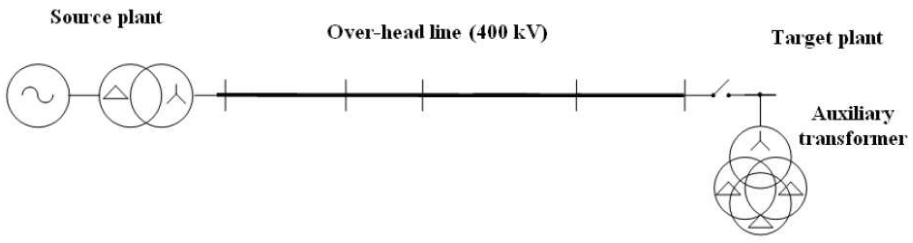

Figure 2-30 Network configuration studied in harmonic resonant overvoltages caused by energising transformer during system restoration [43]

In the system studied in [38], the source plant consists of three generators (total capacity is 900 MW); the length of overhead line is 50 km and the auxiliary transformer is of three-phase, shell-type, 96 MVA and 400/6.8 kV.

The possible influential parameters considered in the study include:

- Circuit breaker closing time ;
- Residual flux in the transformer core.
- Direct-axis sub-transient reactance value of the generators;
- Phase-to-earth line capacitance (i.e., the variation of conductors' heights);

To represent the random closing times, it was assumed that: the first pole of the circuit breaker is closed anytime within one cycle (20 ms for 50 Hz system); relative to the first pole being closed, the second and third poles are closed within a standard deviation (one cycle). Regarding the random residual flux, it was assumed that: the residual flux values are in a range of ±0.8 pu of peak nominal flux; the sum of the three-phase residual flux is recognized as zero. The possible range of the sub-transient reactance variation was assumed to be ±15% of the nominal value; the range for the phase-to-earth line capacitance was assumed to be ±5% of the base value. In the studies, 25 deterministic combinations of sub-transient reactance and line capacitance were formed; for each combination, 100 runs were carried out with stochastic residual flux and closing times.

Based on the same type of network, a similar study was performed in [43]. Compared to the work shown in [38], the main differences made in [43] include:

- Adding transformer air-core reactance as a stochastic parameter and it was described by a Uniform distribution covering ±20% of a base value;
- The stochastic variation of sub-transient reactance and phase-to-earth line capacitances were described by a Uniform distribution covering their corresponding ranges;
- Circuit breaker closing time were represented using the approach shown in section 2.2.3;
- The residual flux was modelled by two parameters: the maximum residual flux amplitude (φ_0) and a parameter identifying the flux pattern; twelve equally probable residual flux patterns were considered, which includes: $\{\varphi_0, -\varphi_0/2, -\varphi_0/2\}$, $\{\varphi_0, -\varphi_0, 0\}$ and $\{-\varphi_0, \varphi_0/2, \varphi_0/2\}$ for all the possible phase permutations.

The above contributions are focusing on stochastic simulation related to harmonic resonant overvoltages. So far, no statistical analysis has been made on voltage dips studies yet.

2.4 Possible approaches for mitigating transformer inrush

Mitigating approaches for transformer inrush were developed based on controlling one or more of the key factors governing transformer inrush transients, such as:

- Point-on-wave voltage at the instant of energisation;
- Magnitude and polarity of the residual flux in the transformer core at the instant of energisation;
- Equivalent resistance of the primary winding circuit;
- Impedance of the power supply circuit;
- Inductance of the air core in between the energising winding and the transformer core.

The oldest mitigation strategy to reduce inrush current is the use of the pre-insertion resistor as an intermediate step in closing a switch [1, 105]. When a transformer draws a large inrush current, the voltage drop across the pre-insertion resistor helps reduce the voltage applied across the transformer and hence the flux in the transformer, quickly reducing the inrush current. The effectiveness of this method is largely influenced by the time of inserting the resistance and that of by-passing it. Although this method is simple, it requires upgrading existing substation breakers, which is expensive; in addition, if a pre-insertion resistor is not properly by-passed after the switching process, the breaker could be damaged.

Reducing residual flux in the transformer core could be a possible strategy for reducing inrush currents. In [106], it was shown that residual flux can be significantly reduced by using a low, variable frequency voltage source to demagnetize the transformer. This method has only been shown in simulation but has not yet been realized experimentally.

Modifying transformer design may help reduce inrush current. The modification suggested by [107] is to change the distribution of the coil winding in a way to increase the transient inductance of the primary coil. The one presented in [108] employs an auxiliary winding to create an air gap in the transformer core so as to control the core reluctance. These methods have only been tested in laboratory on small single-phase

transformers. It is however challenging and costly to modify the design of large power transformers.

Techniques involving the control of circuit breaker closing time are probably the most widely discussed for mitigating inrush current. The most effective technique is to optimize the circuit breaker closing time according to transformer core residual flux [109]. The basic principle is that: measure the residual flux in the core during transformer de-energisation; with the residual flux known, calculate the optimum voltage angle resulting in the measured residual flux equal to the prospective flux; the inrush current could be eliminated if the energisation is carried out at the optimum voltage angle. Applying this technique requires installation of additional measurement equipment on the transformer terminals, which is costly. In addition, its performance is very sensitive to the accuracy of residual flux measurement and circuit breaker operation.

The influence of tap position on the magnitudes of inrush current has been addressed in [110]. It was considered that adjusting tap changer position to the lowest possible energisation voltage could result in smaller inrush current. So far, this strategy is the most commonly applied. The effectiveness of this technique has been proven in the cases of energising generator step-up transformers in high voltage networks [51, 85].

2.5 Summary

This chapter reviewed the published work studying transformer energisation transients, regarding the following aspects:

- Approaches for calculating transformer inrush current;
- Modelling system components in EMTP for transformer energisation studies;
- Investigation case studies of transformer energisation transients;
- Possible measures for mitigating transformer inrush current.

The main findings from previous research are summarized as follows:

For calculation of inrush currents:

- Simple analytical equations can only provide rough estimation of inrush current for single phase transformers; for studying the network-wide impacts of three-phase transformer energisation transients in large-scale networks, the use of

EMTP-type simulation tools are preferred.

For modelling system components in EMTP to study transformer energisation transients:

- BCTRAN+ and single-phase STC transformer models, which only require commonly available transformer test report data and empirical parameters, are more frequently used;
- Constant frequency distributed model (Bergeron model) is preferred for representing transmission overhead lines and cables;
- Circuit breaker can be simplified as ideal time-controlled switch but attention should be paid to modelling closing time span;
- Source network can be modelled by an ideal sine-wave source and a Thevenin equivalent impedance of the part of the network not under study;
- Loading can be treated as constant impedance model with constant resistance in parallel with constant inductance.

For investigation of transformer energisation transients:

- Mechanical forces on transformer winding generated by inrush currents can be larger than that generated by short-circuit currents; the longer duration stress imposed by the inrush currents can lead to reduction of insulation capability and may cause insulation failures a certain time after transformer energisation;
- Energising a transformer into a system where there are adjacent transformers already connected can induce sympathetic interaction which can dramatically change the duration of the inrush transient; line resistance and the losses in the transformer loop are the key factors influencing sympathetic interaction, while line inductance and transformer loading have negligible effects;
- The inrush currents resulted from transformer energisation are rich in harmonics, with the second harmonic as the dominant one; this characteristic can be utilized to prevent the protection relay from mistaking the inrush with internal faults; however, it incurs harmonic resonant overvoltages in systems with low resonant frequencies and low degree of damping;
- Significant voltage dips can be produced by transformer energisation; the dip magnitude is influenced by circuit breaker closing time, residual flux, the number of transformers being energised simultaneously, system loading and source strength;

- Transformer energisation transients are decided by stochastic parameters; Monte-Carlo simulation have been applied to statistically estimate inrush current for a single phase transformer and harmonic overvoltages;
- Existing approaches for mitigating inrush current are costly to be applied and they all have limitations which restrict their application.

The literature review further indicates that:

- For studying transformer energisation transients in EMTP, system components modelling can be targeted on the frequency range between 0.1 and 1 kHz;
- Investigation of sympathetic interaction between transformers is only limited to simple theoretical analysis and parametric studies; understanding of the impact of sympathetic interaction on other energisation transients is lacking;
- Voltage dips caused by transformer energisation were deterministically assessed under the commonly agreed worst case energisation condition in most of previous studies; however, the probability of reaching such a condition is unclear yet;
- Although sympathetic interaction between wind turbine transformers was addressed, the relations between sympathetic interaction and energisation sequence have not been systematically studied.

In this thesis, voltage dips caused by transformer energisation and sympathetic interaction between transformers are investigated in two systems: one is a 400 kV transmission grid and the other one is a 33 kV wind farm collection grid; modelling approaches summarized from the literature review are taken as the modelling guidelines for developing network models in ATP/EMTP for the two systems; the following topics, which were not systematically addressed in the literature, are the main research focuses:

- Investigate the influence of sympathetic inrush on voltage dips caused by transformer energisation;
- Stochastically estimate voltage dips caused by energisation of large GSU transformer;
- Identify the energisation sequence resulting in less sympathetic inrush between wind turbine transformers.

Chapter 3 Field Measurements, Network Model Development and Validation

When accommodating new generation connections, several long-duration voltage dip events occurred due to energising large GSU transformers into a 400 kV transmission system with long transmission lines between the supply sources and the transformers being energised. The long duration voltage dip events triggered low voltage alarms and led to power quality issues at the downstream distribution grids. In order to investigate the possible influential factors, assess the severities of the events and guide future plant operation, a number of field measurements were carried out to evaluate the voltage and current variations; based on this, a detailed network model was developed and validated against the field measurement results, which help further systematic simulation assessments. In this chapter, the system configuration, voltage dip events, field measurements, network model development and validation are given in detail.

3.1 South West Peninsula system

National Grid's transmission system in England & Wales consists of approximately 7200 km of overhead lines and 700 km of underground cables, operating at 400 kV and 275 kV, as shown on the left in Figure 3-1. The transmission system in the South West, as shown on the right in Figure 3-1, consists of a 360 km loop of 400 kV double-circuit transmission lines starting from Melksham substation in Wiltshire, running through Hinkley Point and Taunton, down to Alverdiscott and Indian Queens, and back through Landulph, Langage, Exeter, Mannington and Nursling, where it connects with the rest of the transmission system at Lovedean in Hampshire. Network with such a loop arrangement reliably supplies the local demand. The peak demand is about 2000 MW in the region of the South West Peninsula (as indicated by the shaded area in Figure 3-1). However, for many years, the total installed capacity in South West Peninsula, mainly from Hinkley Point nuclear stations, has been only about 1400 MW, which implies this region was heavily relying on the power feeding from nearby networks.

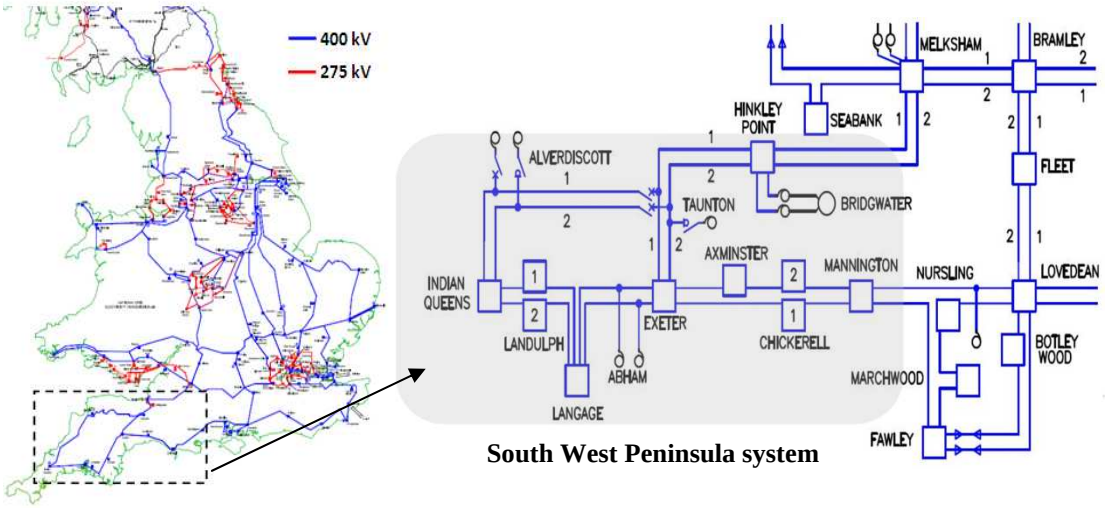

Figure 3-1 South West Peninsula system as part of National Grid's transmission system in England & Wales

In 2009, a new Combined Cycle Gas Turbine (CCGT) power plant, with total installed capacity of 905 MW, was commissioned and connected to the Lagage substation, which is to underpin the National Grid's reinforcement to the South West Peninsula system. In the future, it is estimated that the local demand will modestly increase, yet significant renewable generations are to be installed, driven by the commitments to connect more low carbon generations to the transmission system. As shown in Table 3-1, substantial amounts of generations have been approved and they will be connected to the South West Peninsula in the near future.

Table 3-1 Plan of new generation installations at the South West Peninsula system [111]

Area	Completion Date	Generation Name	Substation	Plant Type	Total Installed Capacity (MW)
South West	31/10/2014	Atlantic Array Stage 1	Alverdiscott 400 kV	Wind Offshore	302
South West	31/10/2015	Atlantic Array Stage 2			404
South West	31/10/2016	Atlantic Array Stage 3			404
South West	01/09/2017	Hinkley Point C Stage 1	Hinkley Point 400 kV	Nuclear	1670
South West	31/10/2017	Atlantic Array Stage 4	Alverdiscott 400 kV	Wind Offshore	405
South West	01/09/2018	Hinkley Point C Stage 2	Hinkley Point 400 kV	Nuclear	1670

To accommodate these incoming generations, it is important to assess the impacts caused by generation connection on the system reliability and power quality. Indeed, during the connection of the CCGT power plant, long duration voltage dips occurred when GSU transformers were energised, which are detailed in the following sections.

3.2 Transmission grid under detailed study

The shaded network in Figure 3-1 is illustrated by the schematic diagram in Figure 3-2. All substations are renamed by capital letters to facilitate the descriptions thereafter.

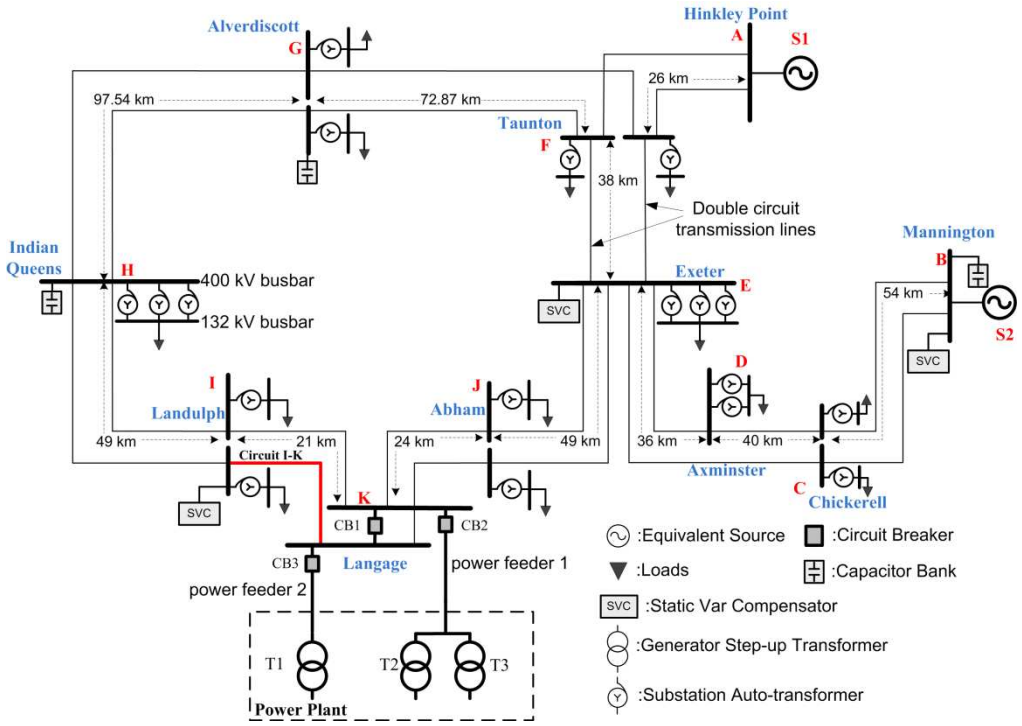

Figure 3-2 Schematic diagram of South West Peninsula system under detailed studies

The system consists of 11 substations, some of which accommodates a number of autotransformers (400/132/13 kV, 240 MVA, YNa0d11). Substations are linked by 400 kV double circuit transmission lines with lengths ranging from 21 to 97.54 km. The networks beyond substation A and B are represented by two equivalent sources, because there are generating plants located around these two substations. There are capacitor banks located at the substations H, G and B, Static Var Compensator (SVC) devices connected at substation I, E and B, and a synchronous compensator connected at H (not explicitly shown in Figure 3-2). The substation K, which provides transmission access to the power plant, comprises two bus sections linked by a coupling circuit breaker CB1 which is normally closed; there are two 400 kV circuits connecting substation K with I and two 400 kV circuits connecting K with J, respectively; through power feeder 1, two GSU transformers, T2 (345 MVA, 400/19 kV, YNd1) and T3 (415 MVA, 400/21 kV, YNd1), are connected to the busbar of substation K via CB2; through power feeder 2, GSU transformer T1 (345 MVA, 400/19 kV, YNd1) is connected via CB3.

3.3 Voltage dip events

In order to connect the power plant to the transmission grid, energisation of the GSU transformers from the high voltage network should be performed first to gain power supply from the main grid; the external supply is then used to power the auxiliary equipment which are necessary for heating up the gas and steam turbines; finally the generators can be synchronized.

At the commissioning stage of the power plant, two attempts were made to simultaneously energise GSU transformers T2 and T3. Prior to the first attempt:

- the synchronous compensator located at substation H, whose capacity is 140 MW, was not connected;
- the coupling circuit breaker CB1 at substation K was closed;
- all circuits in the 400 kV transmission grid were in service;
- GSU transformer T1 was already connected to the grid through power feeder 2, but the generator unit was not synchronized.

When the first attempt was conducted by closing the CB2, voltage dips were observed in the South West system, as shown in Figure 3-3 (voltages shown are line-to-line voltage).

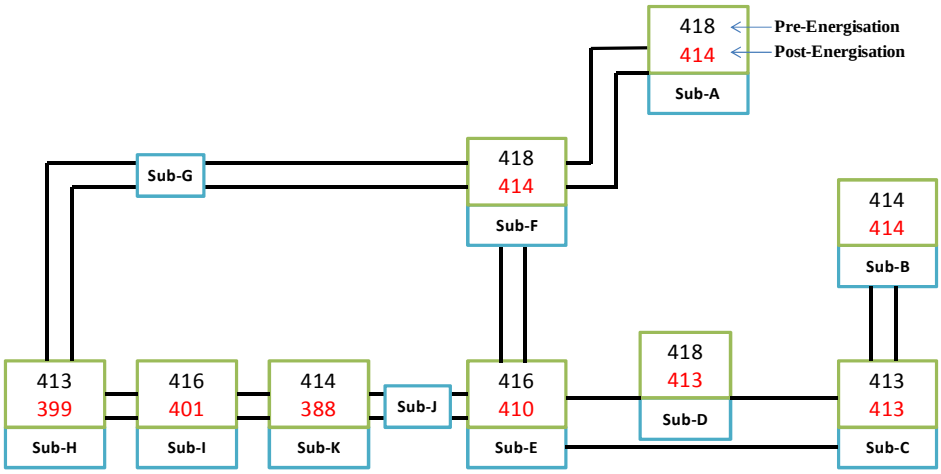

Figure 3-3 South West Peninsula voltage depression resulted from the first attempt

Voltage dips in those substations in proximity to the power plant were relatively large; the maximum voltage dip was observed at substation K, which was about 7.8%. As consequences of the dips, there were responses from reactive compensation around the South West system; low voltage alarms in the Integrated Energy Management System were triggered and downstream distribution utilities were affected.

Several days after the first attempt, the CB2 was opened for carrying out further commissioning, which led to the second attempt of energising T2 and T3. The initial system conditions prior to the second attempt were similar to those in the first attempt except that more proactive measures were taken to reinforce reactive power support. Dynamic System Monitoring equipment was set up at substation K to sensitively capture voltage and current variations. During the second attempt, three-phase inrush currents were captured by the current transformers located at power feeder 1, which are shown in Figure 3-4. As can be seen, the maximum peaks of phase A and phase B are almost the same, both of which are about half that of phase C. In addition, three-phase RMS (root mean square) voltage dips were also measured at substation K, which are shown in Figure 3-5. It can be seen that: the resulted three-phase voltage dips were unbalanced; the biggest voltage dip appeared at phase C, which was about 7%.

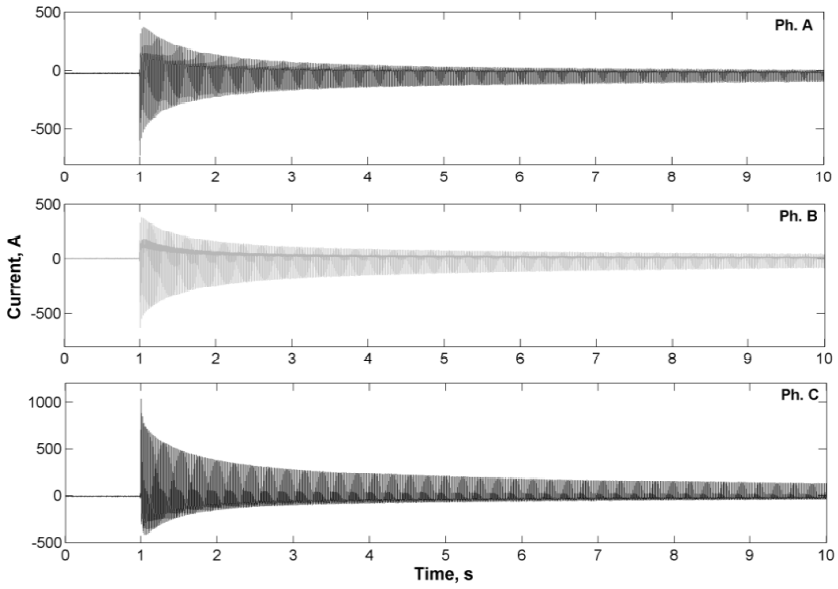

Figure 3-4 Three-phase inrush currents measured in the second attempt

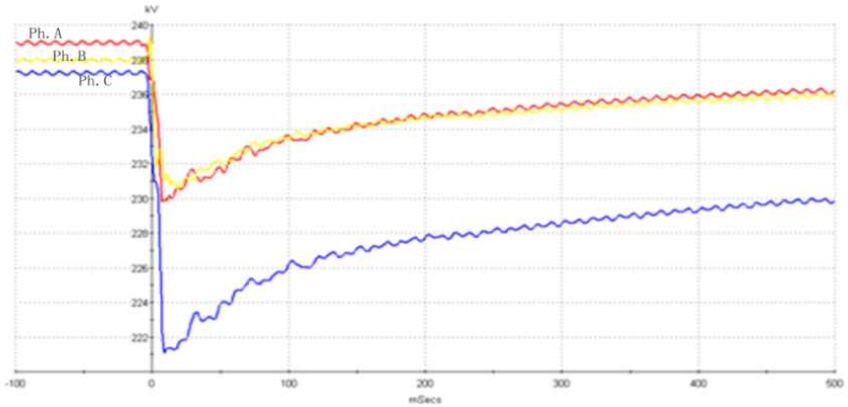

Figure 3-5 RMS voltage dips measured at substation K in the second attempt

3.4 Further field measurements

Since energisation of GSU transformers is a common operation, there are concerns that it would cause severe disturbances. Therefore, further field measurements were conducted to investigate the transient behavior of transformer inrush and voltage dips performance, which also helps develop network model for simulation assessments.

During the time of carrying out field measurements, there were four energisation cases, which are illustrated in Table 3-2. The first two energisation cases (Case E1 and Case E2) were trial energisation made by the power plant engineer by quickly pressing and releasing the circuit breaker closing button. The trial energisation might be to reduce the transformer residual flux. In the energisation Case E3 and Case E4, the circuit breaker closing was completely conducted and the corresponding GSU transformers were successfully energised.

Table 3-2 Four energisation cases in the further field measurement

Cases	GSU transformer being energised	Already connected GSU transformer	Outcome
E1	T2 & T3	No	Trial (on and off)
E2	T2 & T3	No	Trial (on and off)
E3	T2 & T3	No	Success (on)
E4	T1	T2 & T3	Success (on)

For all the energisation cases, currents and voltages were simultaneously measured on a couple of locations including:

- Three-phase currents and voltages at power feeder 1;
- Three-phase voltages at substation I;
- Three-phase currents at the circuit I-K linking substation I and K (the circuit position is highlighted in Figure 3-2).

Measurement was not carried out at power feeder 2 because the monitor on that feeder was not working at the time.

3.4.1 Energisation Case E1

For the energisation Case E1, the three-phase currents and voltages observed at power feeder 1 are shown in Figure 3-6 and Figure 3-8, respectively; the three-phase currents observed at circuit I-K and the voltages observed at substation I are shown in Figure 3-7 and Figure 3-9, respectively.

From the current waveforms shown in Figure 3-6, sharp pulses can be seen at the instant

of energisation t_0, which could be due to the charging of stray capacitance. The interval between the energisation instant t_0 and the inrush starting instant t_1 is about 4 ms. Because the transformer is of star-delta-connection, the inrush currents might be qualitatively analysed by the helping effect theory explained in [112]. At t_1, the inrush started in phase B first; from t_1 to t_2, the inrush in phase B was aided by phases A and C through the medium of the delta winding. At t_2, phase A started to experience its own inrush, as the current began to increase rapidly. This imposed demands on phase C from both phase B and phase A. The two demands were in opposite direction and the helping-current from phase C would flow in the direction of the maximum instantaneous demand. From t_2 to t_3, the phase B current was larger than phase A, so the phase C current remained in positive polarity but decreasing. At t_3, the demand from phase A and phase B were equal in magnitude but opposite in polarity, therefore the helping-current from phase C became zero. After t_3, the current magnitude of phase A was larger than that of phase B, the helping-current in phase C therefore increased in negative polarity. At t_4, the inrush in phase B ceased. From t_4 to t_5, phase B and phase C were helping phase A. This whole process could be repeated in the next cycle; however, due to the circuit breaker opening at t_5, the three-phase currents through power feeder 1 returned to zero.

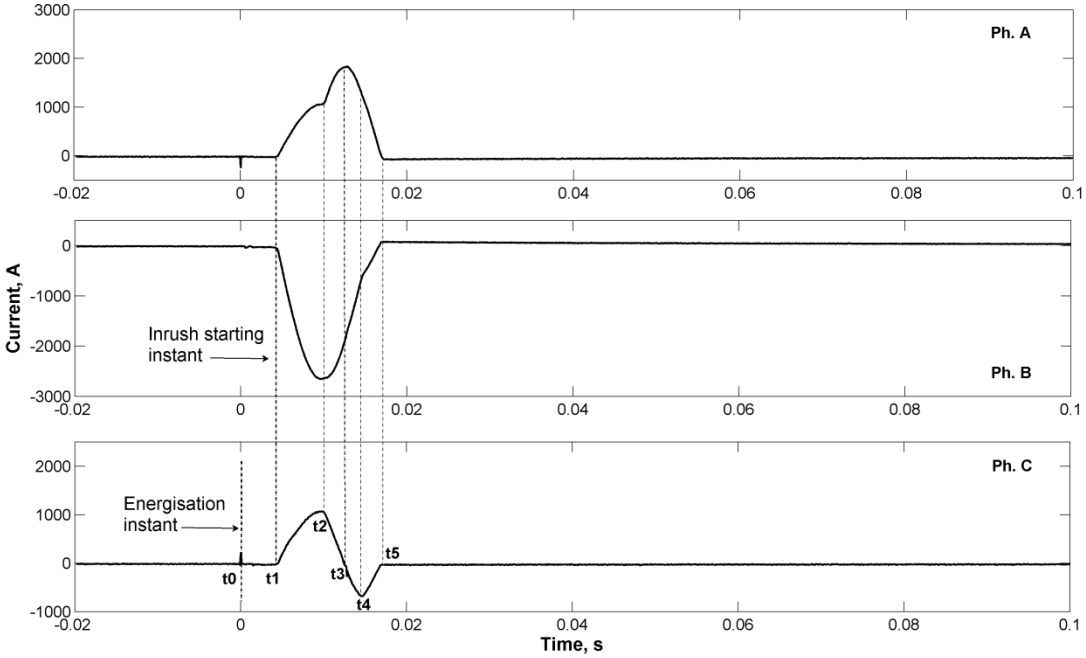

Figure 3-6 Three-phase currents measured at power feeder 1 in Case E1

From the circuit I-K currents shown in Figure 3-7, it can be seen that: before the energisation, the feeder currents only contained steady state load currents flowing

through circuit I-K (the peak magnitudes for phase A, phase B and phase C were 344 A, 346 A and 334 A, respectively); after the energisation, the load currents were superimposed by a portion of inrush currents during the inrush period, which increased current magnitudes of phase B and C and decreased the current magnitude of phase A. After the inrush period, only the load currents flowed through the circuit I-K.

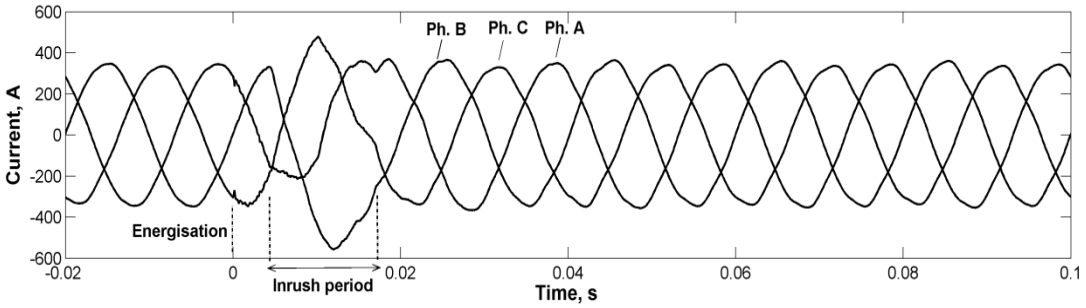

Figure 3-7 Three-phase currents measured at the circuit I-K in Case E1

Figure 3-8 shows the voltage variation observed at power feeder 1. As can be seen, three phases were almost simultaneously energised at the positive-going zero crossing of phase B line-to-ground voltage. The build-up of voltages exhibited distortion due to the influences of the inrush currents. The sharp dip at the voltage trace of phase C was most probably due to the re-ignition when the circuit breaker pole connecting phase C was trying to open at the current zero crossing appeared at the instant t_3 (as shown in Figure 3-6). CB2 was opened at the instant when all three-phase inrush currents decreased to zero (i.e., at the instant t_5 as shown in Figure 3-6). This instant was about 16.9 ms after the energisation instant. The opening of CB2 de-energised the GSU transformers and initiated a ring-down process which involves exchange of energy between electrical field in capacitances and magnetic field in the core of the GSU transformers.

From Figure 3-9, it can be seen that: prior to the energisation, the peak magnitudes of three-phase line-to-ground voltages at substation I for phase A, B and C were 333.8 kV, 333.5 kV and 331.0 kV, respectively. After the energisation, three-phase voltage magnitudes were all reduced by the inrush currents during the inrush period; the most affected phase was phase B whose peak magnitude was reduced by 36.1 kV.

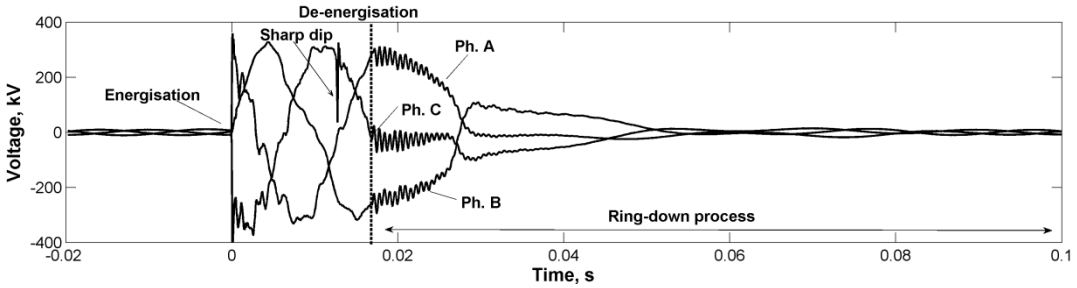

Figure 3-8 Three-phase line-to-ground voltages measured at power feeder 1 in Case E1

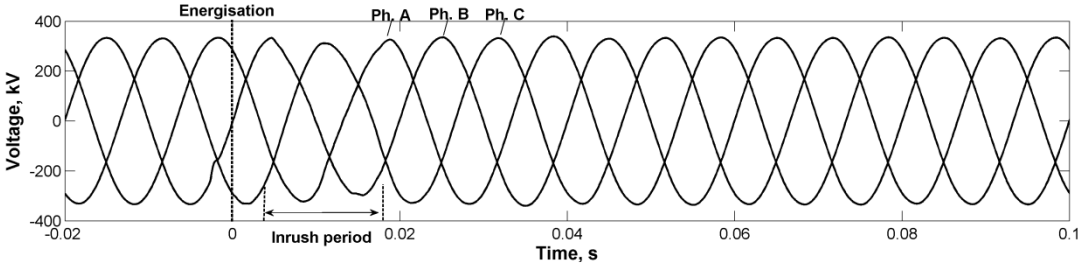

Figure 3-9 Three-phase line-to-ground voltages measured at substation I in Case E1

3.4.2 Energisation Case E2

The energisation Case E2 was carried out about twenty minutes after the Case E1, during which, the closing and opening of CB2 were also finished within one power frequency cycle.

The measured inrush currents are shown in Figure 3-10. The closing time difference among three phases can be interpreted by observing the zoom-in waveforms of the pulse currents: the circuit breaker pole of phase C was the first one being closed, which was followed by the closing of phase A and then the closing of phase B; between the closing of phase C and phase A, the time interval was 0.3 ms; between the closing of phase C and phase B, the time interval was 1.5 ms. The time interval between the energisation instant of phase C and the inrush starting instant was about 4.5 ms, which is 12.5% longer than that observed in Case E1. It can be also seen that the inrush started from phase B first and, from the inrush starting instant to its peak, it was accompanied by the helping-effect currents from phase A and phase C; after its peak, inrush also appeared in phase A. The total inrush time only lasted for about 8.2 ms which is less than half cycle. The inrush current peak magnitudes were significantly lower than those observed in Case E1. As can be seen in Figure 3-11, during the inrush period, the small inrush current being superimposed on the load currents flowing through circuit I-K, only caused a slight distortion.

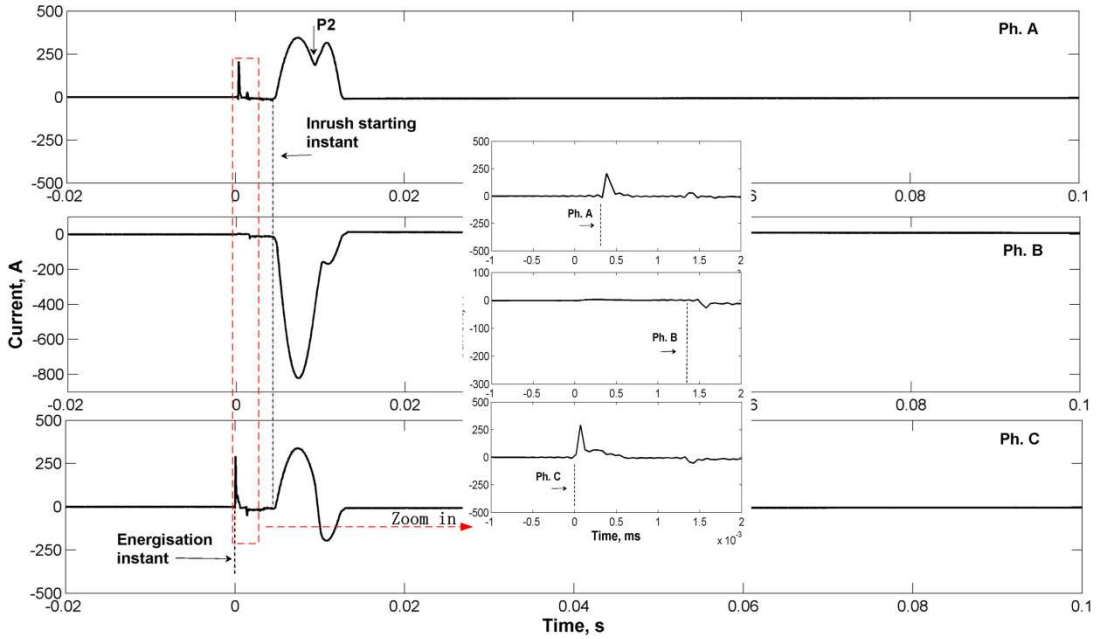

Figure 3-10 Three-phase currents measured at power feeder 1 in Case E2

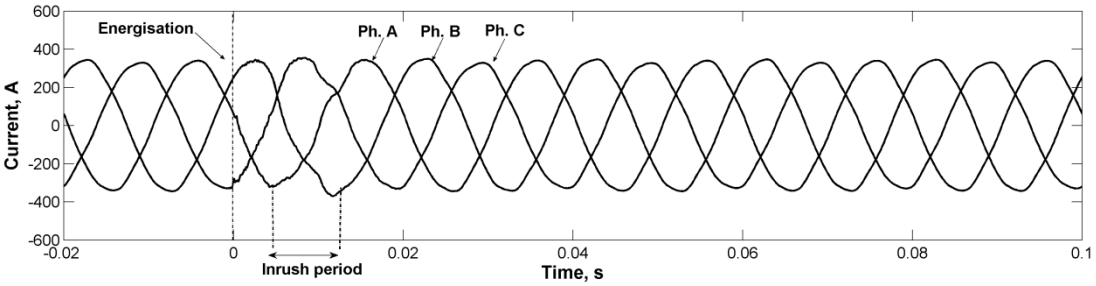

Figure 3-11 Three-phase currents measured at circuit I-K in Case E2

The voltage waveforms measured at power feeder 1 are shown in Figure 3-12. It can be seen that: phase A was energised almost at the negative-going zero crossing; however, it was not the phase which experienced the biggest inrush peak. In fact, the peak magnitude of phase B inrush current was the biggest, according to Figure 3-10. This indicates that the forming of inrush might be influenced by residual flux. Once the inrush currents decreased to zero, the transformers were de-energised. The de-energisation time was about 13 ms after the energisation instant. Following the de-energisation, the ring-down transient began. Due to the small inrush current magnitudes, the voltages observed at substation I after the energisation were only slightly affected, as shown in Figure 3-13.

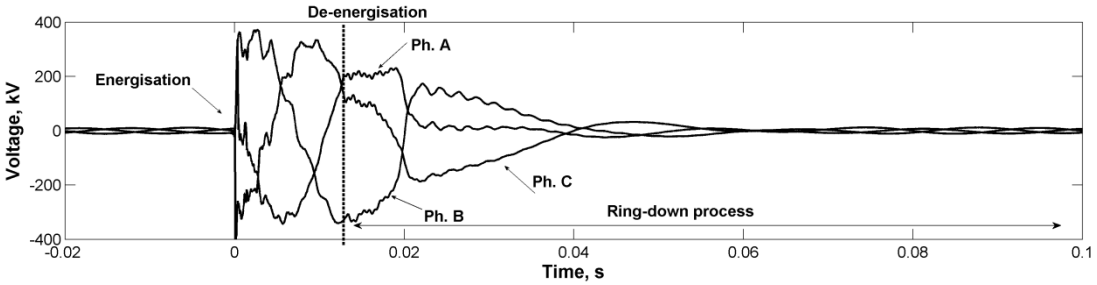

Figure 3-12 Three-phase line-to-ground voltages measured at power feeder 1 in Case E2

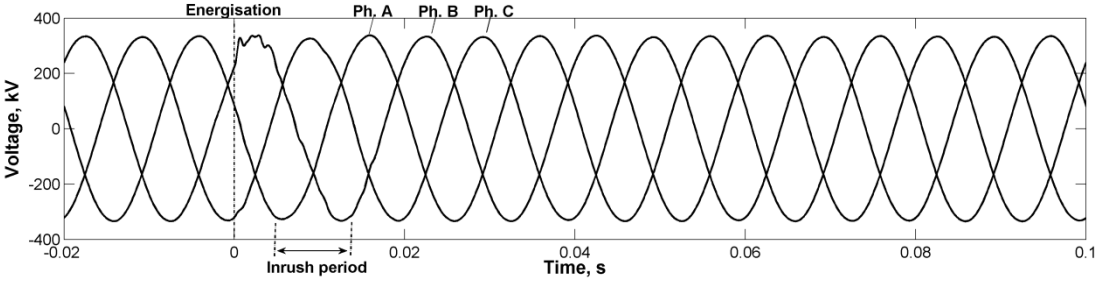

Figure 3-13 Three-phase line-to-ground voltages measured at substation I in Case E2

3.4.3 Energisation Case E3

In the energisation Case E3, the GSU transformers T2 and T3 were successfully energised. The measured three-phase currents are shown in Figure 3-14. It can be interpreted that: the interval between the energisation instant and the inrush starting instant is about 2.4 ms; the inrush started from phase C first and then followed by phase B; phase A was the phase helping the inrush in phase C and B; the first peaks of phase A, phase B and phase C were of 950 A, 2160 A and 1400 A, respectively.

In Figure 3-15, the inrush currents with a longer time range is illustrated. As can be seen, about seven cycles after the energisation, the inrush current waveforms of phase B and phase C abruptly jumped. This abrupt change of inrush current waveform could be due to the inaccurate measurement caused by the saturation of the current transformer (CT). It will be further addressed in the section regarding CT modelling and simulation.

The variation of three-phase currents measured at circuit I-K is illustrated in Figure 3-16. Prior to the energisation, the magnitudes of the measured three-phase load currents were about 336 A, 340 A and 326 A for phase A, phase B and phase C, respectively. After the energisation, the load currents were superimposed by a portion of inrush currents.

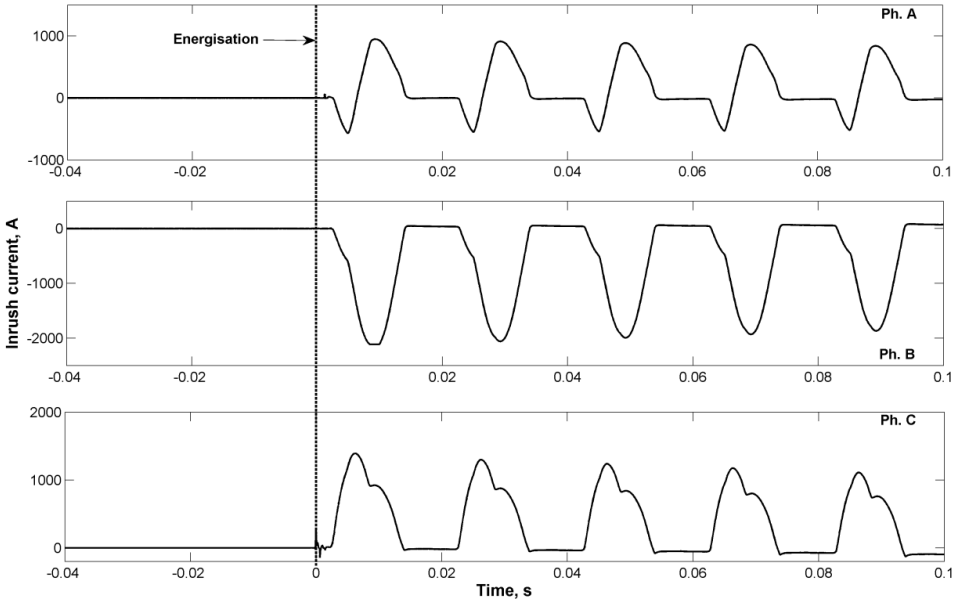

Figure 3-14 Three-phase currents measured at power feeder 1 in Case E3 (initial cycles)

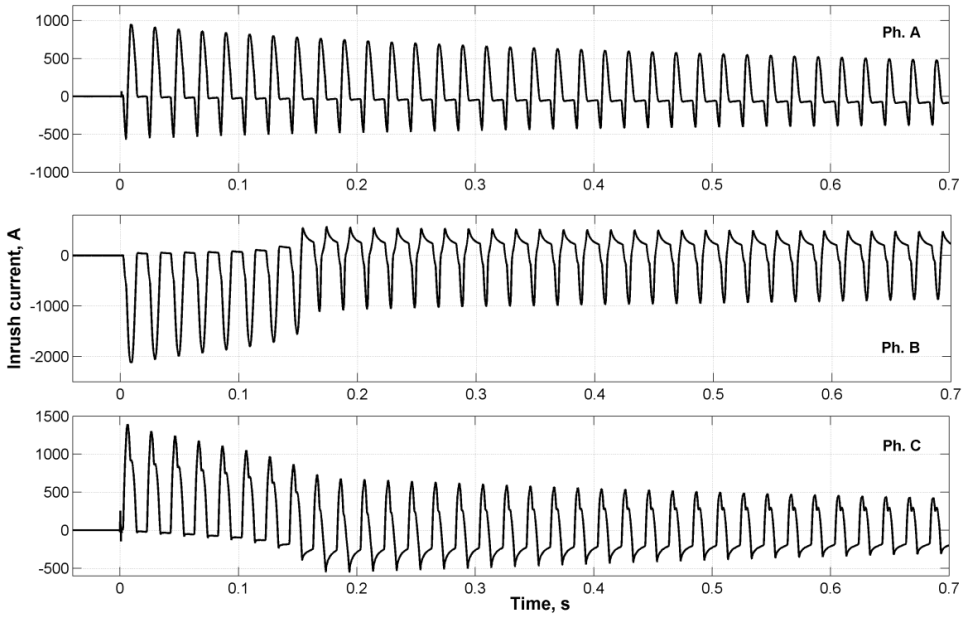

Figure 3-15 Three-phase currents measured at power feeder 1 in Case E3 (long duration)

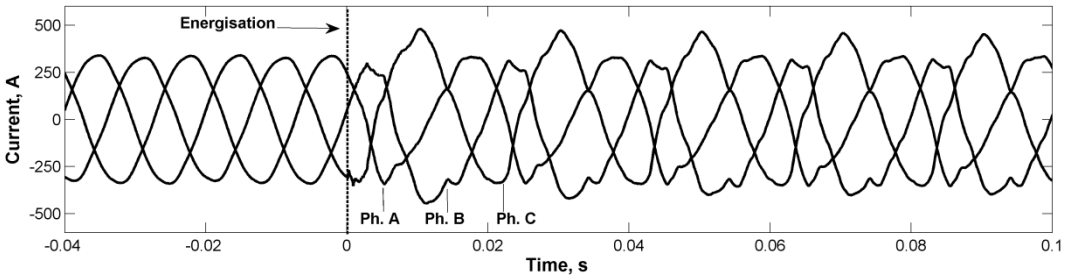

Figure 3-16 Three-phase currents measured at the circuit I-K in Case E3

Before and after energisation, three-phase voltages observed on power feeder 1 are shown in Figure 3-17. The closing time, as one of the important initial conditions for

inrush transients, can be identified. It can be interpreted that: the closing of circuit breaker was made on phase C first at about 5 ms behind the negative-going zero crossing of phase C line-to-ground voltage; the other two phases were energised both with a closing time delay of about 1 ms. If the residual fluxes of the energised transformers were zero, the closing time would have resulted in minimum peak of inrush current on phase C. However, Figure 3-14 shows that the phase A was of minimum inrush current peak, which could be due to the existence of residual flux in the transformer core. Comparing the peak magnitudes of inrush currents with that resulted from the second attempt presented in section 3.3, it can be seen the maximum peak is twice as much as that shown in Figure 3-4.

The RMS variations of the voltages observed at substation I are shown in Figure 3-18 (Note that the RMS calculation for field measurement results was based on one power frequency cycle window and refreshed half power frequency cycle). It can be seen that the dip magnitudes were about 5.5 kV (2.3%), 14.2 kV (6%) and 9.35 kV (4%) for phase A, B and C, respectively. In addition, it can be identified that the rate of the initial voltage dip recovery was faster than that of the later stage, which will be shown that it was due to the SVC compensation.

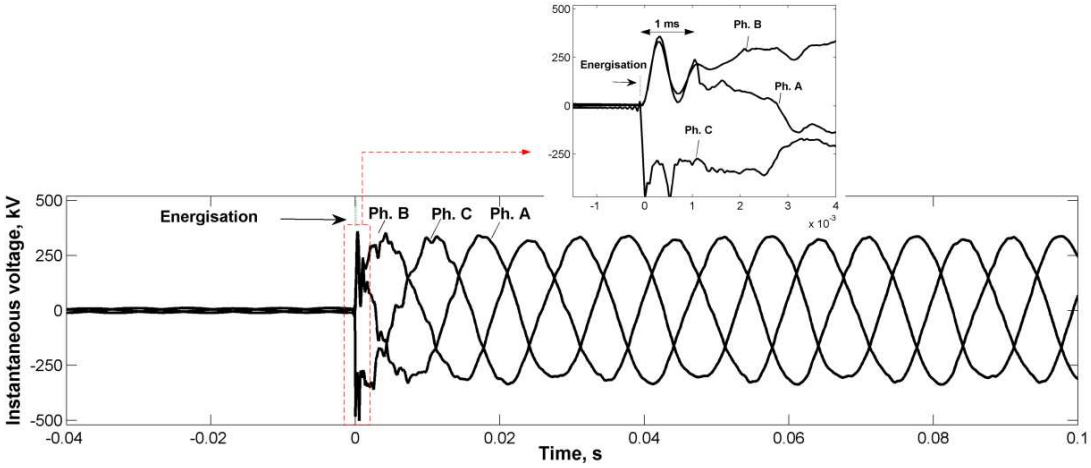

Figure 3-17 Three-phase line-to-ground voltages measured at power feeder 1 in Case E3

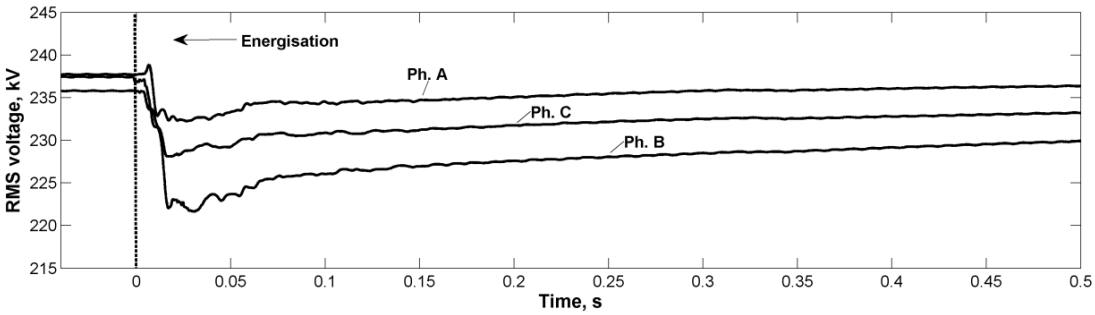

Figure 3-18 Three-phase RMS voltage dips measured at substation I in Case E3

3.4.4 Energisation Case E4

In the Case E4 energisation, T1 was energised, with T2 and T3 already connected. Voltages and currents were measured at the same locations as in the previous cases.

The three-phase currents observed at power feeder 1 are shown in Figure 3-19 in terms of instantaneous current waveforms for a short-time range and in Figure 3-20 in terms of RMS current waveforms for a long-time range. In addition, three-phase voltages observed on power feeder 1 in terms of RMS value are shown in Figure 3-21; three-phase currents observed at the circuit I-K are shown in Figure 3-22.

As can be seen in Figure 3-19, the magnetizing currents of GSU transformers T2 and T3 became gradually larger after transformer energisation, which indicates the initiation of sympathetic inrush. The growth and the decay of the sympathetic inrush currents are further illustrated in Figure 3-20 which shows that the sympathetic inrush currents took about 2 seconds to reach their maximum magnitudes (the largest maximum magnitude appeared in phase C, which is about 120 A in RMS) and the decay lasted more than 25 seconds. With the presence of the long duration sympathetic inrush, it can be seen in Figure 3-21 that the system took a long time to achieve full recovery of three-phase voltages.

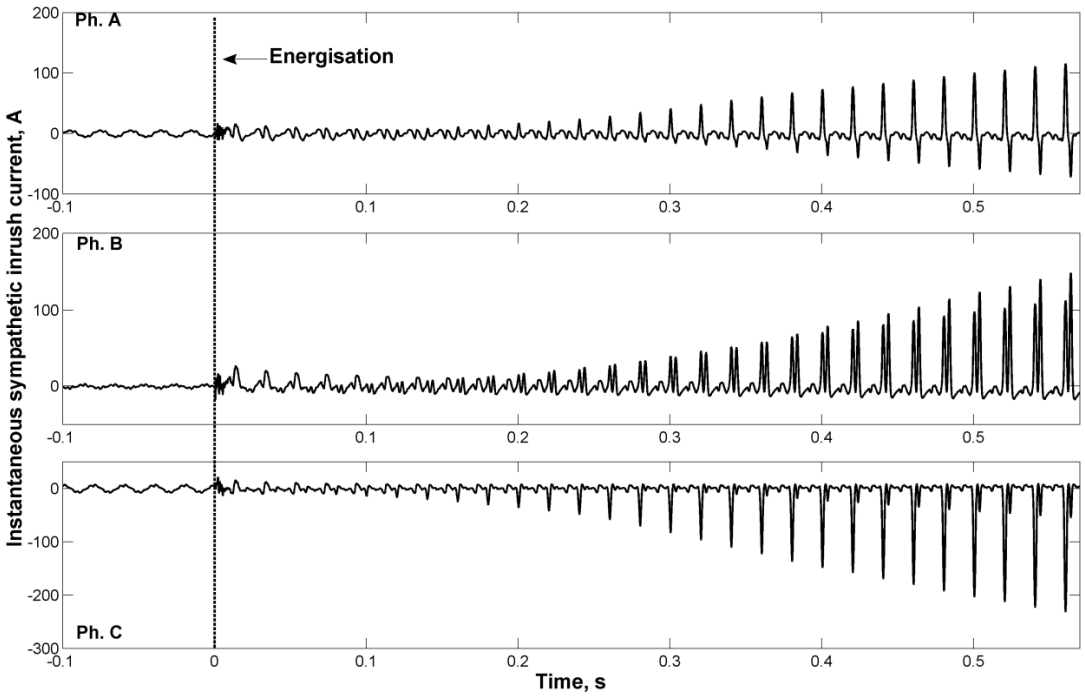

Figure 3-19 Sympathetic inrush currents measured at power feeder 1 in Case E4

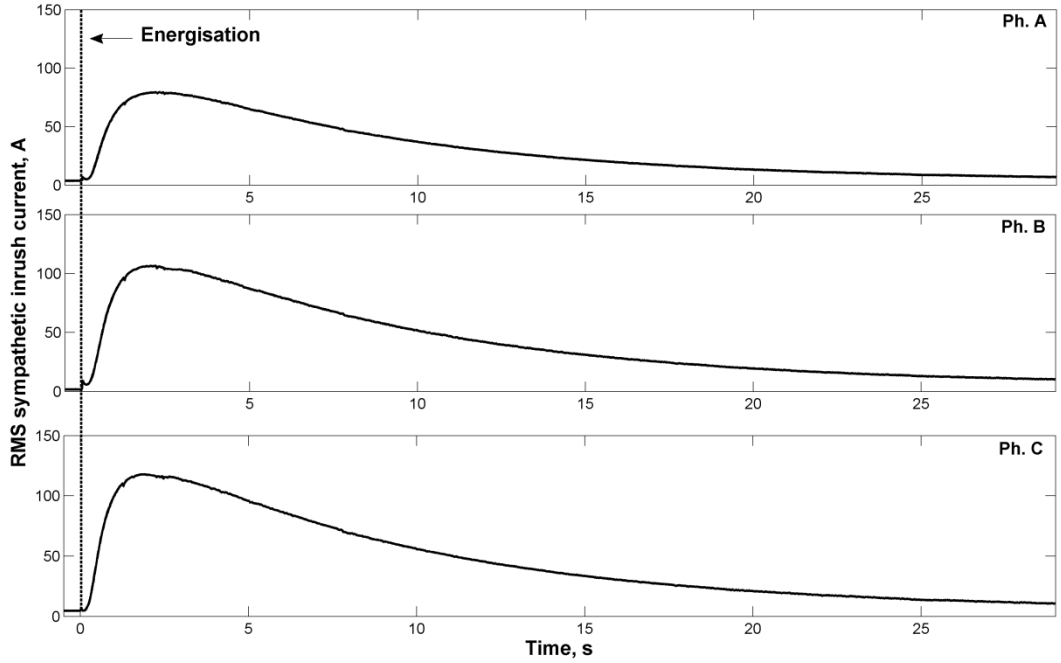

Figure 3-20 RMS sympathetic inrush current measured at power feeder 1 in Case E4

Similar to the one shown in Figure 3-16, the currents measured at circuit I-K shown in Figure 3-22 can be divided into two parts: the first part is, before energisation, the steady state load currents flowing through the circuit; the second part is, after energisation, the steady state load currents superimposed by a portion of transformer inrush currents.

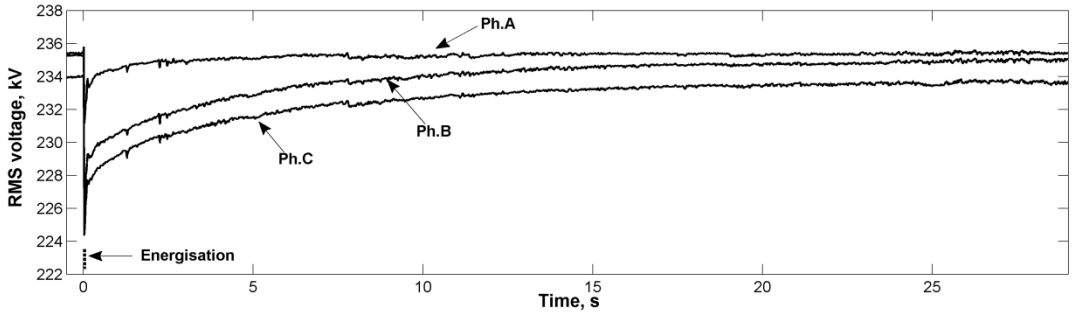

Figure 3-21 RMS voltage dips measured at substation I in Case E4

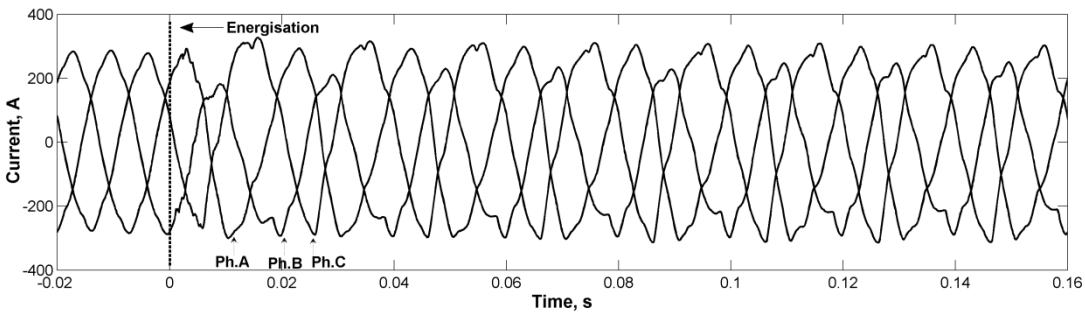

Figure 3-22 Currents measured at circuit I-K in Case E4

The above field measurement results provide some insights of transformer inrush current transients (in terms of initiation, waveform pattern, decay and peak magnitudes)

and also show the possible influences of transformer inrush current on voltage dips (in terms of the degrees of unbalance among three phases, dip magnitudes and recovery trends). These results will be taken as the benchmarks for validating network models.

3.5 Network model development

Field measurement results indicate that the system would experience unacceptable long duration voltage dips during energisation of GSU transformers, therefore further studies are required to assess this transient phenomenon and its impacts on power system operation. Due to the difficulty in carrying out more field measurements, computer simulation is preferred to conduct more detailed studies. This section describes the development of a network model using ATP/EMTP based on the 400 kV transmission network shown in Figure 3-2.

3.5.1 Equivalent source and impedance

The source S1 and S2 were represented by ideal voltage source. Equivalent source impedances to represent source strength were derived from the short-circuit levels at substation A and B, which are 7.1 GVA and 6.4 GVA, respectively.

3.5.2 Transmission lines

Modelling of double circuit transmission lines are based on following parameters:

- Line length;
- Line dimension;
- Resistivity and diameter of phase conductor and earth wire;
- Number of conductors in a bundle;
- Ground resistivity;
- Transposing scheme.

The lengths of the 400 kV double-circuit transmission lines in the South West system can be referred to Figure 3-2. The longest one is between substation H and G, which is about 97 km. They are based on the similar type of tower structure, as shown in Figure 3-23. Specifically, **a, b** and **c** define the horizontal distances between the phase conductors and the tower central; **g, d, e** and **f** define the vertical heights of phase conductor and earth wire relative to ground surface. They are all determined in accordance to the tower designs shown in Table 3-3. In the table, some other

information including the type of conductor, conductor diameter and resistivity, together with the number of conductors in a bundle, are also provided. Figure 3-24 shows how the tower designs and transposing schemes are associated with each double-circuit line between two substations. With all the line data taken into account, Bergeron model was chosen for modelling transmission lines, because it is more accurate than pi routine for modelling long lines and it is sufficient to represent the line parameters in the frequency range of transformer inrush transient which is normally less than 1 kHz;

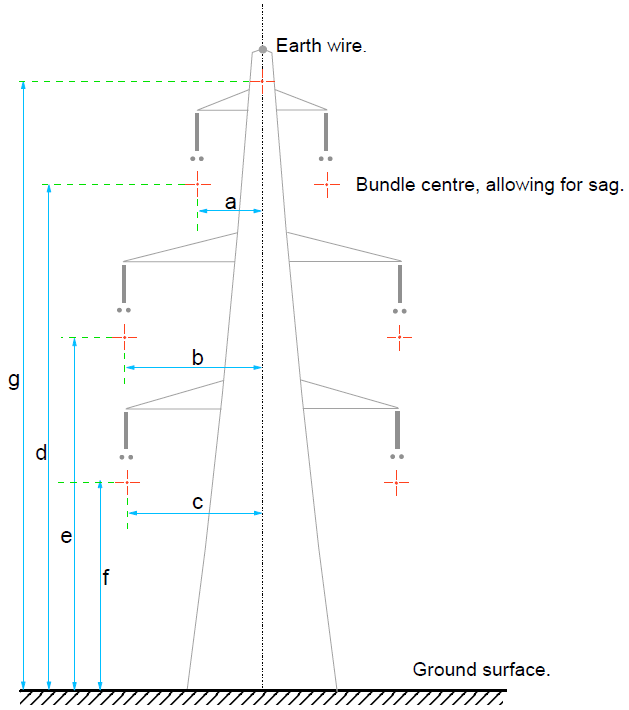

Figure 3-23 Basic tower structure used in South West system [113]

Table 3-3 Line dimension and conductor data [113]

Routine name	**Phase conductor**	**Num.***	**Earth wire**	**Line dimension (m)**						
				a	**b**	**c**	**d**	**e**	**f**	**g**
L2	Z	2	L	5.48	5.71	6.09	27.24	19.47	11.63	34.94
L2/2	RB	2	K	5.48	5.71	6.09	28.54	20.77	12.93	35.60
L6	Z	4	Z	6.93	10.16	8.33	32.26	21.79	12.95	43.09
L6/1	Z	2	Z	6.93	10.16	8.33	32.26	21.79	12.95	43.09

***Num.** represents the number of bundle conductors.*

Conductor name	**Usage**	**Material**	**Outer radius (mm)**	**AC resistance (Ω/km)**
Z = ZEBRA	phase	ACSR	14.31	0.0684
	earthwire	ACSR	14.31	0.0643
L = LYNX	earthwire	ACSR	9.765	0.1489
K = KEZIAH	earthwire	AACSR	9.765	0.1654
RB = RUBUS	phase	AAAC	15.75	0.0558

ACSR: Aluminium Conductors Steel Reinforced; AAAC: All Aluminium Alloy Conductors
AACSR: Aluminum Alloy Conductor, Steel Reinforced.

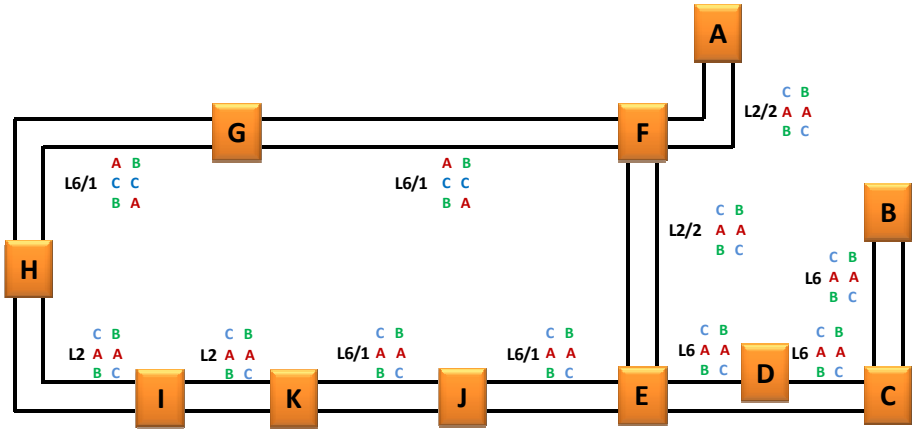

Figure 3-24 Tower designs and transposing schemes associated with double circuit lines

3.5.3 System loading

System loading connected to each substation transformer was modelled by constant lumped impedances connected at 132 kV side, with the power factors of local demands considered. The constant lumped impedance consists of a resistor connected in parallel with an inductor. Based on the system loading data measured at the moment of energisation (as shown in Table 3-4), the values of the resistor were calculated by V^2/P and similarly the values of inductor were calculated by V^2/Q.

Table 3-4 System loading data of the South West system

Substation	V (kV)	P (MW)	Q (MVar)	PF	R (Ohm)	L (mH)
C	132	104	52	0.89	167	1067
D	132	209	89	0.92	84	621
E	132	331	77	0.976	52.5	719
F	132	213	68	0.95	82	813
G	132	187	1.21	0.999	93	45860
H	132	316	138	0.915	55	400
I	132	232	74	0.95	75	750
J	132	252	2.42	0.999	70	22930

V: line-to-line voltage; P: active power; Q: reactive power;
PF: power factor; R: resistor; L: inductor.

3.5.4 Reactive power compensation devices

The reactive power compensation devices in the South West system consist of mechanical switched capacitor banks and Static Var Compensator.

Capacitor bank was modelled by three constant capacitors connected in parallel. In series to each capacitor, the current limiting inductor and resistor for representing losses were also considered. The capacity of each capacitor bank was scaled to 60 MVar.

The SVC device was modelled by a thyristor-controlled reactor (TCR) connected in parallel with a fixed capacitor bank (FC), as shown in Figure 3-25. The TCR comprises a fixed reactor connected in series with a set of by-directional thyristors. A control module to vary the firing angle of the thyristor valves was integrated in the model to continuously change the reactive power output from the reactor. If the TCR is controlled to operate in conduction, the output of SVC is the net difference of the reactive power between the TCR and the FC. If the TCR is off, the output of SVC is then only contributed by the FC.

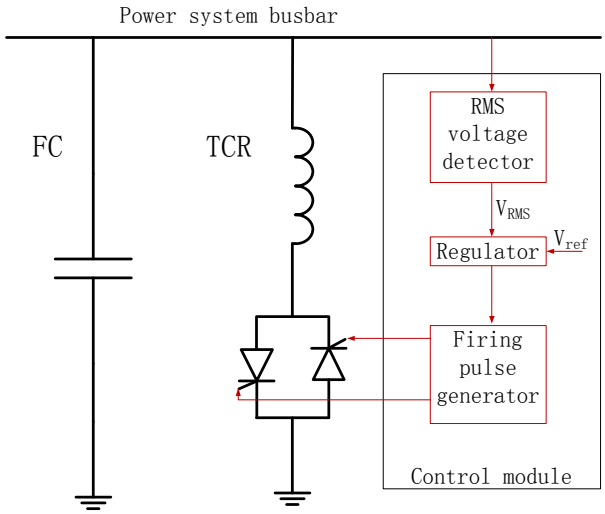

Figure 3-25 Schematic diagram of SVC configuration

The control module, as shown in Figure 3-25, consists of three building blocks:

- RMS voltage detector
- Regulator
- Firing pulse generator

Continuously, the RMS voltage detector processes the phase voltages measured at the 400 kV busbar to provide the RMS value of three averaged line-to-line voltages (V_{RMS}). The V_{RMS} is then compared with the V_{ref} in the regulator to produce a benchmark. The benchmark and the measured line voltages are the inputs for the firing pulse generator to produce firing pulses for controlling the operation of bi-directional connected thyristors, which is achieved by following the procedure shown in Figure 3-26.

First of all, the line voltage is compared with a zero threshold to produce two opposite square waves with a 1 pu magnitude. In this way, the ranges between two adjacent voltage zero crossings suitable to give firing pulses are identified. In the next step, both square waves are processed by an integrator and a high pass filter, resulting in two

triangle waves. Comparing these two triangle waves with a 0.005 threshold, the positive parts of the two triangle waves are selected and then summed to produce another triangle wave with a frequency of 100 Hz. This new triangle wave is then compared with the benchmark obtained from the regulator: the parts of the triangle wave with magnitude less than the benchmark result in zero output; the other parts result in outputs of 0.5. The comparison gives a square wave that is processed by a high pass filter to generate firing pulses. The variation of the benchmark will change the width of the square wave so as to vary the timing of firing pulses. As a result, the reactive power output of the TCR can be varied, which subtracts the output of the FC so as to vary the output of the SVC.

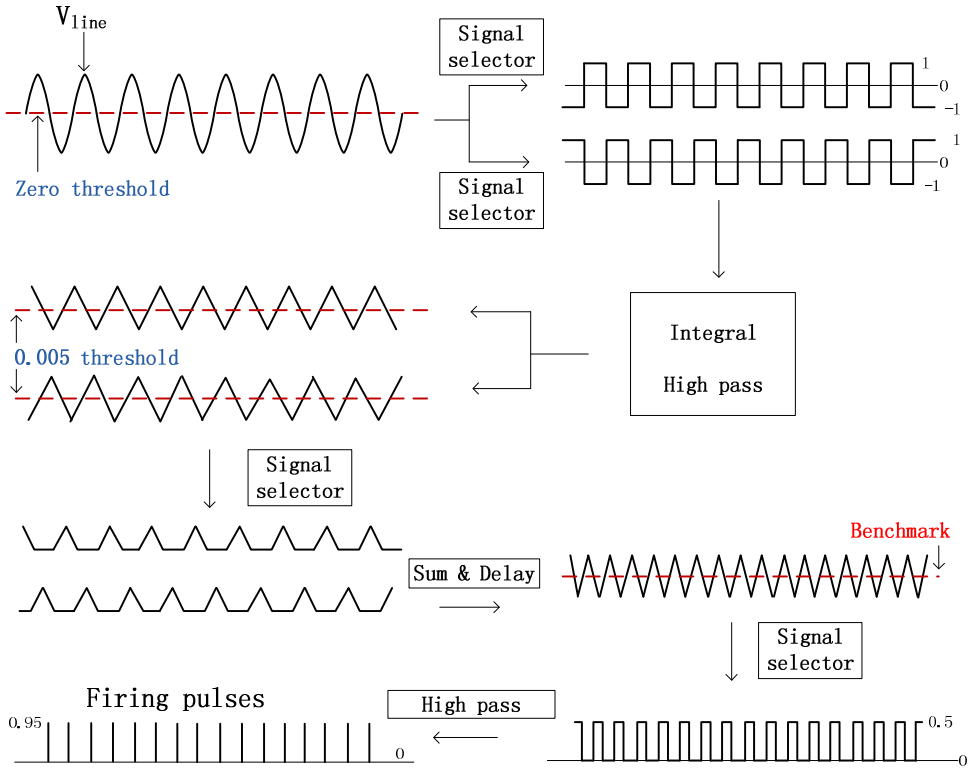

Figure 3-26 Procedure for generating firing pulses to control bi-directional thyristors

3.5.5 Transformers

3.5.5.1 Modelling GSU transformers

The transformer modelling approach suggested and validated in [6] was used to model GSU transformers. It consists of two parts: a linear BCTRAN object to represent transformer short-circuit characteristics; a set of delta connected nonlinear inductors, located at the Low-Voltage (LV) terminal of the BCTRAN object, to represent transformer core saturation characteristics (this model is named here as BCTRAN+).

The test report data of 345 MVA and 415 MVA GSU transformers are shown in Table 3-5 and Table 3-6, respectively. The BCTRAN object utilizes the nameplate data and the short-circuit test data, including rated power, rated voltages, short-circuit impedance, full load losses and winding connection, to model the transformers.

Table 3-5 GSU transformer test report (T1&T2, 345 MVA)

Nameplate data	**[kV]**	**[MVA]**	**[A]**	**Coupling**
HV	400	345	498	YN
LV	19	345	10483	d1
Open-circuit	**E_o[kV,%]**	**[MVA]**	**I_o[%]**	**P_o[kW]**
LV	17.1(90)	345	0.049	126.2
	19(100)	345	0.103	174.1
	20.9(110)	345	0.350	239.9
Short-circuit	**[kV]**	**[MVA]**	**Z%**	**P_s[kW]**
HV/LV	400/19	345	17.8	838.4

Table 3-6 GSU transformer test report (T3, 415 MVA)

Nameplate data	**[kV]**	**[MVA]**	**[A]**	**Coupling**
HV	400	415	599	YN
LV	21	415	11410	d1
Open-circuit	**E_o[kV,%]**	**[MVA]**	**I_o[%]**	**P_o[kW]**
LV	18.9(90)	415	0.05	156.8
	21(100)	415	0.069	211.1
	23.1(110)	415	0.179	290.8
Short-circuit	**[kV]**	**[MVA]**	**Z%**	**P_s[kW]**
HV/LV	400/21	415	17.12	924.7

Open-circuit test data were used to derive saturation curves for the nonlinear inductors. Type-96 nonlinear inductor (enables the setting of initial residual flux) was selected for GSU transformers. The conversion procedure for obtaining hysteresis saturation curves for type-96 nonlinear inductor is shown in Figure 3-27, which consists of four steps:

- Step 1: transform RMS voltage versus current data (V_{rms}-I_{rms}) into peak flux-current data (λ_{peak}-i_{peak}) based on the algorithm presented in [57] (a MATLAB program was specifically developed based on the algorithm for carrying out the transformation);
- Step 2: curve fit the λ_{peak}-i_{peak} data to obtain a piecewise nonlinear saturation curve;
- Step 3: select a positive saturation point from the piecewise nonlinear curve for ATP subroutine HYSDAT [58] to derive a hysteresis loop;
- Step 4: assign an additional point beyond the saturation point to set the saturation inductance deduced from transformer air-core inductance, with the effect of winding leakage inductance considered [52].

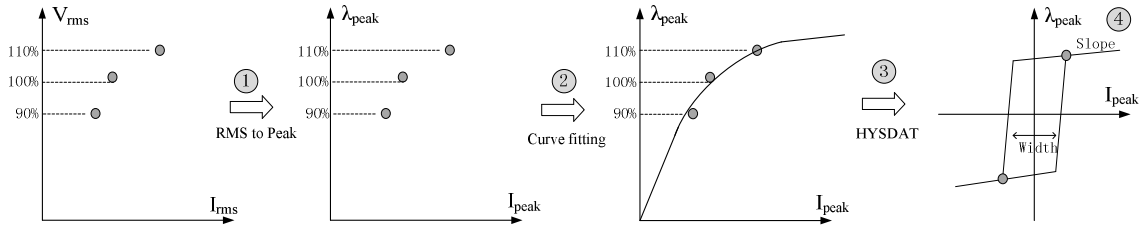

Figure 3-27 Conversion to derive saturation curve for type-96 nonlinear inductor

Figure 3-28 shows the lower half hysteresis curves for the GSU transformers. The saturation points used to define the corresponding major hysteretic loop are appointed; beyond the saturation points, the final slopes of saturation curves are quantified by $\Delta\lambda/\Delta i$.

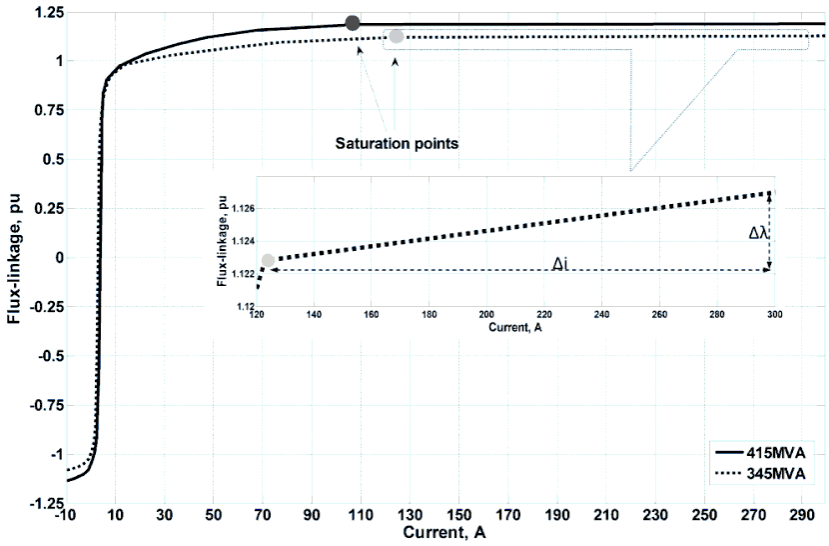

Figure 3-28 lower half hysteresis curves for GSU transformers

It was assumed that the air-core inductance is equal to twice of transformer short-circuit inductance. This assumption is reasonable, because, when an unloaded two winding core type transformer is energised from the HV winding side (usually the outer winding), the cross section area of the air-core cylinder enclosed by the HV winding where the flux goes through under deep saturation is normally about twice the cross section area of the gap between HV and LV windings where the flux goes through during the short-circuit test.

To preliminarily check the accuracy of the models, simulation of open circuit test was applied to the developed BCTRAN+ models for the GSU transformers. Results obtained from testing 415 MVA and 345 MVA GSU transformer models are shown in Figure 3-29 and Figure 3-30, respectively. In both figures, the simulated no-load current and

no-load losses as a function of magnetizing voltage (under 0.9 pu, 1 pu and 1.1 pu of rated voltage) are compared with that given in the transformer test report, which show good agreements between measured and simulation results.

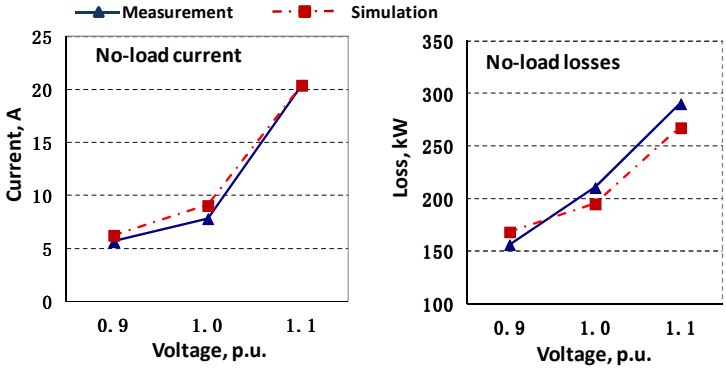

Figure 3-29 Open circuit test results deduced from GSU transformer model (415 MVA) compared to manufacture test results

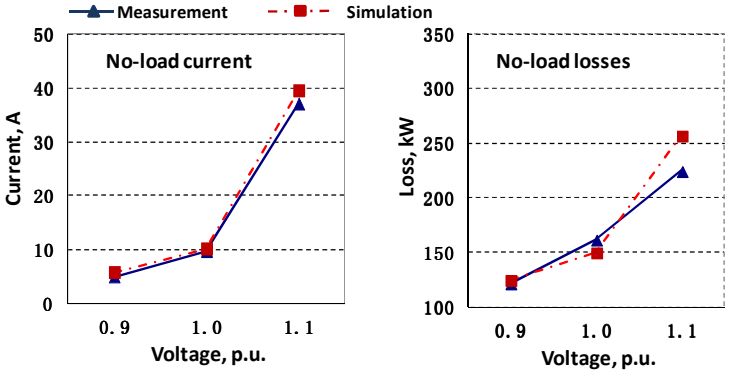

Figure 3-30 Open circuit test results deduced from GSU transformer model (345 MVA) compared to manufacture test results

Furthermore, the BCTRAN+ models were tested regarding inrush current calculation, with results compared with those generated by the more advanced Hybrid Transformer model (including 3-limb and 5-limb core models, as the core configuration of the transformers was unclear). To do the comparison, the $\lambda - i$ curves used in the BCTRAN+ model (i.e., the curves shown in Figure 3-28) were also used to implement the Hybrid Transformer models; the models were energised on the primary side at the same switching angle against an ideal 400 kV voltage source, with residual flux assumed to be zero. The energisation cases, including energising 345 MVA transformer at phase A voltage zero-crossing, energising 415 MVA transformer at phase A voltage zero-crossing and energising 415 MVA transformer at phase A voltage peak, were simulated and the results comparison are shown in Figure 3-31, Figure 3-32 and Figure 3-33, respectively.

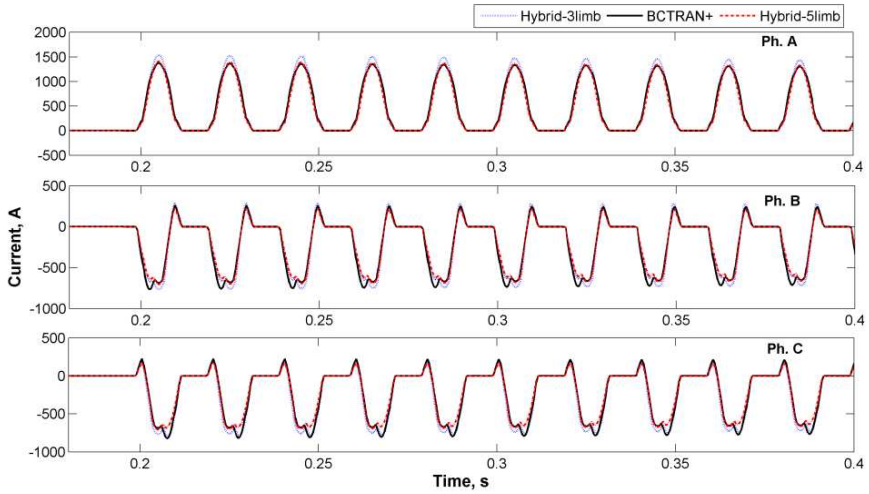

Figure 3-31 Comparison of inrush currents generated by Hybrid and BCTRAN+ for 345 MVA transformer (Energised at phase A voltage zero-crossing)

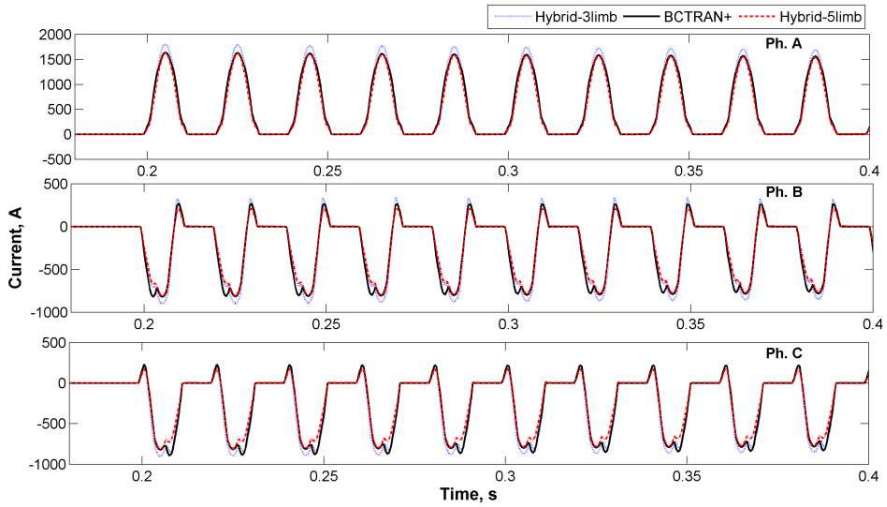

Figure 3-32 Comparison of inrush currents generated by Hybrid and BCTRAN+ for 415 MVA transformer (Energised at phase A voltage zero-crossing)

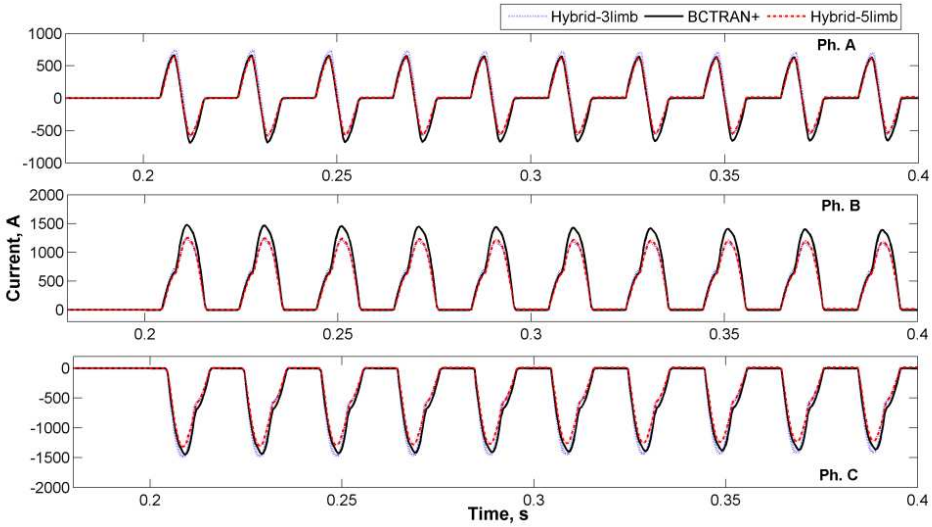

Figure 3-33 Comparison of inrush currents generated by Hybrid and BCTRAN+ for 415 MVA transformer (Energised at phase A voltage peak)

As can be seen, the patterns and magnitudes of the three-phase inrush currents calculated by the BCTRAN+ model can closely match those estimated by the more advanced Hybrid Transformer model. Good agreements were achieved in the energisation cases with different switching angles. This indicates that the relatively simple core topology in the BCTRAN+ model is sufficient to give accurate simulation results.

3.5.5.2 Modelling substation transformers

The way to model substation transformers is similar to that for modelling GSU transformers, which is a BCTRAN object plus a set of delta connected nonlinear inductors. The differences are that: type-93 nonlinear inductors were used for the core representation of substation transformers (because there is no need to model their residual flux condition since they are in service) and they were located at the tertiary winding terminal. As the type-93 nonlinear inductor only requires single-value saturation curve, the procedure to derive the saturation curve for type-93 nonlinear inductor is simpler compared to that for type-96 nonlinear inductor. As shown in Figure 3-34, the basic procedure is the same with that shown in Figure 3-27 but with the step of forming hysteresis loop skipped.

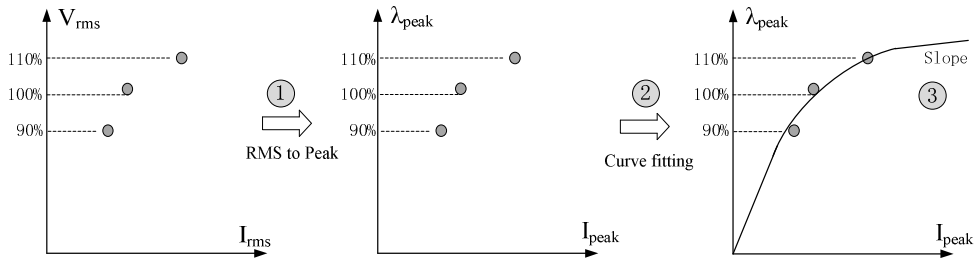

Figure 3-34 Conversion to derive saturation curve for type-93 nonlinear inductor

As shown in Figure 3-35, two saturation curves were derived from transformer test report data: one is for conventional transformers (those manufactured before 1980); the other is for modern transformers. This difference is due to the change of transformer design, manufacture technique and core material around the time of 1980. The nominal magnetizing current of modern transformer is much smaller than that of conventional transformer, and therefore with lower core losses.

The air-core inductances of all the substation transformers were assumed to be four times the transformer short-circuit inductance, as the substation transformers are

autotransformer; this assumption follows the guideline given by CIGRE Study Committee 33 for quantifying the air-core inductance of autotransformer [33].

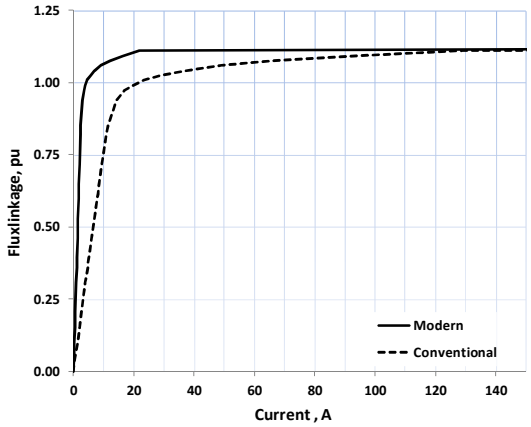

Figure 3-35 Substation transformer saturation curves

3.5.5.3 Modelling Current Transformer

In the field tests, the measurement of inrush currents can be influenced by the performance of current transformer (CT). When the CT is saturated, the shape of inrush currents given on the CT's secondary side can be significantly different from those seen on its primary side. A CT model was developed to simulate such a transient response.

In Figure 3-36, the circuit diagram of the CT model is shown. It is formed by three single-phase transformer models. Each single-phase model consists of an ideal transformer, a type-96 non-linear inductor and a lumped impedance. The ideal transformer is with a ratio of 1200/5. The type-96 non-linear inductors were characterized by the $\lambda - i$ curve shown in Figure 3-37; the curve was derived based on the procedure shown in Figure 3-27. The lumped impedance, whose value was assumed to be $5 + j0.62$ Ohm, represented the relay burden and CT winding impedance.

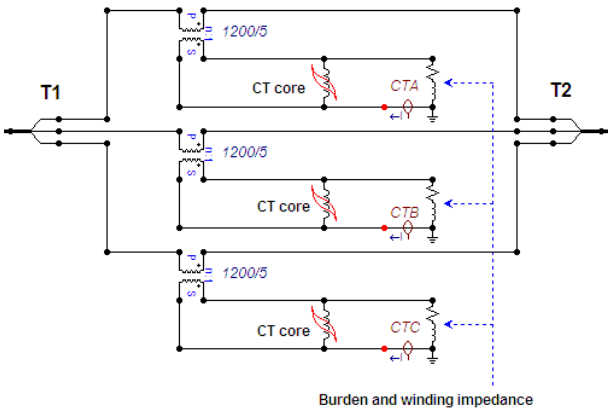

Figure 3-36 Circuit diagram of CT model

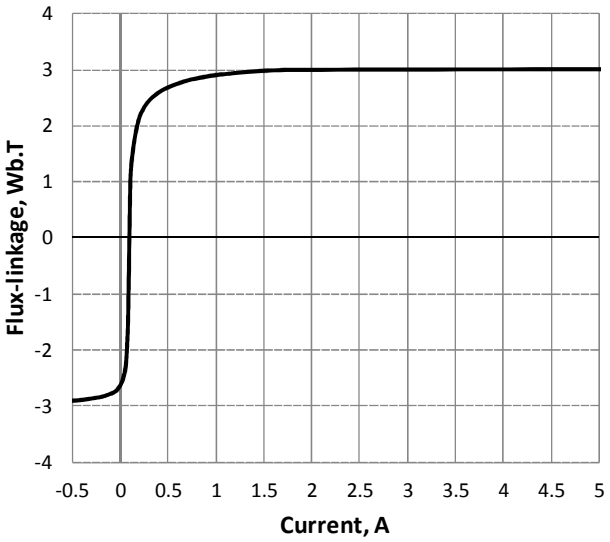

Figure 3-37 CT magnetization characteristic

3.6 Network model validation

The field test results were used to validate the developed network model.

The simulation setup for each validation study consisted of two parts: the first part was the initialization of network condition to define the values of system source voltages, source strength impedance and system loading; the second part was the initialization of energisation condition including the circuit breaker closing time and the transformer residual flux.

Regarding the network condition, the network model was initialized via the following procedure:

- The system source voltages were initialized by referencing the steady state voltages (measured prior to energisation) at substation I: for simulating E1, E2 and E3, the applied source voltage (line-to-line) is 418 kV; for simulating E4, the applied source voltage (line-to-line) is 414 kV;
- It was assumed that the synchronous compensator at substation H was not connected;
- Equivalent source impedances for supply sources S1 and S2 were derived based on the short-circuit levels: 7.1 GVA for S1 and 6.4 GVA for S2;
- Following the loading data provided by the network operator, the loading at each substation was distributed in such a way that each substation transformer was about half loaded: it should be noted that, due to loading variation, the loadings

of substation H and G in the Case E1, Case E2 and Case E3 were set to be 10% more than those in the Case E4.

As for the energisation condition, circuit breaker closing times were interpreted from the measured voltage waveforms and transformer residual fluxes were all assumed.

3.6.1 Validation against Case E1 measurement

For both transformers (i.e., T2 and T3), residual fluxes in phase A, B and C were initialized to -0.3 pu, 0.15 pu and 0.15 pu of peak nominal flux, respectively. T2 and T3 were simultaneously energised at the positive-going zero crossing of phase B line-to-ground voltage. The voltage variation on power feeder 1, inrush current drawn by the T2 and T3, current variation on circuit I-K and voltage variation observed at substation-I were all simulated based on the network model, with results plotted against the measurement in Figure 2-26, Figure 3-39, Figure 3-40 and Figure 3-41, respectively. As can be seen, the waveforms obtained from simulation closely agree with field test results. Specifically, the de-energisation transient is replicated by taking into account the ring-down transient caused by the interaction between cable (the cable was modelled by a lumped capacitance with 0.1 μF) and transformer core nonlinear inductance.

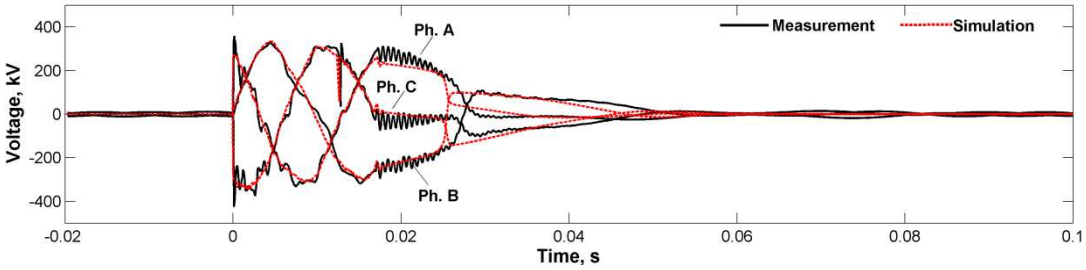

Figure 3-38 Simulated voltages at power feeder 1 compared to those measured in Case E1

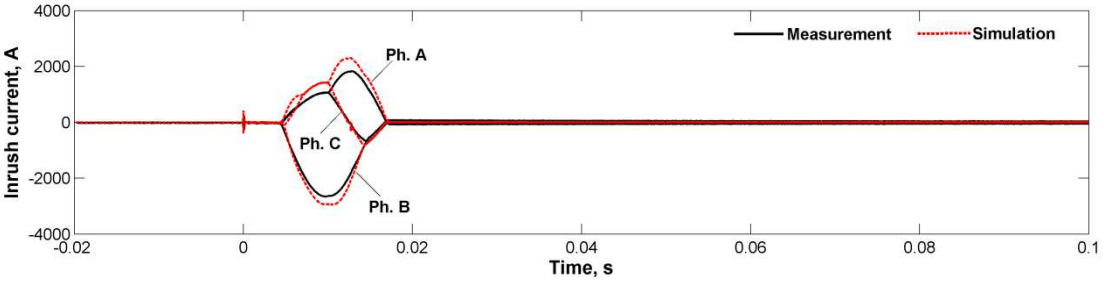

Figure 3-39 Simulated currents at power feeder 1 compared to those measured in Case E1

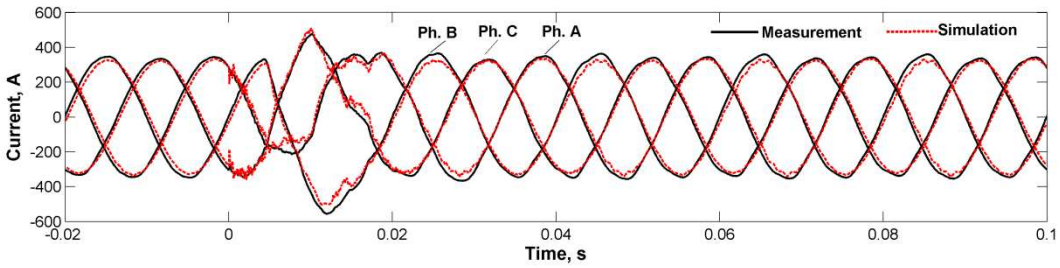

Figure 3-40 Simulated currents at circuit I-K compared to those measured in Case E1

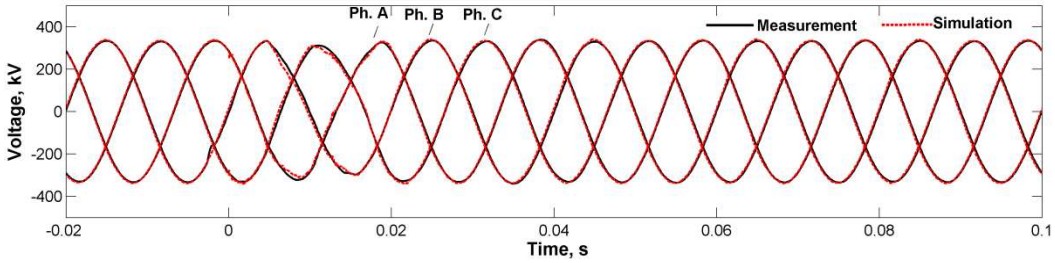

Figure 3-41 Simulated voltages at substation I compared to those measured in Case E1

3.6.2 Validation against Case E2 measurement

For both transformers, residual fluxes in phase A, phase B and phase C were set to 0.64 pu, -0.16 pu and -0.48 pu of peak nominal flux, respectively. Circuit breaker closing time were interpreted based on the voltage measured on the power feeder 1, which indicates that, by referencing the positive-going zero crossing of phase A line-to-ground voltage, phase C, phase A and phase B were energised at 9.27 ms (167°), 9.55 ms (172°) and 10.67 ms (192°), respectively.

The voltage variation observed at power feeder 1, inrush current drawn by the T2 and T3, current variation on circuit I-K and voltage variation at substation-I were all simulated based on the network model, with the results plotted against the measurements shown in Figure 3-42, Figure 3-43, Figure 3-44 and Figure 3-45, respectively. As can be seen, the waveforms obtained from simulation closely agree with test results.

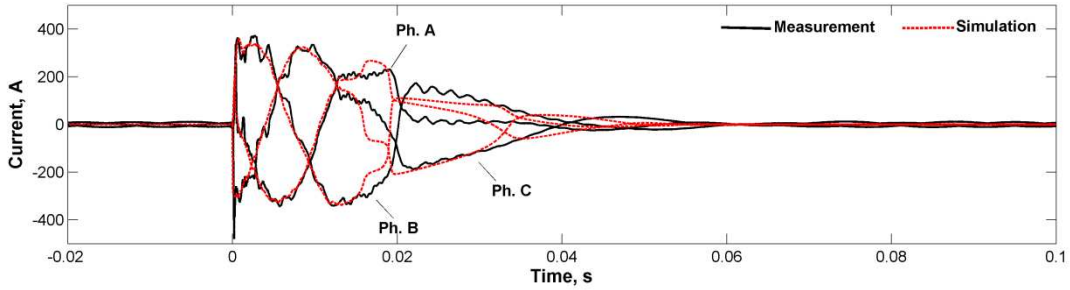

Figure 3-42 Simulated voltages at power feeder 1 compared to those measured in Case E2

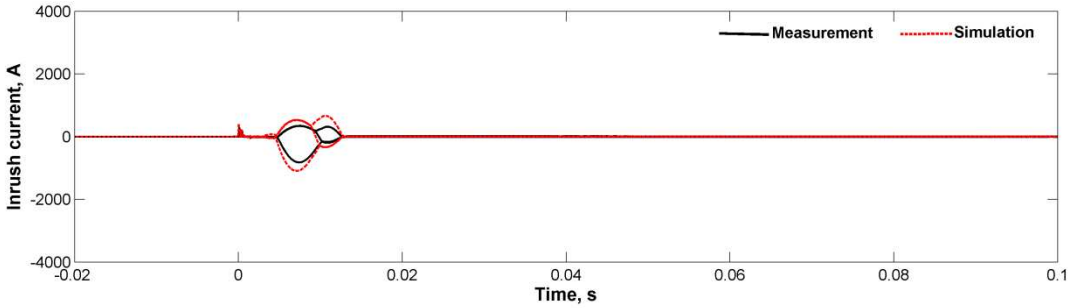

Figure 3-43 Simulated currents at power feeder 1 compared to those measured in Case E2

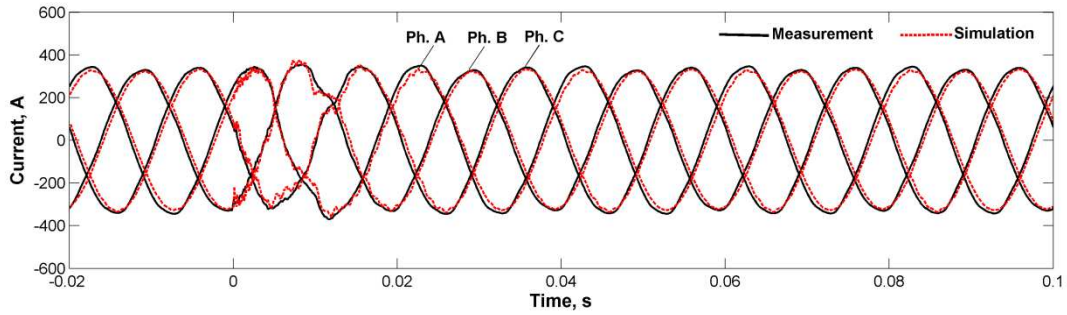

Figure 3-44 Simulated currents at circuit I-K compared to those measured in Case E2

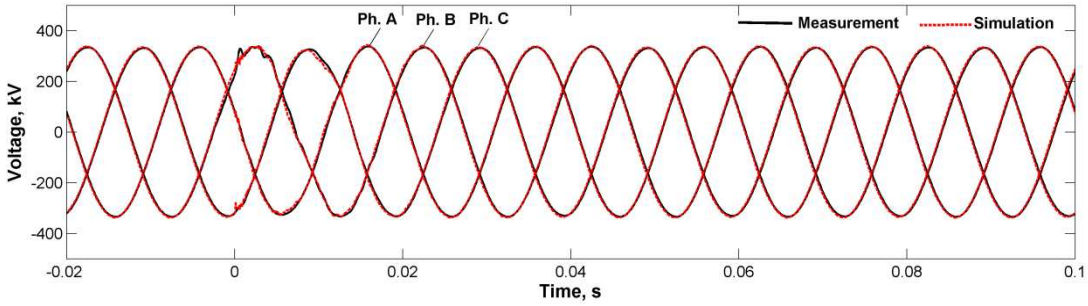

Figure 3-45 Simulated voltages at substation I compared to those measured in Case E2

3.6.3 Validation against Case E3 measurement

To further justify the accuracy of the developed network model, simulation validation was conducted against the Case E3 measurement in which T2 and T3 were energised simultaneously (T1 was not connected during the measurement).

Circuit breaker closing time were interpreted from the voltage waveforms measured on the power feeder 1: phase C was set to be energised first at 5 ms after the negative-going zero crossing of phase C line-to-ground voltage; referencing the closing time of phase C, the other two phases were energised both with a delay of 1.1 ms. Residual fluxes in both T2 and T3 were initialized to -0.385 pu, 0.55 pu and -0.165 pu of peak nominal flux for phase A, phase B and phase C, respectively.

The simulated currents and voltages on power feeder 1, currents flowing through circuit I-K and also the RMS voltage variation at substation I are plotted against field

measurement results in Figure 3-46, Figure 3-47, Figure 3-48 and Figure 3-49, respectively. As can be seen, the simulated waveforms match the measurement results well; specifically, in Figure 3-49, the part of voltage recovery with faster speed is also replicated by considering the response of SVC in the network model.

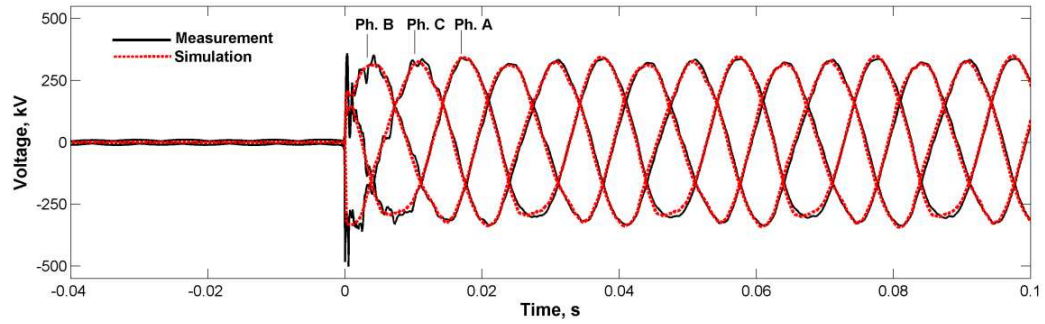

Figure 3-46 Simulated voltages at power feeder 1 compared to those measured in Case E3

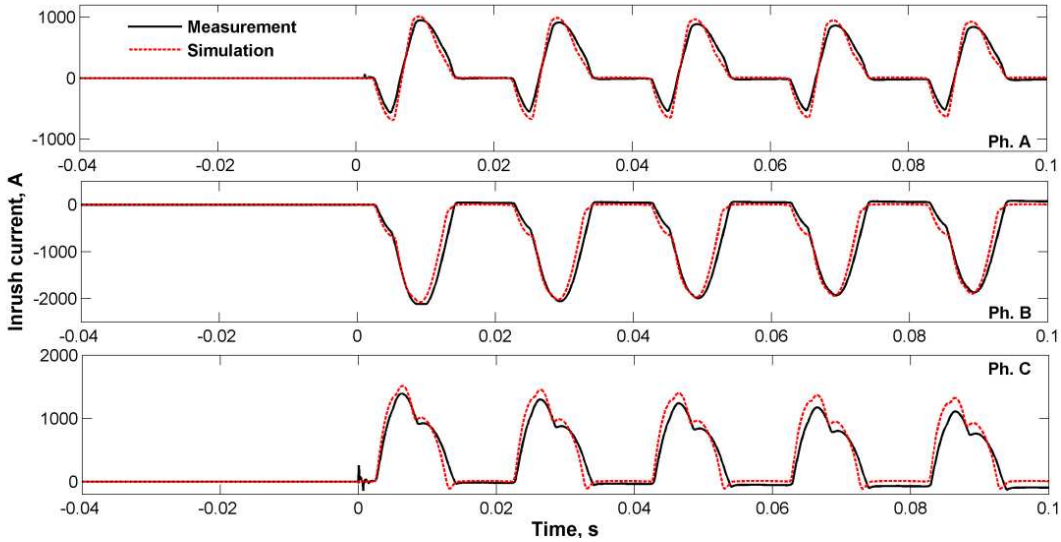

Figure 3-47 Simulated currents at power feeder 1 compared to those measured in Case E3

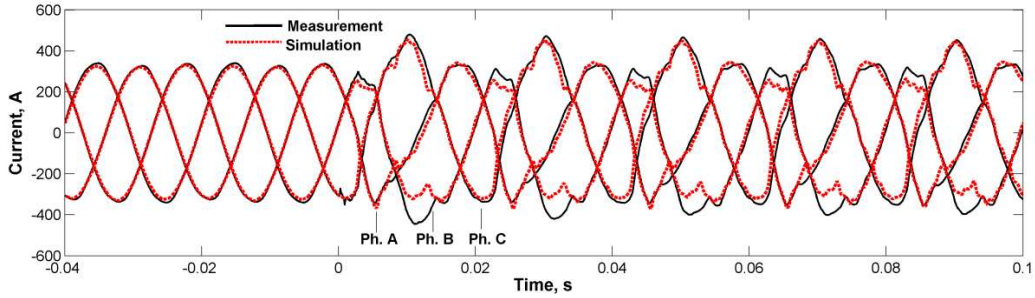

Figure 3-48 Simulated currents at circuit I-K compared to those measured in Case E3

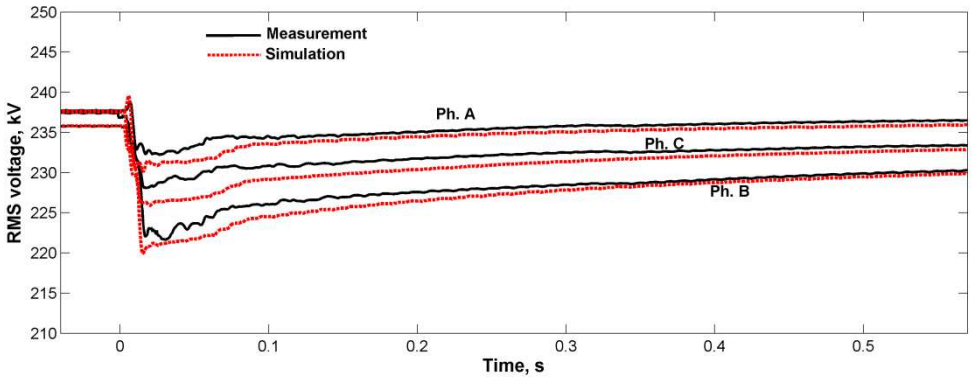

Figure 3-49 Simulated RMS voltage variation at substation I compared to those measured in Case E3

3.6.3.1 Reproduce inrush current waveforms altered by saturated CTs

During the validation against measurement E3, it was found that (as shown in Figure 3-50): good agreement between simulated and measured inrush currents (drawn by T2 and T3) can only be achieved in the first few cycles; after the sixth cycle, the simulated inrush currents cannot replicate the abrupt changes of current peak and waveform pattern of the measured inrush currents in phase B and phase C.

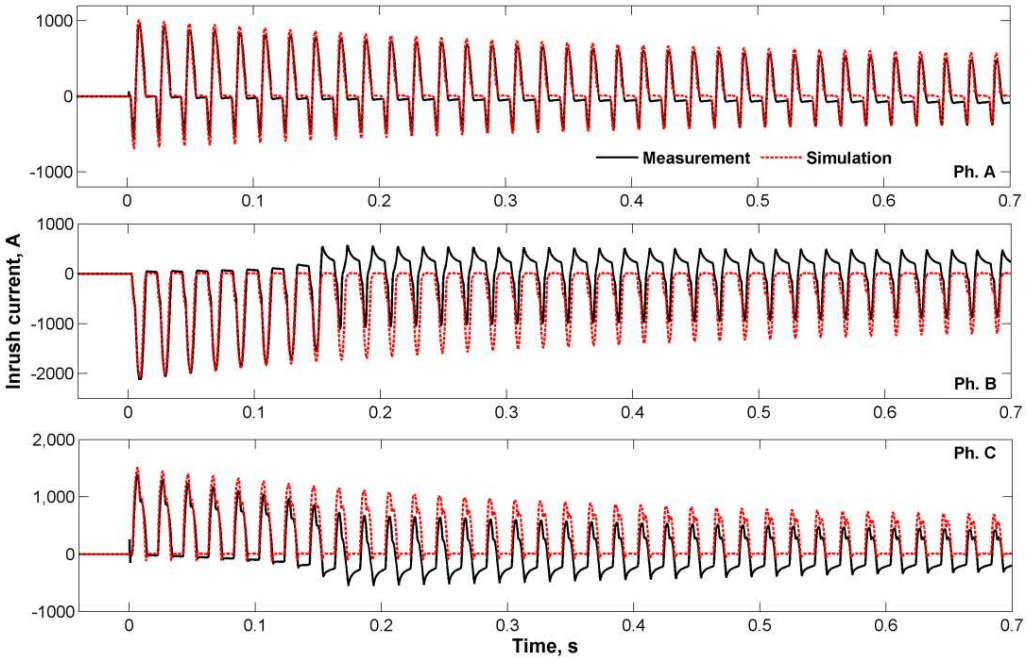

Figure 3-50 Comparison between measured and simulated inrush currents drawn by T2 and T3 in Case E3 (simulated currents observed at the CT primary side)

It is believed that the changes appeared in the measured phase B and phase C currents were due to the CT saturation caused by the significant dc offset components presented in both currents. No obvious change can be observed in the measured phase A current is because its offset dc component was of relatively small magnitude, in which case, good

agreement between simulated and measured currents can still be retained. To confirm such reasoning, the developed CT model was incorporated in the network model to reproduce the inrush currents altered by the CT saturation effects. The simulated inrush currents shown in Figure 3-50 was taken as the input for the CT model, and the resulted secondary side currents of the CT model were obtained and compared with the measured inrush currents in Figure 3-51. As can be seen, the abrupt changes in phase B and C can be very well matched, which indicates that the simulated inrush currents shown in Figure 3-50 are accurate and confirms that the abrupt changes of the inrush currents was due to CT saturation.

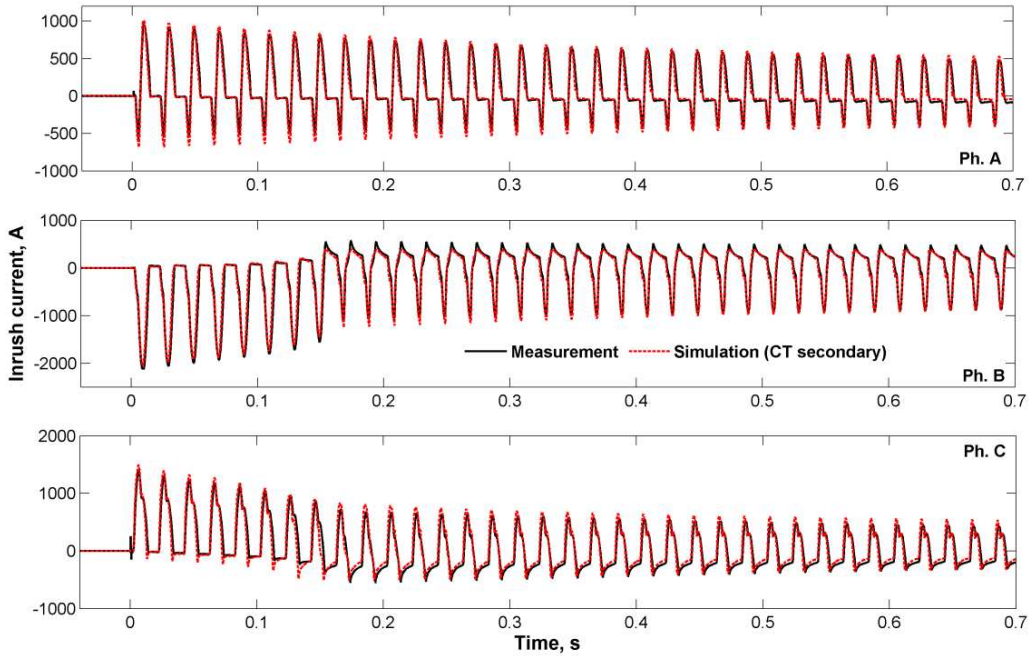

Figure 3-51 Comparison between measured and the simulated currents (observed at the CT secondary side)

3.6.4 Validation against Case E4 measurement

Further validation was also conducted to replicate the results obtained from the Case E4 measurement. In this case, network model was set to simulate energising T1 with transformer T2 and T3 already connected. Circuit breaker closing times were obtained from the measured voltage waveforms in which three phases were energised simultaneously at 4.44 ms (80°, relative to the positive-going zero crossing of phase A line-to-ground voltage); residual fluxes were assumed to be zero. Based on these parameter settings, the simulation results were simultaneously generated by the developed network model.

In Figure 3-52, instantaneous wave shapes of three-phase sympathetic inrush currents were compared, focusing on the initiation of sympathetic inrush. It can be seen that the simulation results can replicate the double-peak patterns, as well as the growing trend and peak magnitudes. Furthermore, the simulated RMS sympathetic inrush currents and the field measurement results were compared in Figure 3-53 in terms of the build-up and decay of sympathetic inrush. Good agreement is achieved in terms of the initiation, the peak instants and magnitudes as well as the decay.

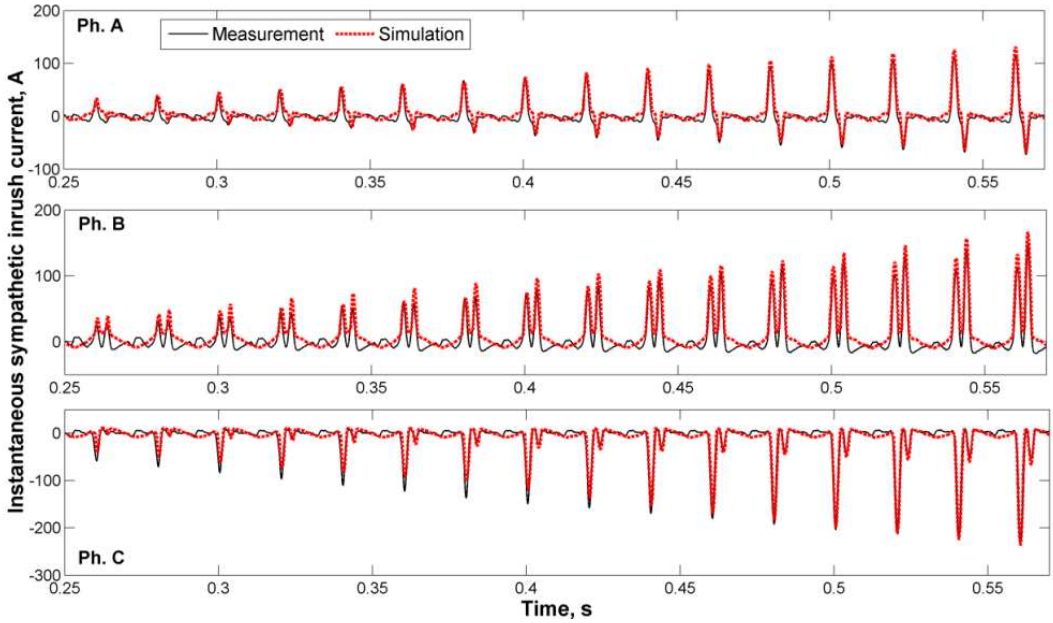

Figure 3-52 Simulated sympathetic inrush currents at power feeder 1 compared to those measured in Case E4

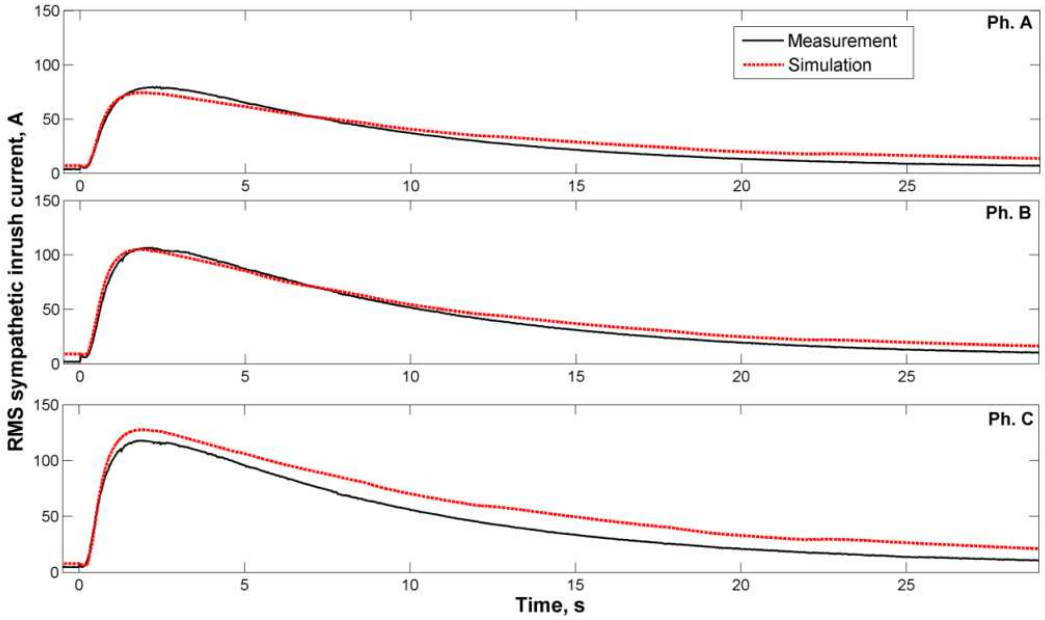

Figure 3-53 Simulated RMS sympathetic inrush currents at power feeder 1 compared to those measured in Case E4

Figure 3-54 illustrates the comparison regarding the long-duration RMS voltage dips, with the dip magnitudes particularly compared in Table 3-7. As can be seen, the simulated voltage dip recovery traces are similar to field measurement results; the largest deviation of dip magnitude is approximately 2.8%.

The comparison in Figure 3-55 is the currents measured at circuit I-K. Good agreement can be seen in the range of steady stage (i.e., prior to energisation), which confirms the correct modelling of system loading. In the range of transient stage (i.e., after energisation), simulation results also show good agreement with field test results. It should be noted that the initial part of voltage recovery was affected by the response of SVC, which has also been correctly replicated in the simulation results. Regarding this SVC effect, more details will be described in Chapter 4.

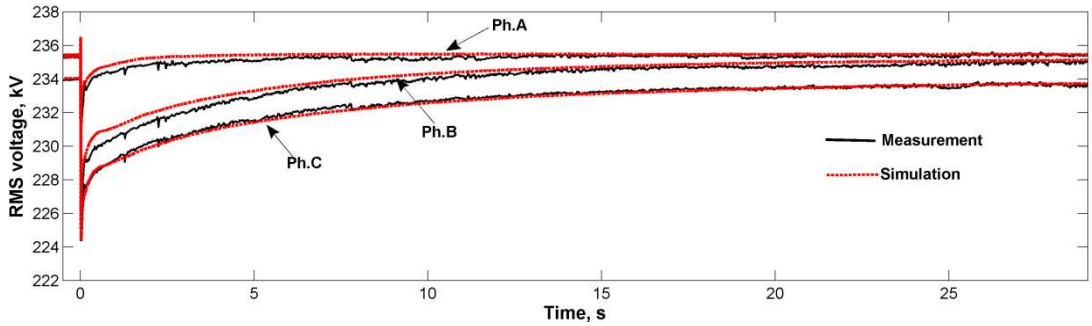

Figure 3-54 Simulated RMS voltage at power feeder 1 compared to those measured in Case E4

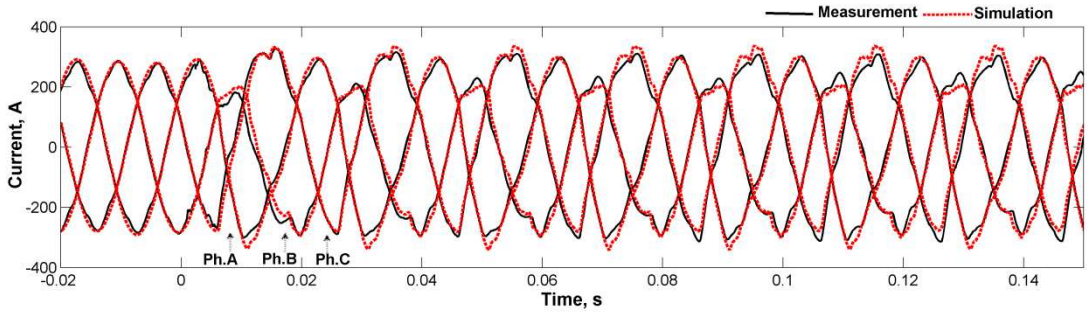

Figure 3-55 Simulated currents at circuit I-K compared to those measured in Case E4

Table 3-7 Comparison of three-phase voltage dip magnitudes

Phase	Dip magnitude (kV)		Deviation
	Field test	Simulation	
A	4.23	4.35	2.8%
B	9.28	9.08	2.1%
C	9.65	9.6	0.5%

3.7 Summary

In this chapter, voltage dip events caused by energising large GSU transformers is reported, in conjunction with field measurements, network model development and its validation. The system under study is a 400/132 kV transmission system featured by long transmission lines between the supply source and the energised transformers.

In the voltage dip events, it was shown that the energisation of GSU transformers can trigger a network-wide voltage dips; the recorded maximum RMS voltage dip was about 7.85% of the initial voltage; the events triggered low voltage alarms and the dips were noticed by the downstream distribution utilities.

In the further field measurements, voltage dips involving sympathetic interaction between GSU transformers were observed, showing that the duration of sympathetic inrush can last more than 20 seconds and so did the full recovery of the resulted voltage dips; in addition, the voltage and current waveforms measured at different locations provide useful benchmarks for network model validation.

Based on the system parameters provided by the network operator, a network model was developed in ATP/EMTP by following the guidelines summarized in Chapter 2. The network model was validated against the field measurement results, showing good agreements. It thus confirms the accuracy of the following modelling approaches:

- The source network can be modelled by an ideal sine-wave source and a Thevenin equivalent impedance of the part of the network not under study;
- The transmission network between the supply source and the energised transformer should be represented in detail, taking into account the transmission lines, system loading and reactive power compensation devices;
- The Bergeron model can be used to represent transmission lines, with line dimension and transposing scheme considered;
- System loading can be represented by lumped constant resistance and inductance connected in parallel;
- Transformers can be represented by the BCTRAN+ model (consisting of a BCTRAN object with a set of delta-connected nonlinear inductors).

In the following chapters, computer simulation assessments of the voltage dips caused by transformer energisation will be carried out based on the validated network.

Chapter 4 Assessment of Voltage Dips Caused by Transformer Energisation Transients Using Deterministic Approach

In this chapter, a comprehensive assessment of voltage dips caused by energising large GSU transformers is deterministically conducted based on the network model developed and validated in Chapter 3.

Being the first step of the assessment, different energisation conditions are analysed and compared, considering circuit breaker closing time, transformer core residual flux, the number of GSU transformers being energised and the number of GSU transformers already connected. Based on the commonly agreed worst case energisation condition, assessment of network-wide voltage dips is performed to investigate the voltage dip patterns under non-outage, single-circuit outage and double-circuit outage situations. Furthermore, sensitivity studies are carried out to identify the key influential parameters. Finally, possible operational measures to control the voltage dips are assessed and an optimized energisation procedure is proposed to effectively and economically reduce the voltage dips caused by transformer energisation.

4.1 Voltage dips under different energisation conditions

Ten case studies were carried out using the validated network model to compare voltage dips under different energisation conditions. The details of these case studies are shown in Table 4-1. They differ from each other in terms of circuit breaker closing time, transformer core residual flux, the number of GSU transformers being energised and the number of GSU transformers already connected. Regarding closing time, it was assumed that the closing time span is zero (the influence of closing time span will be studied by stochastic approaches in Chapter 5); the closing time is referenced to the positive-going zero crossing of phase C line-to-ground voltage. When residual flux is considered, it was assumed that phase A, B and C possess -0.8 pu, 0 and 0.8 pu of peak nominal flux, respectively. Combination of such a closing time and residual flux is

regarded here (and also in the rest of the thesis) as the commonly agreed worst case energisation condition.

It should be noted that, for quantifying the dip magnitude and duration, the following two criteria are used in this chapter and also in the rest of the thesis:

- Dip magnitude: the dip magnitude is defined as the lowest RMS voltage among three phases;
- Dip duration: the 3% dip was taken as the beginning and end threshold for quantifying the voltage dip duration.

The results of the case studies are summarized in Table 4-1, with voltage dip magnitudes and durations observed at the substation-I selected for the comparison, because it is located closest to the substation-K which connects the generating plant.

Table 4-1 Voltage dips observed at substation I under different energisation conditions

Case	GSU transformer		closing time (ms)	Residual flux (pu)			Voltage dips					
							Magnitude (%)			Duration (s)		
	Energised	On-line		A	B	C	A	B	C	A	B	C
1	T1	--	5	0			4.3	3.5	1.8	0.274	0.181	0
2	T1	--	0	0			2.0	2.9	4.4	0	0	0.393
3	T1	T2&T3	0	0			2.0	2.9	4.4	0	0	0.631
4	T1	--	0	-0.8	0	0.8	5.8	5	9.6	0.946	0.636	2.728
5	T1	T2&T3	0	-0.8	0	0.8	5.8	5	9.6	2.90	1.477	6.448
6	T2&T3	--	5	0			7.8	6.4	3.3	0.906	0.601	0.006
7	T2&T3	--	0	0			3.7	5.0	8.2	0.04	0.265	1.12
8	T2&T3	T1	0	0			3.7	5.0	8.2	0.04	0.279	2.614
9	T2&T3	--	0	-0.8	0	0.8	10.7	9.2	18.4	1.576	1.199	3.564
10	T2&T3	T1	0	-0.8	0	0.8	10.7	9.2	18.4	4.0	2.68	7.919

Comparing Case 1 with Case 2, it can be seen that, energising at the peak of phase C voltage only gives small voltage dip on phase C, but results in larger voltage dips on the other two phases, which shows that, in the case of three-phase system, a closing time in favour of one phase may act against the other two phases. This is also evidenced in the comparisons between Case 6 and Case 7.

Comparing Case 2 and Case 4, it can be seen that, when the transformer is energised at the commonly agreed worst case energisation condition, the resulted voltage dips are much higher than those voltage dips resulted from energisation at zero-crossing energisation instant but with zero residual flux. This can also been seen from other comparisons, including the one between Case 3 and Case 5, the one between Case 7 and Case 9 and the one between Case 8 and Case 10.

Under the same closing time and residual flux condition, it can be seen that:

- Energising transformers T2 and T3 together would cause voltage dips with longer dip duration (in most cases) and with magnitude almost twice that caused by energising T1 alone, which, for instance, can be seen from the comparison between Case 4 and Case 9;
- Comparison between Case 4 and Case 5 shows, with the presence of on-line transformers, the voltage dip magnitudes are the same but the durations can be prolonged by more than 100%; similar observation can be seen in the comparison between Case 2 and Case 3, between Case 7 and Case 8, and between Case 9 and Case 10.

The above case studies show that the sympathetic inrush does not affect the voltage dip magnitude, which is obvious because at the initial stage of the energisation transient, voltage dip is mainly determined by the inrush current in the energised transformers, while at this time the sympathetic inrush drawn by the adjacent transformer has yet to build up. With the increase of the sympathetic inrush current, the decay of the inrush current in the energised transformer slows down and as a consequence the dip duration is prolonged. The comparisons made between the case studies indicate that this prolonging effect can be very significant. Comparing Case 4 with Case 5, the dip duration of phase C is prolonged by 136%; similarly, comparing Case 9 with Case 10, the dip duration of phase C is prolonged by 122%.

As far as the case studies of energising only one GSU transformer are concerned, Case 5 is the worst case energisation. Among all of the case studies, Case 10 is the worst energisation case, as it results in the largest dip magnitude and the longest dip duration. Both cases are further analysed in terms of the current and voltage variations.

4.1.1 Current and voltage variation when energising T1 with T2&T3 already connected

Energisation Case 5 is similar to the field measurement Case E4 in Chapter 3: both involve energising T1, with T2 and T3 already connected; however, Case 5 is with more unfavourable closing time and residual flux condition.

The inrush current drawn by T1 after the energisation is shown in Figure 4-1. The maximum current peak appears on phase C and it is about 2500 A. As shown in Figure

4-2 and Figure 4-3, part of the inrush current flows through the double-circuit lines between substation I and K and part of it flows through the lines between substation J and K. The inrush current flowing through the lines between J and K (not observed in the field measurement) is much larger than that flowing through the lines between I and K, which is mainly due to the large impedance of the circuit between substation G and H.

The incursion of sympathetic inrush in transformers T2 and T3 is illustrated in Figure 4-4 (initiation stage) and Figure 4-5 (RMS current, long period). As can be seen, at the initiation stage, sympathetic inrush currents started to build up at about 0.1 second after the energisation; they then took about 1 second to reach their peaks, which is twice faster than that observed in field measurement Case E4. The maximum instantaneous peak value is about 1000 A, and the maximum RMS peak is 391 A. Compared to that observed in field measurement Case E4, the RMS peak is about three times larger.

In Figure 4-6, the three-phase RMS voltage dips are illustrated. It shows that the voltage dip recovery trace started to be altered once the sympathetic inrush currents started to build up, which can be further evidenced by the comparison between Case 4 and Case 5 regarding the voltage dip recovery on phase C (see Figure 4-7).

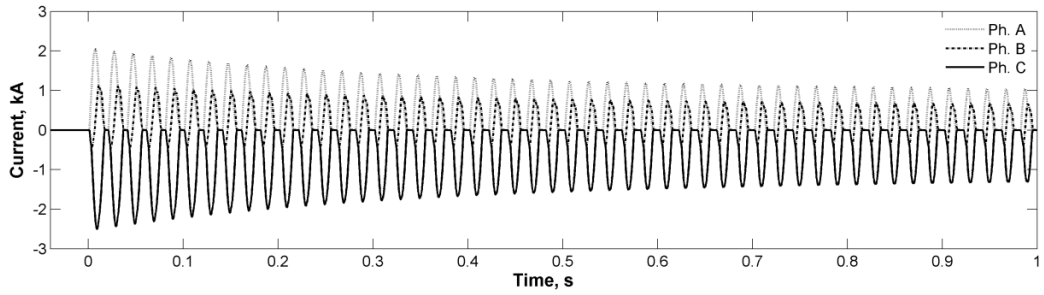

Figure 4-1 Inrush current observed at power feeder 2 (Case 5)

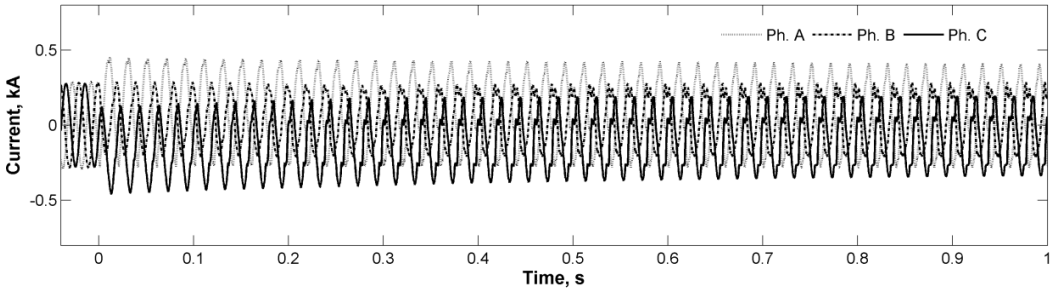

Figure 4-2 Currents flowing through one of the circuits between substation I and K (Case 5)

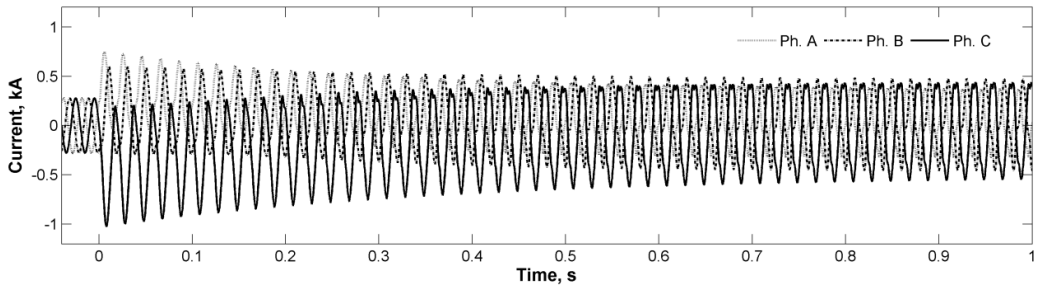

Figure 4-3 Currents flowing through one of the circuits between substation J and K (Case 5)

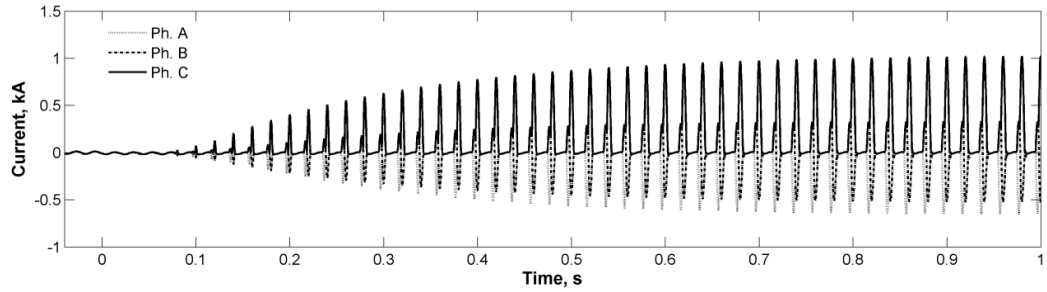

Figure 4-4 Initiation of sympathetic inrush current observed at power feeder 1 (Case 5)

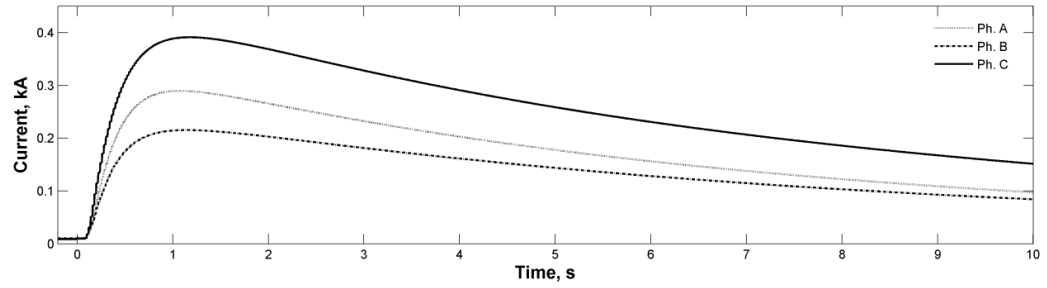

Figure 4-5 RMS sympathetic inrush current observed at power feeder 1 (Case 5)

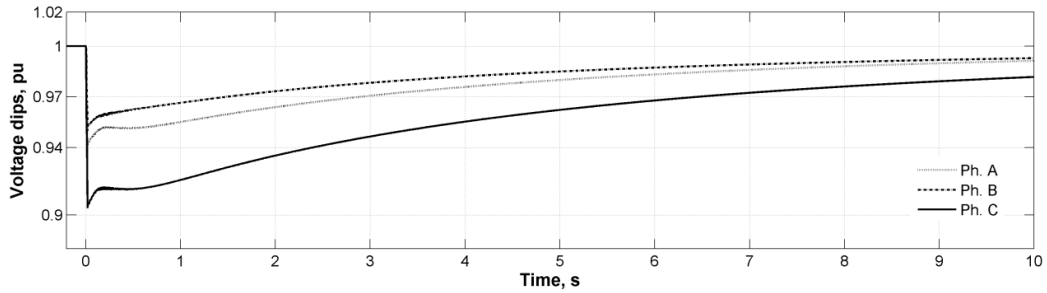

Figure 4-6 Voltage dips observed at Substation I (Case 5)

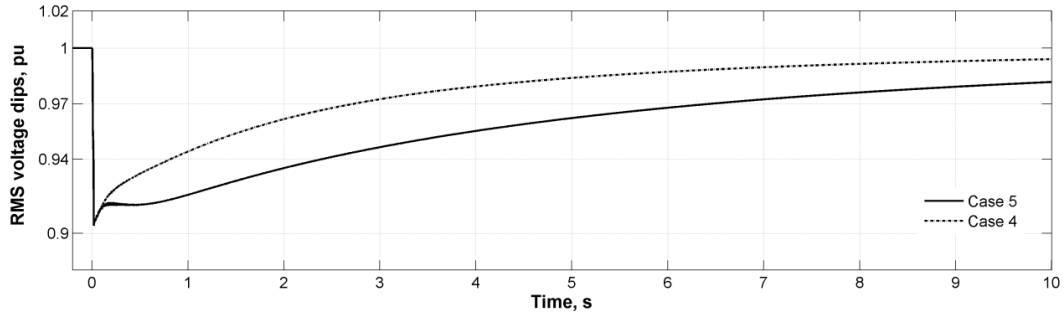

Figure 4-7 Comparison between Case 5 and Case 4 regarding phase C voltage dip

4.1.2 Current and voltage variation when energising T2&T3 with T1 already connected

Further analysis of the current and voltage variations in Case 10 was also conducted. In Figure 4-8, the maximum peak of the inrush current drawn by T2 and T3 together is about 4800 A. This current peak is about twice the current peak observed in Case 5, since there are two transformers being energised simultaneously in Case 10. Correspondingly, the magnitudes of the inrush currents observed on the two circuits (Figure 4-9 for I-K, Figure 4-10 for J-K) are proportionally increased.

The sympathetic inrush current drawn by transformer T1 alone (as shown in Figure 4-11 and Figure 4-12), is similar to that drawn by T2 and T3 together (see Figure 4-4 and Figure 4-5 in the analysis of Case 5). This is because the total number of transformers engaging sympathetic inrush in both cases is the same.

In Figure 4-13, the voltage dip of phase C observed in Case 10 is compared with that observed in Case 5. As can be seen, the higher inrush current in Case10 results in voltage dips with magnitude twice that observed in Case 5; the dip duration, however, is of much smaller difference between the two cases, which can be attributed to the similar level of sympathetic inrush for both cases.

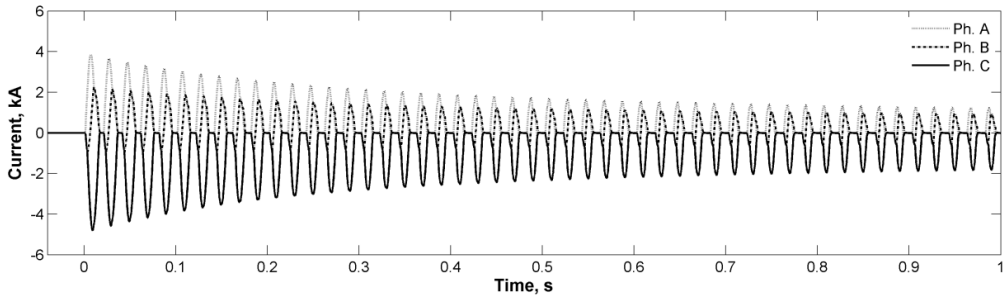

Figure 4-8 Inrush current observed at power feeder 1 (Case 10)

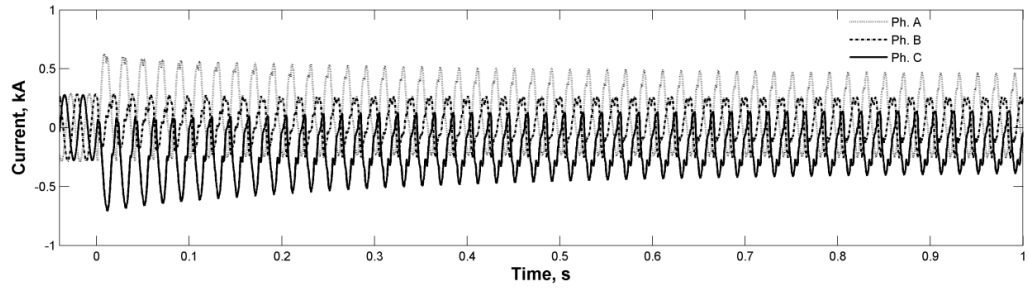

Figure 4-9 Currents flowing through one of the circuits between I and K (Case 10)

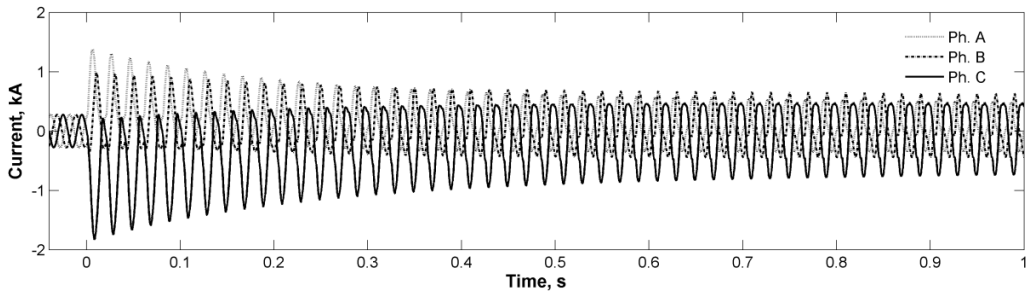

Figure 4-10 Currents flowing through one of the circuits between J and K (Case 10)

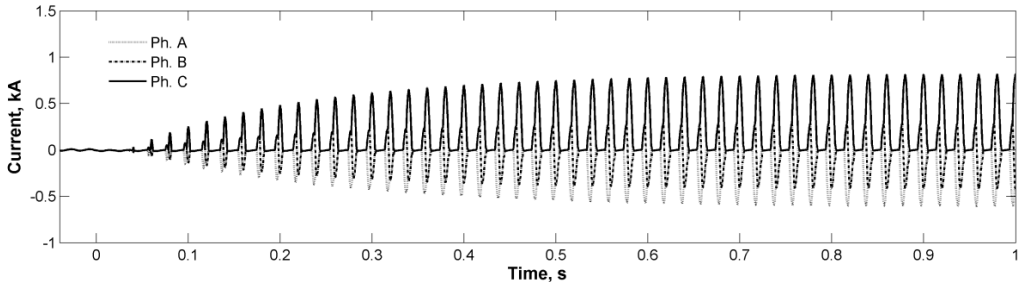

Figure 4-11 Initiation of sympathetic inrush observed at power feeder 2 (Case 10)

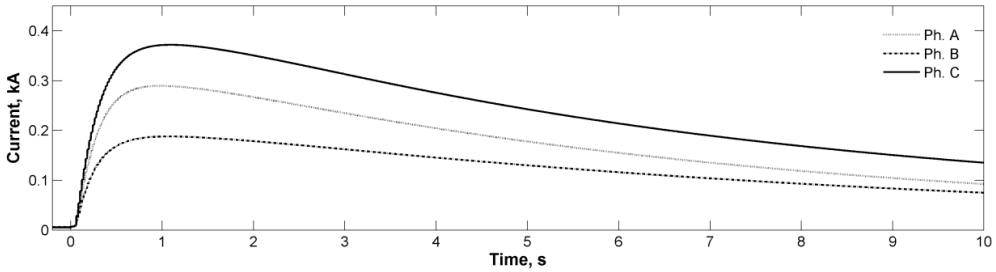

Figure 4-12 RMS sympathetic inrush current observed at power feeder 1 (Case 10)

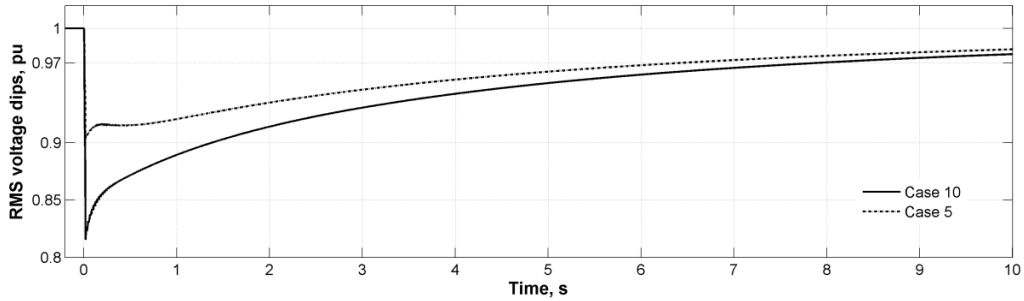

Figure 4-13 Comparison between Case 5 and Case 10 regarding phase C voltage dip

4.2 Network-wide voltage dips

Based on Case 10, network-wide voltage dips were further investigated by focusing on the following aspects:

- Network-wide voltage dip pattern under non-outage condition;
- Network-wide voltage dip pattern under single-circuit outage condition;
- Network-wide voltage dip pattern under double-circuit outage condition.

4.2.1 Network-wide voltage dip pattern under non-outage condition

Non-outage condition means there is no circuit outage in the network. Case 10 was performed under the non-outage condition, with voltage dip magnitudes and durations observed in phase C at substations D, E, F, G, H, I and J analyzed in detail (because phase C is subjected to the biggest voltage dips under Case 10 energisation).

Figure 4-14 shows the patterns of voltage dip magnitudes of phase-C on both 400 kV and 132 kV side. It can be seen that the two patterns are almost identical. This indicates that, as far as dip magnitude is concerned, the voltage dips appear on the 132 kV side are not much affected by the substation transformers in the system studied. The dip magnitude observed at each substation is found to be related to the distance between the substation and the supply source and also the distance between the substation and the energised transformers. For those substations (including H, I and J) located in the proximity of the energised transformer and relatively far away from the supply source, the observed dip magnitudes are relatively large; for those substations (including D, E, F and G) located relatively far away from the energised transformer and close to the supply source, the observed dip magnitudes are relatively small.

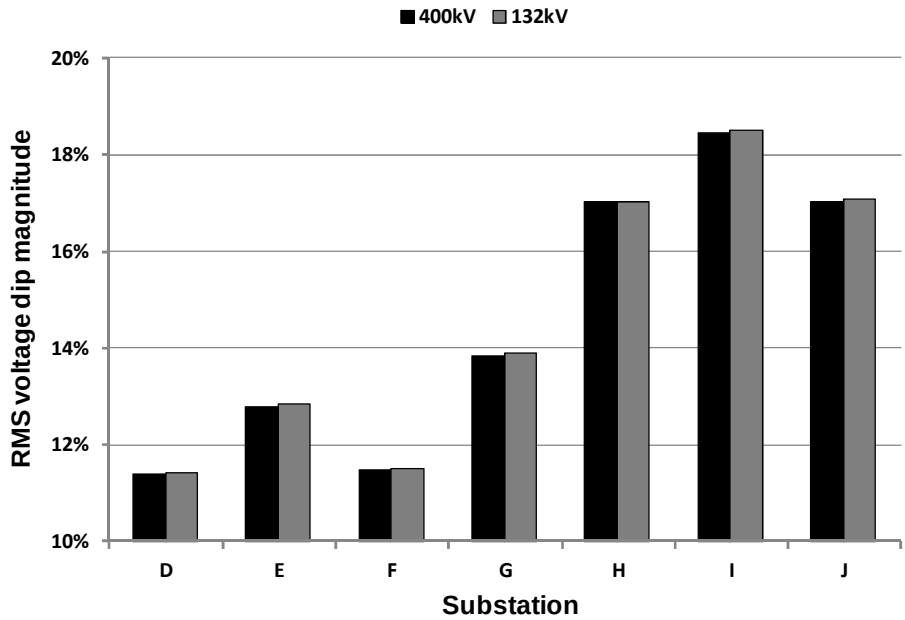

Figure 4-14 Patterns of voltage dip magnitudes across all the network substations (voltage dips observed at substation autotransformers' 400 kV side versus 132 kV side)

Figure 4-15 shows the patterns of voltage dip duration observed on 400 kV and 132 kV side. It can be seen that the dip durations on 132 kV side are longer. The prolonged voltage dip duration at 132 kV side is attributed to the sympathetic inrush of substation

transformers which is further illustrated by voltage dip traces at substation I shown in Figure 4-16. It can be seen that both sides witness the same amount of voltage dip magnitude, however, the recovery at 132kV side starts to be affected by sympathetic inrush about two cycles after the energisation and continues to be affected for more than 9 seconds. The substation transformers located at substation I and J have been found to be the most affected, because their electrical distances to the GSU transformers are the shortest. The above findings show that the energisation of GSU transformers can trigger a network-wide sympathetic inrush, because the sympathetic phenomena can extend to substation transformers.

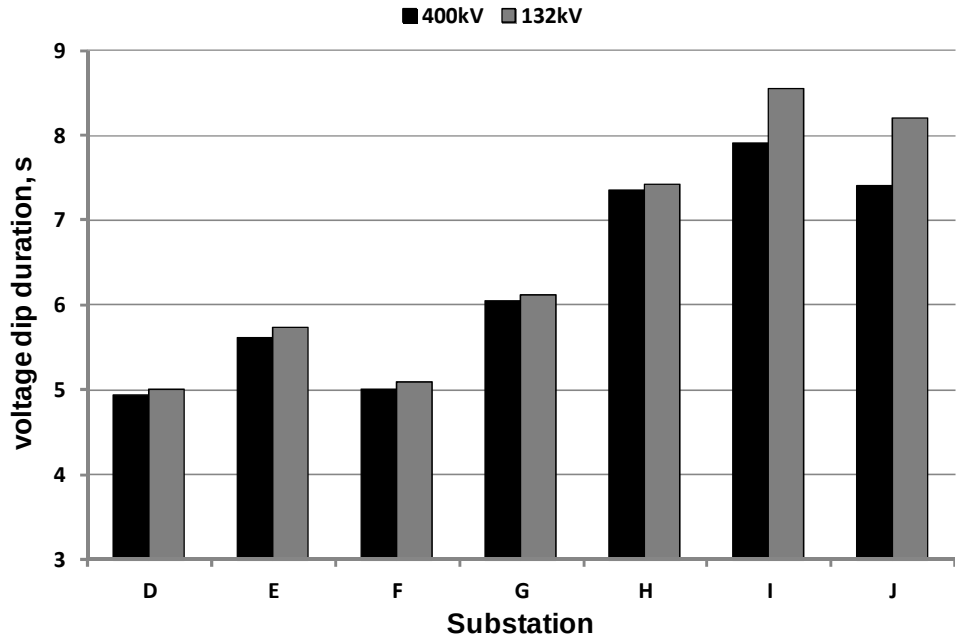

Figure 4-15 Patterns of voltage dip duration across all the network substations (400 kV side versus 132 kV side)

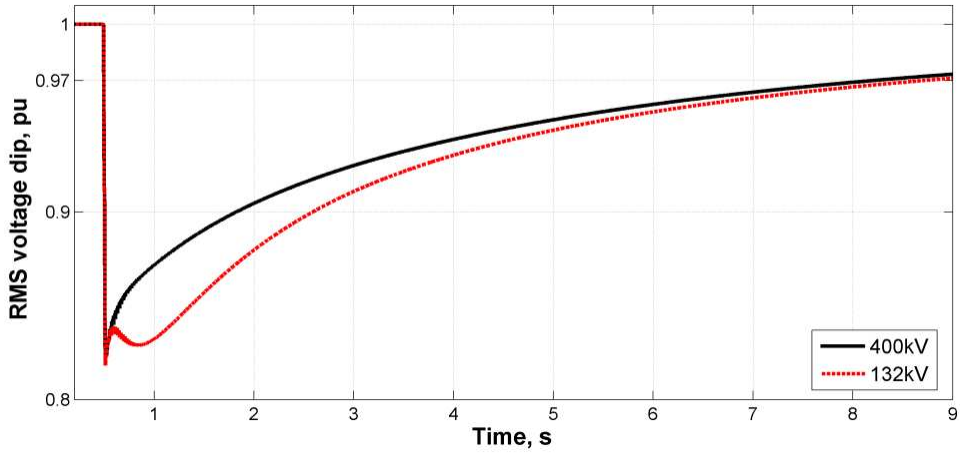

Figure 4-16 Voltage dip recovery traces observed at 400 and 132 kV busbars of substation I

4.2.2 Network-wide voltage dip pattern under single-circuit outage

The network may be subjected to single-circuit outage under maintenance or fault condition. In fact, as reported by the network operator, transformer energisation did occur during maintenance of one of the double-circuit lines.

To understand the impacts of single-circuit outage on the voltage dip pattern, various single-circuit outage scenarios were simulated based on Case 10 energisation condition. In the simulation studies, voltage dips in phase C were observed at substations D, E, F, G, H, I and J and compared with those obtained under non-outage condition. The relatively severe voltage dips scenarios have been found under the A-F and J-E single-circuit outage, which are shown in Figure 4-17 and Figure 4-18. Note that in both figures, the sub-figure on the left shows the comparison regarding the voltage dip magnitude whilst the sub-figure on the right shows the comparison regarding the dip duration. From the comparisons, it can be seen that: single-circuit outage only results in slight increase of voltage dips; the maximum increase of dip magnitude and duration both appear at substation J.

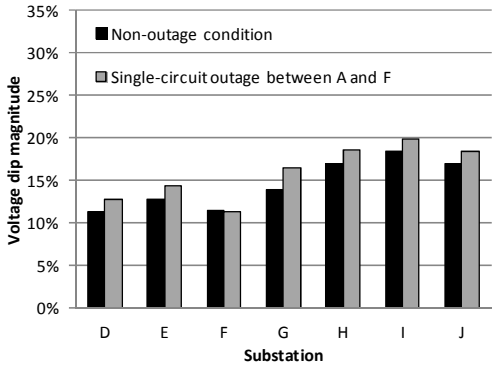

(a) Dip magnitude

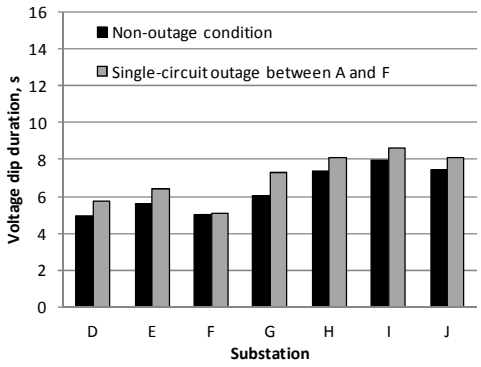

(b) Dip duration

Figure 4-17 Voltage dips caused by single-circuit outage between substation A and F

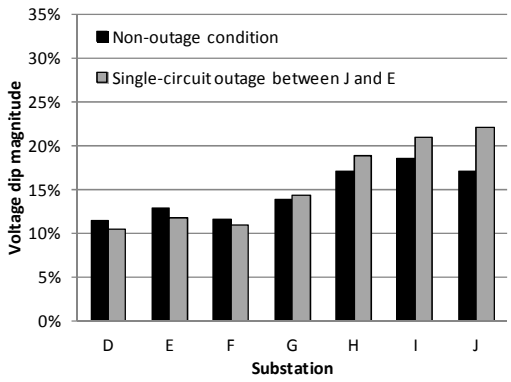

(a) Dip magnitude

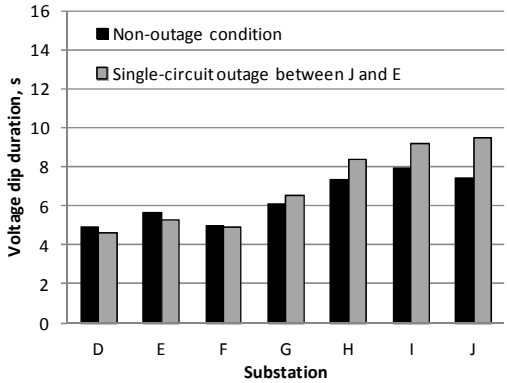

(b) Dip duration

Figure 4-18 Voltage dips caused by single-circuit outage between substation J and E

4.2.3 Network-wide voltage dip pattern under double-circuit outage

Under some circumstances, the network may be subjected to outage of both circuits connecting between two adjacent substations. This may occur when one circuit of the double-circuit line is under maintenance and the other circuit coincidently experiences a fault condition. Network-wide voltage dips caused by energisation under such a situation were examined using the Case 10 energisation and the results were compared with the voltage dip pattern observed under non-outage network condition. It was found that:

- Outage of both circuits between substation A and F or B and C leads to increase of voltage dips in all the substations, which can be seen in Figure 4-19 and Figure 4-20, respectively; specifically, A-F double-circuit outage causes larger voltage dips than that caused by B-C double-circuit outage; similar effects were found in the cases of C-D and D-E double-circuit outage;
- In many cases of double-circuit outage, the voltage dip pattern is only slightly affected; these cases include outage of double circuits between the following substations: F-G, F-E, G-H, H-I and I-K; especially, the case of I-K double-circuit outage actually results in less sever voltage dips in most of substations, which is illustrated in Figure 4-21;
- The most unfavorable scenario is found to be the J-E double-circuit outage; in that case, as shown in Figure 4-22, the largest voltage dip magnitude becomes over 30%, with duration over 14 s. The large increase of voltage dip magnitude is mainly due to the significant increase of the length of the transmission lines between the supply source and the energised GSU transformers.

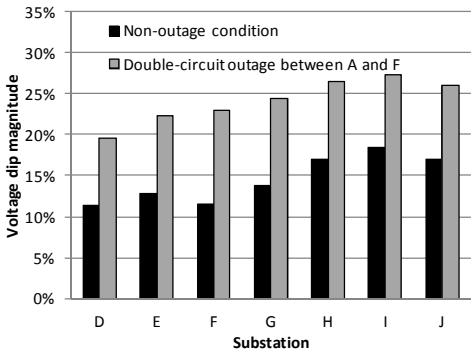

(a) Dip magnitude

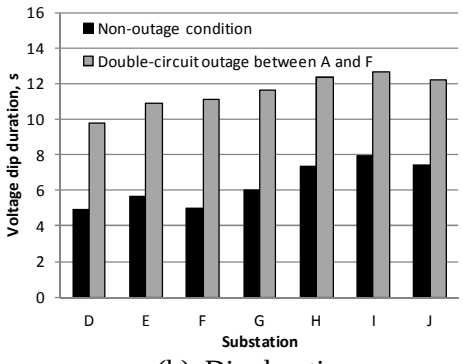

(b) Dip duration

Figure 4-19 Voltage dips caused by double-circuit outage between substation A and F

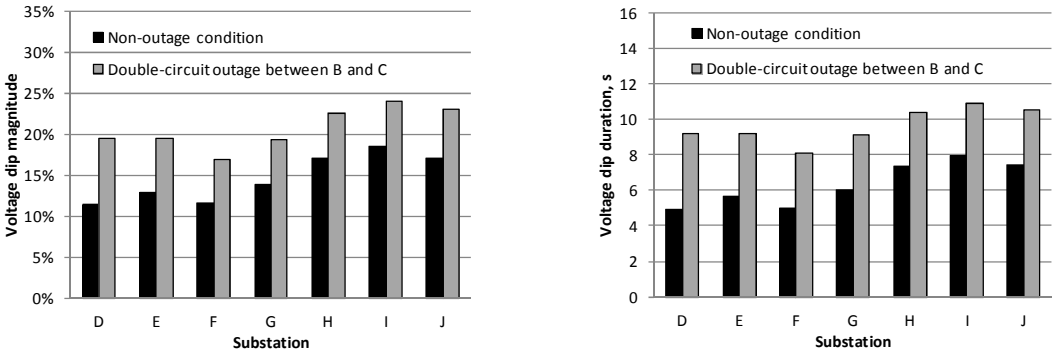

Dip magnitude (a) Dip duration

Figure 4-20 Voltage dips caused by double-circuit outage between substation B and C

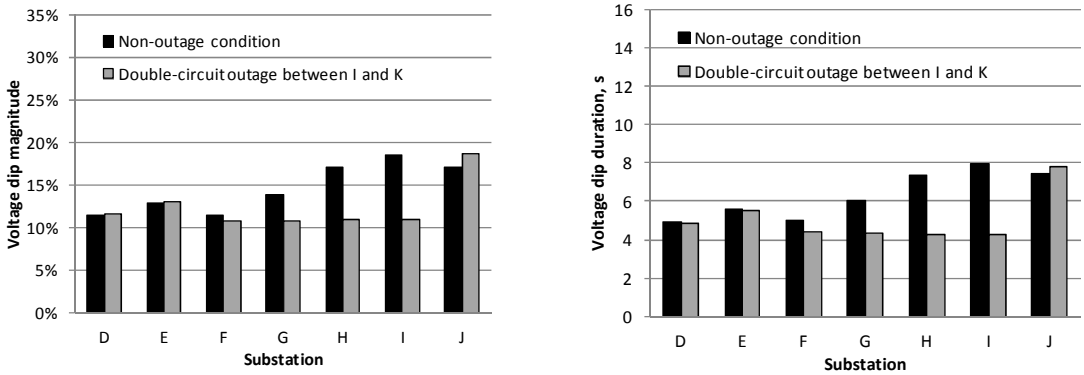

(a) Dip magnitude (b) Dip duration

Figure 4-21 Voltage dips caused by double-circuit outage between substation I and K

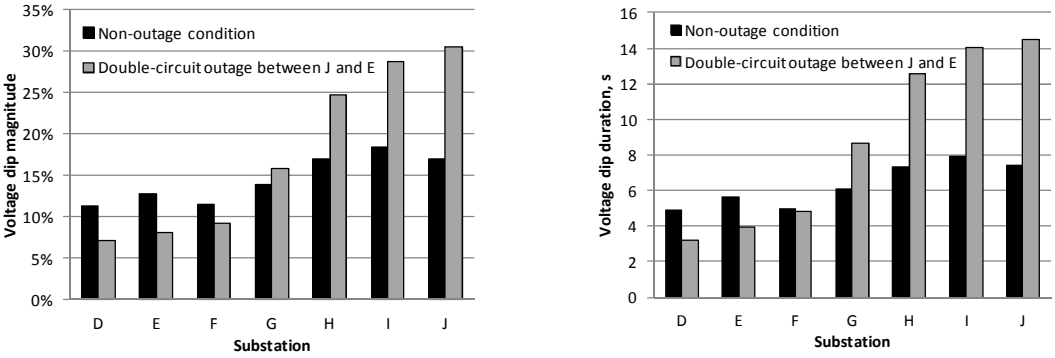

(a) Dip magnitude (b) Dip duration

Figure 4-22 Voltage dips caused by double-circuit outage between substation J and E

4.3 Sensitivity assessment

The voltage dips caused by transformer energisation are influenced by multiple parameters. Sensitivity assessment was carried out to identify the most influential parameters. Here, the concerning parameters include the system source strength, system loading, GSU transformer load losses and GSU transformer core saturation inductance. Closing time and residual flux were not taken into account in the sensitivity study because they were treated as fixed parameters forming the worst energisation condition.

The energisation Case 10 was selected as the base case for the sensitivity assessment. The sensitivity assessment addressed variations of the concerning parameters between +100% and -50% of their values in the base case (i.e. up to 200% variation was applied).

The results of the sensitivity study are shown in Figure 4-23 in which voltage dips due to variation of transformer load losses, core saturation inductance, source strength and system loading are shown in Figure 4-23 (a), Figure 4-23 (b), Figure 4-23 (c) and Figure 4-23 (d), respectively.

In general, it can be seen that: both the core saturation inductance and the supply source strength exhibit significant impact on dip magnitude; the dip duration is largely affected by the variation of transformer load losses as well as the supply source strength; the impact of system loading variation on voltage dip duration and magnitude is moderate.

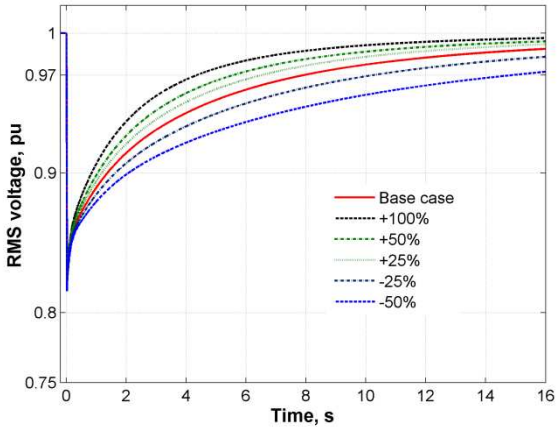

(a) Effects of transformer load losses variation

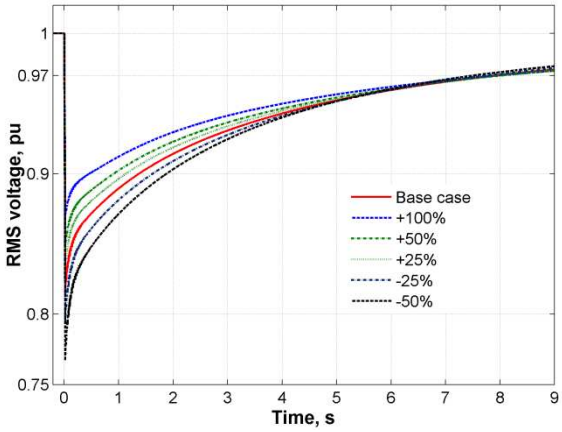

(b) Effects of transformer core saturation inductance variation

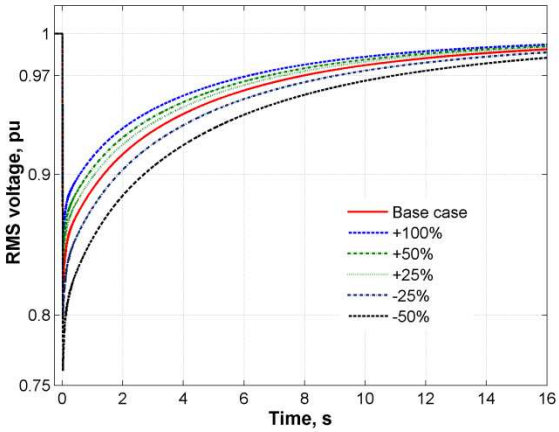

(c) Effects of source strength variation

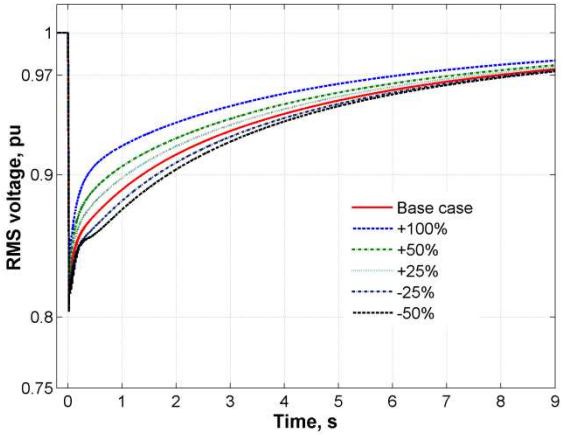

(d) Effects of system loading variation

Figure 4-23 Voltage dips influenced by variation of key parameters

Furthermore, two sensitivity factors were used to quantify the effects of the parameter variations on the voltage dip magnitude and duration: one is dip magnitude deviation V_d

and the other is dip duration deviation T_d. These two factors are presented in Figure 4-24 as an example which compares the phase C voltage dip between two cases: the base case (plotting in solid line) and the case with 100% increase of source strength (plotted in dotted line). The percentage of dip magnitude deviation is deduced from $100\times(V_1-V_{base})/V_{base}$; similarly, the percentage of dip duration deviation is calculated by $100\times(T_1-T_{base})/T_{base}$.

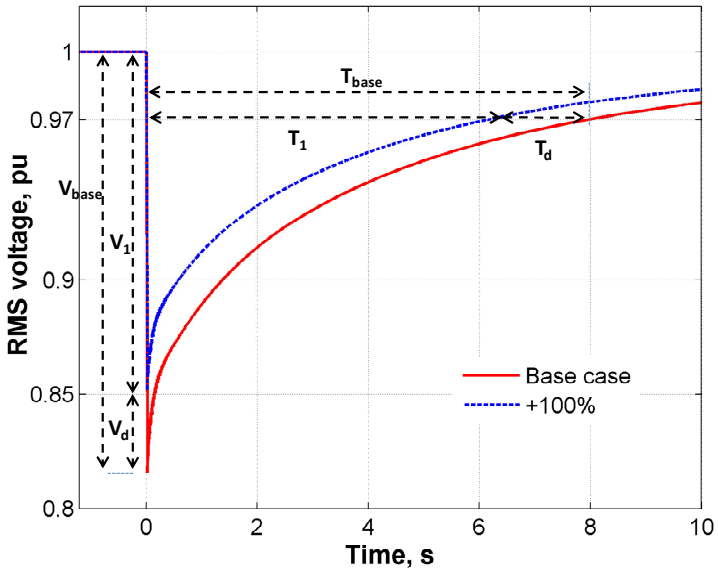

Figure 4-24 Example for illustrating two sensitivity factors V_d and T_d

Based on the results shown in Figure 4-23, the two sensitivity factors were analysed and the obtained quantities of the deviations are detailed and compared in Figure 4-25 and Figure 4-26, respectively. In both figures, each column represents the deviation caused by variation of a certain parameter.

Figure 4-25 illustrates that change of core saturation inductance presents the biggest impact on dip magnitude. Source strength is the second most influential one. In fact, in the reduced cases, the impact of source strength variation on voltage dip magnitude is comparable with that caused by variation of core saturation inductance. The variation of system loading only results in minor impact on dip magnitude. The variation of transformer copper losses barely impacts the dip magnitude.

In Figure 4-26, it can be observed that change of transformer load losses dominates the impact on voltage dip duration (e.g., 50% reduction of transformer load losses could increase dip duration by 88%); the cases of reduced full-load losses have more impact than those of increased. The second most influential parameter is again the source

impedance. 50% reduction of source strength will increase the duration by 36.5%. Variation of system loading only shows minor impact on voltage dip duration, which is similar to its impact on dip magnitude. The variation of core saturation inductance shows very little impact on voltage dip duration, however, exhibits great impact on dip magnitude. It should be noted that, although the above analysis focuses on phase C, the other two phases also exhibit the same trend.

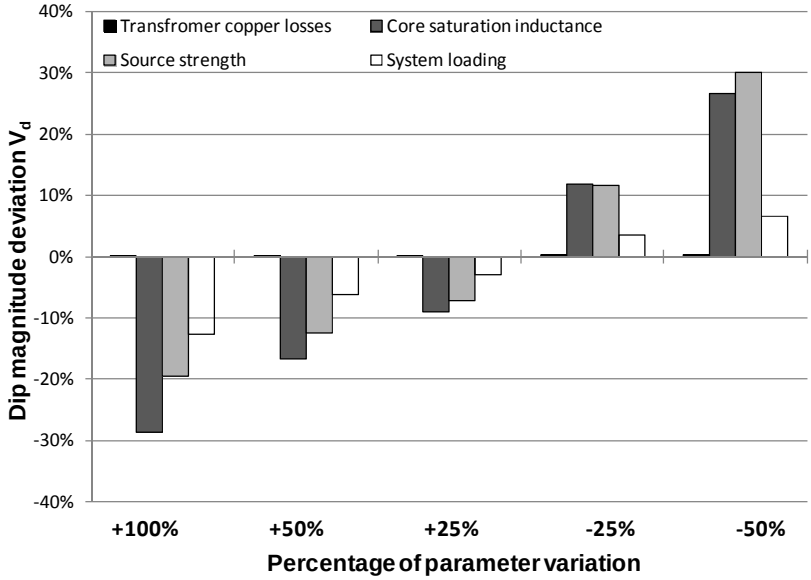

Figure 4-25 Impacts of parameter variation on voltage dip magnitude

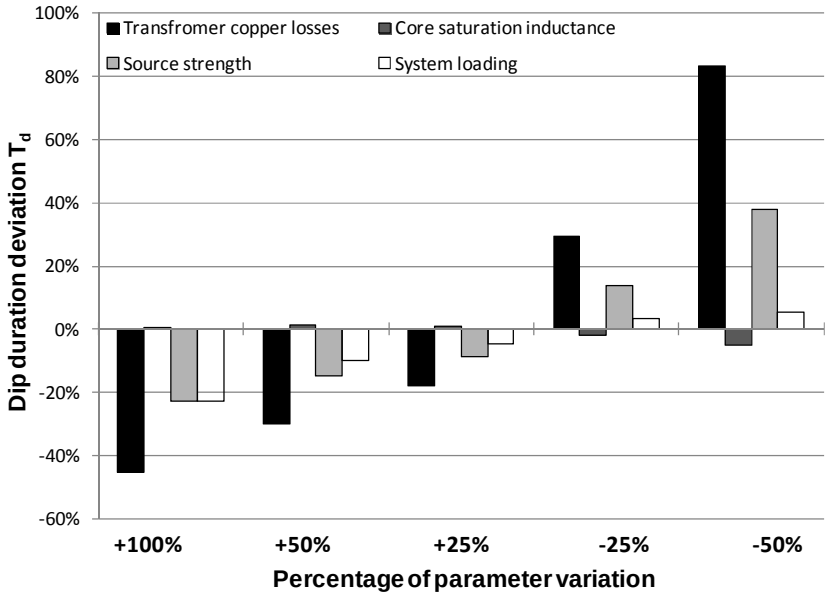

Figure 4-26 Impacts of parameter variation on voltage dip duration

The minor impact of system loading variation suggests that the system loading condition is of less concern when carrying out transformer energisation in the network studied, which can be attributed to the low ratio of maximum substation loading to the source strength (which is less than 0.09), i.e., the source strength is too strong relative to

system loading. However, it is noteworthy that for those systems having a higher ratio of system loading to source strength, the effect of system loading might become more obvious. The network studied here is characterized by long transmission lines between supply source and the transformers being energised, and therefore the effect of source strength, to some extent, has been offset by the impedances of long transmission lines; in those systems where the supply source is located closer to the transformers being energised, the impact of source strength variation would be more significant. The variation of core saturation inductance directly influences the magnitude of inrush currents and thus produces great impact on the dip magnitude; however, most transformers up to date are only tested at factory up to 110%; open circuit test at higher voltages is required for more accurate estimation of core saturation inductance. On the other hand, the saturation inductance only slightly affects the decay time constant of inrush transients (due to the saturation inductance relatively small compared to network impedance), and therefore shows little impact on the dip duration. The significant impact of transformer load losses on dip duration is because the decay of sympathetic inrush is highly determined by the losses of the GSU transformers and the losses of the connection between them. Due to the short electrical distance between the GSU transformers, the amount of load losses of the GSU transformers is the key contributor to the damping of sympathetic inrush and therefore imposes the greatest impact on dip duration.

4.4 Operational measures for controlling voltage dips

With Case 10 energisation under non-outage condition as the base case, some operational measures were studied to effectively and economically mitigate the voltage dips caused by transformer energisation, which include:

- Adjusting tap changer position;
- Application of SVC device;
- Application of mechanical switched capacitors (MSC);
- Opening of the coupler circuit breaker.

The key benefit of these operational measures is that they utilized the devices already existing in the system and do not incur any additional cost.

4.4.1 Utilization of tap changer

The GSU transformers are equipped with on-load tap changers which can be positioned to a maximum tap to give 1.15 pu of the rated voltage. Positioning at this maximum tap increases the number of turns to be energised, which has two potential effects: one is that the nominal operating flux is lowered because of the smaller voltage per turn; the other is it increases the winding air-core inductance. To approximate the first effect, the values of the peak flux-linkages in the original flux-current curves were times by a factor of 1.15; for the second effect, the values of the core saturation inductances of T2 and T3 were both increased by 40% (this amount was estimated by the transformer short-circuit inductances measured under the maximum tap). The modified saturation curves of the transformer T2 and T3 are shown in Figure 4-27(a) and Figure 4-27(b), respectively.

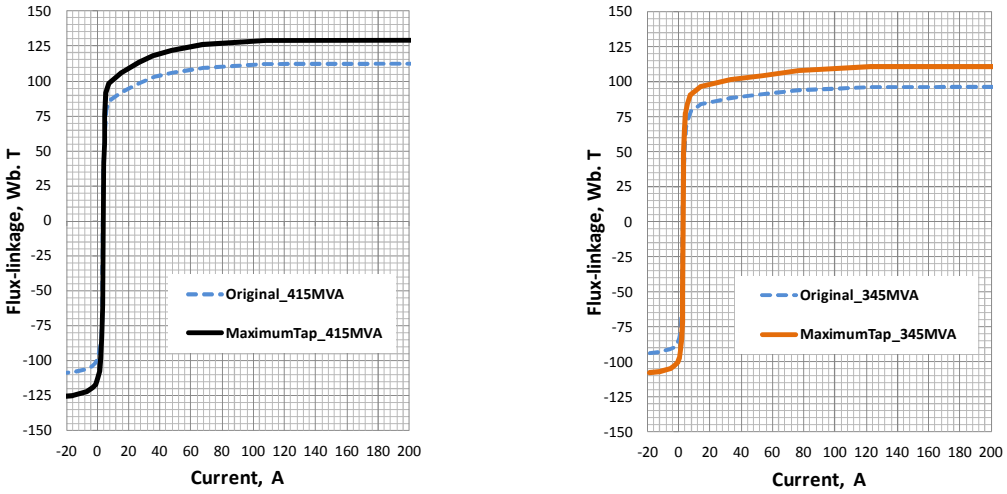

(a) GSU T2 (b) GSU T3

Figure 4-27 Modified saturation curves for approximating maximum tap effect

By applying the approximated saturation curves to the transformer T2 and T3, energisation Case 10 was simulated. In Figure 4-28 and Figure 4-29, the resulted network-wide voltage dip magnitudes and durations are compared to those observed in the base case, which shows that: both dip magnitude and duration can be reduced; the reduction on dip magnitude (about 24%) is much larger than that on dip duration (about 7%). The reduction of dip magnitude is largely attributed to the increase of core saturation inductance, which is in line with the findings in the sensitivity assessment.

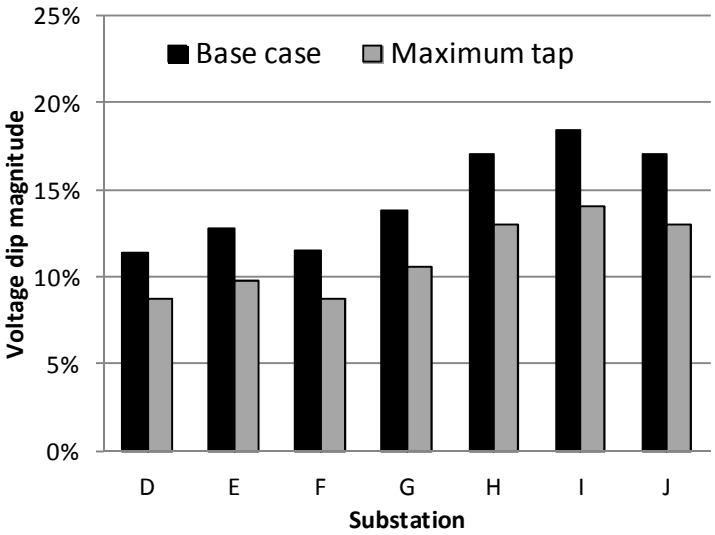

Figure 4-28 Voltage dip magnitudes observed in the case with GSU transformers set to their maximum tap

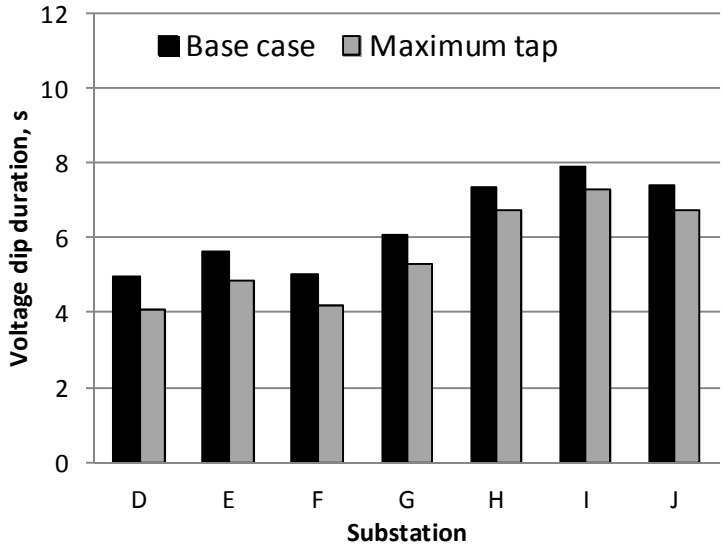

Figure 4-29 Voltage dip duration observed in the case with GSU transformers set to their maximum tap

4.4.2 Application of SVC

The SVC can give immediate reactive power compensation to the transmission system. Under transformer energisation, the voltage dip performance is further studied when the SVC is involved, taking into account the possible variation of SVC's capacity, response time and distance to the GSU transformers being energised.

4.4.2.1 SVC capacity

In this study, it was assumed that the location of the SVC is at the 400 kV busbar of substation K and its response time is fixed at 120 ms. With different capacities, including 75 MVar, 150 MVar and 300 MVar, the effect of the SVC capacity on voltage

dip performance was simulated. Regarding the effects on voltage dip magnitude, the results obtained are shown in Figure 4-29; regarding the effects on voltage dip duration, the results obtained are shown in Figure 4-31; both were compared with the patterns observed in the base case. As can be seen, application of SVC device has negligible impacts on dip magnitude but helps speed up the voltage dip recovery; the recovery can be observed on all the substations; faster recovery can be achieved by the SVC with larger capacity; applying 300 MVar SVC can result in 39% reduction of dip duration. The negligible impacts on dip magnitude can be attributed to the fact that the SVC normally needs several cycles to respond to the voltage dips within which maximum dip magnitude has already been reached.

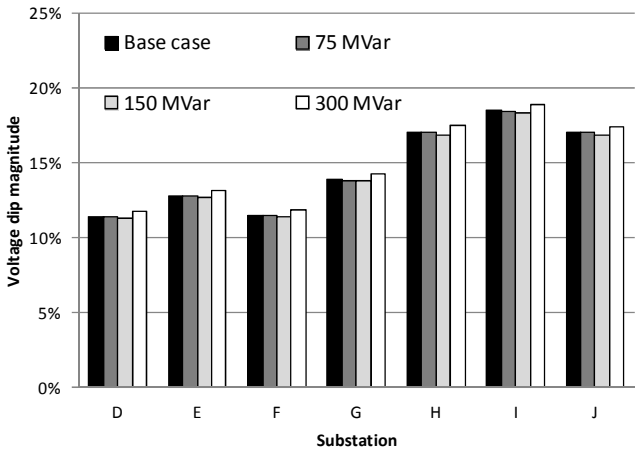

Figure 4-30 Effect of SVC with different capacities on dip magnitude

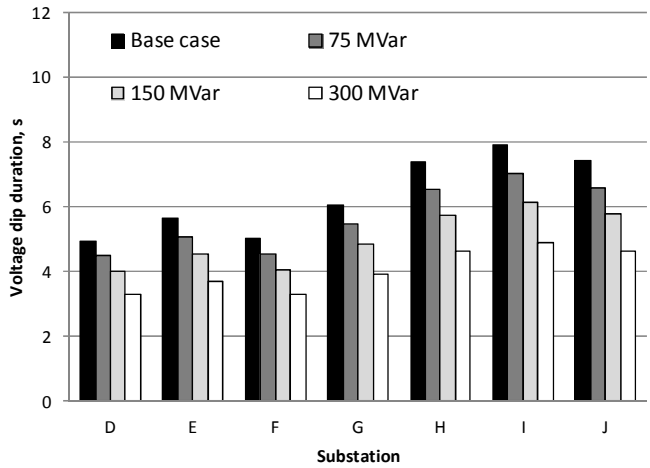

Figure 4-31 Effects of SVC with different capacities on dip duration

4.4.2.2 SVC response time

With the capacity of SVC fixed at 300 MVar and its location at the 400 kV busbar of substation K, possible effect of response time variation on the SVC performance was studied. The values of response time under study include 80 ms, 120 ms and 160 ms. It

is shown in Figure 4-32 that the effect of SVC on voltage dip duration is not affected by the variation of SVC response time.

4.4.2.3 SVC location

With the capacity of SVC fixed at 300 MVar and its response time at 120 ms, further studies were conducted to see whether the location of SVC may affect the dip duration. Besides locating the SVC at substation K, two other locations were considered: substations E and H. In Figure 4-33, the obtained patterns of dip duration are contrasted to that observed in the base case. As can be seen, the substations nearest to the SVC location will benefit the most; therefore it is desirable to locate SVC close to the substation where the transformers are to be energised.

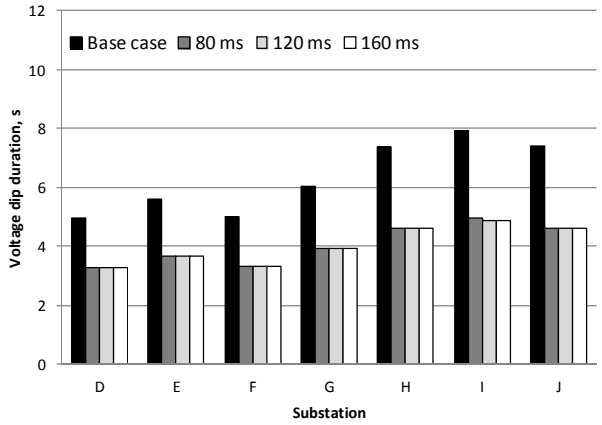

Figure 4-32 Effects of SVC with different values of response time on dip duration

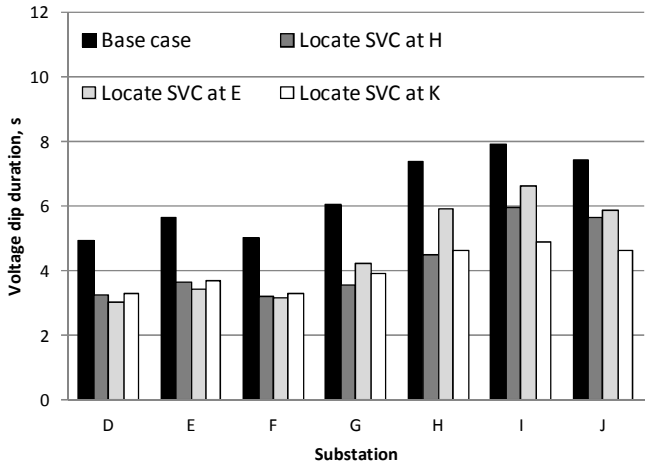

Figure 4-33 Patterns of voltage dip duration at 400kV side for various SVC locations

4.4.3 Application of MSC

Although switching in capacitors also shows similar ability to speed up the voltage recovery, it might cause other negative disturbances to the system, such as switching

overvoltages and voltage overshoot. Therefore, application of switching in capacitor banks is not suggested here as a remedial solution.

4.4.4 Opening coupler circuit breaker

The two busbars at the substation K is coupled by a circuit breaker CB1. To make the substation operating solid, CB1 is normally in the closed position, which is a condition for all the cases studied above. As one of the possible operational measures, it is interesting to evaluate the effect of opening the coupler CB1 on the voltage dip performance. This was conducted by simulating the energisation Case 10 with the CB1 being opened. Results obtained are compared with that observed in the base case, as shown in Figure 4-34 and Figure 4-35 for voltage dip magnitude and duration, respectively.

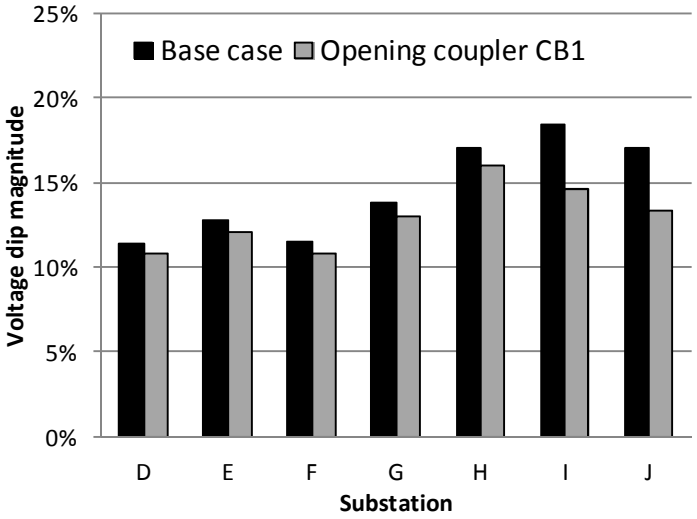

Figure 4-34 Effects of opening coupler CB1 on dip magnitude

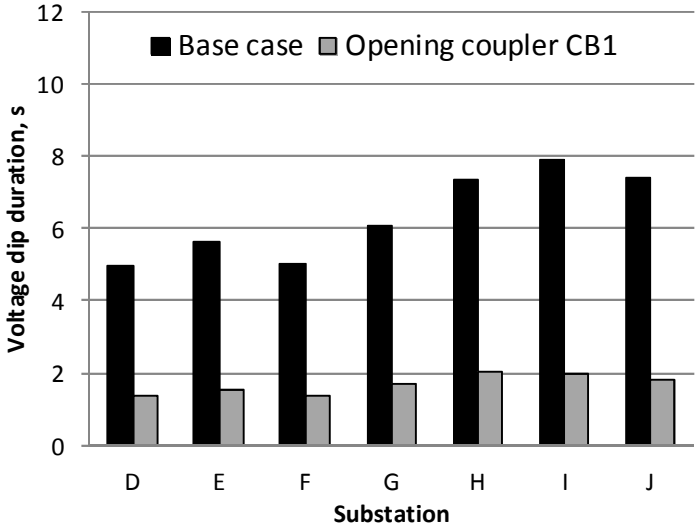

Figure 4-35 Effects of opening coupler CB1 on dip duration

As can be seen, opening the coupler CB1 moderately reduces the dip magnitudes (about 21%) but significantly reduces the dip duration (nearly 75%). This great impact on duration is largely attributed to the fact that: the opening of CB1 adds long transmission lines into the connection between the GSU transformer T1 and GSU transformers T2&T3, which effectively increases the losses of the connection between the GSU transformers. As the decay of sympathetic inrush is highly determined by the losses of the connection between the GSU transformers and their own losses, the increase of connection losses significantly reduces the dip duration.

4.4.5 Combining operational measures

The above analysis shows that adjusting the tap changer to the maximum tap, applying SVC device and opening coupler circuit breaker can effectively relieve voltage dips. These three mitigation approaches were combined together to simulate the energisation Case 10. Note that in the study, it was assumed that the SVC is of 300 MVar, 120 ms response time and located at substation K. Again, the simulated voltage dip magnitude and duration patterns are compared with those observed in the base case, which are shown in Figure 4-36 and Figure 4-37, respectively. As can be seen, by simultaneously applying all the possible operational measures, the dip magnitude at substation I can be reduced by 37% and the dip duration by 85%.

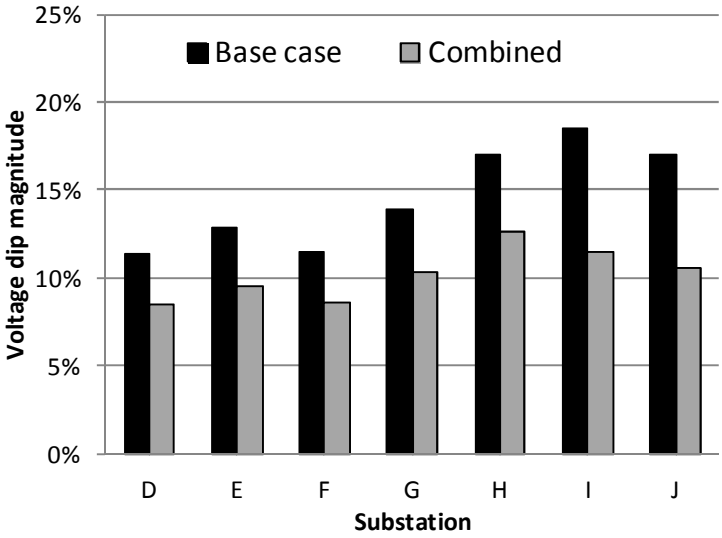

Figure 4-36 Dip magnitude pattern simulated under combined case

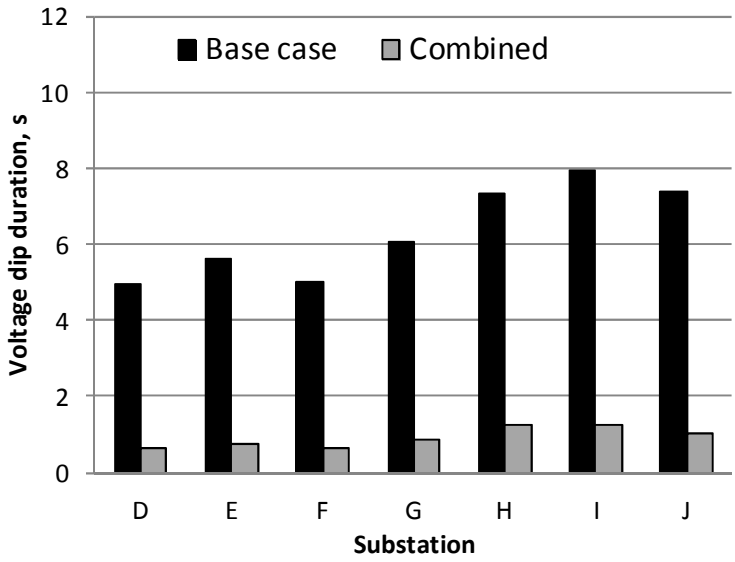

Figure 4-37 Dip duration pattern simulated under combined case

4.5 Summary

In this chapter, the voltage dips due to energising large GSU transformers was comprehensively studied based on a real 400/132 kV network, with special attention paid to the influences of sympathetic inrush. The network model developed and validated in Chapter 3 was used for carrying out the simulation studies.

The degrees of voltage dips under different energisation conditions were assessed. It was found that, under the worst case energisation condition: with two GSU transformers simultaneously energised, the maximum dip in the present system is at the substation closest to the transformers being energised and its magnitude is about 18% and duration about 3.5 seconds; with the presence of sympathetic interaction, the magnitude of sympathetic inrush current can be more than twice the transformer rated current; the sympathetic inrush can prolong the dip duration from 3.5 seconds to 7.9 seconds. The voltage dips caused at 400 kV transmission system side can propagate into 132 kV distribution system and the dip duration on 132 kV side is longer due to the sympathetic inrush of substation transformers.

Network-wide voltage dips were assessed under non-outage network condition. The dip magnitude observed at each substation was found to be related to the distance between the substation and the supply source and also the distance between the substation and the energised transformers. Those substations located in the proximity of the energised transformer and relatively far away from supply source would experience larger dip

magnitudes.

Furthermore, the network-wide voltage dips were assessed when the network under line outage situations. It was found that: under single-circuit outage, the network voltage dips performance is similar to that observed under non-outage network condition; however, if there is double-circuit outage, both dip magnitude and duration can be significantly exacerbated; in the present system under study, the most unfavorable double-circuit outage can increase the dip magnitude to about 30% and the duration to about 14 seconds.

Considering sympathetic inrush and voltage dips are controlled by multiple parameters, sensitivity assessment was carried out to identify the most influential parameters on dip magnitude and duration. It was found that transformer core saturation inductance has the most profound impact on the voltage dip magnitude; however, this parameter is not readily available from factory test report. The amount of transformer load losses has been proven as the key influential parameter on determining the duration of sympathetic inrush and voltage dip.

Based on the understanding obtained from the deterministic assessment, possible operational measures to control the voltage dips were explored. It was found that:

- Adjusting tap changer to its maximum tap can reduce voltage dip magnitude by 24% and duration by 7%;
- Applying 300 MVar SVC next to the GSU transformer being energised can reduce the dip duration by 39%;
- Opening the coupler circuit breaker can contribute about 75% reduction of dip duration and 21% reduction of dip magnitude;
- If these operational measures are applied simultaneously, the dip magnitude and duration can be reduced by 37% and 85%, respectively.

Chapter 5 Assessment of Voltage Dips Caused by Transformer Energisation Transients Using Stochastic Approach

Transformer energisation, as mentioned in the previous chapters, may cause significant inrush current that could induce adverse impacts on power systems and the transformer itself; the severity of these impacts is determined by several key parameters which can be classified as external and internal for the transformer. External parameters include the circuit breaker closing time, strength of the supply source and system loading; internal parameters include residual flux and saturation characteristics of the transformer core. In most of previous research, deterministic combinations of these key parameters are normally used for assessing the most adverse impacts and the commonly agreed one is the worst energisation condition characterized by simultaneous energising transformer at the voltage zero crossing of one phase and its corresponding residual flux set to be with maximum magnitude and polarity in line with flux build-up.

However, since the circuit breaker closing time, transformer core residual flux as well as system conditions are normally of stochastic nature, the assessments performed using the deterministic approach as mentioned above could underestimate the outcome or at least unable to give the probability distribution of the occurrence of inrush transients, therefore, they cannot assist the realistic estimation of the adverse impacts of inrush transients on the system. Hence, recently, a number of studies were devoted to studying the impacts of parameter uncertainties on the calculation of transformer energization transients [43, 104, 114]. The studies extended the few deterministically-defined studies to many stochastically-defined case studies by considering the stochastic nature of the key parameters.

In this chapter, Monte Carlo approach is used to stochastically evaluate voltage dips caused by transformer energisation in the South West system. The 400 kV transmission network model developed and validated in Chapter 3 is coordinated with MALAB program to perform the Monte Carlo simulation. It is aimed to identify the dip

frequency pattern and the likelihood of reaching the dip magnitude resulted from the commonly agreed worst case energisation condition, with their sensitivities to the variation of circuit breaker closing time span, transformer core residual flux, system condition and the number of transformers being energized together also investigated.

5.1 Monte Carlo simulation platform

5.1.1 Monte Carlo simulation

Monte Carlo simulation is a procedure of iteratively performing stochastic sampling experiments with a system model [115]. In each iteration, the values of the stochastic variables consisted in the system model are re-sampled from their corresponding distribution functions, based on which, a simulation is conducted to estimate the system performance. Through performing a large number of statistical sampling experiments, the response of a system to the stochastic variables can be approximately obtained. The more experiments being performed, the more accurate the approximation can be achieved towards the real performance of the system.

5.1.2 MATLAB-ATP interfacing simulation platform

Monte Carlo simulation requires a large number of simulations where the only difference between each case is a stochastic variation of a few stochastic parameters. Manually carrying out such a simulation (editing and running the ATP program) requires tremendous efforts and may easily cause mistakes. It is therefore preferable to automate such a simulation process. A MATLAB-ATP interfacing simulation platform was specifically designed and established for automating the Monte-Carlo simulation. This platform coordinates the advantages of the MATLAB and ATP: ATP package executes the transient simulation; MATLAB generates and modifies the values of the stochastic variables as the inputs for simulation, controls Monte Carlo simulation and processes the simulation results.

Arbitrary number of simulation runs can be carried out. For each simulation run, the coordination of MATLAB and ATP for Monte-Carlo simulation follows such a procedure:

- First, the random number generators in MATLAB are called upon to generate values for the stochastic variables such as closing time and residual flux;
- Second, MATLAB opens the ATP program and writes the generated values of

the stochastic variables to the ATP program;

- Third, the ATP-solver is called upon by MATLAB to execute the modified ATP program;
- Fourth, once ATP simulation has completed, an ATP PL4 file is generated and MATLAB calls another program (PL4toMAT) to convert the ATP PL4 file to MAT file which can be read by MATLAB;
- Fifth, the data stored in the MAT file are processed to obtain results such as the maximum inrush current peaks, the maximum dip magnitudes, the distribution of dip magnitudes and so on.

5.2 Stochastic parameters determination

5.2.1 Potential stochastic parameters

The key influential parameters that could affect transformer inrush-induced voltage dips are transformer core saturation inductance, transformer copper losses, closing time, residual flux, system loading and source strength.

Supposing detailed design data are available, transformer core saturation inductance can be determined by the core and winding dimension; transformer copper losses can be determined by the winding material, cross section area and length, which indicates they are fixed by transformer design. Therefore, the two parameters can be regarded as deterministic parameters.

As mentioned in Chapter 2, closing time and residual flux are normally of stochastic nature. In general, when the closing of a circuit breaker is uncontrolled, the signal to initiate breaker closing is stochastic with respect to the ac voltage wave; in addition, the breaker poles of three-phase do not close simultaneously, but with some closing time scatters which may vary with time and maintenance [116]. Hence, the circuit breaker closing time is featured by the stochastic signalling time to order the closure of three poles and the stochastic closing time span between the three poles.

Transformer residual flux is largely influenced by the ring down process initiated by transformer de-energisation [117]. Resulted from this process, the residual flux in the transformer core can be influenced by a number of factors including de-energisation instants, circuit breaker chopping characteristics, transformer core material, winding capacitances and other system capacitance connected to the transformer [118]. The

uncertain properties of transformer residual flux can be categorized by two folds: one is the magnitudes of residual flux in three phases and the other is their distribution among three phases. Up to date, knowledge about these two aspects include: residual core flux can be as high as 85% of peak nominal flux; residual flux in cores of three phase transformers must inherently sum to zero [117, 118].

The amount of loads connected to the system could have daily and seasonal variations. Similarly, the source strength may vary with system configurations and generation connections. Therefore, to certain extend, both of these two parameters are of stochastic feature.

5.2.2 Quantification of stochastic parameters

For the above-mentioned stochastic parameters, each one can be quantified by a range defined by minus and plus certain percentages of a nominal value; in addition, the range can be characterized by a probability distribution using Uniform, Gaussian, Exponential or any other distribution functions.

Normally, Uniform distribution is used to describe the ranges of source strength and system loading; Uniform distribution can also be used to describe ranges of switching angle and residual flux in the case of single phase system. In the case of three-phase system, two procedures shown in Figure 5-1 and Figure 5-2 are used for quantifying the closing time and residual flux.

Utilizing the approach suggested in [43], modelling of the stochastic closing time followed the procedures shown in Figure 5-1. First, a common order time T_cot, which is the same for three poles of the circuit breaker, is defined by a Uniform distribution ranging in one power frequency cycle. Second, the maximum closing time span (MCTS), i.e. the time interval between the first pole and the last pole to close, is defined. Third, the MCTS is used to define the range of the closing offset time for each pole T_offset_i (i represents phase A, B or C); the range is assumed to be from –MCTS/2 to +MCTS/2, referring to the T_cot; in addition, a probability distribution is assigned to define the offset time range. Finally, the closing time of each pole can be determined by the summation of T_cot and T_offset_i which are stochastically generated based on their corresponding ranges and distributions.

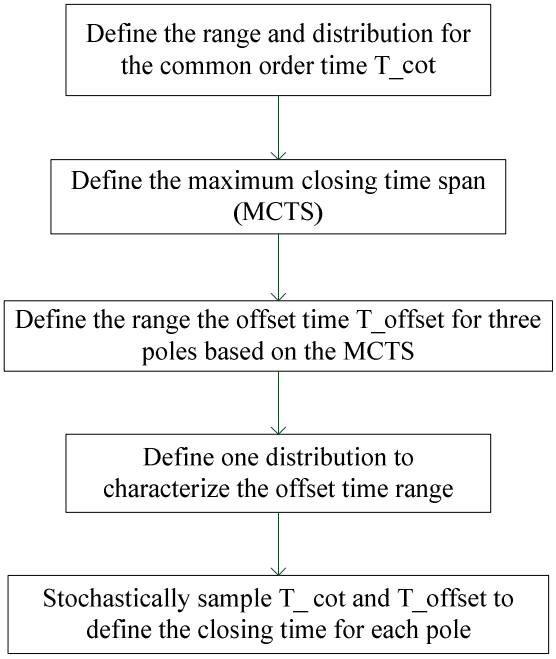

Figure 5-1 Procedure for generating stochastic circuit breaker closing time

For generating three-phase residual fluxes, it is commonly assumed that: the residual flux of each phase is in a range whose absolute maximum value is no more than peak nominal flux; the three-phase residual fluxes should sum to zero. With these assumptions, the three-phase residual fluxes were generated through the procedure shown in Figure 5-2. As can be seen, the first step is to define the maximum residual flux Resi_max (normally in terms of the percentage of the peak nominal flux) for determining the residual flux range (i.e. from –Resi_max to +Resi_max); in the second step, a probability distribution is assigned to characterize the residual flux range; in the third step, based on the range and probability distribution, two residual flux values Resi_1 and Resi_2 are stochastically generated; then, a check loop is called upon to verify whether the absolute value of the sum of Resi_1 and Resi_2 is smaller than Resi_max, which is to ensure that |Resi_3| = |-Resi_2-Resi_1| < Resi_max; if not, go back to the second step; if yes, proceed to the fifth step to calculate Resi_3; finally, Resi_1, Reis_2 and Resi_3 are stochastically assigned to phase A, B and C, respectively.

Both procedures were programmed in MATLAB to generate the stochastic circuit breaker closing time and transformer core residual flux as the inputs for ATP to carry out transient calculations.

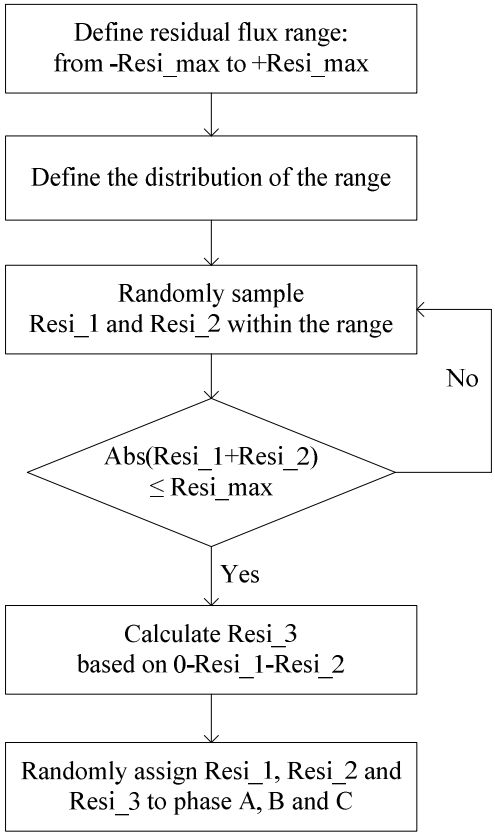

Figure 5-2 Procedure for generating stochastic transformer core residual flux

5.3 Preliminary assessment on a single-phase circuit

A preliminary assessment of voltage dips caused by transformer energisation was carried out based on a single phase circuit. The single-phase circuit is a simplification of the three-phase South West system, which is shown in Figure 5-3. The circuit consists of:

- an ideal voltage source;
- an equivalent series impedance, representing the source strength;
- a set of shunt connected resistance and inductance, representing the system loading;
- an ideal circuit breaker, whose closing time can be controlled;
- an ideal transformer connected in series with an impedance and a nonlinear inductor, representing a single phase transformer;
- an measurement unit which observes instantaneous voltage and current and calculates RMS voltage dip.

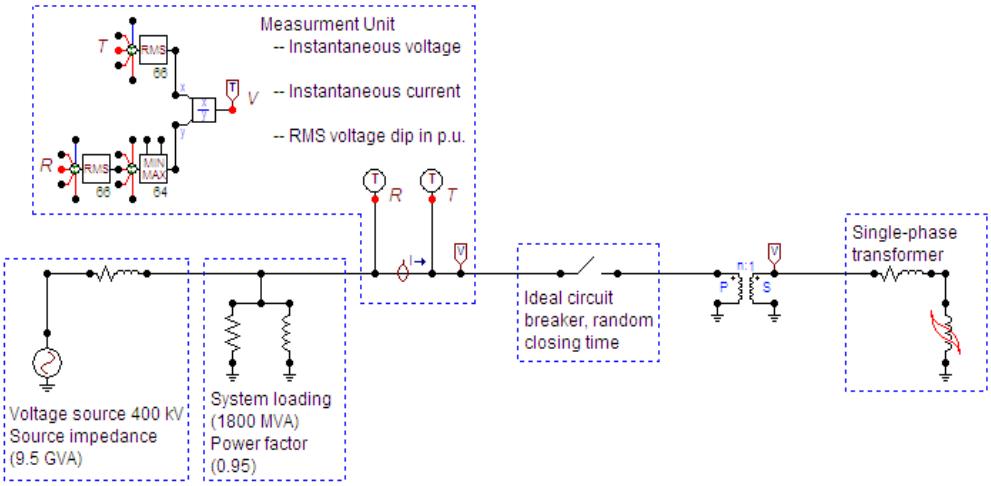

Figure 5-3 Single phase simulation circuit for preliminary Monte Carlo simulation

Initially, a determinstic worst case simulation was carried out based on the commonly agreed worst case energisation condition (i.e., the circuit breaker was closed at the postive-going zero crossing of the applied voltage and the transformer core retained 0.8 pu of peak nominal flux with positive polarity), with the system condition set as: the source fault level is of 9.5 GVA (X/R ratio is 10), the system loading is of 1800 MVA (power factor is 0.95 inductive). The resulted inrush currents and voltage dips observed at the transformer primary terminal are shown in Figure 5-4 and Figure 5-5, respectively. As can be seen, the first peak of the inrush current, the voltage dip magnitude and duration were 4.63 kA, 12% and 1.02 s, respectively. These were taken as the base values to scale the results obtained from the following case studies within this section.

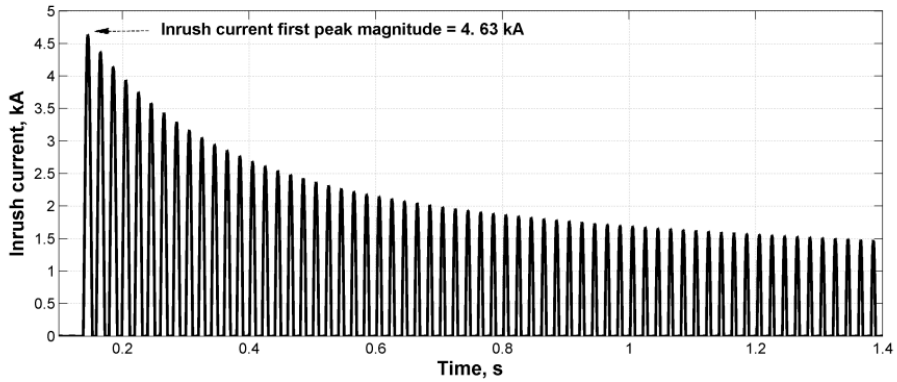

Figure 5-4 Inrush current resulted from energising a single phase transformer under the worst energisation condition

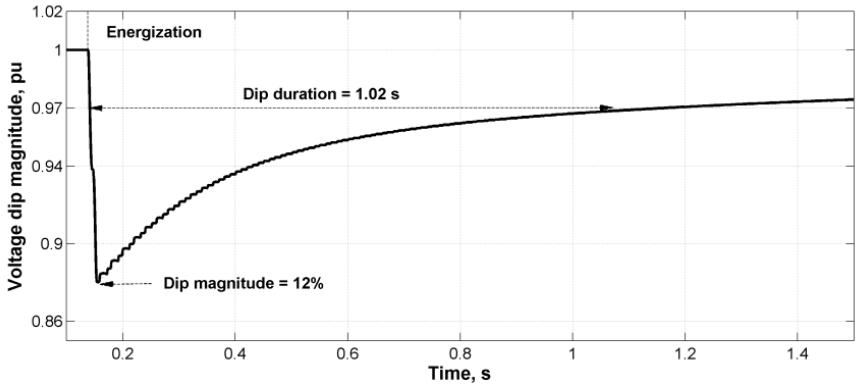

Figure 5-5 Voltage dips resulted from energising a single phase transformer under the worst energisation condition

Further, stochastic simulaiton was performed based on the single phase circuit. The simulation consists of two cases, which are shown in Table 5-1.

Table 5-1 Case studies of stochastic estimation of voltage dips caused by energising a single phase transformer

Case	Closing time		Residual flux		System condition	
	Range	Distribution	Range	Distribution	Range	Distribution
P1	One power frequency cycle	Uniform	±0.8 pu of peak nominal flux	Uniform	fixed	
P2					±25%	Uniform

In Case P1, only the circuit breaker closing time and the transformer core residual flux were considered as stochastic variables; both of them were defined by Uniform distribution; the range for the closing time was one power frequency cycle and the range for the residual flux was between -0.8 and +0.8 pu of peak nominal flux; the system conditions were fixed at the level identical to those set in the worst case simultion (i.e., 9.5 GVA source strength, 1800 MVA loading).

In Case P2, besides considering the variation of stochastic closing time and residual flux (range and distirbution of the two variables were considered to be the same as in Case P1), the variation of system condition (e.g., source strength and system loading) was also considered and its range was considered to be ±25% (i.e., the source strength varied in a range from 75 to 125% of 9.5 GVA and the system loading varied in a range 75 to 125% of 1800 GVA); both ranges were charaterized by Unifrom distribution. It should be noted that the X/R ratio of the source impedance and the power factor for the system loading were assumed to be constant.

For both case studies, 1000 runs were conducted. The distributions of closing time and residual flux obtained from Case P1 are shown in Figure 5-6 and Figure 5-7, respectively.

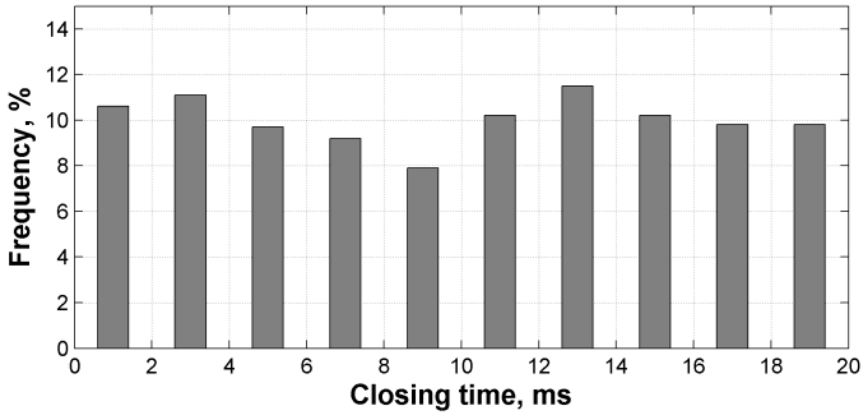

Figure 5-6 Distribution of closing time in Case P1

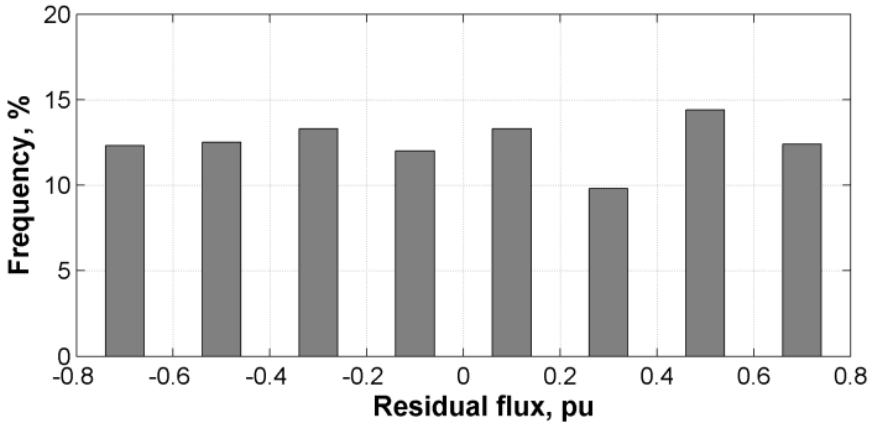

Figure 5-7 Distribution of residual flux in Case P1

The resulted voltage dips of Case P1 are illustrated as follows:

- Scatter diagrams: relative dip magnitudes and relative dip durations plotted against the relative inrush current peaks, which are shown in Figure 5-8 and Figure 5-9, respectively;
- Bar charts: illustrating the frequency of different dip magntiudes and durations, as shown in Figure 5-10 and Figure 5-11, respectively.

As can be seen in Figure 5-8, based on the base values obtained from the worst case simulation (e.g., the highest inrush current first peak 4.63 kA and the worst case dip magnitude 12%), the resulted inrush current peaks and voltage dip mangitudes are in per unit values by scaling to 4.63 kA and 12%, respectively; each voltage dip magnitude is corresponding to a specific inrush current peak; there is an approximate linear relationship between the voltage dip magntiude and the inrush current peak; the larger

the inrush current peak, the larger the dip magntiude. There are two worst case boundaries: the horizontal one is set by the worst case dip magnitude and the vertical one is set by the highest inrush current first peak. None of the results obatined from Case P1 study can exceed the two boudaries.

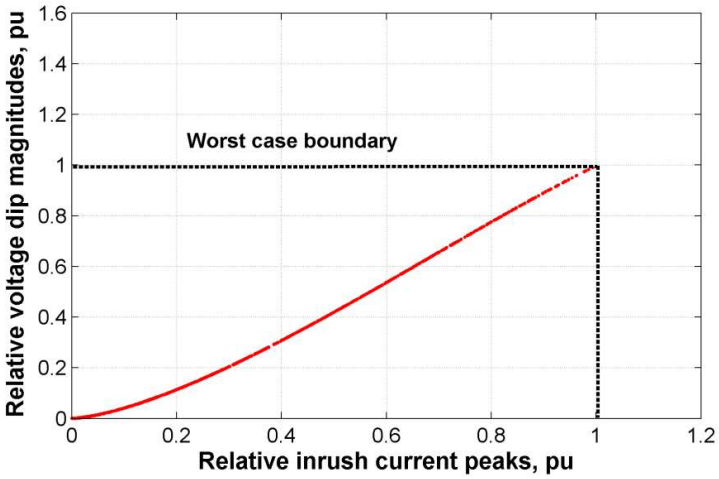

Figure 5-8 Relative voltage dip magnitudes plotted against relative inrush current peaks

Similar observations can be made in Figure 5-9 regarding the relation between the dip duration and the inrush current peak; the section of zero dip duration is attributed to those dips with magnitudes samller than the 3% dip threshold.

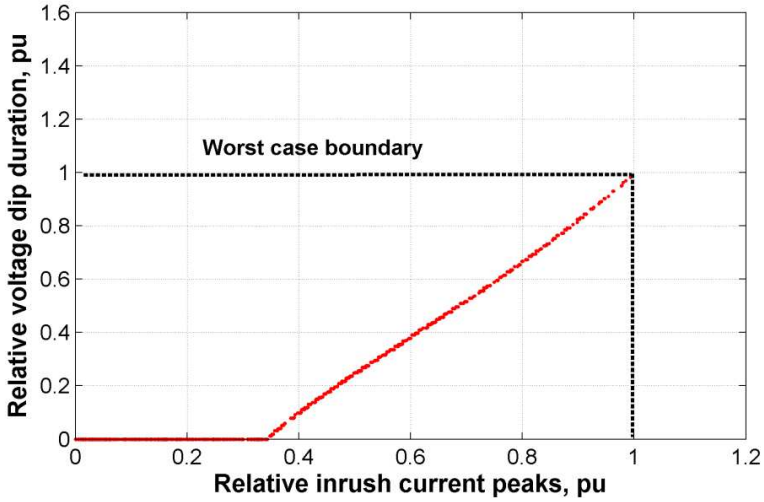

Figure 5-9 Relative voltage dip magnitudes plotted against relative inrush current peaks

Figure 5-10 illustrates the distribution of the relative voltage dip magntidutes. As can be seen, about 50% of the dips are with magntiudes smaller than 0.2 pu of the worst case dip magnitude; only about 6% of the dips are with magnitudes larger than 0.8 pu of the worst case dip magnitude. The distribution of the relative voltage dip durations is shown in Figure 5-11. Benchmarking the 3% dip threshold, about 55% of the dips are with

duration equal to zero and less than 5% of the dips are with duration larger than 0.8 pu of the worst case dip duration.

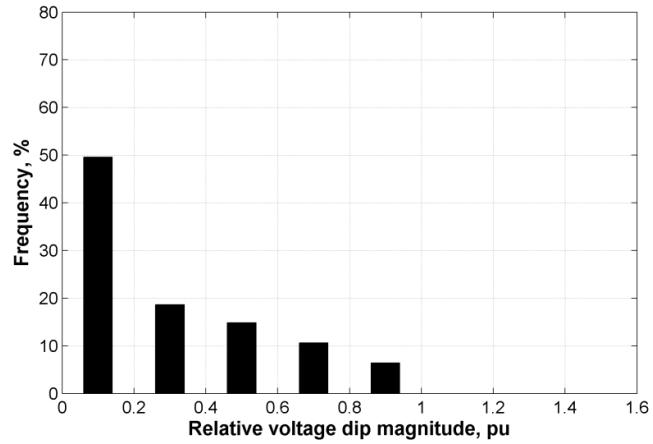

Figure 5-10 Frequency of voltage dips at different dip magnitude ranges

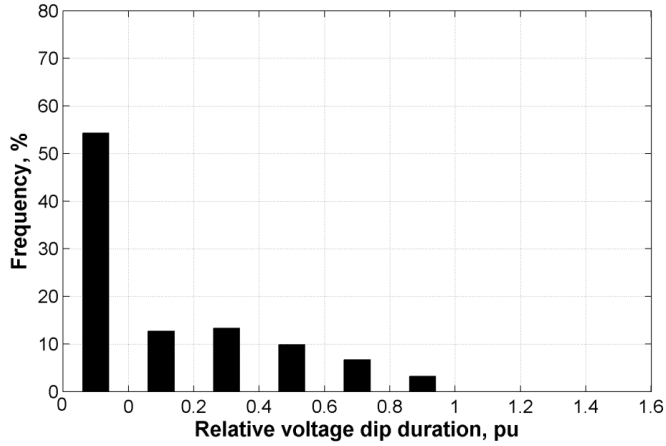

Figure 5-11 Frequency of voltage dips at different dip duration ranges

The resulted voltage dips of Case P2 stochastic simulation are illustrated as follows (similar to Case P1, the obtained dip mangitudes, durations and inrush peaks are in per unit values by scaling to 12%, 1.02 s and 4.63 kA, respectively):

- Scatter diagrams: relative dip magnitudes and relative dip durations plotted against the relative inrush current peaks, which are shown in Figure 5-12 and Figure 5-13, respectively;
- Bar charts: showing the frequency of different dip magntiudes and durations, which are shown in Figure 5-14 and Figure 5-15, respectively.

In Figure 5-12, the scattered points indicate that the same inrush current peak may result in a variaty of voltage dip magnitudes, mainly due to the vairation of system condition; the width of the scatter range is proportional to the inrease of inrush current peak. Benchmarking the scattered points with the worst case boundaries, most of the points are capped inside; a few points are out of the voltage dip mangitude boundary in the

cases of weak source strength; yet none of them can be of magnitudes exceeding both boundaries.

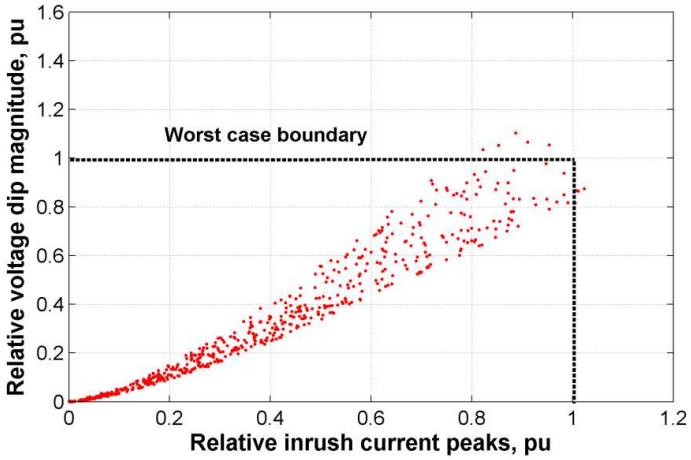

Figure 5-12 Relative inrush first peaks plotted against relative dip magnitudes

Similarly, the relative inrush current first peaks are ploted against the realtive voltage dip durations, as shown in Figure 5-13. It shows that: when the inrush current peak is smaller than 0.3 pu of the worst case inrush current peak, the dip duration is zero, i.e., the voltage dip mangitude is smaller than the 3% threshold; when the inrush current peak is bigger than 0.3 pu of the worst case, the voltage dip duration increases with the inrush current peak magnitude; again, due to the vairation of system condition, the possible voltage dip durations corresonponding to one inrush current peak is scattered. The width of the scatter range is also propotional to the inrease of inrush current peak.

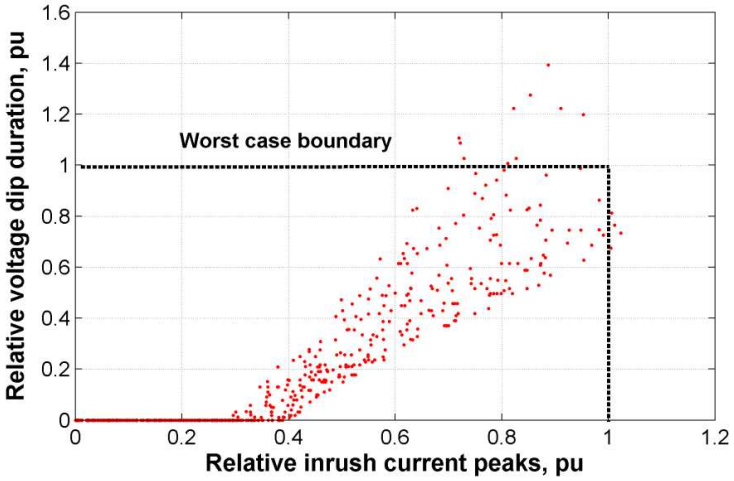

Figure 5-13 Relative inrush first peaks plotted against relative dip durations

Figure 5-14 shows the frequency of occurrence of different voltage dip mangitudes. As can be seen, the proportion of dips with magnitudes less than 0.2 pu of the worst case dip magnitude is about 65% which is larger than that observed in Case P1; only about 6% of dips are of magnitudes larger than 0.8 pu of the worst case dip magnitude.

Figure 5-15 shows the frequency of occurrence of different voltage dip durations. As can be seen, about 70% of the dips are of zero duration; the proportion of dips with duration reaching the worst case level is less than 1%.

The above findings suggest that the chance to encounter a voltage dip with a scale matching that estimated by the commonly agreed worst case energisation condition is very low. This can be attributed to the fact that, for any value of residual flux, there exists a counteracting closing time that results in nearly zero inrush current, whereas the probability is small for a maximum residual flux with a right polarity to meet a closing time at voltage zero crossing.

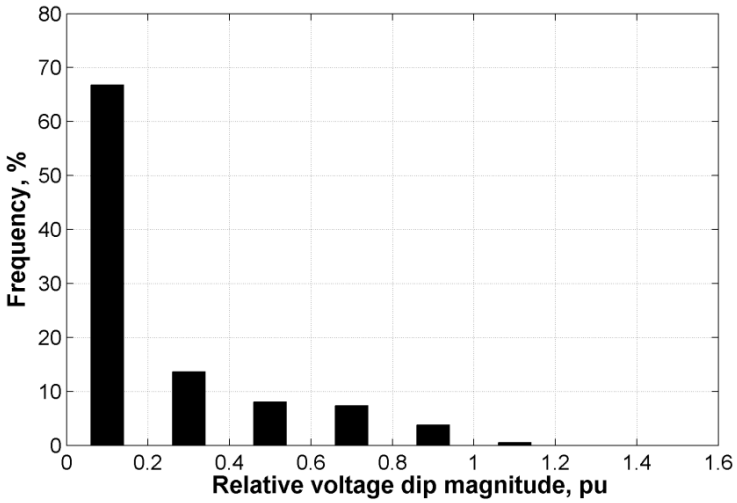

Figure 5-14 Frequency plot of votlage dip magnitudes relative to the worst case dip magnitude

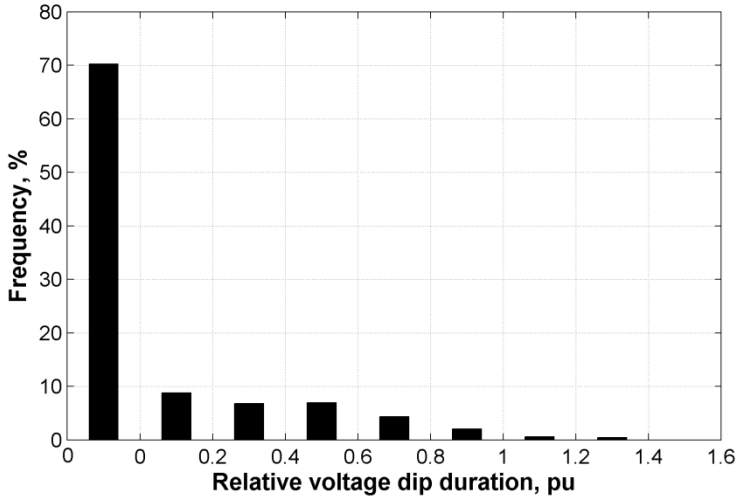

Figure 5-15 Frequency plot of votlage dip duration relative to the worst case dip magnitude

The preliminary study on the single phase circuit illustrates the influence of random parameter variation on the outcomes of the inrush transient and the associated voltage dips. It forms a basis for carrying out stochastic assessment for three-phase circuits.

5.4 Stochastic assessment of voltage dips caused by energising three-phase transformers

Besides studies on single phase circuit, voltage dips caused by transformer energisation were also stochastically assessed in the three-phase circuit based on the South West system. The assessment consists of the following sections:

- Identify the dip frequency pattern resulted from energising one three-phase transformer in the South West system;
- Study the influences of closing offset time distribution and residual flux distribution on the dip frequency pattern;
- Study the influences of the variation of source strength and system loading on the stochastic estimation of the dip frequency pattern;
- Study the dip frequency pattern when multiple transformers are simultaneously energised.

5.4.1 Simulation setup

The network model developed and validated in Chapter 3 was used as the basis for the stochastic simulation, which is briefly described as follows: system equivalent sources were represented by ideal voltage source connected in series with Thevenin equivalent impedances; transmission line was represented by Bergeron model; all the loads and shunt devices, such as capacitor banks, were modelled by constant impedances and they were directly connected to the 400 kV busbars; transformer modelling mainly takes into account winding resistances, leakage inductances and transformer saturation characteristics, and this was realized by the use of an BCTRAN model with hysteretic inductor (type-96) externally connected to the low-voltage winding terminal. It should be noted that, since the main focus of the stochastic assessment is the voltage dip magnitudes on the 400 kV side, the 400/132 kV substation transformers were not taken into account in the model.

5.4.2 Design of case study

To conduct the stochastic assessment, several different case studies were considered, which are shown in Table 5-2:

1) A base case for the stochastic estimation, named as Case S1, is calcuated to identify the dip frequency pattern; it considers energising only one GSU

transformer (T1) with the closing time and residual flux treated as stochastic parameters and system condition (e.g., system loading and source strength) fixed;

2) Influences of closing time on the dip frequency pattern are studied in Cases S2, S3, S4 and S5; specifically, Cases S2 and S3 consider the influence of the MCTS, Cases S4 and S5 study the influence of the closing offset time distribution;
3) Influences of residual flux distribution on the dip frequency pattern are studied in Cases S6, S7 and S8;
4) Influences of the variation of system condition including system loading and source strength are considered in Case 9;
5) In Cases S10 and S11, the dip frequency patterns resulted from simultaneously energizating two transformers are assessed and compared with that obtained in the base case.

Table 5-2 List of case studies conducted in stochastic assessment

<table>
<tr><th rowspan="2">Case</th><th colspan="2">Offset time</th><th>Residual flux</th><th rowspan="2">Energised Transformer /Network condition</th></tr>
<tr><th>Range (ms)</th><th>Distribution</th><th>Distribution</th></tr>
<tr><td>S1</td><td>±2.5</td><td>Gaussian</td><td rowspan="5">Uniform</td><td rowspan="8">Only T1 is energised

Fixed network condition</td></tr>
<tr><td>S2</td><td>0</td><td>--</td></tr>
<tr><td>S3</td><td>±5</td><td>Gaussian</td></tr>
<tr><td>S4</td><td rowspan="8">±2.5</td><td>Uniform</td></tr>
<tr><td>S5</td><td>Exponential</td></tr>
<tr><td>S6</td><td rowspan="8">Gaussian</td><td>Gaussian</td></tr>
<tr><td>S7</td><td>Exponential_1</td></tr>
<tr><td>S8</td><td>Exponential_2</td></tr>
<tr><td>S9</td><td rowspan="3">Uniform</td><td>Only T1 is energised

network condition ±25% variation (Uniform)</td></tr>
<tr><td>S10</td><td rowspan="2">T2 & T3 are energised

Fixed network condition</td></tr>
<tr><td>S11</td></tr>
</table>

For all the case studies, the common order time is of one power frequency cycle range defined by Uniform distribution and the residual flux is of a range between -0.8 pu and +0.8 pu of peak nominal flux.

The dip magnitude observed in the case of energising T1 under the commonly agreed worst case energisation condition (9.6%, named here as WCDM1) is selected as the

base value to be referred to by all the dip magnitudes obtained from Case S1 to S9. Similarly, the dip magnitude observed in the case of energising T2 and T3 under the commonly agreed worst case energisation condition (18.4%, named here as WCDM2) is used as the base value for scaling all the dip magnitudes obtained from Case S10 to S11.

5.5 General dip frequency pattern

In Case S1, the offset time of each pole was considered to follow a Gaussian distribution whose mean is zero (i.e., three poles tend to be closed simultaneously) and whose standard deviation is MCTS/6 (note that the MCTS was assumed to be 5 ms). As for the residual flux, it was assumed to be characterized by Uniform distribution. After 1000 runs, the probability distributions of the offset time for three-phase poles and three-phase residual fluxes were obtained and they are shown in Figure 5-16 and Figure 5-17, respectively. The frequency of voltage dips in three phases at substation I are shown in Figure 5-18 and Figure 5-19 regarding dip magnitude and duration, respectively. To test whether 1000 runs is sufficient, 5000 stochastic runs were conducted and the resulted patterns were compared with those obtained from 1000 runs. Dip frequency patterns out of 5000 runs of Case S1 were obtained and plotted in Figure 5-20 (for the frequency distribution of dip magnitude) and Figure 5-21 (for the frequency distribution of dip duration). Comparing the two bar charts with those obtained from 1000 runs, the differences between them are very small, indicating that it is sufficient to make the subsequent studies based on 1000 runs.

As can be seen, the dip frequency patterns of each phase are almost identical to each other, indicating that the dip frequency pattern observed on one of the phases can represent those observed on the other two phases. Therefore, analysis of the simulation results can be focusing on one phase and the phase chosen here is phase C.

By observing the dip frequency of phase C shown in Figure 5-18, it can be seen that: out of 1000 stochastic dip events, over 80% of the dips are with magnitudes less than 0.6 pu of WCDM1; no more than 6% of the dips are with magnitudes larger than 0.8 pu of WCDM1; only about 0.2% of the dips are with magnitudes larger than the WCDM1 and their magnitudes are about 1.1 pu of WCDM1. This larger dip magnitude suggests that calculation based on the commonly agreed worst case energisation condition

(which assumes zero closing time span) may underestimate the worst case dip magnitude by 0.1 pu.

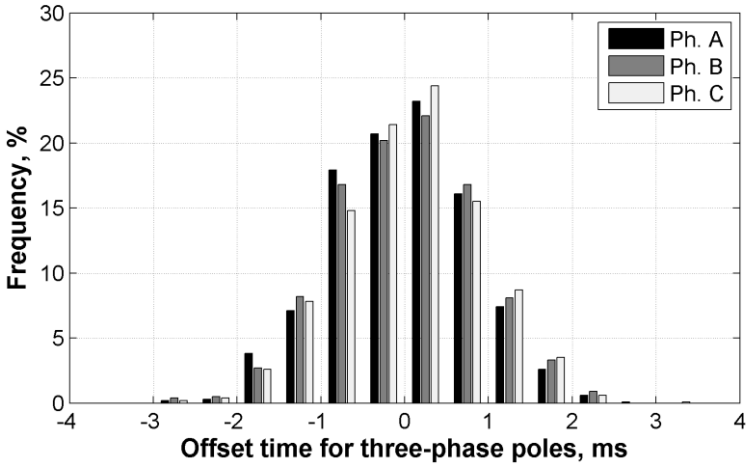

Figure 5-16 Distribution of offset closing time for three-phase poles in Case S1

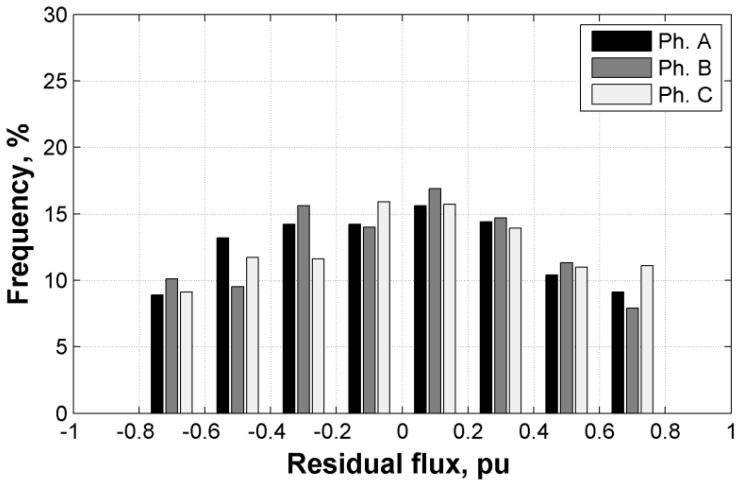

Figure 5-17 Distribution of residual flux in Case S1

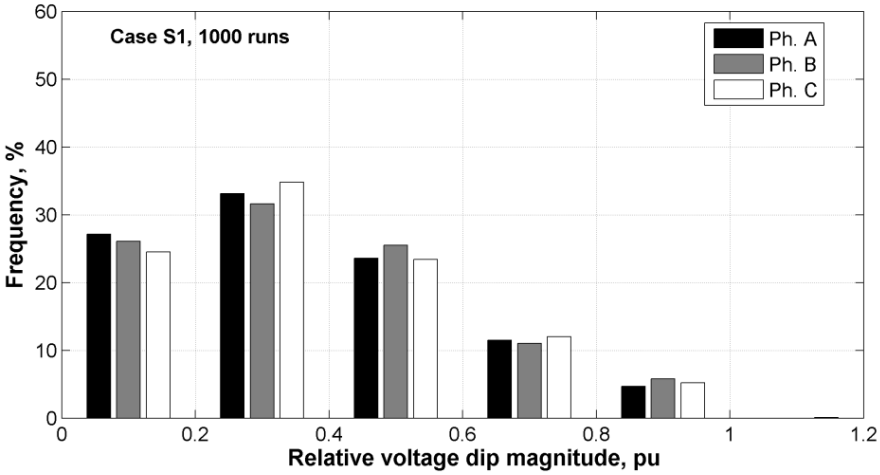

Figure 5-18 Frequency of dip magnitude of each phase at substation I out of 1000 stochastic runs

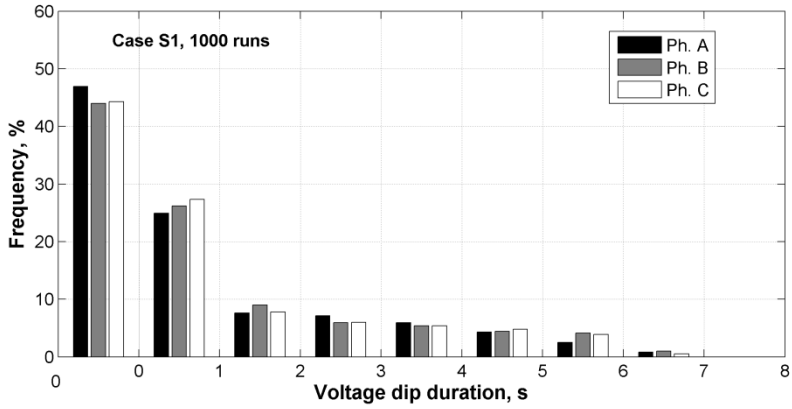

Figure 5-19 Frequency of dip duration in each phase at substation I out of 1000 stochastic runs

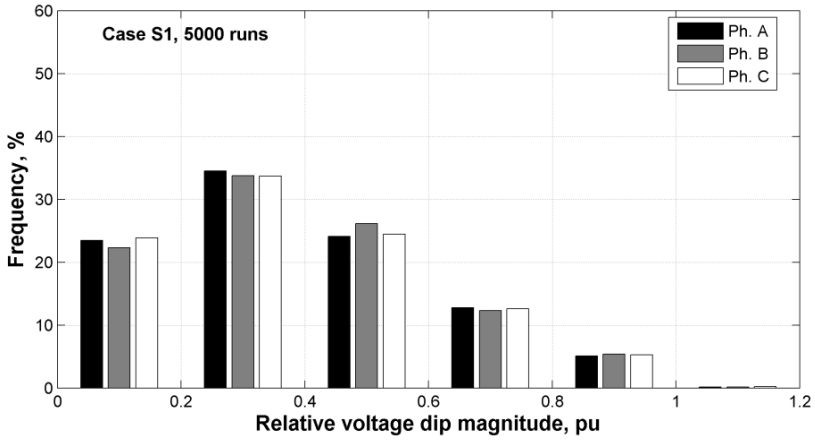

Figure 5-20 Frequency of dip magnitude in each phase at substation I out of 5000 stochastic runs

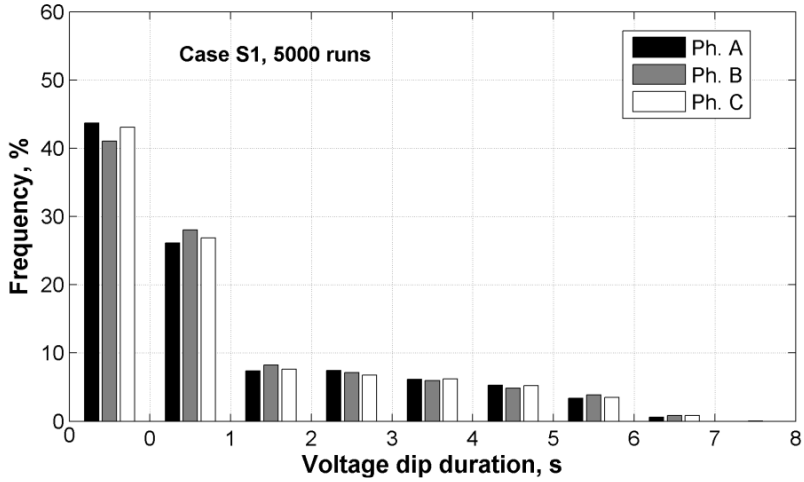

Figure 5-21 Frequency of dip duration in each phase at substation I out of 5000 stochastic runs

5.6 Influences of closing time span

5.6.1 Maximum closing time span

The MCTS may vary between circuit breakers. This variation may affect the outcome of the dip frequency pattern identified in the base case S1. To address this concern, two

case studies were conducted: one with zero closing time span (Case S2) and the other one with 10 ms MCTS (Case S3). For both cases, the distributions of closing offset time and residual flux are the same as those used in the Case S1. Similar to Case S1, 1000 runs were made for Case S2 and Case S3 to predict the dip frequency patterns of phase C at substation I; these two patterns are compared with that obtained from Case S1 in Figure 5-22 (It should be noted that the comparison made on phase C can represent the comparison made on the other two phases, because the dip frequency patterns of three phases are almost identical to one another). As can be seen, there is not much difference between any two of the dip frequency patterns. This indicates that the dip frequency pattern is not sensitive to the variation of MCTS.

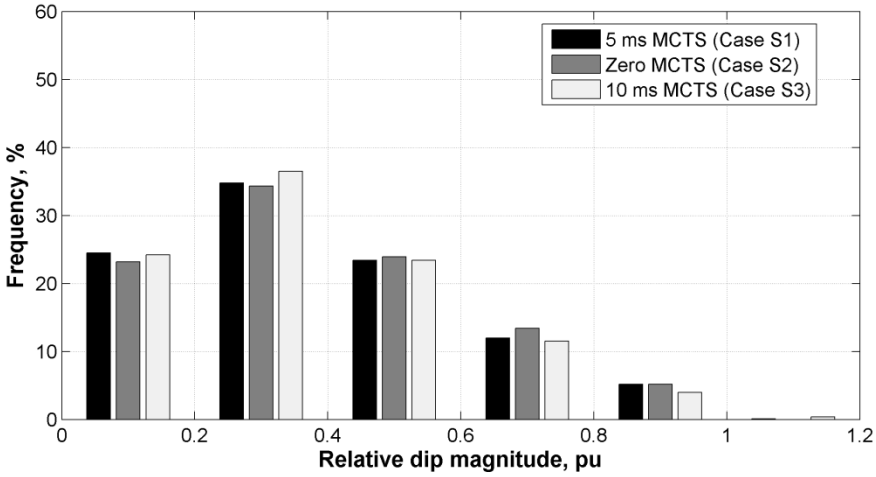

Figure 5-22 Frequency of voltage dip magnitude in phase C at substation I under different values of closing time span

5.6.2 Closing offset time distribution

Closing offset time with Gaussian distribution should be common because circuit breaker poles tend to be closed simultaneously [43]. However, circuit breakers can be of different characteristics due to different operating mechanisms, frequencies of maintenance and levels of wearing. Therefore, closing offset time might be characterized by other distributions. Here, two more closing offset time distributions, Uniform and Exponential, were considered to study the influence of closing offset time distribution on the dip frequency pattern. Both distributions were established within a range of ±MCTS/2 (noted that the value of the MCTS is 5ms, the same as in Case S1). The Exponential distribution was designed to make more closing offset time samples concentrated on the ends of larger values. After 1000 runs, the frequency of the closing offset time resulted from the Uniform and Exponential distributions are shown in Figure

5-23 and Figure 5-24, respectively. Obviously, compared with closing offset time with Guassian distribution, the samples of larger offset time are largely increased in the case of Exponential distribution.

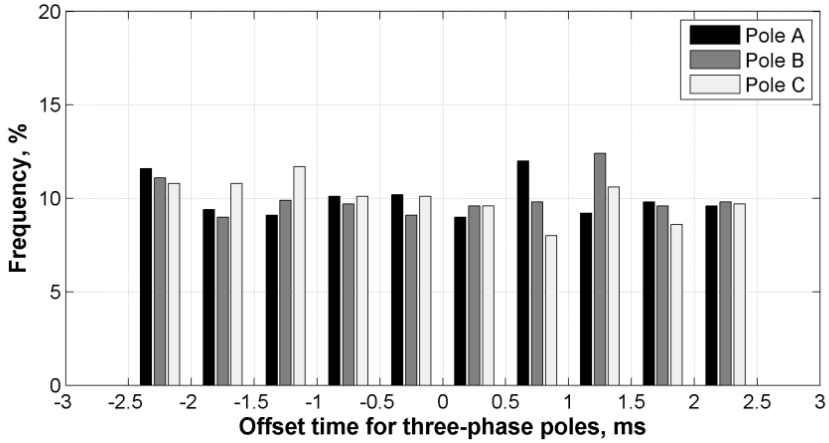

Figure 5-23 Uniform closing offset time distribution within ±2.5 ms range

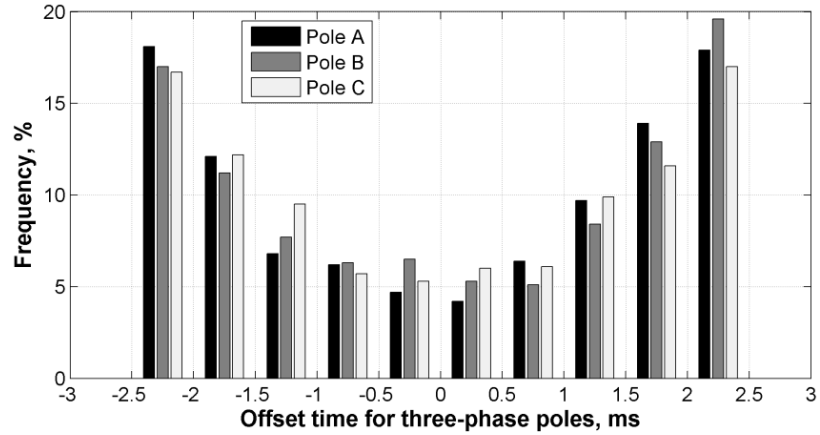

Figure 5-24 Exponential closing offset time distribution within ±2.5 ms range

Prediction of the dip frequency pattern of phase C at substation I with Uniform and Exponential closing offset time was conducted in Case S4 and Case S5. The results are compared with that obtained in Case S1 in Figure 5-25. As can be seen, the dip frequency patterns are very similar to one another; the dip magnitudes are mostly concentrated in the range between 0.2 and 0.4 pu of WCDM1; the frequency of dip magnitudes larger than 0.8 pu of WCDM1 is less than 6% out of 1000 runs.

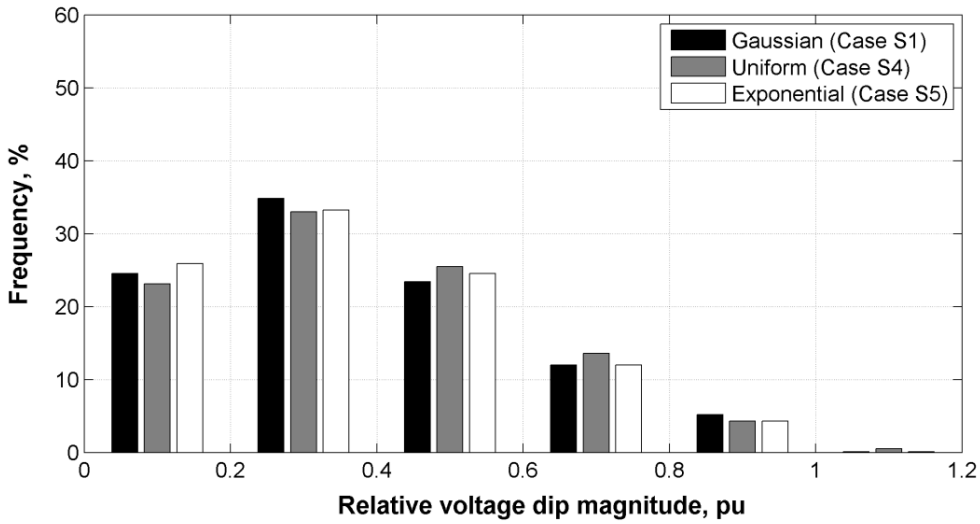

Figure 5-25 Frequency of voltage dip magnitudes in phase C at substation I for different closing time span distributions

5.7 Influences of residual flux distribution

Up to date, little knowledge is known about the residual flux distribution in the transformer core. This uncertainty gives rise to the need of evaluating the influence of residual flux distribution on dip frequency pattern. Besides the Uniform distribution considered in the Case S1, stochastic estimation of voltage dip frequency was made based on other residual flux distributions including Gaussian and Exponential. The Exponential distribution is of two types: the Exponential_1 was designed to make more residual flux samples concentrate on the maximum ends; the Exponential_2 was designed to make more residual flux samples concentrate on the minimum ends. All the residual flux distributions were generated following the procedure shown in Figure 5-2 based on the range between -0.8 and +0.8 pu of peak nominal flux. The probability distributions of three-phase residual fluxes generated out of 1000 runs are shown in Figure 5-26, Figure 5-27 and Figure 5-28 for the Gaussian, Exponential_1 and Exponential_2 distributions, respectively. As can be seen, the absolute magnitudes of the residual flux samples are concentrated between 0.2 and 0.6 pu of peak nominal flux in the case of Gaussian distribution, between 0 and 0.4 pu in the case of Exponential_1 and between 0.6 and 0.8 pu in the case of Exponential_2.

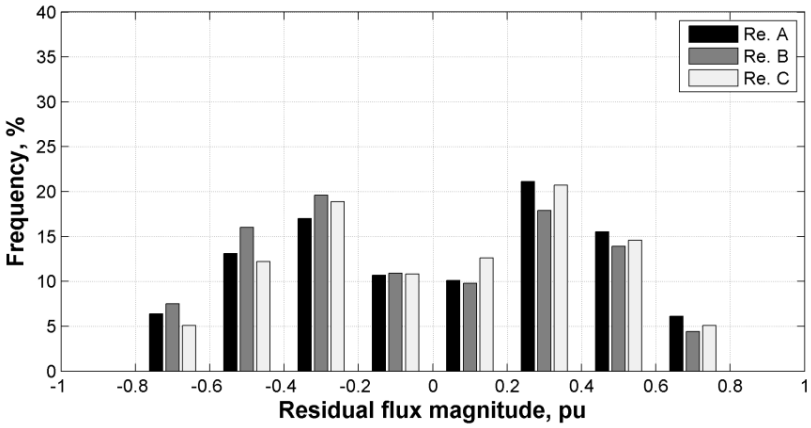

Figure 5-26 Gaussian residual flux distribution

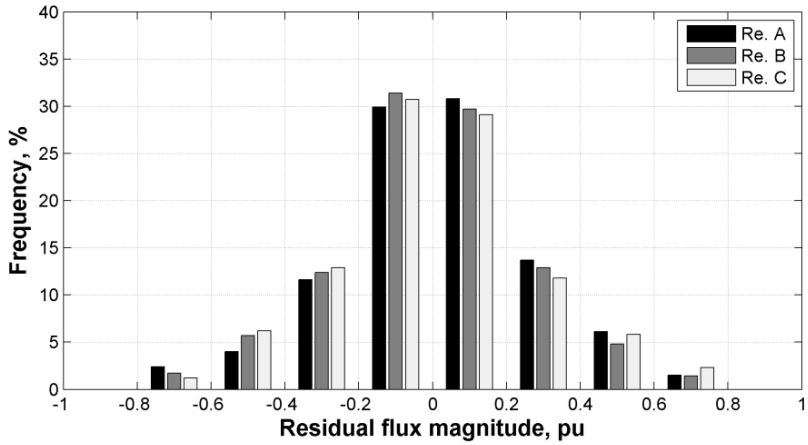

Figure 5-27 Exponential_1 residual flux distribution

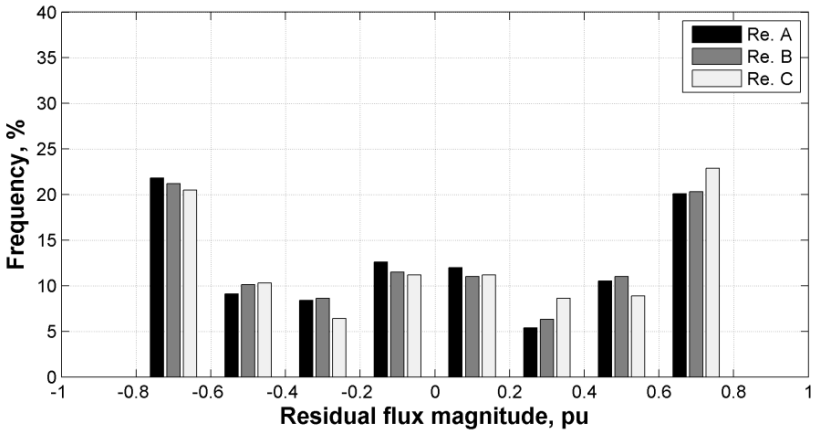

Figure 5-28 Exponential_2 residual flux distribution

The dip frequency patterns observed on phase C at substation I were generated under the above three residual flux distributions, which were compared with that obtained under Case S1 in Figure 5-29. As can be seen, the dip frequency pattern resulted from Gaussian residual flux distribution is almost the same with that given by Case S1; in the case of Exponential_1, the frequency of dips with magnitudes less than 0.6 pu of

WCDM1 is increased to about 90%, whilst the frequency of dips with magnitudes larger than 0.8 pu of WCDM1 is reduced to less than 2%; residual flux with Exponential_2 distribution increases the frequency of dips between 0.8 and 1 pu of WCDM1 from 5% to 11%, but it does not result in substantial increase of the dips with magnitudes exceeding 1 pu of WCDM1. These findings suggest that the dip frequency pattern is sensitive to the distribution of residual flux. For transformers prone to retain residual flux of high magnitudes, the frequency of dips with magnitudes close to the worst case dip magnitude is higher.

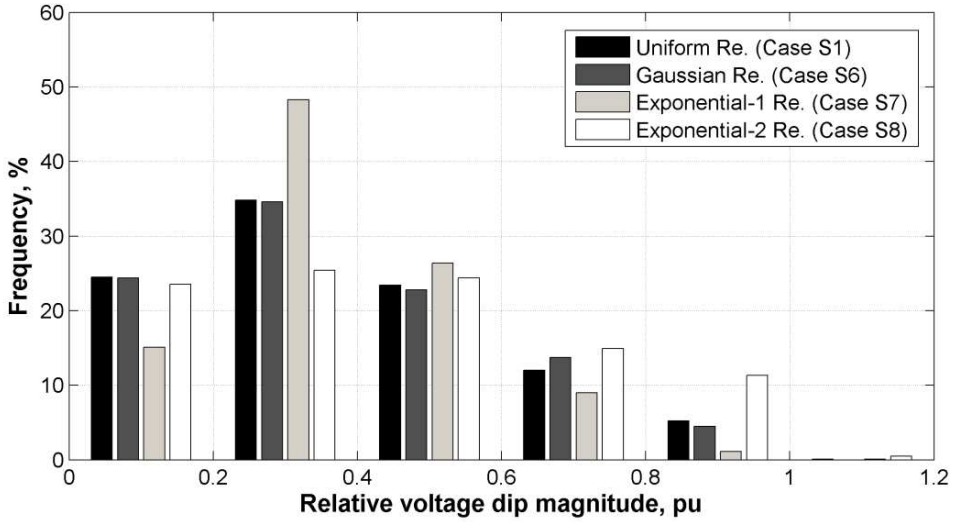

Figure 5-29 Frequency of voltage dips in phase C at substation I for different residual flux distributions

5.8 Influences of system condition variation

In the real system, the source strength and system loading might also vary in a certain range. The influence of this variation on the dip frequency pattern was studied in Case S9. As shown in Table 5-3, the variation of source strength is modelled by ±25% variation of the base case fault level; the source impedance angle varies between 75° and 85°; the variation of system loading is modelled by ±25% variation of half nominal loading and with its power factor varies between 0.9 and 0.999 (due to the simulation program limitation, 0.999 was used to approximate the power factor of 1.0). All of the variations were assumed to follow Uniform distribution. The variation of residual flux and closing time were the same as those assumed in Case S1.

The dip frequency pattern observed on phase C at substation I was calculated and compared with that of Case S1, as shown in Figure 5-30. As can be seen, the two

patterns are very similar to each other. This indicates that, the dip frequency pattern estimated by Case S1 is not sensitive to ±25% variation of system condition.

Table 5-3 Possible ranges and PDFs for random parameters

Parameter	Variation range	Distribution
Source strength	±25% of the base case fault level	Uniform
Source impedance angle	75°-85°	Uniform
Load power factor	0.9-0.999 inductive	Uniform
System loading	±25% of half nominal loading	Uniform

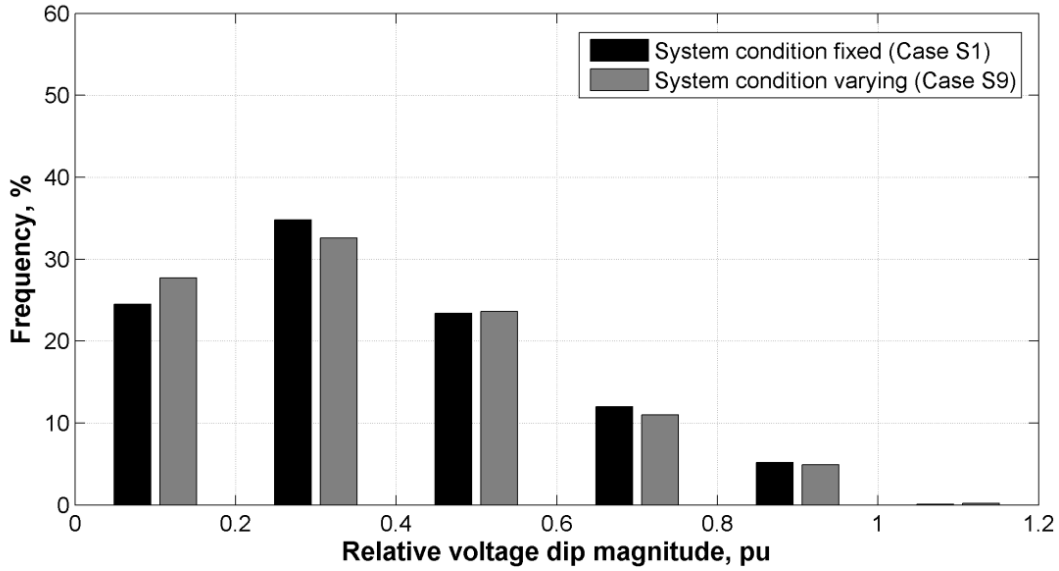

Figure 5-30 Frequency of voltage dips in phase C at substation I (comparing Case S9 with S1)

5.9 Influences of energising multiple transformers

In previous case studies, the energisation only involves one transformer. In certain circumstances, multiple transformers being energised at the same time might be experienced. The dip frequency pattern resulted from such energisation was studied by using the case of energising GSU transformers T2 and T3 together in the South West system, which involves two scenarios: one is Case S10 in which the level of residual flux for both transformers were assumed to be the same; the other is Case S11 in which the residual flux for both transformers are independent. (Note: for both cases, the modelling of the stochastic closing time and residual flux was the same as in Case S1 in terms of their ranges and distributions).

The dip frequency patterns for both cases were obtained after 1000 runs. The dip frequency pattern of phase C at substation I obtained from Case S10 simulation is compared with that of Case S1 in Figure 5-31. Figure 5-32, similar comparison between Case S11 and Case S1 is given. It can be seen that: if the transformers being energised

simultaneously are of the same residual flux, the dip frequency pattern is identical to that observed in the case of energising one transformer only; if the transformers are of stochastically different residual flux, the frequency of dips with magnitudes between 0.2 and 0.6 pu of worst case dip magnitude is increased, whilst the frequency of dips with other magnitudes decreased, which indicates that the likelihood of reaching the worst case dip magnitude is reduced.

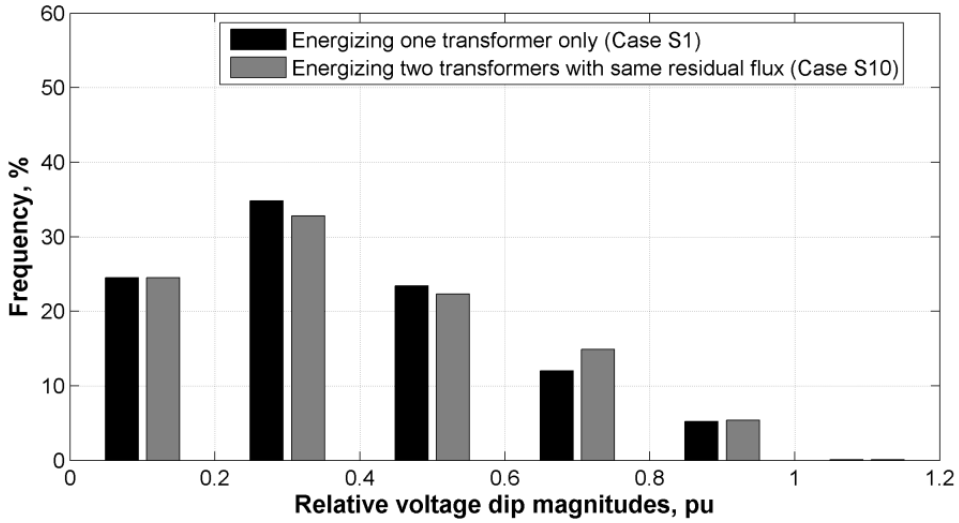

Figure 5-31 Frequency of voltage dips in phase C at substation I of Case S10 contrasting with that of Case S1

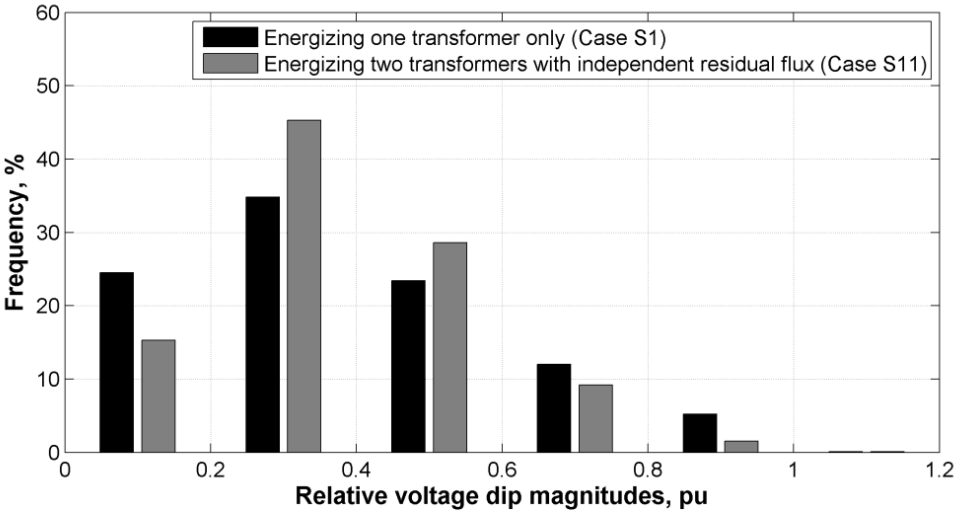

Figure 5-32 Frequency of voltage dips in phase C at substation I of Case S10 contrasting with that of Case S1 (two transformers with different residual flux)

5.10 Summary

In this chapter, Monte Carlo simulation has been conducted to stochastically assess the voltage dips caused by transformer energisation in the South West Peninsula 400 kV

grid, using the network model developed and validated in Chapter 3. The simulation was automated by an ATP-MATLAB interfacing platform which uses ATP to handle transient calculation and MATLAB to generate simulation inputs, control Monte Carlo runs and process results.

A dip frequency pattern was produced over 1000 stochastic runs and it was found to be sensitive to the distribution of residual flux but insensitive to the distribution of closing offset time. This suggests that it is important to model the residual flux distribution in transformer core while closing offset time distribution can be of less concern. In addition, it was shown that the dip frequency pattern is insensitive to the system condition when varying in a range of ±25% of the base case condition. The voltage dip frequency pattern can be extended to cover the condition in which a number of transformers are being energised simultaneously.

Furthermore, it was found that the probability of reaching the worst case dip magnitude (estimated by the commonly agreed worst case energisation condition) is lower than 0.5%, indicating that the worst case scenario is unlikely to occur in a system; in fact, about 80% of the dips are likely to be with magnitudes lower than 0.6 pu of the worst case. Nevertheless, it was shown that there are dips with magnitudes exceeding the worst case dip magnitude, indicating the inadequacy of the deterministic assessment approach by using the commonly agreed worst case energisation condition.

Chapter 6 Assessment of Transformer Energisation Transients Due to Offshore Wind Farm Connection

To acquire more green energy, increasing installations of larger offshore wind farms are being designed and commissioned. The total installed capacities of offshore wind farm in counties such as Germany, UK and China are planned to be 10 GW, 18 GW and 30 GW by 2020, respectively [119-121]. The capacities of individual offshore wind farm and wind turbine are also expanding: offshore wind farms with installed capacity reaching 1 GW have been proposed [122]; wind turbines with rated capacity reaching 10 MW are commercially available [123].

Typical electrical system for an offshore wind farm involves a collection grid within the wind farm and a transmission system to deliver the power to the onshore main grid. The collection grid begins from the wind turbine transformers (usually at the base of the wind turbine tower) which steps up the generation voltage from typically 690 V to a medium voltage of 25-40 kV [124]. Depending on the wind farm total capacity and the capacity of individual wind turbine, a large offshore wind farm may accommodate dozens or even more than a hundred wind turbine transformers, as can be seen from the top ten existing offshore wind farms (up to 2012) listed in Table 6-1 [125]. Usually, the wind turbine transformers are distributed over a number of cable feeders; each feeder may contain 5-10 wind turbines.

During the energisation of wind farm collection grid, there are two potential factors to be considered: one is the possible voltage dip experienced at the point-of-common-coupling between the electrical system of the wind farm and the utility company [75], which concerns grid code compliance; the other is the sympathetic interaction between wind turbine transformers [126], which on one hand may prolong the resulted voltage dips and on the other hand prolong the mechanical and thermal stresses imposed on the wind turbine transformers (according to the IEC 60076-16:2011 standard [127], due to frequent energising wind turbine transformers during wind farm operation, wind turbine transformers can be frequently exposed to mechanical and thermal stresses of inrush

currents). Both factors have not been thoroughly addressed for large offshore wind farm connections.

In this chapter, modelling and simulation methodologies gained from the studies conducted in Chapter 3 and Chapter 4 are used to develop network model of an existing large offshore wind farm collection grid, based on which, deterministic and statistical approaches presented in Chapter 4 and Chapter 5 are both employed to assess voltage dips and sympathetic inrush caused by energising wind turbine transformers under various scenarios. The assessment aims to provide guidance on planning and operating offshore wind farms, especially focusing on identifying an optimum energisation sequence to reduce sympathetic interaction between wind turbine transformers.

Table 6-1 List of top ten operational offshore wind farms [125]

Offshore Wind Farm	Capacity (MW)	Turbine Capacity (MW)	Turbine Number	Year	Country
Walney (phases 1&2)	367	3.6	102	2012	UK
Thanet	300	3	100	2010	UK
Horns Rev II	209	2.3	91	2009	Denmark
Rødsand II	207	2.3	90	2010	Denmark
Lynn and Inner Dowsing	194	3.6	54	2008	UK
Robin Rigg	180	3	60	2010	UK
Gunfleet Sands	172	3.6	48	2010	UK
Nysted (Rødsand I)	166	2.3	72	2003	Denmark
Bligh Bank (Belwind)	165	3	55	2010	Belgium
Horns Rev I	160	2	80	2002	Denmark

6.1 Offshore wind farm under study

The Nysted offshore wind farm collection grid and its connection with onshore main grid are shown in Figure 6-1. At the point-of-common-coupling, there is a 132 kV onshore substation where a 40 MVAr shunt reactor is installed to compensate cable-generated reactive power. From the point-of-common-coupling to the offshore platform of the collection grid is a 132 kV transmission link consisting of 18.3 km onshore cable and 10 km offshore cable. A main transformer (180/90/90 MVA, 132/33/33 kV) is located at the offshore platform; its HV terminals are connected to the transmission link and LV terminals connected to eight 36 kV cable feeders (labelled from A to H, distance between two adjacent feeders is about 850 m). The electrical circuit of feeder-A is taken as an example and illustrated in detail. As can be seen, each feeder contains nine 2.5 MVA, 33/0.69 kV wind turbine transformers. The HV side of the wind turbine transformer is connected with a circuit breaker, and the LV side is connected with a

small amount of auxiliary load. The cable connecting two adjacent wind turbine transformers is 505 m long.

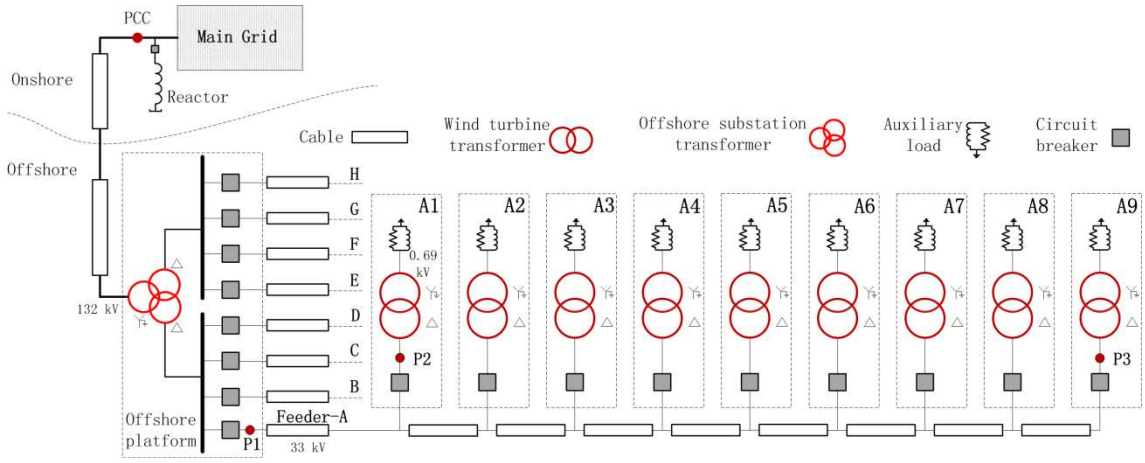

Figure 6-1 Layout of Nysted offshore wind farm collection grid and its connection with onshore main grid

6.2 Measurement of energisation transients

In [128], inrush currents caused by simultaneous energisation of all the wind turbine transformers connected to feeder-A were measured (at the time of conducting the energisation, all the wind turbine transformers were connecting a 0.37 kW auxiliary load; in addition, the secondary side of wind turbine transformer A1 was connecting a capacitor bank rated at 180 kVAR). Measurements of three-phase voltages and currents were carried out at three locations (as indicated in Figure 6-1):

- P1: the terminal of the offshore platform circuit breaker linking feeder-A;
- P2: the primary side of the wind turbine transformer A1 which is the closest to the offshore platform;
- P3: the primary side of the wind turbine transformer A9 which is farthest away from the offshore platform;

(Note that P1 was located between circuit breaker and 33 kV cable; both P2 and P3 were located between circuit breaker and wind turbine transformer).

Three-phase voltages measured at P1, P2 and P3 are shown in Figure 6-2 (a), Figure 6-2 (b) and Figure 6-2 (c), respectively. In the figures, the base value of the measured voltages is the phase-to-ground voltage (which is $33/\sqrt{3}$ kV). As can be seen, right after the energisation, there were high frequency oscillations of the voltages around the energisation instants, which provoked the occurrence of overvoltages. The overvoltages observed at P3 were slightly higher than those observed at the other two measurement

points. The high frequency oscillation of three-phase voltages decayed within about 1 ms. After the decay, certain level of voltage distortion can still be seen.

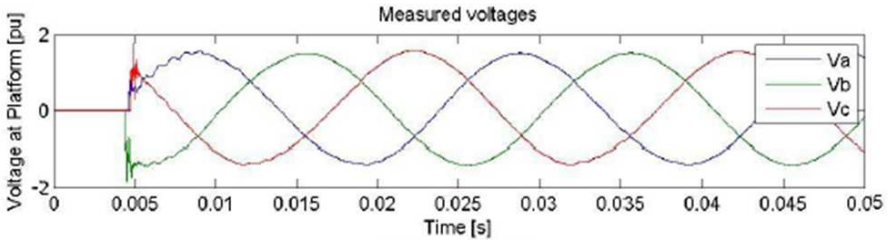

(a) Voltages measured at location P1

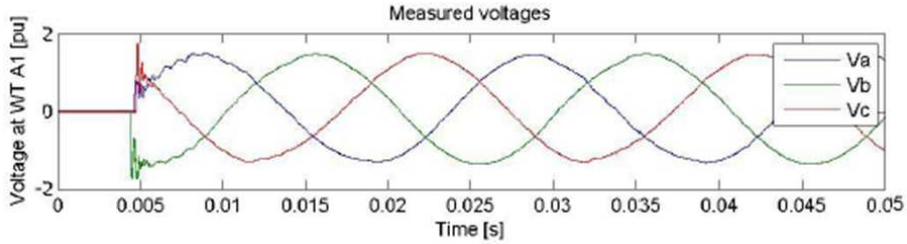

(b) Voltages measured at location P2

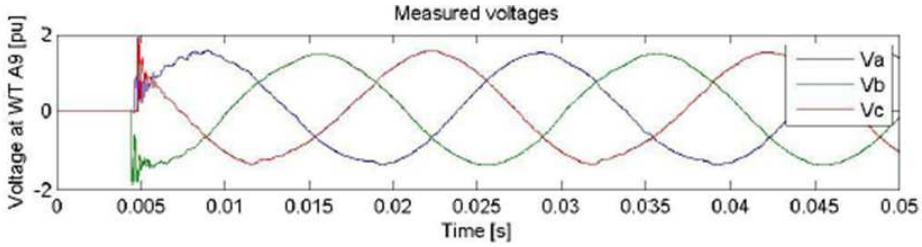

(c) Voltages measured at location P3

Figure 6-2 Measured three-phase voltages during energisation of feeder-A [128]

Voltage waveforms measured at P1 around the energisation instants are further illustrated in Figure 6-3. Closing time deviations can be observed: phase B was the first one being closed at the instant near the voltage peak of negative half cycle; the closure of phase A was delayed by 0.22 ms and the closure of phase C was delayed by 0.47 ms.

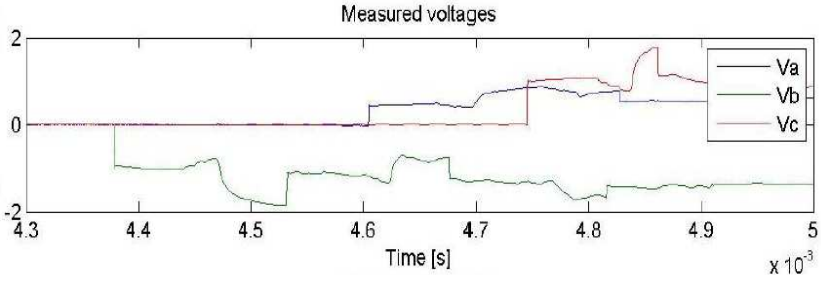

Figure 6-3 Voltage waveforms around the energisation instants (at location P1) [128]

Three-phase currents were also measured at P1, P2 and P3, which are shown in Figure 6-4 (a), Figure 6-4 (b) and Figure 6-4 (c), respectively. In the figures, the base value for the currents measured at P1 is 420 A; for the currents measured at P2 and P3, the base

value is 43 A. As can be seen, spiky currents appeared at the instants of energisation; the magnitudes of the spiky current measured at P1, P2 and P3 were about 668 A, 24 A and 19 A, respectively. After energisation, the time to saturation was about 5 ms. Saturation of wind turbine transformers led to the occurrence of inrush. The inrush currents can be observed at all the three measurement points. By inspecting the first cycle of the inrush currents measured at different locations, it can be seen that their patterns are similar to one another. The more oscillatory currents observed at P2 compared to those observed at P1 and P3 is due to the effect of the capacitor bank connected at the secondary side of wind turbine transformer A1.

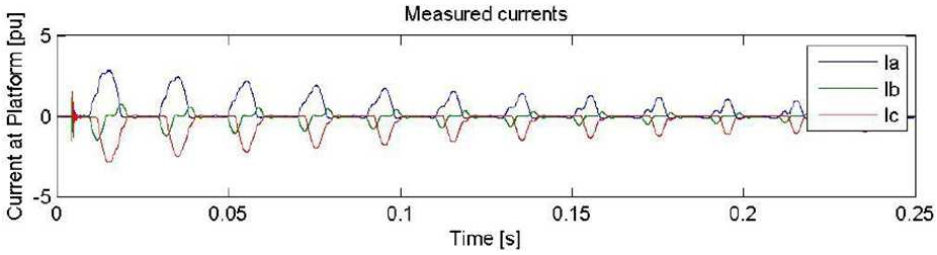

(a) Inrush currents measured at location P1

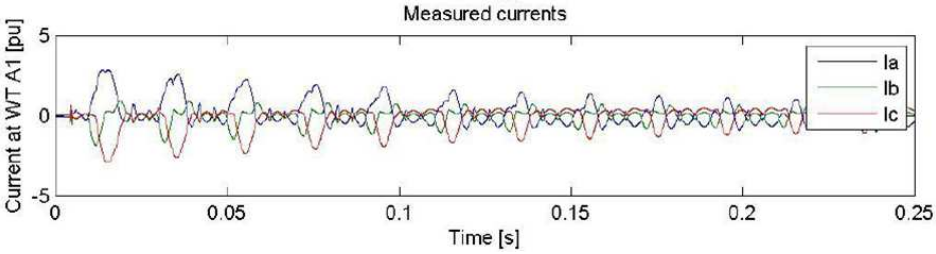

(b) Inrush currents measured at location P2

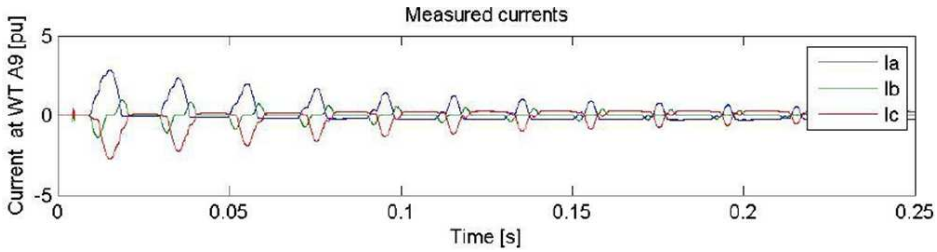

(c) Inrush currents measured at location P3

Figure 6-4 Measured three-phase currents during energisation of feeder-A [128]

The first peak magnitudes of three-phase inrush currents are illustrated in Table 6-2. It can be deduced that the inrush current peak magnitude (1191 A) measured at P1 was close to nine times the peak magnitude of the inrush current drawn by transformer A1. After the first inrush current peak, the inrush currents started to decay. In Figure 6-5, the peak magnitudes of the first ten cycles of the phase A inrush current measured at P1 are plotted, which shows that it decayed by about 60% (from 1191 A to 446 A) within 180

ms. For the same time span (180 ms), phase B inrush current decayed by 68% and phase C by 62.5%.

Table 6-2 Inrush current first peaks resulted from energisation of feeder-A

Inrush current peaks	Platform current P1 (A)	A1 current P2 (A)	A9 current P3 (A)
Phase A	1191	124	123
Phase B	-605	-78	-58
Phase C	-1182	-121	-115

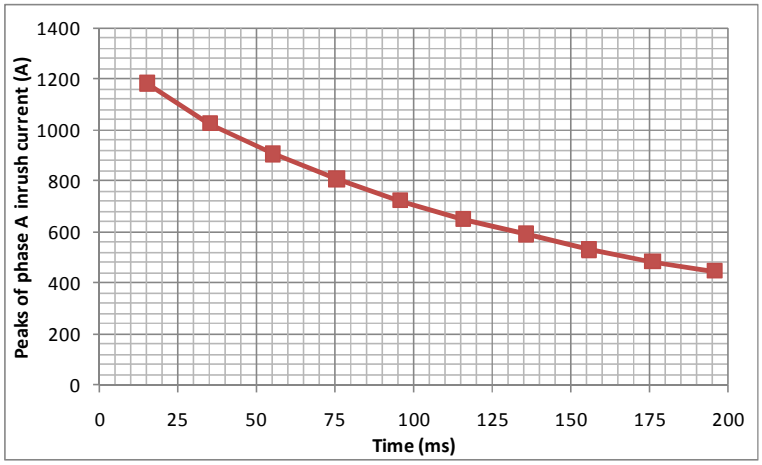

Figure 6-5 Decay of phase A inrush current peaks measured at P1

6.3 Modelling of offshore wind farm collection grid

Modelling of offshore wind farm collection grid mainly considered the modelling of wind turbine transformers, offshore substation transformers, circuit breakers, external grid and their interconnections. Wind turbine generators are normally not connected prior to the energisation of collection grid and therefore they were not considered in the network model.

Wind farm collection grid models developed in previous research, including those presented in [36], [75], [102], [103] and [50], showed that: the auxiliary load on the secondary side of the wind turbine transformer can be neglected or simply represented by a constant resistance; the nominal pi model can be used to represent cables; an ideal voltage source connected with an equivalent source impedance can be used to represent the external grid. These modelling experiences together with those obtained in Chapter 3 were used to develop the collection grid model of the Nysted offshore wind farm using ATP/EMTP.

The developed network model is shown in Figure 6-6. As can be seen, it consists of four

building blocks. Block 1 models the connection with the onshore main grid, which was represented by an ideal voltage source connected in series with an equivalent source impedance; the shunt reactor was modelled by linear inductor. In block 2, the 132 kV onshore cable and offshore cable were represented by a number of pi sections. In block 3, the Hybrid Transformer model was used to represent the offshore platform transformer. Block 4 is the main part of the wind farm collection grid model and it is mainly formed by circuit breakers, cable sections and wind turbine transformers: the circuit breakers were modelled by ideal time-controlled switch; the 33 kV cable sections were represented by nominal pi model; the wind turbine transformers were modelled by BCTRAN+. Further details of the building blocks are described in the following subsections. This network model can be expanded to include more feeders.

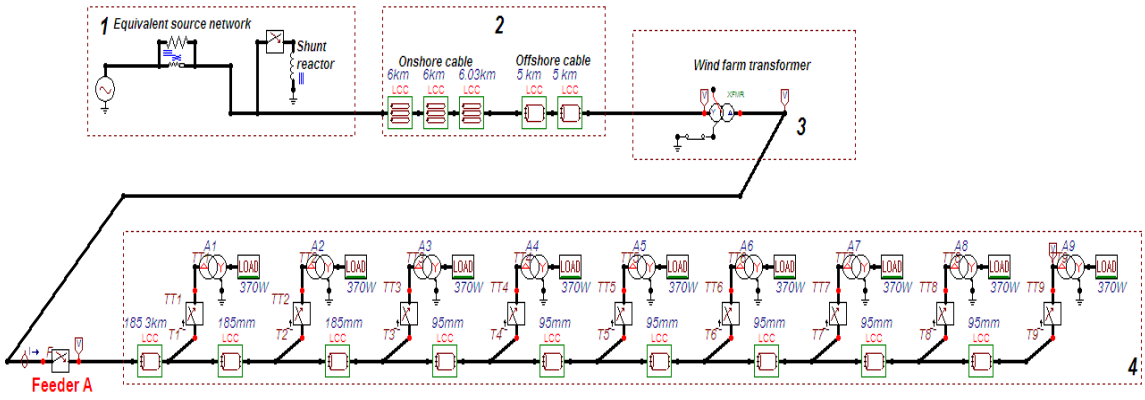

Figure 6-6 Complete network model of the Nysted wind farm collection grid and its connection with the main grid

6.3.1 Modelling of supply source

The onshore main grid, i.e., the system beyond the point-of-common-coupling, was represented by a network equivalent circuit consisting of an ideal voltage source and a Thevinin equivalent source impedance; a resistance in parallel with the source impedance was used to improve the numerical stability of the simulation [76]. The values of the source impedance were estimated from the fault level of the 132 kV busbar at which the wind farm is connected, the X/R ratio of the source impedance was assumed to be 6 [129] and the value of the resistance in parallel with the source impedance was assumed to be 150 Ohm. The shunt reactor was modelled by three star-connected linear inductors which are of 1387 mH.

6.3.2 Modelling of cables

Due to the low frequency nature of transformer energisation transients, nominal pi model was considered to be suitable for representing cables. To calculate cable parameters, namely impedance and admittance matrix, following cable geometrical data and material properties were defined in the pi model routine [130]:

1) Geometry: location of each conductor, inner and outer radii of conductor, insulation and shielding layers, burial depth of the cable system;

2) Material properties: resistivity and relative permeability of conductors, relative permeability and permittivity of the insulating material outside conductors.

The data used to define the geometry and material properties of the 132 kV single-core onshore cable, 132 kV and 33 kV three-core submarine cables are given in Table 6-3 and Table 6-4, respectively (note that cables between A9 and A3 is of 95 mm^2 cross sectional area and cables between A3 and the offshore platform is of 185 mm^2 cross sectional area, which follows the design used in Lillgrund offshore wind farm [131]).

Table 6-3 132 kV single core onshore cables [132]

Cross-section of conductor [mm^2]	1200
Laying depth [m]	1
Flat formation spacing [m]	0.25
Resistivity [Ohm.m] Al	3.6E-8
Radius of conductor [m]	0.0214
Thickness of conductor shielding [m]	0.0018
Thickness of insulation [m]	0.015
Thickness of insulation shielding [m]	0.0018
Thickness of lead sheath [m]	0.003
Thickness of anti-corrosion sheath [m]	0.004
Total radius [m]	0.04685

Table 6-4 132 and 33 kV three-core offshore cables [133]

Voltage level	132 kV	33 kV	33 kV
Cross-section of conductor [mm^2]	800	185	95
Laying depth [m]	1	1	1
Resistivity [Ohm.m] Cu	2.3E-8	2.3E-8	2.3E-8
Radius of conductor [m]	0.016	0.0079	0.0056
Thickness of conductor shielding [m]	0.001	0.0004	0.0004
Thickness of insulation [m]	0.015	0.008	0.008
Thickness of insulation shielding [m]	0.00075	0.0008	0.0008
Thickness of lead sheath [m]	0.0028	0.001	0.0008
Total radius of one core cable [m]	0.04	0.0195	0.0175
Inner radius of wire armour [m]	0.087	0.048	0.043
Outer radius of wire armour [m]	0.093	0.053	0.048
Thickness of anti-corrosion sheath [m]	0.004	0.004	0.004
Total radius [m]	0.097	0.057	0.052

6.3.3 Modelling of wind turbine transformer

Wind turbine transformer was represented by BCTRAN+ model which makes use of BCTRAN model to represent transformer short-circuit characteristic and a set of delta connected hysteresis type-96 inductors attached on the low-voltage side to model core saturation characteristic.

As mentioned before, the BCTRAN model can be derived based on transformer test reports (mainly using short circuit and open circuit test data). The information obtained from manufacturer for modelling the wind turbine transformer using BCTRAN is given in Table 6-5. The core saturation effects were modelled by three wye-connected type-96 hysteretic inductors whose saturation characteristic is shown in Figure 6-7. The air-core inductance of the transformer was assumed to be twice the transformer short-circuit inductance.

Table 6-5 Main electrical information for modelling wind turbine transformers [128]

Parameters	Value
Rated power [MVA]	2.5
Connection group	Dyn7
Rated primary voltage [kV]	33
Rated secondary voltage [kV]	0.69
Copper losses [kW]	22
No-load losses [kW]	5.5
Short-circuit impedance [%]	8.3

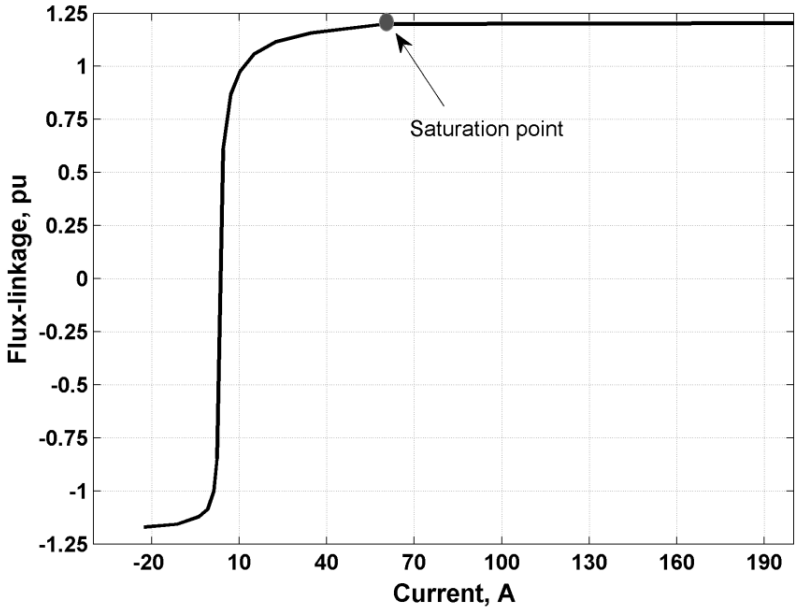

Figure 6-7 Saturation curve of wind turbine transformers

6.4 Network model validation

The developed network model was used to simulate the case of simultaneous energising the entire feeder-A (as the one presented in the Section 6.2). The simulation setting of network model parameters is given in Table 6-6. Source voltage level, circuit breaker closing times were derived from the field measured voltage waveforms. Validation of the network model was conducted by comparing the simulated inrush current and voltage waveforms with those obtained from field measurements, focusing on waveform patterns, peak magnitudes and decay trends.

Table 6-6 Network model parameter settings for simulating field measurement results

Parameters	Setting		Note
Source voltage level	107.7 kV		Peak value of 132 kV (L-L).
Source impedance	R_p=0.3 Ohm, X_p=3.454 Ohm		Derived from 5 GW fault level
Circuit breaker closing time	Ph. A	3.55 ms	Closing time reference: positive-going zero crossing of phase B voltage; Only applied to feeder circuit breaker.
	Ph. B	3.33 ms	
	Ph. C	3.72 ms	
Residual flux	Ph. A	0	Applied to all wind turbine transformers; Base value is peak nominal flux.
	Ph. B	+0.306 pu	
	Ph. C	–0.306 pu	

In Figure 6-8, the simulated voltage waveforms at location P1 are compared with those obtained from the measurements. The high frequency voltage oscillation appearing around the energisation instant is not well replicated, due to the frequency response range of the network model components is up to 1 kHz. Nevertheless, the simulated voltages agree reasonably well with the measured voltages in terms of circuit breaker closing times, peak magnitudes and waveform patterns.

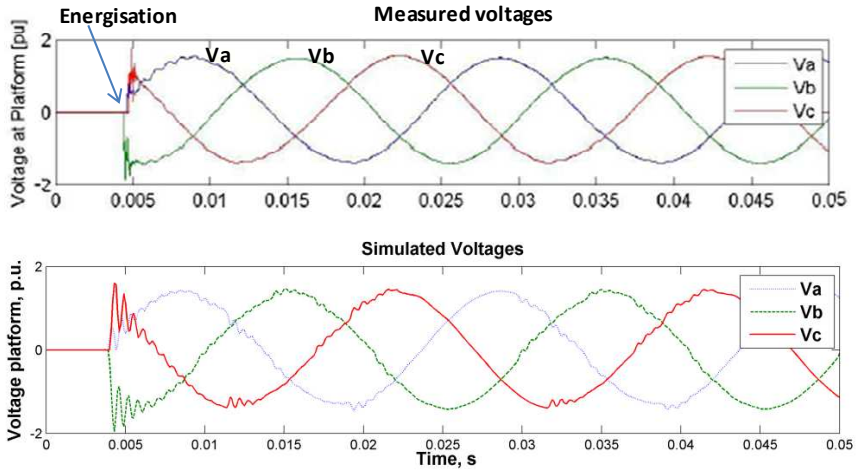

Figure 6-8 Comparison of voltage variation during energisation

The simulated three-phase inrush currents drawn by wind turbine transformer A9 are compared with measurements in Figure 6-9. In addition, the total inrush currents drawn

by all the wind turbine transformers located at feeder-A are compared with measurements in Figure 6-10. As can be seen from both comparisons, the peak magnitudes and patterns of the simulated three-phase inrush currents are very similar to those of the measured inrush currents. This indicates that the network model is not only capable to estimate the inrush currents drawn by a stand-alone wind turbine transformer but also the total inrush currents drawn by an array of wind turbine transformers.

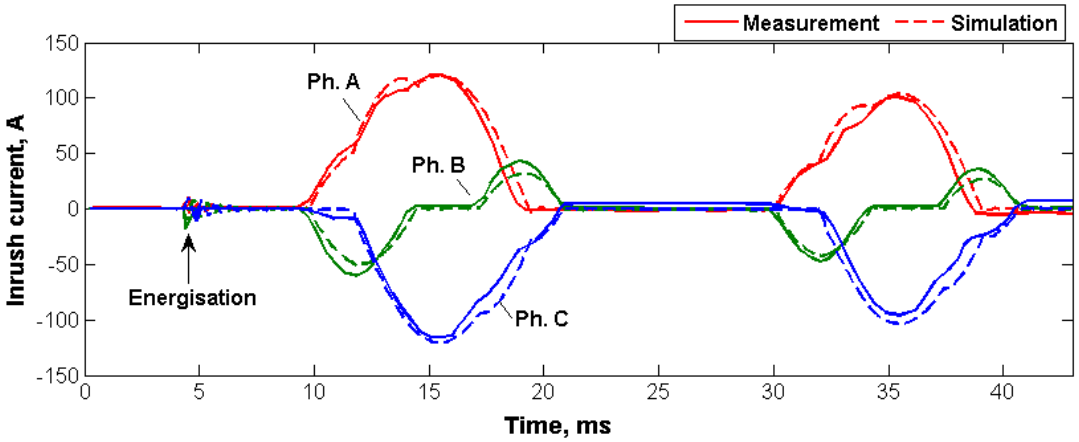

Figure 6-9 Comparison between measurement and simulation regarding the inrush currents drawn by wind turbine transformer A9

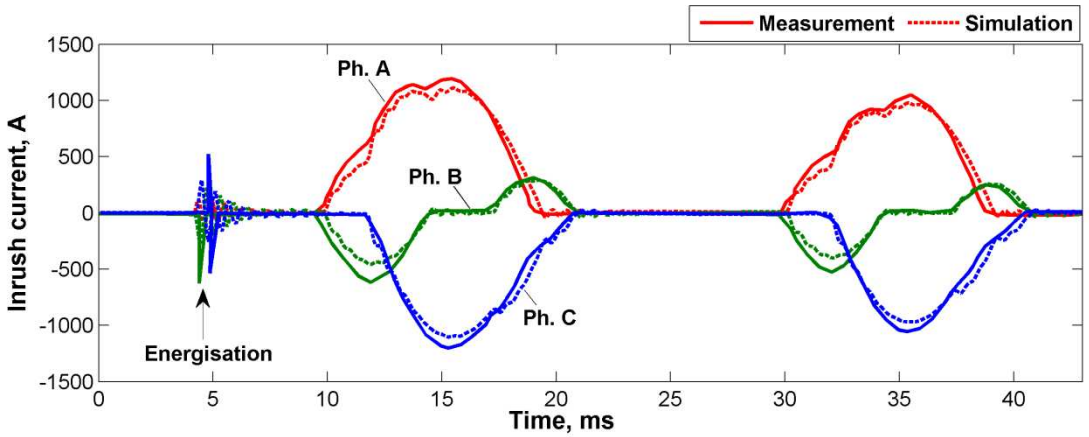

Figure 6-10 Comparison between measurement and simulation regarding the total inrush currents drawn by nine wind turbine transformers in feeder-A

The inrush current decay trends were also compared between the simulated waveforms and measured ones. The one shown in Figure 6-11 compares the inrush currents drawn by all the wind turbine transformers connected at feeder-A. In Figure 6-12, two decay trend comparisons are shown, one compares the phase A inrush current drawn by wind turbine transformer A1 (in red curves) and the other compares the phase A inrush current drawn by wind turbine transformer A9 (in blue curves). Each trend line indicates the decay of inrush current peak magnitudes during the first twelve cycles. As can be

seen, the comparisons show that the decay trends of simulated inrush currents match well with those measured decay trend lines. This indicates that the system parameters that determining the decay time constants of the transformer inrush transients are correctly represented by the network model.

Specifically, the comparisons in Figure 6-12 also shows the faster decay of inrush currents in wind farm transformer A9 than that in A1 and this is also well replicated in the simulation results, which indicates the losses associated with the cable sections between A1 and A9 are accurately represented. This is important for studying sympathetic inrush between wind turbine transformers, as the amount of cable section losses would significantly influence sympathetic interaction between wind turbine transformers.

The above validation comparisons indicate that the network model is capable to reproduce field measurement results in terms of inrush current patterns, peak magnitudes and decay trends, which confirms the accuracy of the developed network model.

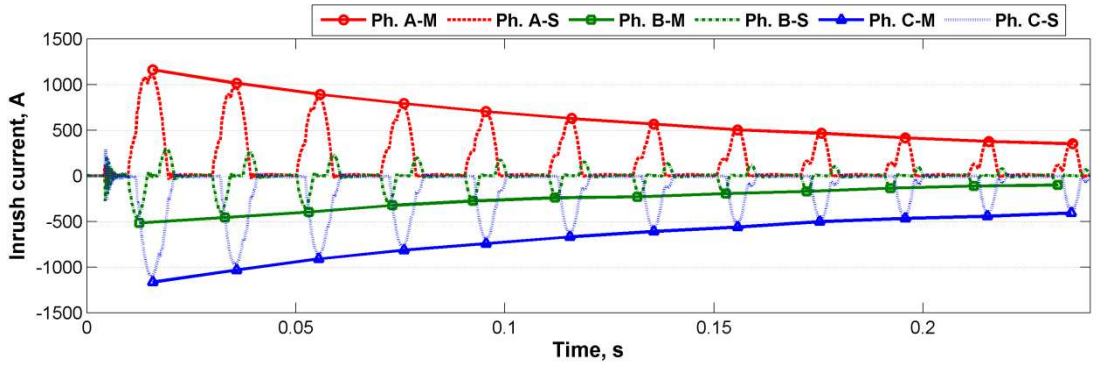

Figure 6-11 Decay trend comparison regarding feeder inrush currents

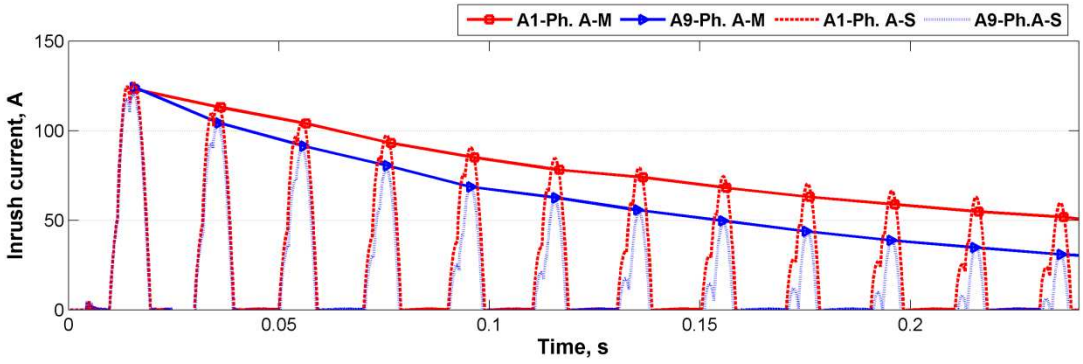

Figure 6-12 Decay trend comparisons regarding the inrush current drawn by transformer A1 and that drawn by A9

6.5 Voltage dips caused by energising wind turbine transformers

Using the validated wind farm collection grid model, voltage dips at the point-of-common-coupling (as shown in Figure 6-1) caused by energising wind turbine transformers were assessed.

6.5.1 Consideration of source strength variation

Possible ranges of 132 kV fault levels are collected from National Grid's Seven Year Statement [134]. As far as the National Grid Electricity Transmission (NGET) system is concerned, the fault level ranges from 864 MVA to 4964 MVA. In the following sections, the source strength corresponding to the 4964 MVA fault level is termed as the strong source strength; the source strength corresponding to the 864 MVA fault level is termed as the weak source strength.

6.5.2 Voltage dips caused by energising wind turbine transformers

For evaluating voltage dips caused by energising wind turbine transformers, six cases of energising feeder-A were studied, which are shown in Figure 6-13. In each case, the horizontal column is corresponding to the number of wind turbine transformer being energised simultaneously. In Case W4, for example, the energisation involves three sequential energisations represented by three separate horizontal columns and each column represents three wind turbine transformers being energised together. For all the case studies, it was assumed that the energisation is conducted under the commonly agreed worst case energisation condition (i.e., for residual flux, phase A, B and C retain -0.8 pu, 0 and +0.8 pu of peak nominal flux, respectively; for closing time, simultaneous energisation at the positive-going zero crossing of phase C line-to-ground voltage); the energising direction is from A1 to A9. Under such condition, all the cases were tested against the strong and the weak source strength of the NGET system and the results are shown in Table 6-7 and Table 6-8, respectively. Note that 3% voltage dip was taken as the beginning and end threshold for quantifying the dip duration. As can be seen, the voltage dips caused by energising an individual wind turbine transformer (in Case W6) is much less than 3% and far less than that caused by energising a large GSU transformer. In fact, under the strong source strength, a feeder of wind turbine transformers can be energised simultaneously without breaching the ER-P28 limit;

under the weak source strength, up to three wind turbine transformers are allowed to be energised together.

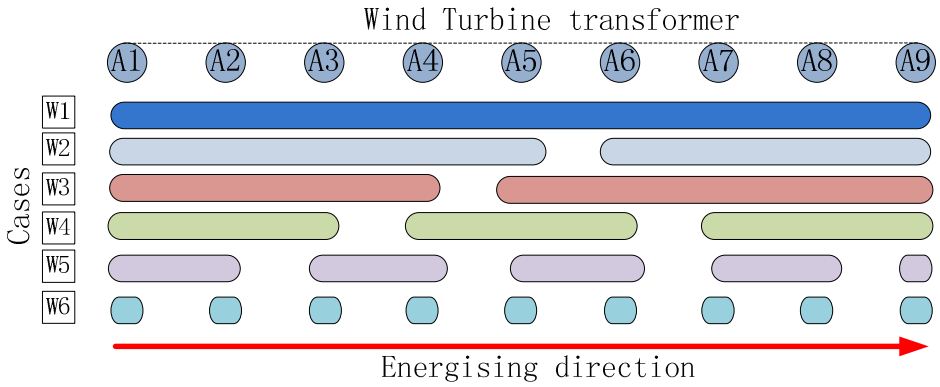

Figure 6-13 Case studies of energising wind turbine transformers in one feeder

Table 6-7 Voltage dips resulted from energising a feeder of wind turbine transformer under the strong source strength

Case	Voltage dips					
	Phase A		Phase B		Phase C	
	Magnitude (%)	Duration (ms)	Magnitude (%)	Duration (ms)	Magnitude (%)	Duration (ms)
W1	0.55	0	1.24	0	1.2	0
W2	0.3	0	0.81	0	0.75	0
W3	0.3	0	0.75	0	0.72	0
W4	0.2	0	0.52	0	0.47	0
W5	0.13	0	0.36	0	0.32	0
W6	0.06	0	0.18	0	0.16	0

Table 6-8 Voltage dips resulted from energising a feeder of wind turbine transformer under the weak source strength

Case	Voltage dips					
	Phase A		Phase B		Phase C	
	Magnitude (%)	Duration (ms)	Magnitude (%)	Duration (ms)	Magnitude (%)	Duration (ms)
W1	2.9	0	6.6	80	5.8	65
W2	1.8	0	4.4	51	3.7	30
W3	1.7	0	4.2	32	3.7	20
W4	1.1	0	2.89	0	2.4	0
W5	0.75	0	2.0	0	1.65	0
W6	0.35	0	1.0	0	0.85	0

6.5.3 Stochastic estimation of voltage dips caused by energising wind turbine transformers

In Case W1, the voltage dip magnitude resulted from energising a feeder of wind turbine transformers under the worst energisation condition is 6.6% and the dip duration is 80 ms (as can be seen from Table 6-8). The likelihood of reaching such a dip was further analysed by using stochastic simulation. In the simulation setup, the circuit

breaker closing time was defined by one cycle Uniform distributed common-order-time and a Gaussian distributed closing offset time (mean value equal to 0 and standard deviation equal to 0.833 ms); the range of the residual flux was defined as ±0.8 pu and of Uniform distribution (note that the residual flux in each wind turbine transformer is independently assigned). The results obtained from 1000 stochastic runs are shown in Figure 6-14 for the frequency of occurrence of dip magnitude and Figure 6-15 regarding the frequency of occurrence of dip duration. The results indicate that: the frequency of reaching the worst case voltage dip is actually negligible; over 95% of the dips are with magnitudes less than 0.6 pu of the worst case.

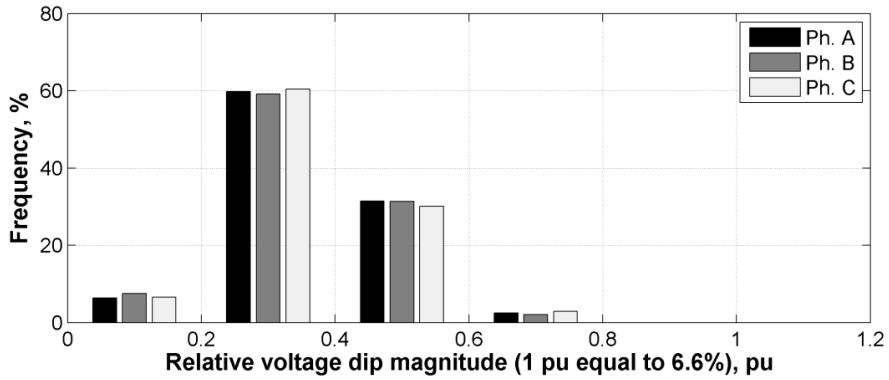

Figure 6-14 Frequency of voltage dip magnitude in three phases at the point-of-common-coupling under energising a feeder of wind turbine transformers

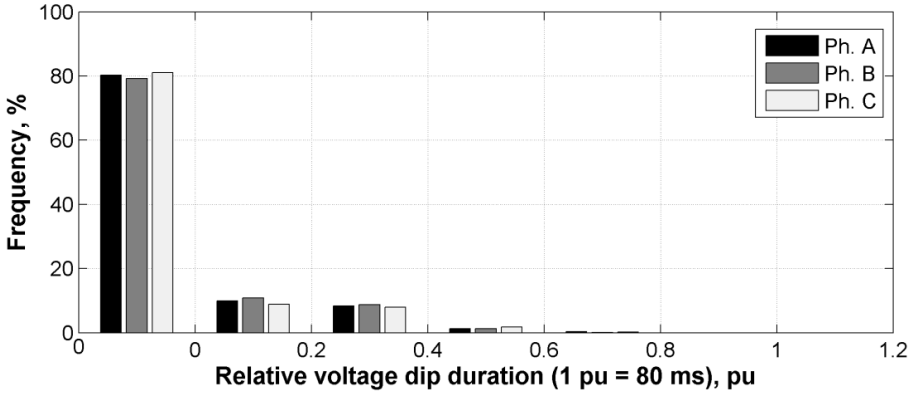

Figure 6-15 Frequency of voltage dip duration in three phases at the point-of-common-coupling under energising a feeder of wind turbine transformers

6.5.4 Effect of transformer winding connections on voltage dips propagation

Effects of transformer winding connections on voltage dips propagation from 132 kV side to 33 kV side were studied. The possible winding connections of the 132/33 kV transformers operating at the distribution grid are YNd1, YNd11 or YNyn0 [135]. The voltage dips (resulted from Case W1 energisation) after propagating through the transformers with these winding connections were observed on the secondary side of

132/33 kV transformers and compared with those observed at the point-of-common-coupling, as shown in Figure 6-16.

As can be seen, on the secondary side of 132 kV transformer with YNyn0 connection, the observed three-phase voltage dips are identical with those observed at the point-of-common-coupling (this finding is similar to the voltage propagation through the 400/132 kV autotransformer shown in Figure 4-14); for the voltage dips observed on the secondary side of 132 kV transformer with YNd1 and YNd11 connections, the biggest voltage dip has been increased by 12.5%, comparing with those observed at the point-of-common-coupling; in addition, the transformer with YNd1 connection changes the phase with the biggest voltage dip from phase B to phase C.

The above analysis indicates that grid transformer with YNyn0 connection has no impact on the propagation of three-phase voltage dips; the grid transformer with YNd1 or YNd11 connection would increase the dip magnitude seen by the end users.

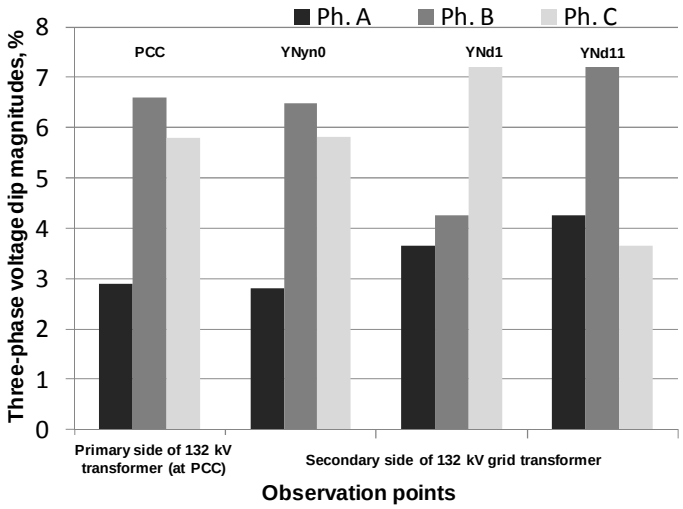

Figure 6-16 Effects of transformer winding connections on voltage dip propagation

6.5.5 Voltage dips caused by consecutive energisation of wind turbine transformers

Since each wind turbine transformer is normally equipped with a circuit breaker, consecutive energisation of a group of transformers may be preferred rather than simultaneous energisation of all the transformers connected at the feeder. Under such practice, if there is a need to quickly energise a feeder of wind turbine transformers, the time interval between two consecutive energisations would be short. With the time interval shorten, the voltage dip limit given by the grid code become smaller (according

to ER-P28, see Figure 2-21); for examples, the limit is about 1.3% if the interval is 1 minute; about 0.4% if the interval is 1 second.

Supposing the time interval between two consecutive energisations is 1 second, voltage dips caused by Case W4, W5 and W6 were further tested (Case W2 and W3 were not tested because the voltage dip magnitudes resulted from these cases already exceeded the grid code limit). For all the cases, the energisation was conducted under the commonly agreed worst case energisation condition against the weak source strength and the energisation direction was from the end closest to the offshore platform to the end farthest from the offshore platform.

Results are shown in Figure 6-17, Figure 6-18 and Figure 6-19, respectively. As can be seen, the maximum dip magnitudes resulted from consecutive energisation under Case W4, W5 and W6 are 2.95%, 2% and 1.2%, respectively. These dip magnitudes all exceed the 0.4% limit stated in the grid code. This indicates that, under the assumed energisation condition, the time interval between two consecutive energisations cannot be as short as 1 second. By comparing the maximum dip magnitudes with those limits given in Figure 2-21, it can be deduced that: to comply with the dip limits, the interval for Case W4 should be more than 12.5 minutes; for Case W5, it should be more than 3.3 minutes; for Case W6, the time interval is the shortest, which is about 1 minute. This shows that consecutively switching in only one transformer at a time is the recommended way to energise a feeder of wind turbine transformers while keeping the lowest risk of exceeding the grid code limit.

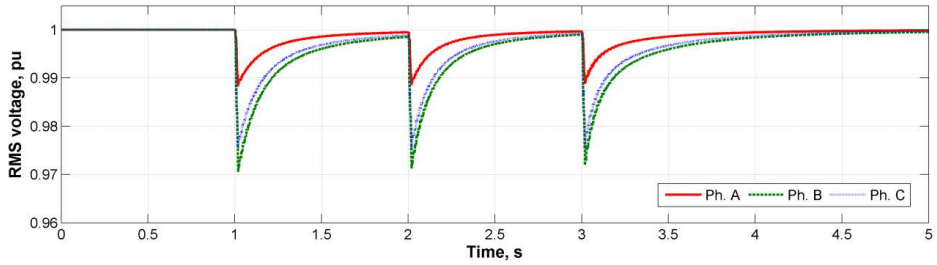

Figure 6-17 Voltage dips caused by consecutive energisation under Case W4

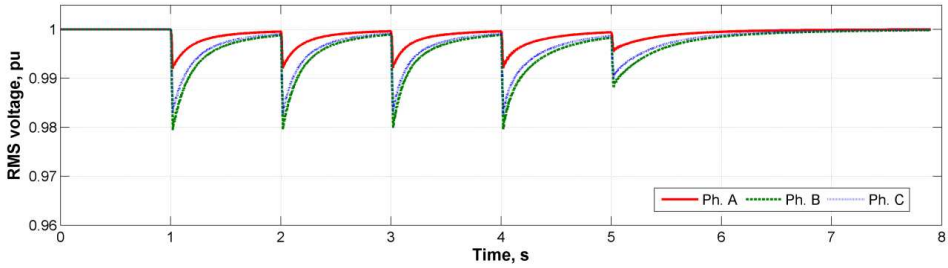

Figure 6-18 Voltage dips caused by consecutive energisation under Case W5

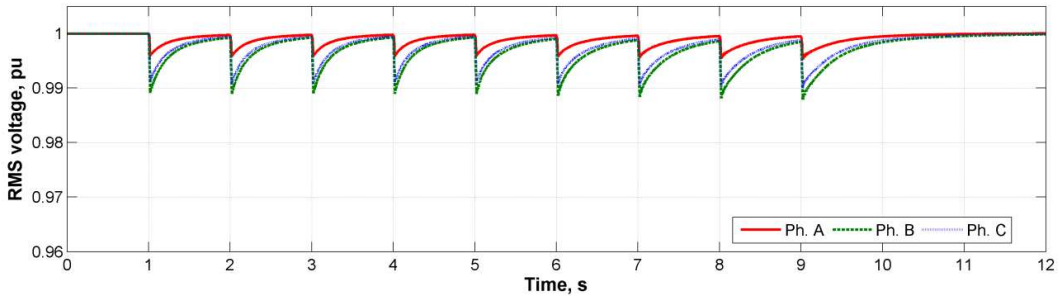

Figure 6-19 Voltage dips caused by consecutive energisation under Case W6

6.6 Sympathetic inrush between wind turbine transformers

Since wind turbine transformers are electrically close to each other, sympathetic inrush between them is a potential concern. In view of this, the potential sympathetic inrush interaction resulted from the above energisation cases were evaluated, as presented in the following sections.

6.6.1 Sympathetic inrush caused by energisation of multiple transformers

From Case W1 to Case W5, several wind turbine transformers being energised together is involved. Such energisation of multiple transformers, compared to energising one stand-alone wind turbine transformer, generates higher inrush current and larger voltage dips, which is evidenced particularly in Case W1. Thus, sympathetic inrush caused by energisation of multiple wind turbine transformers is studied in the following two subsections, in which, all the energisation case studies were carried out under the commonly agreed worst case energisation condition against the weak source strength.

6.6.1.1 Sympathetic inrush in the adjacent already connected feeder

In Figure 6-20, the configuration of two feeders (feeder-A and feeder-B) connected to offshore platform is schematically shown: feeder-A is to be energised and feeder-B is already connected. The distance of the cable connection between transformer A1 and B1 is defined as the electrical distance between the two feeders. With different electrical distances, Case W1 energisation of feeder-A transformers were conducted to assess the possible sympathetic inrush induced on feeder-B. Figure 6-21, Figure 6-22 and Figure 6-23 show the results corresponding to 1, 2 and 3 km electrical distance, respectively.

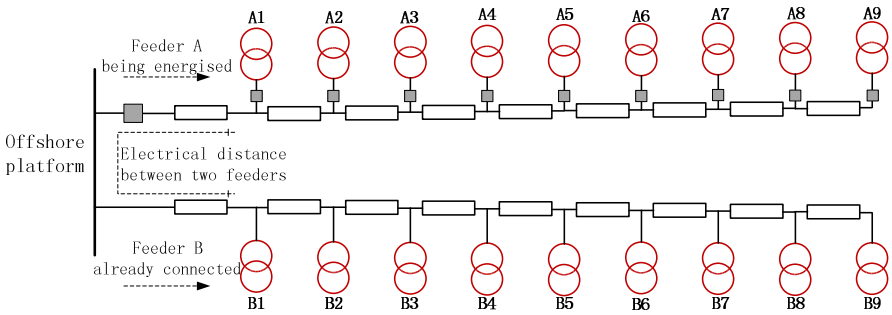

Figure 6-20 Schematic diagram of two wind farm feeders connected at offshore platform

As can be seen, in the case with 1 km electrical distance, the maximum instantaneous peak of the total sympathetic inrush current drawn by feeder-B transformers is about 130 A and the duration of the sympathetic inrush is less than 0.9 second. Compared to the sympathetic inrush currents drawn by large GSU transformers, the degree of sympathetic inrush is much less significant. As the electrical distance between two adjacent feeders increases, both the peak magnitude and the duration of sympathetic inrush currents decrease considerably, because the submarine cables connected between the two feeders provide resistive damping that suppresses the sympathetic inrush.

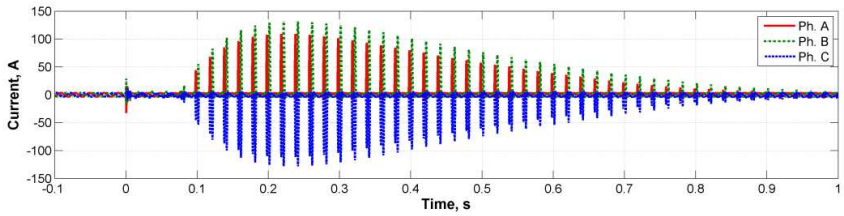

Figure 6-21 Sympathetic inrush currents drawn by the already connected feeder (1 km electrical distance between two feeders)

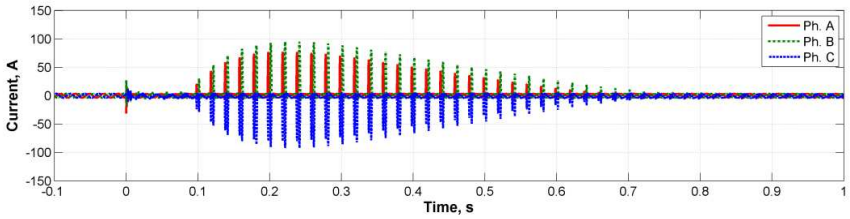

Figure 6-22 Sympathetic inrush currents drawn by the already connected feeder (2 km electrical distance between two feeders)

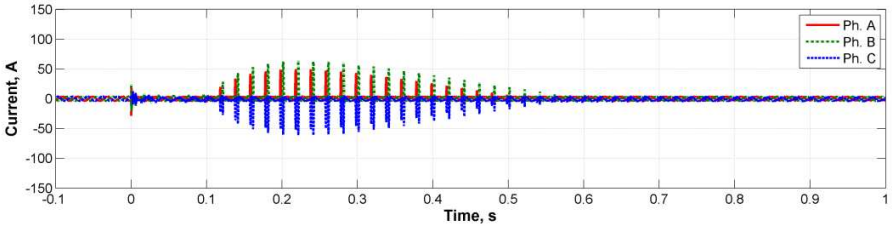

Figure 6-23 Sympathetic inrush currents drawn by the already connected feeder (3 km electrical distance between two feeders)

Furthermore, similar studies were carried out for other energisation cases involving energisation of multiple transformers. For Case W2 and W3 (with 1 km electrical distance), it was found that the maximum peak of the total sympathetic inrush currents is about 75 A and the duration of the sympathetic inrush is about 0.75 second. For Case W4 and W5 (with 1 km electrical distance), the sympathetic inrush current is negligible, which suggests that, in the present offshore wind farm grid, sympathetic interaction between two feeders could be of little concern if no more than three wind turbine transformers are being energised together.

6.6.1.2 Sympathetic inrush between transformers being energised together

When carrying out energisation of multiple transformers, the residual fluxes in wind turbine transformers being energised may differ from each other. Figure 6-24 shows an extreme condition that: the four transformers near to the offshore platform (A1-A4) possess maximum residual flux opposite to the flux build up; the other five wind turbine transformers (A5-A9) possess maximum residual flux in line with the flux build-up.

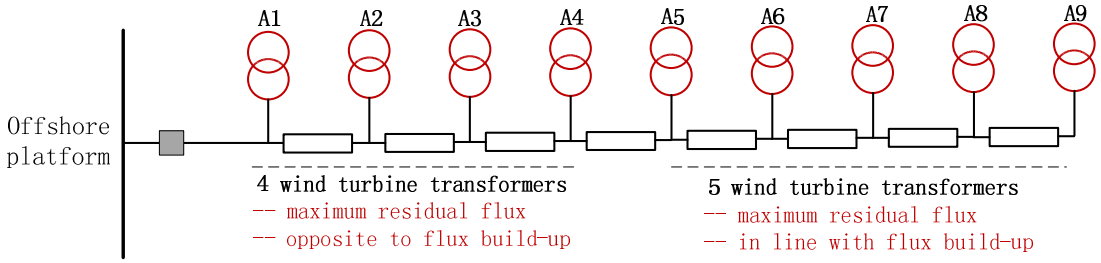

Figure 6-24 Wind turbine transformers with different residual flux condition

Simultaneous energisation of these nine wind turbine transformers was simulated under the worst energisation condition against the weak source strength. The currents observed at the primary sides of these wind turbine transformers are shown in Figure 6-25. Although the transformers were energised simultaneously, inrush took place in the wind turbine transformer A5, A6, A7, A8 and A9, whilst sympathetic inrush took place in the wind turbine transformer A1, A2, A3 and A4. This indicates that: sympathetic interaction could even be induced between the energised transformers if their residual flux conditions are different; the transformers which are relatively less saturated would be forced to engage sympathetic inrush by the relatively more saturated transformers.

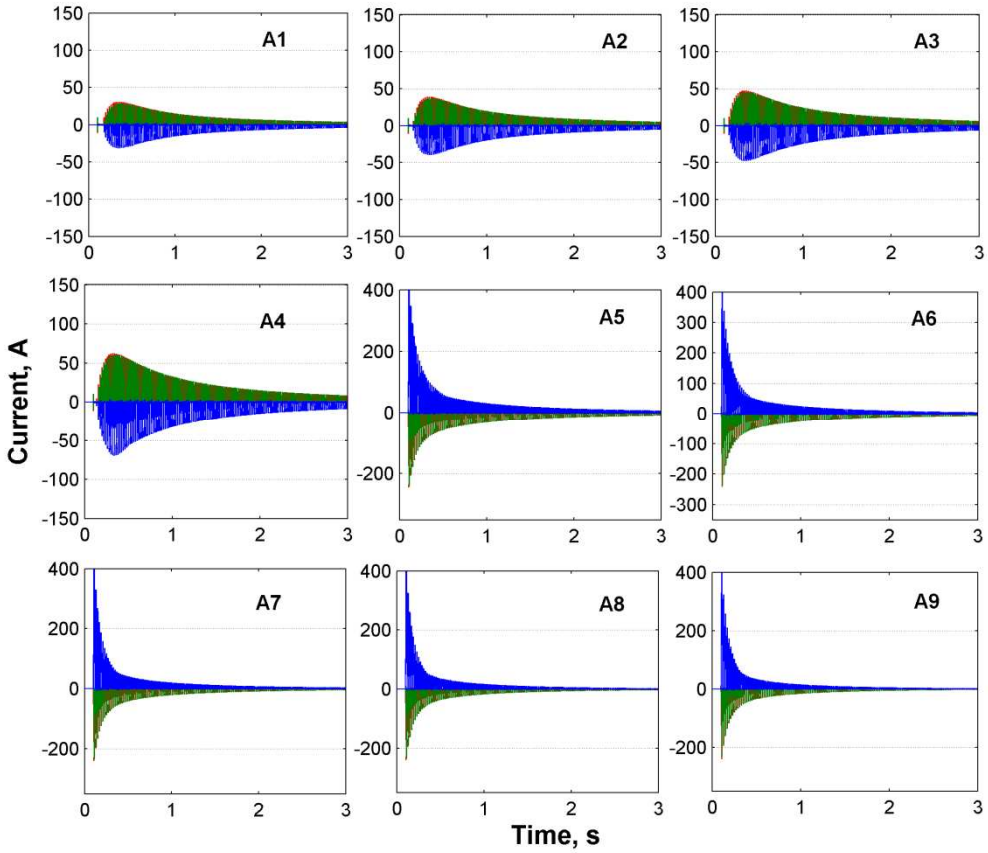

Figure 6-25 Sympathetic and inrush currents in the wind turbine transformers being energised together

6.6.2 Sympathetic inrush caused by independent energisation

Independent energisation of wind turbine transformer means energising only one wind turbine transformer at a time. In the case of such energisation, the concern over sympathetic inrush focuses on the wind turbine transformers within the same feeder, as there is negligible effect on other feeders (according to the findings in section 6.6.1.1). Using the validated network model, two independent energisation cases (Case W6_1 and Case W6_2) were simulated under the commonly agreed worst case energisation condition against the weak source strength:

- Case W6_1 concerns energising A9 with other transformers already connected;
- Case W6_2 regards energising A1 with other transformers already connected.

Under the Case W6_1 energisation, the resulted sympathetic inrush currents at the already connected wind turbine transformers are shown in Figure 6-26. As can be seen, sympathetic inrush currents are induced in A8, A7, A6, A5 and A4. A8 exhibits the largest sympathetic inrush peak which is about 25 A. From A7 to A4, the magnitudes of maximum peaks decrease from 24.5 to 4.6 A. Regarding the duration of sympathetic

inrush, the longest one is also seen at A8 and the shortest one is seen at A4. The sympathetic inrush currents in transformers A1, A2 and A3 are of negligible level. Such a distribution of sympathetic inrush current could be attributed to following reasons:

- When the high inrush currents drawn by A9 flow through the feeder cables, there is voltage distortion being built up by the resistive elements of the cable sections, especially on those 33 kV cable sections because of their higher resistivity; since A8 is the closest to A9, the resistive voltage distortion seen by A8 is the most significant and therefore the largest sympathetic inrush is built up in A8;
- From A8 further away down to A4, smaller and smaller sympathetic inrush currents could be induced, due to the increasing electrical distance from A9 causing bigger losses and shorter feeder cable for building up resistive voltage distortion;
- The established sympathetic inrush currents would balance out the distortion caused by inrush currents of A9 so that very little offset flux can be seen in A1, A2 and A3, therefore they were of negligible sympathetic inrush footprints.

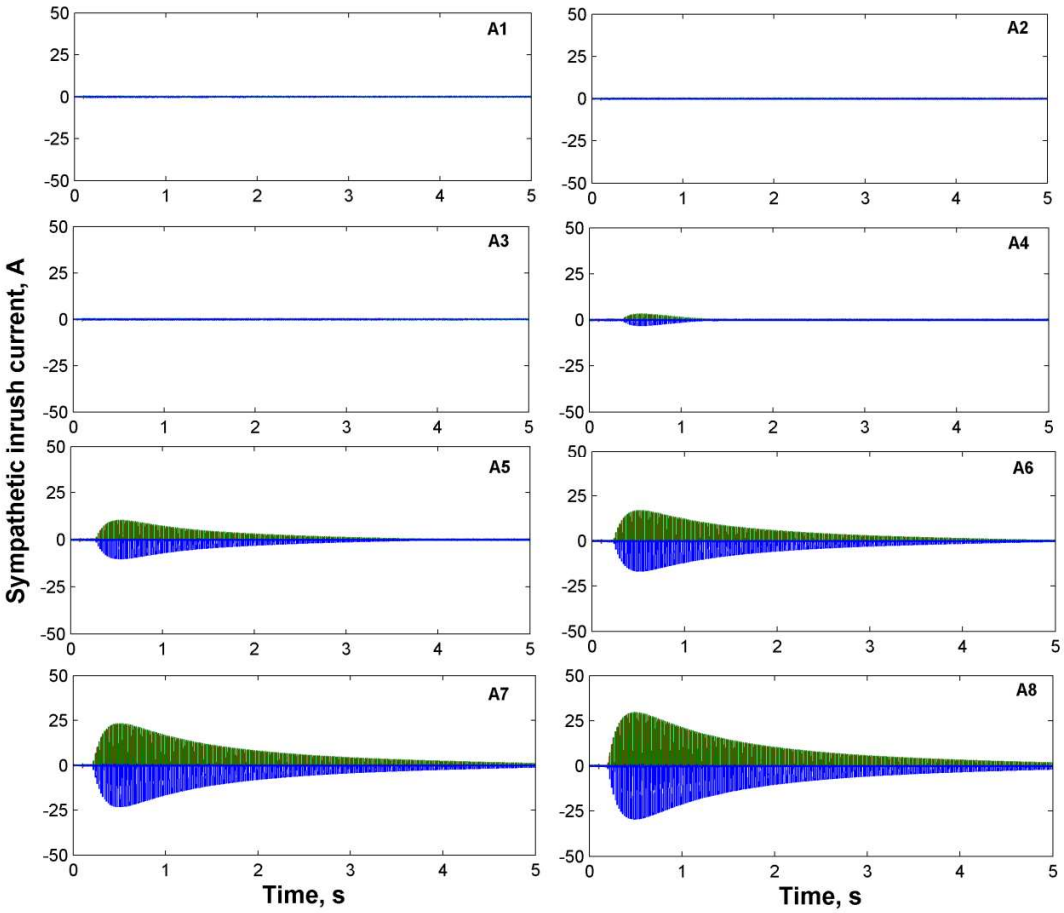

Figure 6-26 Sympathetic inrush currents observed in Case W6_1 simulation

In Case W6_2, A1 is the wind turbine transformer being energised with other wind turbine transformers already connected. The simulation results of this case are illustrated in Figure 6-27. Following the energisation, the peaks of sympathetic inrush currents induced in the already connected wind turbine transformers are relatively the same. This is because the wind turbine transformers experience almost the same amount of resistive voltage distortion built up on the cables connecting between the supply source and the wind turbine transformer A1. The duration of the sympathetic inrush currents, however, exhibits considerable differences. The duration of sympathetic inrush in A2 is the largest, for it is located closest to A1; as the electrical distance between A1 and other already connected wind turbine transformers increases, the duration of sympathetic inrush decreases. However, in contrasting to the results given by Case W6_1, the initiation process of all the sympathetic inrush currents is much slower and the maximum peaks are much smaller, which suggests that the resistive voltage distortion across the system between supply source and A1 is much smaller than that in Case W6_1.

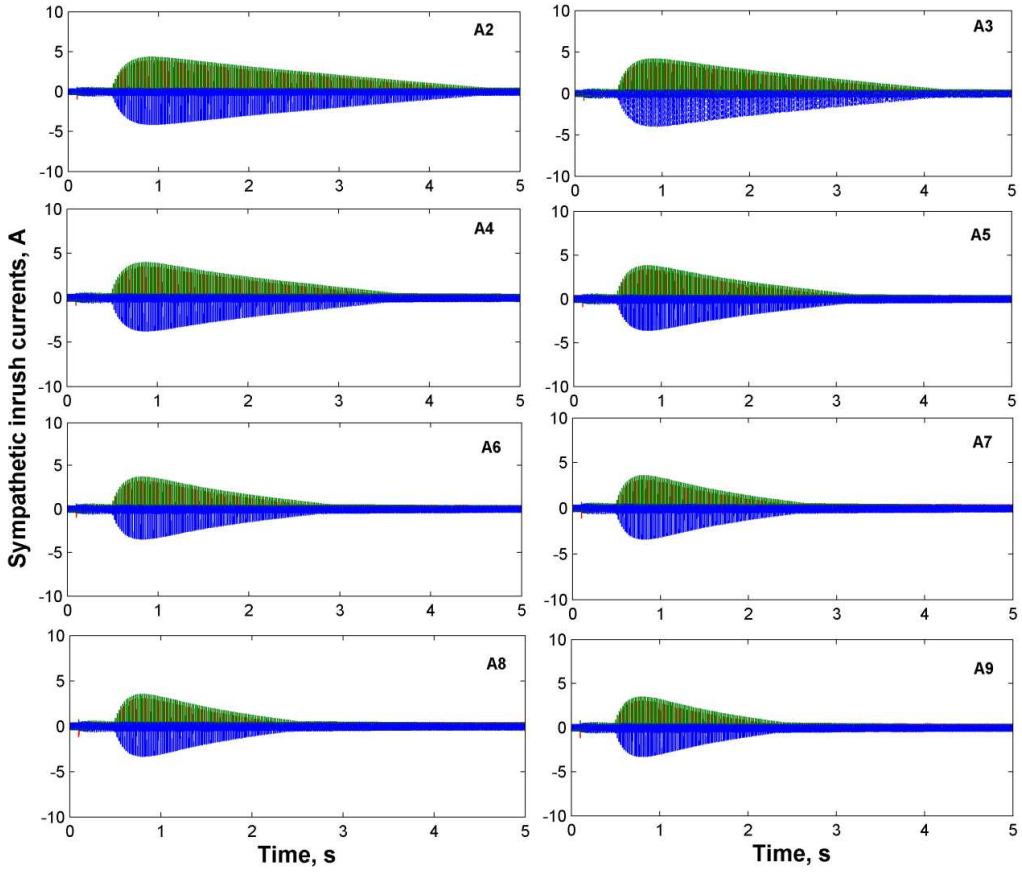

Figure 6-27 Sympathetic inrush currents observed in Case W6_2 simulation

From the above two case studies, it can be deduced that the degree of sympathetic inrush induced on each wind turbine transformer is largely related to the location of the wind turbine transformer being energised and the relative location of the other already connected wind turbine transformers.

6.7 Identification of energisation sequence resulting in less sympathetic inrush between wind turbine transformers

The above two case studies imply that the sequence of energising wind turbine transformers would affect the amount of sympathetic inrush currents being induced on each wind turbine transformer. In this section, potential relationships between energisation sequence and sympathetic inrush level are evaluated, aiming to identify the energisation sequence resulting in less sympathetic inrush between the wind turbine transformers.

6.7.1 Sympathetic inrush level

As illustrated in Figure 6-28, the level of sympathetic inrush is defined by the multiplication of the RMS peak of the sympathetic inrush current and its duration, with its unit is defined as A·s. This sympathetic inrush level is aimed to qualitatively represent the degree of over-fluxing involved in the sympathetic inrush process which might impair the wind turbine transformers in terms of mechanic and thermal effects. Note that the threshold chosen to define the start and the end of sympathetic inrush duration is 1.12 times of the RMS nominal magnetizing current of wind turbine transformer (this threshold was chosen because it is larger than the maximum RMS magnetizing current and is reliable enough to detect the initiation of sympathetic inrush).

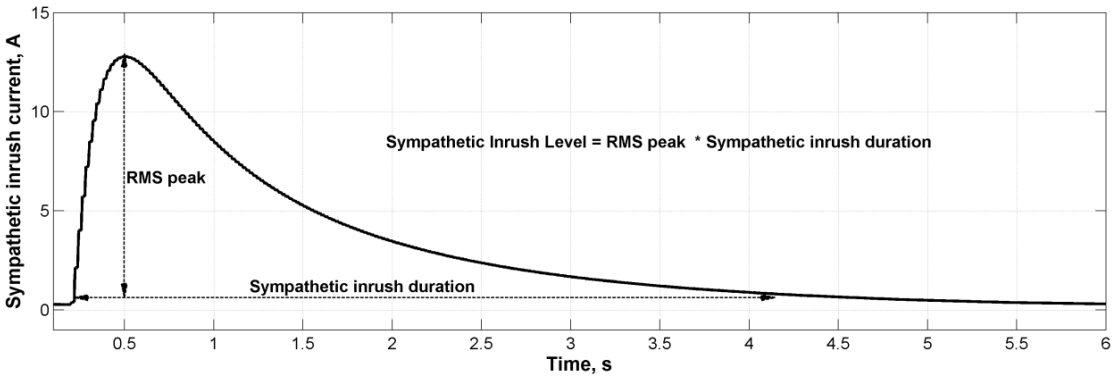

Figure 6-28 Definition of sympathetic inrush level

6.7.2 Energisation sequence

Four energisation sequences were considered for independently energizing the transformers in feeder-A of the Nysted offshore wind farm, which are listed below and also detailed in Table 6-9:

Sequence 1 (S1): starts energisation from the wind turbine transformer closest to the offshore platform towards the one farthest from the offshore platform (i.e., from A1 to A9);

Sequence 2 (S2): starts energisation from the wind turbine transformer farthest from the offshore platform towards the one closest to the offshore platform (i.e., from A9 to A1);

Sequence 3 (S3): starts from both ends towards middle;

Sequence 4 (S4): starts from middle towards both ends.

Table 6-9 Sequences for energising wind turbine transformers in a feeder

Sequence	Wind turbine transformer being energised								
	1	2	3	4	5	6	7	8	9
S1	A1	A2	A3	A4	A5	A6	A7	A8	A9
S2	A9	A8	A7	A6	A5	A4	A3	A2	A1
S3	A1	A9	A2	A8	A3	A7	A4	A6	A5
S4	A5	A4	A6	A3	A7	A2	A8	A1	A9

6.7.3 Study procedure correlating sympathetic inrush level and energisation sequence

The flowchart shown in Figure 6-29 illustrates the study procedure to correlate energisation sequence and the sympathetic inrush level:

- First, an energisation sequence is defined;
- Second, initialize the energisation condition in terms of circuit breaker closing time and the residual flux in the wind turbine transformer to be energised;
- Third, simulate the energisation of the targeted wind turbine transformer;
- Fourth, record the sympathetic inrush currents induced on other adjacent wind turbine transformers and calculate the sympathetic inrush level;
- Fifth, check if all the wind turbine transformers have been energised; if not, update the topology by connecting the newly energised transformer and then move back to the second step;
- Finally, calculate the total sympathetic inrush level accumulated on each wind turbine transformer.

As an example, let us consider applying the study procedure to assess energisation sequence S1. The energisation starts from energizing A1; at this first energisation, no sympathetic inrush can be observed, as other wind turbine transformers are not connected yet. From the second energisation onward to the last one, each energisation would induce sympathetic inrush on the previous energised transformers, i.e., following S1, energizing A2 would cause sympathetic inrush in A1 and energizing A4 would cause sympathetic inrush in A1, A2 and A3. For each energisation, the level of sympathetic inrush of each transformer is recorded. Finally, these levels recorded in all the energisations are summed together to represent the accumulated sympathetic inrush level for each wind turbine transformer. In this way, after following S1 to energise all the transformers, eight sympathetic inrush levels would be accumulated on each phase of A1 but zero on A9 as it is the last one being energised.

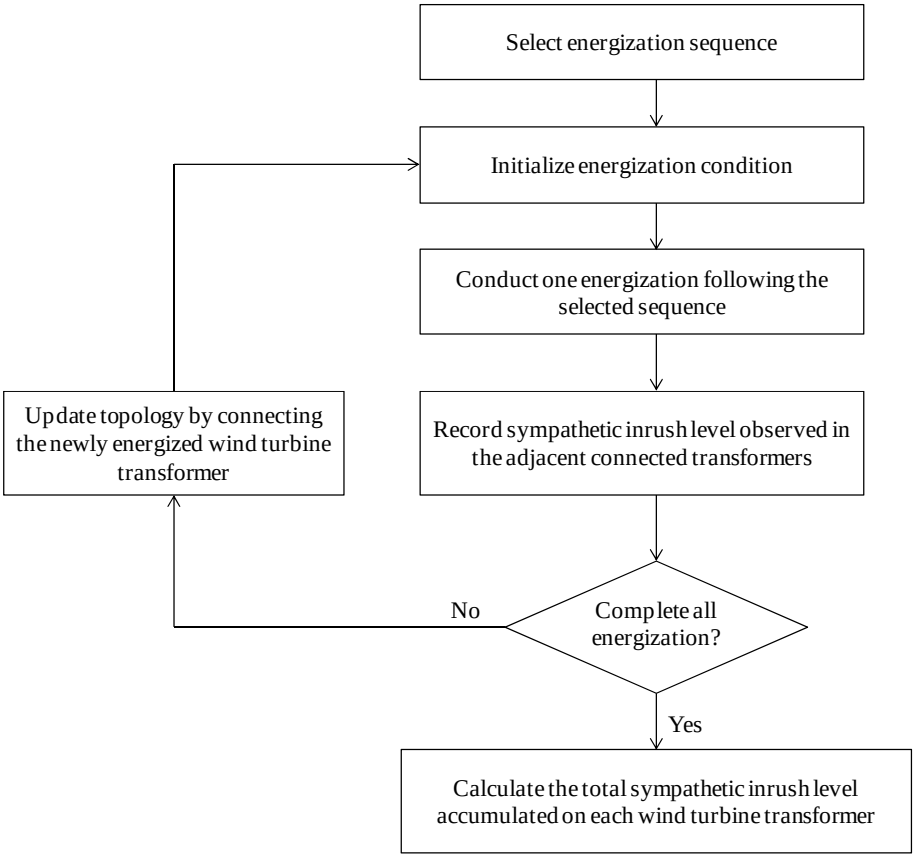

Figure 6-29 Procedure to correlate energisation sequence and sympathetic inrush level

6.7.4 Assessment of sympathetic inrush level under different energisation sequences using deterministic approach

Utilizing the study procedure, the sympathetic inrush levels that would be accumulated in each wind turbine transformer under the four energisation sequences were

deterministically assessed. In the assessment, the energisation condition for all the energisation events was initialized to the commonly agreed worst case energisation condition (same as in previous studies, i.e., three phases were simultaneously energised at the positive-going zero crossing of phase C line-to-ground voltage; residual flux of phase A, B and C was of -0.8 pu, 0 and +0.8 pu of peak nominal flux, respectively).

The simulation results given by assessing sequences S1, S2, S3 and S4 are shown in Figure 6-30, Figure 6-31, Figure 6-32 and Figure 6-33, respectively. In all the figures, the wind turbine transformer is indicated by the number shown on the horizontal axis; each column group represents the sympathetic inrush level of three phases accumulated on each wind turbine transformer under a particular energisation sequence.

As can be seen, for any column group, the sympathetic inrush level accumulated on phase C is the highest among the three phases (this is due to the specific energisation condition). The following analysis focuses on the sympathetic inrush level of phase C only. Regarding the maximum accumulated sympathetic inrush level, the one in S1 is about 130 A·s; in S2, the maximum level is about 295 A·s, which is almost identical to that appear in S3 and is more than twice in S1; in S4, the maximum level is about 205 A·s. Comparing the severity of sympathetic inrush associated with each wind turbine transformer, A8 and A9 would experience the most intensive sympathetic inrush if S2 or S3 is followed, whilst A5 and A6 would be more vulnerable if S1 or S4 is applied. It can also be seen that the wind turbine transformers located close to the platform, including A1, A2 and A3, experience rather small level of sympathetic inrush under all the energisation sequences. In addition, aggregation of all the accumulated sympathetic inrush levels under each energisation sequence was made (in total, four aggregations) and they are compared in Table 6-10. It can be seen that the aggregation of the accumulated sympathetic inrush levels resulted from S1 is the lowest, followed by S3, S4 and S2.

The above results indicate that, when a feeder of wind turbine transformers are to be sequentially energised, to result in less sympathetic inrush, wind turbine transformers should be energised from the one closest to the offshore platform towards the one farthest from the offshore platform, because it gives the smallest level of sympathetic inrush on a stand-alone wind turbine transformer and also the least aggregated sympathetic inrush effects compared to other energisation sequences.

Table 6-10 Aggregation of sympathetic inrush levels resulted from each energisation sequence

Energisation sequence	S1	S2	S3	S4
Aggregation of sympathetic inrush level (A·s)	1434	1796	1581	1590

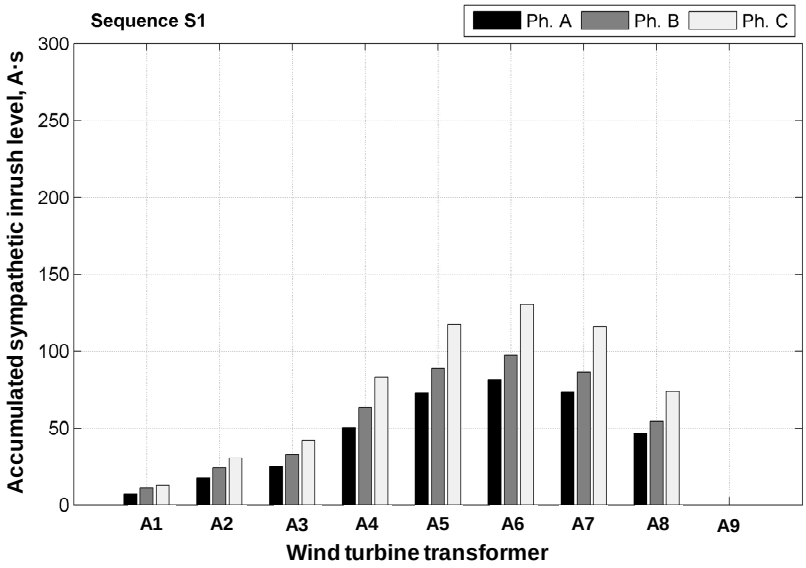

Figure 6-30 Accumulated sympathetic inrush level on each wind turbine transformer resulted from deterministic testing of S1

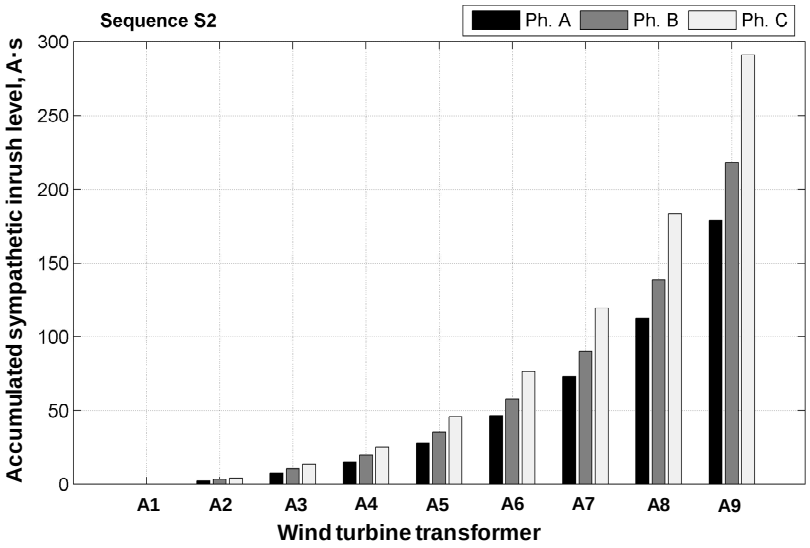

Figure 6-31 Accumulated sympathetic inrush level on each wind turbine transformer resulted from deterministic testing of S2

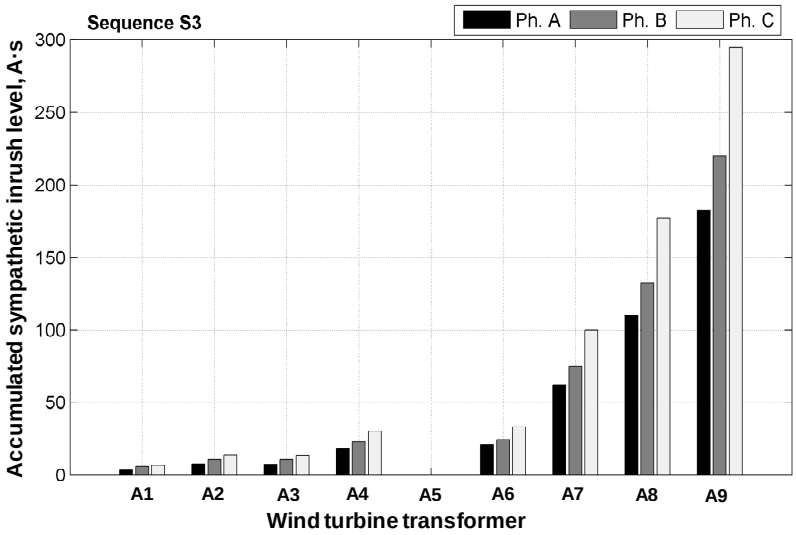

Figure 6-32 Accumulated sympathetic inrush level on each wind turbine transformer resulted from deterministic testing of S3

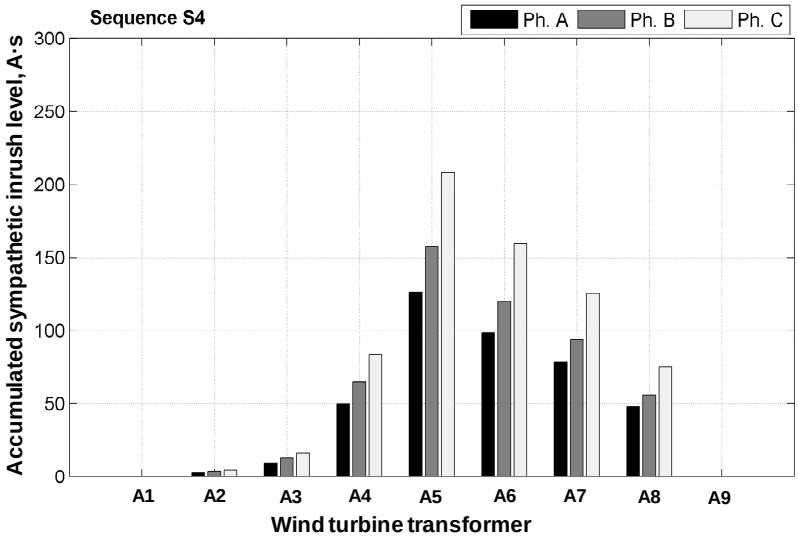

Figure 6-33 Accumulated sympathetic inrush level on each wind turbine transformer resulted from deterministic testing of S4

6.7.5 Assessment of sympathetic inrush level under different energisation sequences using stochastic approach

In the previous section, the energisation sequence resulting in less sympathetic inrush is deterministically identified based on the worst case energisation condition. However, in reality, the initial condition for each energisation is stochastic, due to the uncertainty of circuit breaker closing time and transformer core residual flux. It is suspected that, when these stochastic parameters are considered, the findings given by the deterministic assessment may become less significant or even invalid. Therefore, following the procedure shown in Figure 6-29, stochastic simulation were performed to study the sympathetic inrush level under the above-mentioned four energisation sequences with

energisation condition stochastically initialized, aiming to confirm the findings obtained from the deterministic assessment.

The energisation condition was stochastically initialized as follows: the closing time of each circuit breaker pole was defined by a common-order-time (same for three poles, uniformly distributed over one power frequency cycle) plus a Gaussian distributed closing offset time (with the mean value equals to zero and standard deviation equals to 0.833 ms) [43]; the range of the residual flux was defined as between -0.8 pu and +0.8 pu of the peak nominal flux and it was characterized by Uniform distribution (note that the residual flux in each wind turbine transformer was independently assigned). For each energisation sequence, 1000 stochastic simulation tests were carried out.

By using box plot, results obtained from stochastic testing energisation sequence S1, S2, S3 and S4 are presented in Figure 6-34, Figure 6-35, Figure 6-36 and Figure 6-37, respectively. In these figures, each column represents 1000 sympathetic inrush levels accumulated on phase C of a specific wind turbine transformer (the results of other two phases are similar to that of phase C); the central mark on each box is the median; the lower and upper edges of the box are the 25th and 75th of the percentiles; the length of the whisker is defined by w whose value is 1.5 (this value corresponds to 99.3% coverage if the data are normally distributed); points are displayed using + as outliers if they are larger than $Q_{75}+w\cdot(Q_{75}-Q_{25})$, where Q_{25} and Q_{75} are the 25th and 75th percentiles, respectively.

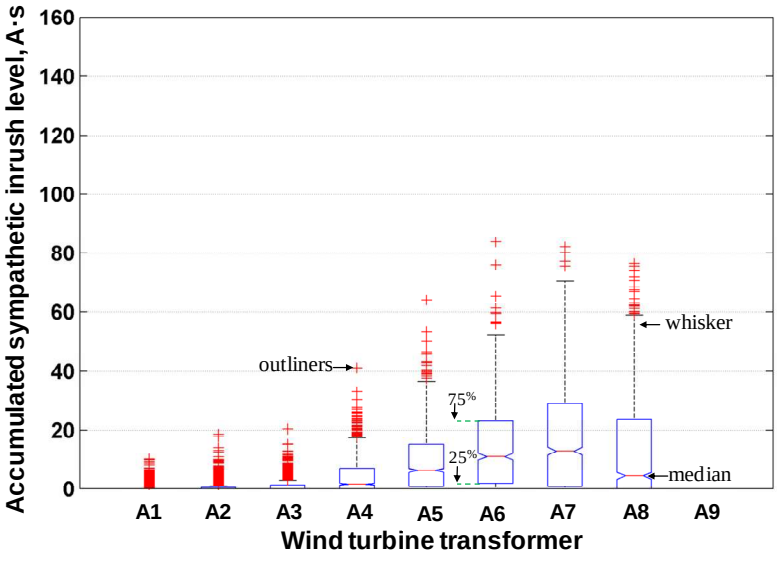

Figure 6-34 Accumulated sympathetic inrush level of each wind turbine transformer resulted from stochastic testing of S1

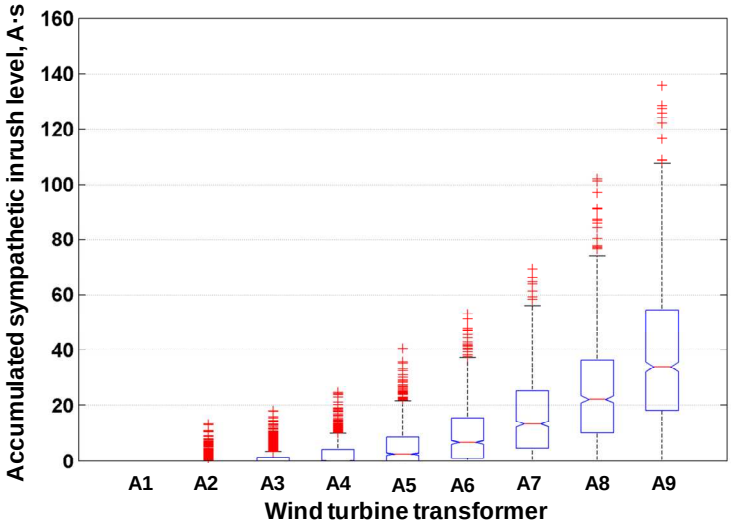

Figure 6-35 Accumulated sympathetic inrush level of each wind turbine transformer resulted from stochastic testing of S2

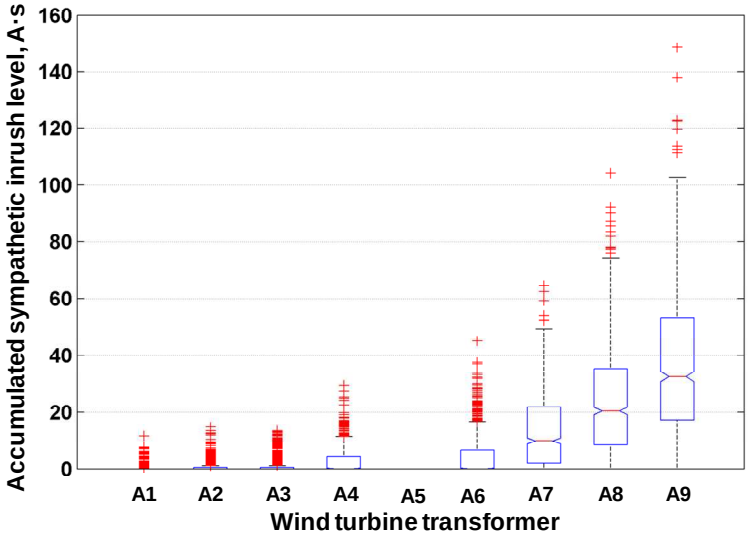

Figure 6-36 Accumulated sympathetic inrush level of each wind turbine transformer resulted from stochastic testing of S3

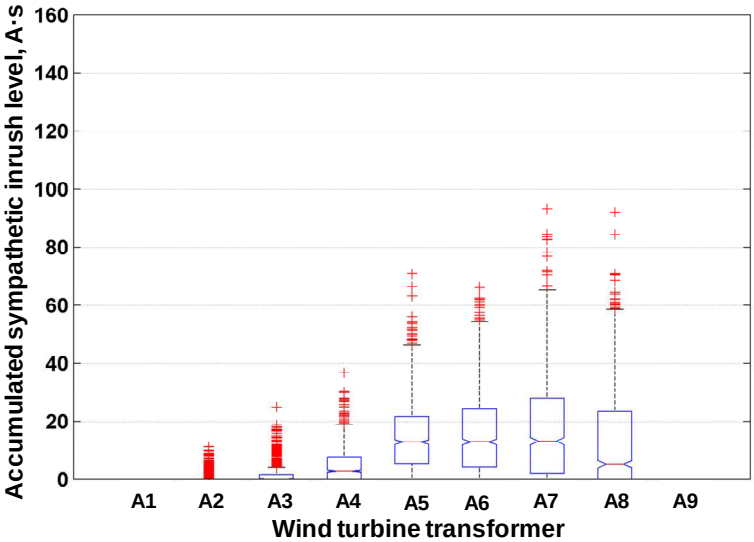

Figure 6-37 Accumulated sympathetic inrush level of each wind turbine transformer resulted from stochastic testing of S4

As can be seen from Figure 6-34 to Figure 6-37, the accumulated sympathetic inrush level for each wind turbine transformer is scattered, due to the presence of stochastic energisation conditions. The scatter ranges are relatively small for transformers A1, A2, A3 and A4 and are relatively large for A6, A7, A8, which are evidenced in all energisation sequences. The scatter range for A5 is relatively large in S1, S2 and S4, while the scatter range for A9 is relatively large in the case of S2 and S4. The relatively large scatter ranges for A5, A6, A7, A8 and A9 indicate that wind turbine transformers located at these positions are likely to be affected by sympathetic inrush, which is also evidenced by the findings obtained in previous deterministic studies.

As far as the median of each column is concerned, the lowest one is still found to be in S1 and the profile of accumulated sympathetic inrush level formed by nine wind turbine transformers is similar to that showed in Figure 6-30, which suggests that S1 is the energisation sequence which would induce minimum sympathetic inrush between wind turbine transformers. Therefore, the findings gained from the deterministic assessment are further validated by the stochastic studies.

6.8 Summary

In this chapter, a network model of a wind farm collection grid was developed and validated against field measurement results obtained in literature, which was then used to study voltage dips and sympathetic inrush caused by energising wind turbine transformers.

Regarding voltage dips, the above case studies show that, in the studied system, energising one wind turbine transformer against the weak source strength can only result in dip magnitude of no more than 1%, therefore causes no concern on breaching grid code requirements. Concerns may be raised in the cases of simultaneously energising multiple wind turbine transformers, because the resulted voltage dips may reach 6.6%, even though stochastic estimation shows that the probability of reaching such a dip magnitude is very low. The winding connection of 132/33 kV transformers should be carefully considered, as it may change the phase with the biggest voltage dip magnitude and result in larger dip magnitude seen by the end users. In addition, care should be taken if consecutive energisation of wind turbine transformers (with time

interval shorter than 750 seconds) is carried out, because the voltage dip limit is further tightened.

Regarding the sympathetic inrush caused by energising wind turbine transformers, the performed studies consist of two parts: one is to on energisation of multiple wind turbine transformers and the other is on energisation of a stand-alone wind turbine transformer.

In the case of energisation of multiple transformers, it was found that: the degree of sympathetic interaction between two adjacent feeders is rather minor, because the cable connection between the feeders can contribute significant resistive losses; one should be cautious that sympathetic inrush may occur between the transformers being energised together, if they have a different residual flux.

In the case of energisation of a stand-alone transformer, it was found that the degree of sympathetic inrush is largely related to the location of the wind turbine transformer being energised and the relative location of the other already connected transformers. Furthermore, the potential relationships between energisation sequence and sympathetic inrush level were deterministically and stochastically evaluated, suggesting that the energisation sequence that would result in less sympathetic inrush level between wind turbine transformers is to energise wind turbine transformers from the one closest to the offshore platform to the one farthest from the offshore platform.

Chapter 7 Conclusion and Future Work

7.1 Concluding remarks

This thesis investigates voltage dips and sympathetic inrush caused by energising generator step-up transformers in two types of generation connection: one is a CCGT plant connected to a 400 kV transmission grid and the other is a large offshore wind farm connected to a 132 kV distribution grid. The studies mainly consist of four parts:

1) Network model development and validation. Two network models, one for a 400 kV grid, and the other for an offshore wind farm collection grid, were developed in ATP/EMTP and validated against multiple sets of field measurement results.
2) Deterministic studies of voltage dips in the transmission grid. This includes: comparative assessment of voltage dips under various energisation conditions and the network-wide voltage dips under non-outage and outage conditions; identifying the influence of sympathetic inrush on voltage dips; carrying out sensitivity studies to identify the key influential parameters; exploring operational approaches to reduce voltage dips and sympathetic inrush.
3) Stochastic estimation of voltages in the transmission grid. First, an ATP-MATLAB interfacing simulation platform was established to enable stochastic assessment using Monte Carlo method. Second, the possible stochastic parameters were determined and the procedures to generate stochastic values for the parameters were developed. Then a preliminary stochastic simulation based on a single phase circuit was conducted, forming the basis for stochastic studies of three-phase transformer energisation transients. Finally, the stochastic simulation investigation was performed on the 400 kV grid, including: calculating the probability distribution of voltage dip magnitudes and durations; identifying the probability of reaching the worst case voltage dips; testing the sensitivity of the results to various closing offset time and residual flux distributions.

4) Assessment of transformer inrush transients due to offshore wind farm connections: voltage dips caused by energising wind turbine transformers under different scenarios were assessed; in particular, sympathetic inrush between wind turbine transformers were studied, which helped identify the energisation sequence resulting in less sympathetic inrush between wind turbine transformers.

Main contributions of this thesis work are likely to be the following:

1) Developing network models suitable for simulating network-wide voltage dips and sympathetic inrush between transformers;
2) Quantifying the influence of sympathetic inrush on voltage dips caused by transformer energisation;
3) Assessing the probability of encountering the worst case voltage dips during energisation;
4) Identifying the optimum energisation sequence for reducing sympathetic inrush between wind turbine transformers.

The summary of simulation results and key findings is given as follows.

Field measurement, network model development and validation

Through analysing the field measurements which were carried out in the 400 kV transmission grid, it was shown that the energisation of GSU transformers can trigger a network-wide voltage dips (i.e., voltage dips not only appear at the substation connected by the transformer being energised but also at other substations in the network); the recorded maximum RMS voltage dip was about 7.85%; the measured sympathetic inrush currents showed that the duration of sympathetic inrush lasted for more than 20 seconds and so did the full recovery of the resulted voltage dips.

Based on the system parameters provided by the network operator, a 400 kV grid network model was developed in ATP/EMTP by following the modelling guidelines summarized through the literature review. The successful validation of the network model confirms that: the source network can be modelled by an ideal sine-wave source and a Thevenin equivalent impedance of the part of the network not under study; the transmission network between the supply source and the energised transformer should be represented in detail, taking into account the transmission lines, system loading and reactive power compensation devices; the constant frequency line model can be used to

represent transmission lines, with line dimension and transposing scheme considered; system loading can be represented by lumped constant resistance and inductance connected in parallel; transformers can be modelled by the BCTRAN routine with transformer core externally represented by three delta-connected type-96 non-linear inductors.

Deterministic studies of voltage dips caused by energising large GSU transformers

The validated network model was utilized to carry out a comprehensive study on voltage dips using deterministic approach. Through assessing the degrees of voltage dips under different energisation conditions, it was found that: in the present system with two GSU transformers simultaneously energised under the worst energisation condition, the maximum voltage dip, observed at the substation closest to the transformers being energised, would be of magnitude about 18% and duration about 3.5 seconds; with the presence of sympathetic interaction, the dip duration can prolonged by 125% (increased from 3.5 seconds to 7.9 seconds); the voltage dips propagating to 132 kV side can be of longer dip duration due to the sympathetic inrush of substation transformers.

Furthermore, assessing the network-wide voltage dips for the complete network under non-outage condition suggests that: the dip magnitudes observed at each substation are related to the distance between the substation and the supply source and also the distance between the substation and the energised transformers; those substations located in the proximity of the energised transformer and relatively far away from supply source are subjected to larger dip magnitudes.

With line outage taken into account, it was found that: the network-wide voltage dip outcome under single-circuit outage situation is similar to that observed under non-outage condition; however, if there is double-circuit outage resulting in significant network topology change, both dip magnitude and duration can be significantly exacerbated; in the system under study, the most unfavorable double-circuit outage can increase the dip magnitude from 18% to about 30%.

The sensitivity assessment shows that: transformer core saturation inductance has the most profound impact on the voltage dip magnitude; the amount of transformer copper losses is the most influential parameter on determining the voltage dip duration.

Possible operational measures to control the voltage dips were found to be adjusting GSU tap changer to maximum tap, opening the coupler circuit breaker and applying SVC. It was found that, if these operational measures are applied simultaneously, the dip magnitude and duration resulted from worst case energisation can be reduced by 37% and 85%, respectively.

Stochastic assessment of voltage dips caused by transformer energisation

Monte Carlo simulation was conducted to extend the few deterministically-defined case studies to many stochastically-defined case studies. A dip frequency pattern was identified based on over 1000 stochastic runs and it was found to be sensitive to the distribution of residual flux but insensitive to the distribution of closing offset time. In addition, it was shown that the dip frequency pattern is insensitive to the system condition variation in a range of ±25%. Furthermore, it was found that the probability of reaching the worst case dip magnitude (estimated by the commonly agreed worst case energisation condition) is lower than 0.5%, indicating that the worst case scenario is unlikely to occur; in fact, about 80% of the dips are with magnitudes lower than 0.6 pu of the worst case dip magnitude. Nevertheless, it was shown that there exist dips with magnitudes exceeding the worst case dip magnitude, indicating the inadequacy of deterministic assessment approach by using the commonly agreed worst case energisation condition.

Assessing transformer energisation transients due to offshore wind farm connection

Voltage dips caused by energising wind turbine transformers were studied and compared with those caused by energising large GSU transformers. It was found that, in the present system under study, energising a stand-alone wind turbine transformer against the weak source strength can only result in dip magnitude of no more than 1 % (as the fault level of the source network is more than three hundred times larger than the rating of the wind turbine transformer), therefore causes no concern on complying grid code requirements. Concerns may be raised in the case of simultaneously energising a feeder of wind turbine transformers or consecutive energisation of transformers with short time interval.

Regarding the sympathetic inrush caused by energising wind turbine transformers, it was found that although the degree of sympathetic interaction between two adjacent feeders is rather mild (as the cable connection between the feeders can contribute

significant resistive losses), one should be cautious that sympathetic inrush may occur between the transformers being energised together, if they are of different residual flux.

The potential relationships between sympathetic inrush and energisation sequence were both deterministically and stochastically evaluated and the main conclusion reached is that the optimum energisation sequence to achieve less sympathetic inrush between wind turbine transformers is to energise wind turbine transformers from the one closest to the offshore platform to the one farthest away from the offshore platform.

7.2 Future work

Although the work carried out in this thesis has helped fulfill all the initially defined goals and generate a number of useful conclusions, it also raises new questions to be investigated in the future work.

<u>For network model development and validation:</u>

1) For modelling GSU transformers, the transformer air-core inductance was assumed to be twice the transformer short-circuit inductance. It would be interesting to check the accuracy of this assumption by comparing with analytical estimation using transformer winding and core design data.
2) The use of BCTRAN+ model in this thesis does not take into account the influence of transformer core topology. The effect of core topology may be taken into account by using Hybrid Transformer model to represent GSU transformers, if more transformer design information is available. Then it would be interesting to see if Hybrid Model can more accurately simulate sympathetic inrush between GSU transformers.

<u>For assessment of energising GSU transformer into transmission network:</u>

1) In the deterministic case studies, it was assumed that the generators on the secondary side of the GSU transformers were not connected yet. It is possible that one of the generators is already connected while carrying out the energisation of a GSU transformer. In this case, it would be interesting to evaluate the influence of the generator's AVR responses on the outcome of sympathetic inrush.
2) In the stochastic case studies, residual flux is initialized by pre-defined

distributions. In reality, the residual flux in the transformer core is formed by a ring down process. If there is detailed knowledge about disconnection time, circuit breaker chopping characteristic, circuit capacitance and transformer core hysteresis behavior, the ring down process can be more accurately simulated so as to initialize the core residual flux with more realistic distribution and magnitudes. In future work, more efforts can be diverted to evaluating the transformer residual flux formation so as to refine the residual flux distribution.

For assessment of energising wind turbine transformer into offshore wind farm grid:

1) Field measurement of sympathetic inrush between wind turbine transformers would help further validation of the collection grid model and reinforcing the identified energisation sequence. Hence, it is important to carry out field measurement of sympathetic inrush between wind turbine transformers in the future.
2) Wind farm collection grid normally consists of dozens of wind turbines. To represent all the wind turbine generators and transformers is a challenge to the simulation stability and simulation time. An alternative approach might be to represent some of the feeders using aggregated transformer and cable model so that the network model can be simplified for reducing computation effort.
3) The degree of sympathetic inrush between wind turbine transformers might vary with the layout of the wind farm collection grid. The studies carried out in this thesis are focusing on radial layout only. Further studies can be carried out for guiding the energisation of offshore wind farms with other layouts.

References

[1] L. F. Blume, G. Camilli, S. B. Farnham, and H. A. Peterson, "Transformer magnetizing inrush currents and influence on system operation," Transactions of the American Institute of Electrical Engineers, vol. 63, no. 6, pp. 366-375, 1944.

[2] I. Arana, A. Hernandez, G. Thumm, and J. Holboell, "Energization of wind turbine transformers with an auxiliary generator in a large offshore wind farm during islanded operation," IEEE Transactions on Power Delivery, vol. 26, no. 4, pp. 2792-2800, 2011.

[3] N. Chiesa and H. K. Høidalen, "Novel approach for reducing transformer inrush currents: laboratory measurements, analytical interpretation and simulation studies," IEEE Transactions on Power Delivery, vol. 25, no. 4, pp. 2609-2616 2011.

[4] Engineering-Recommendation-P28, "Planning limits for voltage fluctuations caused by industrial, commercial and domestic equipment in the UK," 1989.

[5] "National electricity transmission system security and quality of supply standard," National Grid, Mar. 2012.

[6] L. Prikler, G. Bánfai, G. Bán, and P. Becker, "Reducing the magnetizing inrush current by means of controlled energization and de-energization of large power transformers," Electric Power Systems Research, vol. 76, no. 8, pp. 642-649, 2006.

[7] S. P. Patel, "Fundamentals of transformer inrush," in 64th Annual Conference for Protective Relay Engineers, pp. 290-300, Texas, USA, Apr. 2011.

[8] M. Steurer and K. Frohlich, "The impact of inrush currents on the mechanical stress of high voltage power transformer coils," IEEE Transactions on Power Delivery, vol. 17, no. 1, pp. 155-160, 2002.

[9] J. Faiz, B. M. Ebrahimi, and T. Noori, "Three- and two-dimensional finite-element computation of inrush current and short-circuit electromagnetic forces on windings of a three-phase core-type power transformer," IEEE Transactions on Magnetics, vol. 44, no. 5, pp. 590-597, 2008.

[10] R. Yacamini and A. Abu-Nasser, "Numerical calculation of inrush current in single-phase transformers," IEE Proceedings B: Electric Power Applications, vol. 128, no. 6, pp. 327-334, 1981.

[11] R. A. Turner and K. S. Smith, "Transformer inrush currents," IEEE Industry Applications Magazine, vol. 16, no. 5, pp. 14-19, 2010.

[12] A. Ketabi, A. M. Ranjbar, and R. Feuillet, "Analysis and control of temporary overvoltages for automated restoration planning," IEEE Transactions on Power Delivery, vol. 17, no. 4, pp. 1121-1127, 2002.

[13] R. Yacamini and A. Abu-Nasser, "Transformer inrush currents and their associated overvoltages in HVDC schemes," IEE Proceedings C: Generation, Transmission and Distribution, vol. 133, no. 6, pp. 353-358, 1986.

[14] R. A. Turner and K. S. Smith, "Resonance excited by transformer inrush current in inter-connected offshore power systems," in IEEE Industry Applications Society Annual Meeting, pp. 1-7, Edmonton, Canada, Oct. 2008.

[15] M. M. Adibi, R. W. Alexander, and B. Avramovic, "Overvoltage control during restoration," IEEE Transactions on Power Systems, vol. 7, no. 4, pp. 1464-1470, 1992.

[16] R. Hunt, J. Schaefer, and B. Bentert, "Practical experience in setting transformer differential inrush restraint," in Annual Georgia Tech Protective Relaying Conference, Atlanta, Georgia, May 2007.

[17] X. Lin and P. Liu, "The ultra-saturation phenomenon of loaded transformer energization and its impacts on differential protection," IEEE Transactions on Power Delivery, vol. 20, no. 2, pp. 1265-1272, 2005.

[18] E. Styvaktakis and M. H. J. Bollen, "Signatures of voltage dips: transformer saturation and multistage dips," IEEE Transactions on Power Delivery, vol. 18, no. 1, pp. 265-270, 2003.

[19] M. Nagpal, T. G. Martinich, A. Moshref, K. Morison, and P. Kundur, "Assessing and limiting impact of transformer inrush current on power quality," IEEE Transactions on Power Delivery, vol. 21, no. 2, pp. 890-896, 2006.

[20] Z. Bin, B. Liangen, Z. Peipeng, Z. Jian, Y. Yonghua, Z. Hongguang, G. Qiang, H. Fengjun, N. Shuanbao, and C. Xiqiang, "Analysis on field measured system voltage sag caused by energizing 750 kV no-load transformer and its simulation comparison," Power System Technology, vol. 36, no. 9, 2012.

[21] G. B. Kumbhar and S. V. Kulkarni, "Analysis of smpathetic inrush phenomena in transformers using coupled field-circuit approach," in IEEE Power Engineering Society General Meeting, pp. 1-6, Florida, USA, June 2007.

[22] H. Bronzeado and R. Yacamini, "Phenomenon of sympathetic interaction between transformers caused by inrush transients," IEE Proceedings - Science, Measurement and Technology, vol. 142, no. 4, pp. 323-329, 1995.

[23] J. A. Fleming, "Experimental researches on alternate-current transformers," Journal of the Institution of Electrical Engineers, vol. 21, no. 101, pp. 594-686, 1892.

[24] H. S. Bronzeado, P. B. Brogan, and R. Yacamini, "Harmonic analysis of transient currents during sympathetic interaction," IEEE Transactions on Power Systems, vol. 11, no. 4, pp. 2051-2056, 1996.

[25] W. Yunfei, S. G. Abdulsalam, and X. Wilsun, "Analytical formula to estimate the maximum inrush current," IEEE Transactions on Power Delivery, vol. 23, no. 2, pp. 1266-1268, 2008.

[26] T. R. Specht, "Transformer magnetizing inrush current," Transactions of the American Institute of Electrical Engineers, vol. 70, no. 1, pp. 323-328, 1951.

[27] J. E. Holcomb, "Distribution transformer magnetizing inrush current," Transactions of the American Institute of Electrical Engineers Part III. Power Apparatus and Systems, vol. 80, no. 3, pp. 697-702, 1961.

[28] T. R. Specht, "Transformer inrush and rectifier transient currents," IEEE Transactions on Power Apparatus and Systems, vol. PAS-88, no. 4, pp. 269-276, 1969.

[29] C. E. Lin, C. L. Cheng, C. L. Huang, and J. C. Yeh, "Investigation of magnetizing inrush current in transformers. I. Numerical simulation," IEEE Transactions on Power Delivery, vol. 8, no. 1, pp. 246-254, 1993.

[30] P. C. Y. Ling and A. Basak, "Numerical prediction of magnetising inrush current in transformers " Physica Scripta, vol. 40, pp. 246-248, 1989.

[31] J. Takehara, M. Kitagawa, T. Nakata, and N. Takahashi, "Finite element analysis of inrush currents in three-phase transformers," IEEE Transactions on Magnetics, vol. 23, no. 5, pp. 2647-2649, 1987.

[32] N. Richard and N. Szylowicz, "Comparison between a permeance network model and a 2D finite element model for the inrush current computation in a three phase transformer," IEEE Transactions on Magnetics, vol. 30, no. 5, pp. 3232-3235, 1994.

[33] "Guidelines for representation of network elements when calculating transients," Cigré Working Group 33-02, 1990.

[34] P. G. Boliaris, J. M. Prousalidis, N. D. Hatziargyriou, and B. C. Papadias, "Simulation of long transmission lines energization for black start studies," in 7th Mediterranean Electrotechnical Conference, pp. 1093-1096, Antalya, Turkey, Apr. 1994.

[35] J. A. Martinez and B. A. Mork, "Transformer modeling for low- and mid-frequency transients - a review," IEEE Transactions on Power Delivery, vol. 20, no. 2, pp. 1625-1632, 2005.

[36] M. Rioual and J. C. Reveret, "Energization of step-up transformers for wind-farms: Modeling and its validation by tests performed on a 10 MW site," in IEEE Power & Energy Society General Meeting, pp. 1-7, Calgary, Canada, Jul. 2009.

[37] H. Kuisti, "Energization of an unloaded transmission grid as part of restoration process," in International Conference on Power Systems Transients (IPST), New Orleans, USA, 2003.

[38] F. X. Zgainski, B. Caillault, and V. L. Renouard, "Validation of power plant transformers re-energization schemes in case of black-out by comparison between studies and field tests measurements," in International Conference on Power Systems Transients (IPST), Lyon, 2007.

[39] A. Ebner, "Reduction of voltage stress and inrush current of power transformers using controlled switching," in 20th International Conference and Exhibition on Electricity Distribution, pp. 1-4, Prague, Czech, 2009.

[40] V. Brandwajn, H. W. Donnel, and I. I. Dommel, "Matrix representation of three-phase n-winding transformers for steady-state and transient studies," IEEE Transactions on Power Apparatus and Systems, vol. PAS-101, no. 6, pp. 1369-1378, 1982.

[41] J. A. Martinez, R. Walling, B. A. Mork, J. Martin-Arnedo, and D. Durbak, "Parameter determination for modeling system transients-Part III: Transformers," IEEE Transactions on Power Delivery, vol. 20, no. 3, pp. 2051-2062, 2005.

[42] P. Nunes, A. Morched, M. Teresa, and C. d. Barros, "Analysis of generator tripping incidents on energizing nearby transformers," in Internatinoal Conference on Power Systems Transients (IPST), New Orleans, USA, 2003.

[43] M. M. Duro and R. Denis, "Parameter uncertainty assessment in the calculation of the overvoltages due to transformer energization in resonant networks," in CIGRE session proceeding, Paris, France, 2012.

[44] F. Moore, A. Haddad, H. Griffiths, and M. Osborne, "Switching transients in long AC cable connections to offshore wind farms," in 46th International Universities' Power Engineering Conference (UPEC), pp. 1-6, Soest, Germany, 2011.

[45] B. Mork, F. Gonzalez, D. Ishchenko, D. Stuehm, and J. Mitra, "Hybrid transformer model for transient simulation: Part I - Development and parameters," IEEE Transactions on Power Delivery, vol. 22, no. 1, pp. 248 - 255, Jan. 2007.

[46] E. C. Cherry, "The duality between interlinked electric and gagnetic circuits and the formation of transformer equivalent circuits " Proc. of the Physical Society of London, pp. 101-111, 1949.

[47] G. R. Slemon, "Equivalent circuits for transformers and machines including non-linear effects," Proceedings of the IEE - Part IV: Institution Monographs, vol. 100, no. 5, pp. 129-143, 1953.

[48] H. K. Høidalen, B. A. Mork, F. Gonzalez, D. Ishchenko, and N. Chiesa, "Implementation and verification of the Hybrid Transformer model in ATPDraw," Electric Power Systems Research, vol. 79, no. 3, pp. 454-459, 2009.

[49] N. Chiesa, H. K. Høidalen, and B. A. Mork, "Developments in the hybrid transformer model - core modeling and optimization," in International Conference on Power Systems Transients (IPST), Delft, The Netherlands, Jun. 2011.

[50] R. A. Turner and K. S. Smith, "Assessing P28 guidelines for renewable generation connections," in International Conference on Power Systems Transients (IPST), Delft, The Netherlands, 2011.

[51] A. Pors and N. Browne, "Modelling the energisation of a generator step-up transformer from the high voltage network," in Australasian Universities Power Engineering Conference (AUPEC), pp. 1-5, Sydney, Australia, Dec. 2008.

[52] N. Chiesa, B. A. Mork, and H. K. Høidalen, "Transformer model for inrush current calculations: simulations, measurements and sensitivity analysis," IEEE Transactions on Power Delivery, vol. 25, no. 4, pp. 2599-2608, 2011.

[53] S. N. Talukdar, J. K. Dickson, R. C. Dugan, M. J. Sprinzen, and C. J. Lenda, "On modeling transformer and reactor saturation characteristics for digital and analog studies," IEEE Transactions on Power Apparatus and Systems, vol. 94, no. 2, pp. 612-621, 1975.

[54] S. Prusty and M. Rao, "A direct piecewise linearized approach to convert rms saturation characteristic to instantaneous saturation curve," IEEE Transactions on Magnetics, vol. 16, no. 1, pp. 156-160, 1980.

[55] W. L. A. Neves and H. W. Dommel, "On modelling iron core nonlinearities," IEEE Transactions on Power Systems, vol. 8, no. 2, pp. 417-425, 1993.

[56] N. Chiesa and H. K. Hoidalen, "Analytical algorithm for the calculation of magnetization and loss curves of delta-connected transformers," IEEE Transactions on Power Delivery, vol. 25, no. 3, pp. 1620-1628, 2011.

[57] W. L. A. Neves and H. W. Dommel, "Saturation curves of delta-connected transformers from measurements," IEEE Transactions on Power Delivery, vol. 10, no. 3, pp. 1432-1437, 1995.

[58] "ATP rule book," Leuven, Belgium: Leuven EMTP Center, 1987.

[59] G. W. Swift, "An analytical approach to ferroresonance," IEEE Transactions on Power Apparatus and Systems, vol. PAS-88, no. 1, pp. 42-46, 1969.

[60] D. A. N. Jacobson, D. R. Swatek, and R. W. Mazur, "Mitigating potential transformer ferroresonance in a 230 kV converter station," in IEEE Transmission and Distribution Conference, pp. 269-275, California, USA, 1996.

[61] N. Chiesa and H. K. Høidalen, "Modeling of nonlinear and hysteretic iron-core inductors in ATP," in EEUG EMTP-ATP Conference, Leon, Spain, 2007.

[62] M. Rioual, Y. Guillot, and C. Crepy, "Determination of the air-core reactance of transformers by analytical formulae for different topological configurations and its comparison with an electromagnetic 3D approach," in IEEE Power & Energy Society General Meeting, pp. 1-8, Calgary, Canada, Jul. 2009.

[63] L. F. Woodruff, "Principles of electric power transmission," 2nd ed, New York: Wiley, 1938.

[64] "Tutorial on Electromagnetic Transient Program Applications to Power System Protection," IEEE PES/PSRC Special Publication, 2000.

[65] H. W. Dommel, "Digital computer solution of electromagnetic transients in single-and multiphase networks," IEEE Transactions on Power Apparatus and Systems, vol. PAS-88, no. 4, pp. 388-399, 1969.

[66] J. R. Marti, L. Marti, and H. W. Dommel, "Transmission line models for steady-state and transients analysis," in Joint International Power Conference Athens Power Tech (APT), pp. 744-750, Athens, Greece, Sep. 1993.

[67] H. W. Dommel and et.al., "Electromagnetic transients program reference manual (EMTP theory book)," Portland, OR, 1986.

[68] M. M. Duro, "Damping modelling in transformer energization studies for system restoration: Some standard models compared to field measurements," in IEEE Bucharest Power Tech, pp. 1-8, Bucharest, Romania, Jun. 2009.

[69] J. A. Martinez, J. Mahseredjian, and B. Khodabakhchian, "Parameter determination for modeling system transients-Part VI: Circuit breakers," IEEE Transactions on Power Delivery, vol. 20, no. 3, pp. 2079-2085, 2005.

[70] P. Gomez, "Validation of ATP transmission line models for a Monte Carlo study of switching transients," in 39th North American Power Symposium (NAPS), pp. 124-129, Las Cruces, USA, Sep. 2007.

[71] H. M. Ryan, "High voltage and electrical insulation engineering," 2nd ed London, UK: Institution of Electrical Engineers, 2001.

[72] S. D. Skuletic and P. Mijajlovic, "Experimental investigations of switching overvoltages in 110 kV network of power system of Montenegro," in IEEE Power Tech Conference Proceedings, Bologna, Italy, Jun. 2003.

[73] Z. Zdravković, P. Vukelja, R. Naumov, and M. Vučinić, "Overvoltages during switching of 400 kV, 220 kV and 110 kV circuit-breakers in high voltage networks," in International Conference on Power Systems Transients (IPST), Budapest, Hungary, 1999.

[74] "Modelling guidelines for switching transients," IEEE Modelling and Simulation Working Group 15.08.

[75] K. S. Smith, "Transformer inrush studies for wind farm grid connections," in International Conference on Power Systems Transients (IPST), Montreal, Canada, 2005.

[76] M. Kizilcay, "Energization of 380-kV partial networks for the purpose of fast blackstart after system collapse," in International Conference on Power Systems Transients (IPST), Budapest, Hungary, 1999.

[77] M. R. Iravani, A. K. S. Chandhary, W. J. Giesbrecht, I. E. Hassan, A. J. F. Keri, K. C. Lee, J. A. Martinez, A. S. Morched, B. A. Mork, M. Parniani, A. Sarshar, D. Shirmohammadi, R. A. Walling, and D. A. Woodford, "Modelling and analysis guidelines for slow transients. II. Controller interactions; harmonic interactions," IEEE Transactions on Power Delivery, vol. 11, no. 3, pp. 1672-1677, 1996.

[78] I. Hassan, H. V. Nguyen, and R. Jamison, "Analysis of energizing a large transformer from a limited capacity engine generator," in IEEE Power Engineering Society Winter Meeting, pp. 446-451, Singapore, Jan. 2000.

[79] D. Bi, X. Wang, D. Li, G. Yu, Z. Wang, and W. Wang, "Theory analysis of the sympathetic inrush in operating transformers," Automation of Electric Power Systems, vol. 29, no. 6, pp. 1-8, 2005.

[80] W. Yangguang, Y. Xianggen, Y. Dahai, and X. Tianqi, "Analysis on the influencing factors of transformer sympathetic inrush current," in IEEE Power and Energy Society General Meeting, pp. 1-8, Pittsburgh, USA, Jul. 2008.

[81] C. D. Hayward, "Prolonged inrush currents with parallel transformers affect differential relaying," Transactions of the American Institute of Electrical Engineers, vol. 60, no. 12, pp. 1096-1101, 1941.

[82] M. M. Saied, "A study on the inrush current phenomena in transformer substations," in 36th IEEE Industry Applications Conference, pp. 1180-1187, Chicago, USA, Sep. 2001.

[83] R. Yacamini and H. Bronzeado, "Transformer inrush calculations using a coupled electromagnetic model," IEE Proceedings - Science, Measurement and Technology, vol. 141, no. 6, pp. 491-498, 1994.

[84] S. Schramm, C. Sihler, and S. Rosado, "Limiting sympathetic interaction between transformers caused by inrush transients," in International Conference on Power Systems Transients (IPST), Delft, the Netherlands, 2011.

[85] J. Pontt, J. Rodriguez, J. S. Martin, and R. Aguilera, "Mitigation of sympathetic interaction between power transformers fed by long over head lines caused by

inrush transient currents," in IEEE Industry Applications Conference, pp. 1360-1363, New Orleans, USA, 2007.

[86] W. J. McNutt, W. M. Johnson, R. A. Nelson, and R. E. Ayers, "Power transformen short-circuit strength - requirements, design, and demonstration," IEEE Transactions on Power Apparatus and Systems, vol. PAS-89, no. 8, pp. 1955-1969, 1970.

[87] P. C. Y. Ling and A. Basak, "Investigation of magnetizing inrush current in a single-phase transformer," IEEE Transactions on Magnetics, vol. 24, no. 6, pp. 3217-3222, 1988.

[88] C. E. Lin, C. L. Cheng, C. L. Huang, and J. C. Yeh, "Investigation of magnetizing inrush current in transformers. II. Harmonic analysis," IEEE Transactions on Power Delivery, vol. 8, no. 1, pp. 255-263, 1993.

[89] B. Kasztenny, "Impact of transformer inrush currents on sensitive protection functions," in IEEE PES Transmission and Distribution Conference and Exhibition, pp. 820-823, Dallas, USA, May 2006.

[90] F. Mekic, R. Girgis, Z. Gajic, and t. Ed, "Power transformer characteristics and their effects on protective relays," in 60th Annual Conference for Protective Relay Engineers, pp. 455-466, Texas, USA, Mar. 2007.

[91] A. Wiszniewski, W. Rebizant, D. Bejmert, and L. Schiel, "Ultrasaturation Phenomenon in Power Transformers - Myths and Reality," IEEE Transactions on Power Delivery, vol. 23, no. 3, pp. 1327-1334, 2008.

[92] B. Kasztenny and A. Kulidjian, "An improved transformer inrush restraint algorithm increases security while maintaining fault response performance," in 53rd Annu. Conf. Protective Relay Engineers, College Station, TX, Apr. 2000.

[93] Y. C. Kang, B. E. Lee, S. H. Kang, and P. A. Crossley, "Transformer protection based on the increment of flux linkages," IEE Proceedings - Generation, Transmission and Distribution, vol. 151, no. 4, pp. 548-554, 2004.

[94] J. Pihler, B. Grcar, and D. Dolinar, "Improved operation of power transformer protection using artificial neural network," IEEE Transactions on Power Delivery, vol. 12, no. 3, pp. 1128-1136, 1997.

[95] J. P. Bowles, "Overvoltages in HVDC transmission systems caused by transformer magnetizing inrush currents," IEEE Transactions on Power Apparatus and Systems, vol. PAS-93, no. 2, pp. 487-495, 1974.

[96] D. Lindenmeyer, H. W. Dommel, A. Moshref, and P. Kundur, "Analysis and control of harmonic overvoltages during system restoration," in International Conference on Power Systems Transients (IPST) Budapest, Hungary, 1999.

[97] J. F. Witte, F. P. DeCesaro, and S. R. Mendis, "Damaging long-term overvoltages on industrial capacitor banks due to transformer energization inrush currents," IEEE Transactions on Industry Applications, vol. 30, no. 4, pp. 1107-1115, 1994.

[98] A. M. Miri and C. Sihler, "Damping of resonances at energization of transformers serving large pulse-type loads," IEEE Transactions on Industry Applications, vol. 40, no. 6, pp. 1694-1699, 2004.

[99] D. Povh and W. Schultz, "Analysis of overvoltages caused by transformer magnetizing inrush current," IEEE Transactions on Power Apparatus and Systems, vol. PAS-97, no. 4, pp. 1355-1365, 1978.

[100] M. H. J. Bollen, T. Tayjasanant, and G. Yalcinkaya, "Assessment of the number of voltage sags experienced by a large industrial customer," IEEE Transactions on Industry Applications, vol. 33, no. 6, pp. 1465-1471, 1997.

[101] H. C. Seo and C. H. Kim, "The analysis of power quality effects from the transformer inrush current: A case study of the Jeju power system, Korea," in IEEE Power and Energy Society General Meeting, pp. 1-6, Pittsburgh, USA, Jul. 2008.

[102] T. Ma and A. Cadmore, "System studies of voltage dips resulting from energisation of MV wind turbine transformers," in 18th International Conference on Electricity Distribution, Turin, June 2005.

[103] I. Arana Aristi, "Voltage dip caused by the sequential energization of wind turbine transformers," in European Wind Energy Association Conference, Marseille, France, 2009.

[104] L.Pierrat and T.Tran-Quoc, "Influence of random variables on transformer inrush current," in International Conference on Power Systems Transients (IPST), Lisbon, Portugal, 1995.

[105] J. Hu, B. Bisewski, D. Maki, and M. B. Marz, "Mitigation of voltage drop using pre-insertion resistor during large transformer energization in a weak system: simulation and field verification," in International Conference on Power Systems Transients (IPST), Delft, The Netherlands, 2011.

[106] B. Kovan, F. de Leon, D. Czarkowski, Z. Zabar, and L. Birenbaum, "Mitigation of inrush currents in network transformers by reducing the residual flux with an ultra-low-frequency power source," IEEE Transactions on Power Delivery, vol. 26, no. 3, pp. 1563-1570, 2011.

[107] C. K. Cheng, T. J. Liang, J. F. Chen, S. D. Chen, and W. H. Yang, "Novel approach to reducing the inrush current of a power transformer," IEE Proceedings - Electric Power Applications, vol. 151, no. 3, pp. 289-295, 2004.

[108] V. Molcrette, J. L. Kotny, J. P. Swan, and J. F. Brudny, "Reduction of inrush current in single-phase transformer using virtual air gap technique," IEEE Transactions on Magnetics, vol. 34, no. 4, pp. 1192-1194, 1998.

[109] J. H. Brunke and K. J. Frohlich, "Elimination of transformer inrush currents by controlled switching. II. Application and performance considerations," IEEE Transactions on Power Delivery, vol. 16, no. 2, pp. 281-285, 2001.

[110] H. S. Bronzeado and J. C. d. Oliveira, "The influence of tap position on the magnitude of transformer inrush current," in International Conference on Power Systems Transients (IPST), 1999.

[111] "Hinkley Point C Connection Project - Need Case for the South West and South Wales and Gloucestershire Regions," National Grid, 2011.

[112] W. K. Sonnemann, C. L. Wagner, and G. D. Rockefeller, "Magnetizing Inrush Phenomena in Transformer Banks," Power Apparatus and Systems, Part III. Transactions of the American Institute of Electrical Engineers, vol. 77, no. 3, pp. 884-892, 1958.

[113] "Electrical parameters and impedance characteristics of plant, lines and cables," National Grid technical guidance note, 2002.

[114] M. Bolhasani, S. S. H. Kamangar, and S. Tavakoli, "Determination of distribution function of inrush current in three phase transformer using Monte Carlo method," in 47th International Universities Power Engineering Conference (UPEC), pp. 1-7, Sep. 2012.

[115] J. A. Martinez and J. Martin-Arnedo, "Voltage sag stochastic prediction using an electromagnetic transients program," IEEE Transactions on Power Delivery, vol. 19, no. 4, pp. 1975-1982, 2004.

[116] A. Greenwood, "Electrical transients in power systems," 2nd ed, New York: Wiley, 1991.

[117] N. Chiesa, A. Avendano, H. K. Høidalen, B. A. Mork, D. Ishchenko, and A. P. Kunze, "On the ringdown transient of transformers," in International Conference on Power Systems Transients (IPST), Lyon, France, Jun. 2007.

[118] J. H. Brunke and K. J. Frohlich, "Elimination of transformer inrush currents by controlled switching. I. Theoretical considerations," IEEE Transactions on Power Delivery, vol. 16, no. 2, pp. 276-280, 2001.

[119] "UK renewable energy roadmap," available from http://www.decc.gov.uk/assets/decc/11/meeting-energy-demand/renewable-energy/2167-uk-renewable-energy-roadmap.pdf, accessed date: 25th Jan, 2013.

[120] "Germany's wind energy industry," available from http://www.gtai.de/GTAI/Content/EN/Invest/_SharedDocs/Downloads/GTAI/Fact-sheets/Energy-environmental/fact-sheet-wind-energy-in-germany.pdf, accessed date: 25th Jan, 2013.

[121] "Pushing forward: the future of offshore wind energy," available from http://www.rolandberger.de/media/pdf/Roland_Berger_taC_Offshore_20111206.pdf, accessed date: 25th Jan, 2013.

[122] G. Quinonez-Varela, G. W. Ault, O. Anaya-Lara, and J. R. McDonald, "Electrical collector system options for large offshore wind farms," IET Renewable Power Generation, vol. 1, no. 2, pp. 107-114, 2007.

[123] "SeaTitan 10 MW wind turbine," available from http://www.amsc.com/library/, accessed date: 25th Jan, 2013.

[124] A. B. J. Green, L. J. Fingersh and Y. Wan, "Electrical collection and transmission systems for offshore wind power," in Offshore Technology Conference, Houston, Texas, 2007.

[125] "List of offshore wind farms," available from http://en.wikipedia.org/wiki/List_of_offshore_wind_farms, accessed date: 25th Jan, 2013.

[126] M. Rioual and M. Sow, "Study of the sympathetic interactions when energizing transformers for wind-farms: Description of the phenomena involved and determination of the stresses during their energization," in 7th International Workshop on Large-Scale Integration of Wind Power into Power Systems, Madrid, 2008.

[127] IEC-60076-16, "Power transformers - part 16: Transformers for wind turbine applications," 2011.

[128] I. Arana, "Modelling of switching transients in Nysted offshore wind farm and a comparison with measurements," MSc Thesis, Technical University of Denmark, 2008.

[129] S. Das, N. Karnik, and S. Santoso, "Time-domain modeling of tower shadow and wind shear in wind turbines," ISRN Renewable Energy, 2011.

[130] B. Gustavsen, J. A. Martinez, and D. Durbak, "Parameter determination for modeling system transients-Part II: Insulated cables," IEEE Transactions on Power Delivery, vol. 20, no. 3, pp. 2045-2050, 2005.

[131] J. Jeppsson, P. E. Larsen, and Å. Larsson, "Technical description Lillgrund wind power plant," Vattenfall, Sep 2008.

[132] ABB, "XLPE land cable systems," 2010.

[133] ABB, "XLPE submarine cable systems," 2010.

[134] "National grid seven year statement," available from http://www.nationalgrid.com/uk/Electricity/SYS/current/, accessed date: 15th Nov, 2012.

[135] D. West, "Central networks grid transformer specification," E.ON Central Networks 2008.

Appendix: List of Publications

Peer-reviewed Journal Papers:

[1] **J. S. Peng**, H. Y. Li, Z. D. Wang, F. Ghassemi and P. Jarman, "Influence of sympathetic inrush on voltage dips caused by transformer energization", IET Generation Transmission and Distribution, in press, 2013.

[2] **J. S. Peng**, H. Y. Li, Z. D. Wang, F. Ghassemi and P. Jarman, "Stochastic assessment of voltage dips caused by transformer energization", submitted to IET Generation Transmission and Distribution.

International Conference Papers:

[3] **J.S. Peng**, H.Y. Li, Z.D. Wang and P. Jarman, "Evaluation of Transformer Inrush-induced Voltage Dips", CIRED 21st International Conference on Electricity Distribution, Frankfurt, Germany, 6^{th} -9^{th} June 2011.

[4] R. Zhang, **J.S. Peng**, S.P. Ang, H.Y. Li, Z.D. Wang and P. Jarman, "Statistical Analysis of Ferroresonance in a 400 kV Double-Circuit Transmission System", International Conference on Power Systems Transients (IPST), Delft, Netherlands, 14^{th} -17^{th} June, 2011.

[5] S.P. Ang, **J.S. Peng**, and Z.D. Wang, "Identification of key circuit parameters for the initiation of ferroresonance in a 400-kV transmission system", International Conference on High Voltage Engineering and Application (ICHVE), New Orleans, USA, pp. 73-76, 11^{th}-14^{th} Oct, 2010.

[6] **J.S. Peng**, S.P. Ang, H.Y. Li, and Z.D. Wang, "Comparisons of normal and sympathetic inrush and their implications toward system voltage depression", 45th International Universities Power Engineering Conference (UPEC), Cardiff, Wales, pp. 1-5, 31^{st}-3^{rd} Sep, 2010.